Réponse des systèmes alluviaux aux forçages externes a diverses échelles de temps : de la morphologie fluviale a l'architecture stratigraphique des systèmes continentaux

Frédéric Christophoul

UNIVERSITÉ TOULOUSE III PAUL SABATIER — Université de Toulouse

GÉOSCIENCES ENVIRONNEMENT TOULOUSE — GET

Thèse d'Habilitation à Diriger les Recherches

Réponse des systèmes alluviaux aux forçages externes à diverses échelles de temps : de la morphologie fluviale à l'architecture stratigraphique des systèmes continentaux

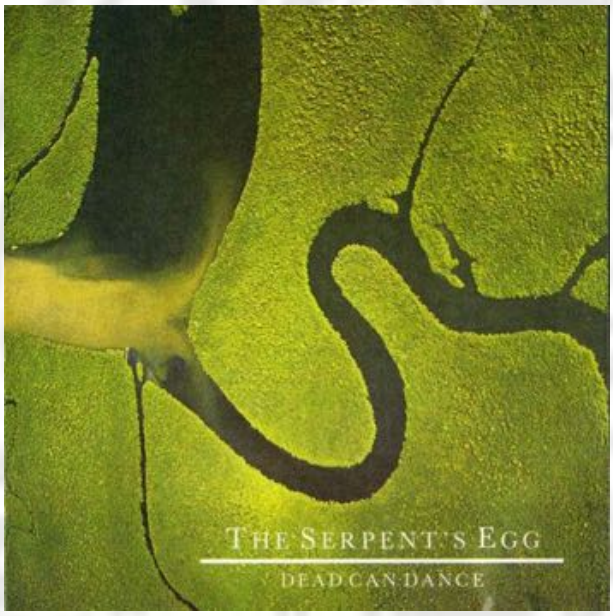

Frédéric Christophoul

Maître de Conférences à l'Université Toulouse III, Paul Sabatier
UMR 5563 Géosciences Environnement Toulouse
- Université de Toulouse - CNRS - IRD - CNES - OMP -
14 Avenue Edouard Belin, F-31400 Toulouse

Soutenue le 24 Novembre 2015

devant le jury composé de :

Isabelle	Cojan	Pr.	Mines ParisTech	Rapporteur
François	Guillocheau	Pr.	Univ. Rennes 1	Rapporteur
François	Métivier	Pr.	IPG Paris	Rapporteur
Mary	Ford	Pr.	ENSG - Univ. de Lorraine	Examinatrice
Stéphane	Bonnet	Pr.	Univ. Toulouse 3	Parrain

Illustration de couverture : Couverture de l'album "The Serpent's Egg" du groupe Dead Can Dance en 1988. Bifurcation entre une anabranche et son chenal parent. Le sens d'écoulement est indiqué par le panache de sédiments en suspension se séparant en deux au niveau de la bifurcation. Localisation inconnue.

"The face of the river, in time,
became a wonderful book which told its mind without reserve,
delivering its most cherished secrets as clearly
as if it uttered them with a voice"
Samuel Langhorne Clemens, dit Mark Twain
"Life on the Mississipi", Twain (1883)

Remerciements

Je tiens remercier Stéphane Bonnet pour avoir accepté d'être mon parrain scientifique pour cette HDR. Je remercie également Isabelle Cojan, François Guillocheau et François Métivier d'avoir accepté de rapporter mon HDR.

Je remercie aussi le Conseil scientifique de l'Université Toulouse III, Paul Sabatier pour m'avoir accordé un an de CRCT et je tiens à exprimer ma gratitude à Mary Ford pour m'avoir accueilli au CRPG durant mon année de CRCT pour travailler sur le projet ANR PYRAMID. Le groupe de sept personnes (chercheurs et étudiants) qu'elle a constitué durant l'année 2014, travaillant sur un projet commun s'est révélé être une vraie motivation pour faire le point sur mes activités de recherche et envisager des projets communs pour les années à venir. Cette collaboration fructueuse se poursuivra dans les années à venir au travers des thèse et post-doc du projet OROGEN financé par Total.

D'un point de vue personnel, je tiens aussi à remercier mes ami(e)s et collègues Markus, Elise, Guillaume, Stéphanie, Cath, Delphine, Dominique, Vincent, Valérie, Joseph et Sébastien pour m'avoir réguliérement tanné en me demandant "tu en es où de ton HDR ?" Leur insistance, parfois lourde, mais toujours bienveillante, aura finalement porté ses fruits.

Enfin, je tiens à témoigner mon éternelle reconnaissance à celles et ceux qui ont été là, le vendredi 26 Septembre 2014 et qui, par leurs conseils ou simplement leur présence ont contribué à ce que cette HDR ne soit pas un ouvrage posthume.

Sommaire

Liste des Figures

Liste des tableaux

Chapitre 1

Curriculum Vitae

1.1 Fiche Résumé

Frédéric CHRISTOPHOUL
Né le 28 mai 1972 à Decazeville (France)
Nationalité Française
Docteur de l'Université Toulouse 3 spécialité : tectonique et sédimentation, depuis le 22 décembre 1999.

Maître de Conférences à l'Université Toulouse 3, Paul Sabatier depuis le 1er Septembre 2002 (CNU 36).
UMR 5563 Géosciences Environnement Toulouse (GET) - Université de Toulouse - CNRS - IRD - OMP
14 Avenue Edouard Belin
F-31400 TOULOUSE
tel : 05 61 33 26 70
mobile : 06 71 72 90 67
courriel : frederic.christophoul@get.obs-mip.fr

Enseignement

- 2014 - CRCT au titre de l'Univ. Toulouse 3, Paul Sabatier.
- 2004 - 2008 Responsable pédagogique de l'année L3 RéoSTE.
- 2002 - 2014 MCU, Univ. Toulouse 3, Paul Sabatier.
- 2000 - 2001 - ATER, Univ. Toulouse 3, Paul Sabatier.
- 2000 - ATER, EGID-Univ. Bordeaux 3, Michel de Montaigne.
- 1998 - 1999 - Vacations, Univ. Toulouse 3, Paul Sabatier.

Thèmes de recherche

- Géomorphologie Fluviale, paramètres de contrôle des morphologies fluviales et des phénomènes d'avulsion.
- Sédimentologie des systèmes fluviatiles, analyse des faciès, architecture stratigraphique.
- Compréhension du fonctionnement autocyclique des systèmes alluviaux/fluviaux et de l'expression géomorphologique et stratigraphique de leur réponse aux forçages externes.

Publications

- 21 articles *(1 sous-presse, 2 en révision, 1 soumis)* de rang A dont 9 en 1er ou 2ème auteur.
- 6 chapitres d'ouvrages dont 2 en 1er auteur.
- 51 communications dans des colloques nationaux et internationaux dont 18 orales.
- 2 conférences invitées.

Projets scientifiques

- à Depuis 2015 - OROGEN - Projet TOTAL-BRGM-INSU, co-encadrement de Thèses et post-docs.
- 2012 - 2016 - ANR (blanc) Minemet (PI : B. Cauuet, UMR TRACE, UT2), coordonnateur partenaire.
- 2012 - 2016 - ANR (blanc) Pyramid (PI : Pr. M. Ford, ENSG, Nancy), coordonnateur partenaire.
- 2008 - 2012 - Interreg SUDOE DO-SMS (PI : J. Darrozes, UMR LMTG Toulouse), participant.
- 2007 - 2011 - ANR (JC) Andes (PI : S. Carretier, UMR LMTG, Toulouse), participant.
- 2003 - BQR (UFR SVT, Univ. Toulouse 3, Paul Sabatier), Co-PI avec Pr. J. Martinod (UMR LMTG).
- 1999 - 2002 - INSU PNSE (PI : P. Baby et J-L. Guyot IRD), participant.

Encadrement

2 thèses de Doctorat, 5 Master 2, 15 Master 1, 2 Licence 3.

Responsabilités collectives

- Depuis 2012 - Membre élu du Conseil Académique CFVU de l'Univ. Toulouse 3.
- 2008 - 2012 - Membre élu du CoNRS section 18 collège B2.
- 2003 - 2008 - Membre élu du CA de l'UFR SVT de l'Univ. Toulouse 3.

Evaluation et expertise scientifique

- 2014 - Evaluateur de projets de pour l'AAP générique de l'ANR.
- depuis 2013 - Membre du jury de l'appel d'offre "Innovation Pédagogique en Licence" et "Masters pluridisciplinaires" de l'DEX de Toulouse.
- 2008-2012 - Evaluation biennale et quadriennale de l'activité des chercheurs dans le cadre du CoNRS.
- Reviews pour le *Journal of South American Earth Sciences, Journal of the Geological Society of London, International Journal of Earth Sciences (ex-Geologische Rundschau), Geomorphology, Comptes Rendus Géosciences et le Bulletin de la Société Géologique de France.*

1.2 Curriculum vitæ étendu

1.2.1 Parcours universitaire

— 22 Décembre 1999 - Thèse de l'Université Toulouse 3, Paul Sabatier : "Discrimination des influences tectoniques et eustatiques dans les bassins liés à des zones de convergence, exemples du Bassin Subandin d'Equateur" mention très honorable.

Directeurs de thèses :
Patrice Baby (DR, IRD).
Joachim Déramond (PR, Univ. Toulouse 3).

Membres du Jury :
Francis Odonne (PR, Univ. Toulouse 3), président du jury.
François Guillocheau (PR Univ. Rennes 1), rapporteur.
Marc Tardy (PR Univ. Chambéry), rapporteur.
Georges Mascles (PR Univ. Grenoble), rapporteur.
Gérard Hérail (DR, IRD), examinateur.

— 1996 - DEA Sed & Pal, cohabilité : Univ. de Dijon, Lyon 1, Aix-Marseille et Toulouse 3. Mention Bien.
— 1995 - Maîtrise des Sciences de la Terre option Géologie, Univ. Toulouse 3. Mention Assez Bien.
— 1994 - Licence des Sciences de la Terre option Géologie, Univ. Toulouse 3.
— 1993 - DEUG Sciences de la Terre, Univ. Toulouse 3. Mention Assez Bien.
— 1990 - Baccalauréat général scientifique (D).

1.2.2 Expériences professionnelles

— 2014 - Actuel - Maître de Conférences à l'Université Toulouse 3, Paul Sabatier, UMR 5563 Géosciences Environnement Toulouse (GET).
— 2014 - Congés pour Recherches et/ou Conversion Thématique obtenu au titre de l'Univ. Toulouse 3. En accueil au Centre de Recherches Pétrographiques et Géochimiques (CRPG), Nancy.
Un CRCT d'un an m'a été accordé par l'Univ., Toulouse 3, Paul Sabatier pour l'année civile 2014. Ma demande de CRCT était principalement motivée par mon implication dans un projet ANR (ANR Blanc PYRAMID 2012-2016, PI : Pr. M. Ford, ENSG/ CRPG, Nancy). Dans le cadre ce de CRCT, je suis actuellement en accueil au Centre de Recherche Pétrographiques et Géochimique (UMR 7358) de Nancy. Dans le cadre du projet Pyramid et au sein des 2 Tâches dans lesquelles je suis impliqué, j'ai été amené à co-encadrer 3 Master 2 GPIR de l'Univ. de Lorraine. J'ai été impliqué dans l'encadrement d'un 4$^{\text{ème}}$ ainsi que dans les travaux d'un doctorant travaillant sur le projet (thèse en cohabilitation Univ. de Lorraine - Univ. de Bergen). A partir de la rentrée 2014, j'assurerai le co-encadrement d'un thèse sur le Bassin Aquitain sur financement mixte RGF-BRGM / Région Lorraine (recrutement du/de la doctorant(e) en cours).

— 2002 - 2014 - Maître de Conférences à l'Université Toulouse 3, Paul Sabatier, UMR 5563 Géosciences Environnement Toulouse (GET).

— 2001 - 2002 - Directeur du Musée Régional de Géologie 'Pierre Vetter', CCSTI - Decazeville.

Le musée Régional de Géologie « Pierre Vetter », du nom de son fondateur et premier directeur, ingénieur géologue aux charbonnages de France a été fondé en 1977 dans un souci de conservation du patrimoine paléontologique des bassins houillers carbonifère terminal du Massif Central. Tombé dans l'oubli pendant près de 15 ans, la municipalité de Decazeville a

eu la volonté de rouvrir ce musée au public et d'en faire un acteur de la diffusion scientifique au plan régional. Mon rôle en tant que directeur a consisté à animer le musée, monter une programmation d'expositions temporaires dans le cadre des Centres de Culture Scientifique, Technique et Industrielle (Ministère de la culture - Ministère de l'Education Nationale). Dans un cadre plus large, j'ai cherché à inscrire le musée dans un réseau régional de diffusion et de vulgarisation des sciences pour un public scolaire et généraliste. J'ai poursuivi l'inventaire, la gestion et mise en valeur de collection paléobotanique du Carbonifère du bassin houiller de Decazeville et mis en place un projet de rénovation muséographique.

— 2000 - 2001 - ATER - Université Toulouse 3, Paul Sabatier.

— 2000 - Vacataire - Bureau des Recherches Géologiques et Minières (BRGM) Aquitaine, Bordeaux. Synthèse sur le contexte géologique des sources d'eaux thermales du sud des Pyrénées Atlantiques.

— 2000 - ATER - Institut EGID - Université Bordeaux 3, Michel de Montaigne.

Durant mon année en tant qu'ATER à l'EGID, j'ai été chargé de l'organisation pédagogique et logistique d'un camp de terrain d'une semaine de géologie structurale sur un transect Zone nord-Pyrénéenne - Zone sous-pyrénéenne dans les Corbières. Ce camp de terrain, légèrement modifié est encore programmé chaque année. J'ai, par ailleurs, pris part à l'encadrement d'un camp de terrain d'un mois en sédimentologie/architecture stratigraphique des bassins sédimentaires dans le bassin Eocène d'Ainsa (Espagne).

— 1998-1999 - Enseignant vacataire, Univ. Toulouse 3, Paul Sabatier.

1.2.3 Activités d'enseignement

Résumé

— 240h ETD par an en moyenne depuis 10 ans.
— 4 responsabilités d'UE.
— 1 responsabilité d'année (L3 RéoSTE, 2004-2008).
— 1 responsabilité d'échanges internationaux (Programme Erasmus, 2004-2008).
— Référent adjoint du Champ Disciplinaire "Sciences de la Terre et Environnement" (depuis 2013).
— 1 an de Congés pour Recherches et/ou Conversion Thématique pour l'année 2014.

Depuis mon recrutement en 2002 sur un profil "sédimentation continentale", je n'ai que marginalement enseigné la sédimentologie (+/- 10h ETD/an). De part ma formation généraliste, je me suis investi dans des enseignements "généralistes" : géologie générale en L3 RéoSTE/RéoTE, camps de terrain de cartographie (L2 et L3 IUP GDE, L3 RéoSTE/ RéoTE, L3 TE, M1 ST et GTPRM, M1 BGSTU et SVTE) et de cartographie géologique (L3 RéoTE, L2 STE, M1 BGSTU, M1 SVTE). Mon changement de thématique de recherche vers la géomorphologie m'a permis de m'investir dans les enseignements de géomorphologie (L3 TE, M1 IUP GDE, M2 STP). Mon profil de recrutement mentionnant une implication dans les enseignements de terrain, ces enseignements constituent une part significative de mon service. Recruté en cours de quadriennal, je me suis adapté aux besoins de la commission pédagogique/ Département en Sciences de la Terre et de l'Environnement. La reconduction tacite des maquettes d'enseignement, d'un quadriennal à l'autre, fait qu'au long de mes douze ans de carrière, mon service d'enseignement est constitué d'une implication en faible volume horaire dans une multitude d'UE et dans un grand nombre de formations.

Volumes horaires

Du fait du sous-encadrement "historique" des Sciences de la Terre et de l'Environnement (Section CNU 35 et 36) à l'Université Toulouse 3, Paul Sabatier, mon service d'enseignement a, depuis mon recrutement, toujours excédé, comme nombre de mes collègues, les 192h ETD statutaires. Après un pic de 357h ETD l'année de ma titularisation (2003-04), mon service s'est stabilisé autour de 230h ETD par an. Ce volume est dans la moyenne (haute) du département. La rationalisation de l'offre de formation et la mise en place d'une gestion centralisée des service d'enseignement m'a permis de revenir plus près des 192h statutaires.

Disciplines enseignées

quadriennal 2003-2007 Durant ce quadriennal, j'ai assuré la responsabilité ainsi que tous les cours cours magistraux de l'UE de pétrographie intervenant au $2^{\text{ème}}$ semestre de L1. J'ai aussi pris la responsabilité d'une UE en MAster 1 SVTE (Prépa CAPES) regroupant des enseignements de sciences de la Terre autour des thèmes : géoressources et risques. Ce enseignements théoriques s'accompagnait d'preuves orales formatées sur les leçons du CAPES pour les thèmes enseignés dans l'UE. A partir de 2004, j'ai pris la responsabilité des échanges Erasmus pour les Sciences de la Terre et de l'Environnement. Dans le cadre de ces échanges, j'ai entretenu et développé les contrats d'échanges avec 11 universités européennes (Madrid Complutense, Madrid Autonoma, Saragosse, Oviedo, Leeds, Vienne, Prague, Milan, Oulu, Heidelberg, Zürich). Le rythme moyen des échanges était de 6 étudiants entrants et 6 sortants. Le pic fut atteint durant l'année 2007-2008 avec 12 étudiants toulousains partant dans une université extérieure. De la même manière, j'ai assuré la responsabilité pédagogique de l'année de L3 IUP GDE devenant en cours de quadriennal L3 RéoSTE suite à la disparition des IUP. Le Tableau 1.1 résume mes enseignements durant cette période.

Code Apogée	intitulé d'UE	Descriptif	CM	TD	Terrain	TP
L1 Mention sciences de la terre						
(*)	Pétrographie	Genèse des roches sédimentaires	22			24
L3 RéoSTE						
ULI5I1CM	Géologie Générale	Genèse des roches sédimentaires et camp de terrain	3			24
ULI6I1CM	Géologie générale	Géologie sédimentaire et camps de terrain	3		30	2
L3 Sciences de la Terre et Environnement						
3L64STM	Cartographie géologique	Camp de terrain			30	
3L62STM	Géomorphologie	Géomorphologie fluviale	3			12
Master 1 SVT et Enseignement (Prépa CAPES)						
3M87STM	Géologie de la France	Cartographie géologique				30
3M88STM (*)	Ressources naturelles et risques	Géologie des hydrocarbures, épreuves orales	5			12
Master 1 Sciences de la Terre						
3M74STM	Bassins Sédimentaires et Stratigraphie séquentielle	Analyse séquentielle des séries fluviatiles, corrélations stratigraphiques, camp de terrain	3	12	24	

(*) : Responsable d'UE.

TABLE 1.1 – Répartition des volumes horaire enseignés durant le quadriennal 2003-2007

quadriennal 2007-2011 Durant ce quadriennal, j'ai assuré les enseignements de stratigraphie séquentielle et d'étude de la subsidence dans les bassins sédimentaires, dans l'UE3M74STM : Bassins Sédimentaires, en remplacement d'un collègue détaché à l'IRD. En cours du quadriennal, j'ai pris la responsabilité de l'UE 3L64STM, camp de terrain cartographie de la Licence 3 STE en prévision du départ en retraite d'une partie de l'équipe pédagogique. j'ai poursuivi le développement des enseignements en Prépa CAPES faisant évoluer les contenus en fonction des modifications des programmes du concours et des rapports des jurys du CAPES. J'ai assuré les enseignements d'

Code Apogée	intitulé d'UE	Descriptif	CM	TD	Terrain	TP
L1 Mention sciences de la terre						
(*)	Pétrographie	Genèse des roches sédimentaires	4,5			8
L3 RéoSTE						
ULI5I1CM	Géologie Générale	Genèse des roches sédimentaires et camp de terrain	3		30	2
ULI6I1CM (*)	Géologie sédimentaire et camps de terrain	Bassins sédimentaires	9	3	30	12
M1 Génie de l'Environnement (IUP GDE)						
UMI8I2CM	Géomorphologie	Géomorphologie fluviale	4		12	
L3 Sciences de la Terre et Environnement						
3L64STM	Cartographie géologique	Camp de terrain			30	
3L62STM	Géomorphologie	Géomorphologie fluviale	3		12	12
Master 1 SVT et Enseignement (Prépa CAPES)						
3M87STM	Géologie de la France	Cartographie géologique				30
3M8VTE2M (*)	Ressources naturelles et risques	Géologie des hydrocarbures, épreuves orales	5		12	
Master 1 Sciences de la Terre						
3M74STM	Bassins Sédimentaires et Stratigraphie séquentielle	Analyse séquentielle des séries fluviales, corrélations stratigraphiques, analyse de la subsidence, systèmes turbiditiques, camp de terrain	6	18	24	

(*) : responsable d'UE, (**) Responsable d'UE par intérim (2 ans).

TABLE 1.2 – Répartition des volumes horaire enseignés durant le quadriennal 2007-2011

analyse des Bassins Sédimentaires en L3 RéoSTE (Stucture des bassins sédimentaires, stratigraphie séquentielle et analyse de la subsidence. Le Tableau 1.2 résume mes activités durant cette période.

quinquennal 2011-2016 En cours de quinquennal en cours, ma charge d'enseignement a été modifiée de manière importante suite à la réforme du concours de recrutement des enseignants du 2nd degré. La mise an place des Master MEEF à réduit la part des enseignements disciplinaires en Master 1 au profit des enseignements de Sciences de l'Education. Ainsi, L'UE "Ressources Naturelles, Risques et Environnement" a été supprimée. Cette suppression m'a permis de développer des enseignements en Master 1 écologie de l'Univ. Toulouse 3 dans l'UE "Interactions sous-sol végétation".

Code Apogée	intitulé d'UE	Descriptif	CM	TD	Terrain	TP
L1 Mention sciences de la terre						
	Approche expérimentale en sciences de la terre	Enseignements généraux			6	32
L3 RéoTE						
ULI5I1CM	Géologie Générale	Genèse des roches sédimentaires et camp de terrain	3			24
ULI6I1CM	Géologie générale	Géologie sédimentaire et camps de terrain	3		30	2
L3 Sciences de la Terre et Environnement						
3L64STM	Cartographie géologique	Camp de terrain			30	
3L62STM	Géomorphologie	Géomorphologie fluviale	3		12	
Master 1 SVT et Enseignement (Prépa CAPES)						
3M87STM	Géologie de la France	Cartographie géologique			30	
3M8VTE2M (*)	Ressources naturelles et risques	Géologie des hydrocarbures, épreuves orales	5		12	
Master 1 Ecologie						
EM8BECBM	Interactions sous-sol végétation	Géomorphologie structurale et fluviale	4	2	12	

(*) : responsable d'UE.

TABLE 1.3 – Répartition des volumes horaire enseignés durant le quinquennal 2011-2016

après 2016 Depuis 1998 et le début du renouvellement de la génération recrutée avec la massification du nombre des étudiants à l'université (fin des années soixante), la politique de l'Axe pédagogique « Science de la terre et Environnement » (anciennement Commission Pédagogique) a mené au recrutement de 8 enseignants-chercheurs sur des profils incluant le mot clé « sédimentation ». Ces recrutements ont permis de constituer un groupe de 8 permanents. Malgré un potentiel d'enseignement important, ce groupe peine à faire émerger le pôle toulousain en tant qu'école reconnue de géologie sédimentaire au plan national. Dans les deux prochaines années, vont débuter les discussions en vue de la mise en place du quinquennal 2016-2021. Dans ce cadre, je souhaite m'investir dans ces discussions afin de faire émerger une formation cohérente, au niveau Licence et Master. Dans cette optique, je pense recentrer mes interventions en Licence en sédimentologie et plaéoenvironnements sur un nombre réduit d'UE, en m'y impliquant que de plus forts volumes horaires afin d'assurer un meilleur suivi de la formation des étudiants.

1.2.4 Encadrement et formation par la recherche

Résumé

- 3 thèses de doctorat (1 en cours).
- 5 stages de Master 2 (Univ. Toulouse 3 ; Univ. de Lorraine Nancy).
- 15 stages de maîtrise / TPE Master 1 ST ou ESE (Univ. Toulouse 3).
- 2 Stages de L3 Réorientation en Sciences de la Terre.
- 1 DESU de l'Univ. Toulouse 3.
- 1 Thèse d'ingénieur de l'Université Centrale de Quito (Equateur).

Post-doctorat

- A compter de la rentrée 2015 « Topographic growth, basin flexure and sediment flux in early mountain belt/foreland basin systems : Cretaceous-Palaeogene evolution of the central-eastern Pyrenees » Co-encadrement avec M. Ford, R. Pik (CRPG, Nancy) et H. Sinclair (Univ. Edimbourg). Financement TOTAL (projet Orogen).

Thèses de doctorat

Encadrement

- depuis 2014 - Santiago Yepes, « Quantification des volumes de sédiments transportés par le Rio Orénoque. » Financement IRD / Gouvernement du Venezuela. Co-encadrement avec A. Laraque (DR, IRD) et J-M. Martinez (CR, IRD).
- 2005 - 2009 - Isabel Carolina Bernal Carrera, « Transferts de masses entre une chaine et son piedmont : aspect géomorphologiques et hydro-sédimentologiques. Exemple du méga-cône du Napo-Pastaza (Equateur-Pérou)», soutenance 25 novembre 2009. Financement programme Alban (Union Européenne). Actuellement Professeur à l'Ecole Polytechnique Nationale de Quito (Equateur). Ex-vice-ministre chargée des mines dans le gouvernement de la République d'Equateur. Co-encadrement, J. Darrozes (MC, Univ. Toulouse 3) et A. Laraque (CR, IRD).

- 2003 - 2006 - José David Burgos Zambrano, « Mise en place et évolution d'un cône de piémont : exemple du mégacône du Napo-Pastaza depuis le néogène » soutenance avril 2006. Co-encadrement, Patrice Baby (DR IRD). Financement IRD. Actuellement, chef d'exploration dans l'industrie pétrolière, Petroamazonas, Equateur.

- 2003 - 2007 - Cindy Maisonnave « Développement du réseau hydrographique sur un piedmont orogénique, sédimentologie et traçage de sources, exemples de l'Eocène du bassin d'avant-pays nord-pyrénéen ». Thèse non soutenue. Financement MENSR.

Collaboration

— a partir de 2016 - XXXXXXX . « Reconstruction of early orogen dynamics in the Pyrenees : development and application of in situ double dating U/Pb and U/He by laser ablation on detrital zircons ». Encadrement R. Pik, M. Ford (CRPG, Nancy) et H. Sinclair (Univ. Edimbourg). Financement TOTAL (Projet OROGEN).
— depuis 2014 - Paul Angrand. Evolution 3D d'un bassin d'avant-pays de type rétro-prisme riche en sel : le Bassin Aquitain, Nord Pyrénées. Encadrement M. Ford (ENSG/CRPG, Nancy) et Cédric Carpentier (Univ. de Lorraine- UMR Géoressources, Nancy). Financement RGF-BRGM / Région Lorraine.

— 2013 - en cours - Arjan Grool. Retroforeland basin dynamics : the north-pyrenean foreland basin. Encadrement : M. Ford (ENSG/CRPG, Nancy) et R. Huismans (Univ. Bergen, Norvège). Financement ANR / Univ. Bergen.

Masters 2

— Géraldine Rougier, 2014. Sedimentological and tectonic studies in the Central Aquitaine basin : constraints on subsidence and deformation of a retro-foreland basin. M2 GIPR (Univ. de Lorraine), encadrement à 30% avec M. Ford (PR, ENSG, Nancy) et A-G. Bader (BRGM Orléans).
— Louis Hemmer, 2014. Tectonics and sedimentary evolution of the Aquitaine retro-foreland basin along the ECORS profile : Construction of a balanced cross section and quantitative subsidence analysis. M2 GIPR (Univ. de Lorraine), encadrement à 50% avec M. Ford (PR, ENSG, Nancy).
— Larissa Ngombi Mavoungou, encadrement à 50% avec M. Ford (PR, ENSG, Nancy).
— Aymeric Lansac, 2012. Origine de la dissymétrie des réseaux de terrasses du piémont nord-pyrénéen. Encadrement à 50% avec V. Regard (MCU, UMR 5563 GET).
— XXX XXXX, 2006. Volumes de glace dans les vallées pyrénéennes lors du dernier maximum d'extension glaciaire : influence sur le rebond isostatique post-glaciaire. Encadrement à 50% avec J. Darrozes (MCU, UMR 5563 GET).

Masters 1

— Jade Faure, David Vallois et Laure Viprey, 2014. Mise en évidence des chenaux de la basse terrasse de la Garonne par tomographie électrique. Encadrement à 30% avec Muriel Llubes et Joseph Martinod (UMR 5563 GET).
— Adélaïde Wyndicka et Marie Gombert, 2013. Cartographie des placers alluviaux du Roussillon (Forêt du Réart, Pyrénées Orientales). Encadrement à 100%.
— Bérangé Moussirou et Romain Metge, 2012. Géomorphologie sismique du bassin Maranon (Pérou). Encadrement à 50% avec Gérôme Calvès (MCU, UMR 5563 GET).
— Suzie Gire, 2012. Le cône de Lannemezan : étendue stratigraphique et géographique. Encadrement à 100%.
— Flavien Denis, 2011. Dissymétrie des réseaux de terrasses fluviales sur les tributaires du piedmont Nord-Pyrénéen. Encadrement à 50% avec Vincent Regard (MC, UMR 5563, LMTG).
— Guillaume Baby et Laurent Mondouch, 2011. Sédimentologie du Paléocène-Eocène du bassin d'avant-pays Nord-Pyrénéen. Encadrement à 50% avec Markus Aretz (MC, UMR 5563 LMTG).
— Krystel Segura, 2009. Cartographie des migrations du cours inférieur du Rio Ucayali, Bassin de l'Amazone, nord-Pérou. Encadrement à 100%.
— Freedy Nzue Nzue, 2009. Le continental Terminal du Bassin des Iullemeden (Niger). Encadrement à 50% avec D. Chardon (PRU, UMR 5563 LMTG).
— Gilles Tichy, 2007. Cartographie 3D de la base des terrasses de la Garonne entre Cazères et

Muret. Encadrement à 50% avec Eric Maire (IR, CNRS, UMR Géode).
— Agathe Sutra, 2005. Reconstitution du style fluviatile de la molasse Eocène de Carcassonne à Tourouzelle. Encadrement à 50% avec Elie-Jean Debroas (IE, UMR 5563 LMTG).
— Krystel Tiberi, 2004. Cartographie des morphologies fluviales du Rio Napo (Equateur, Pérou). Encadrement à 50% avecJ-C. Soula (MC, UMR 5563 LMTG).
— Matthieu Mondou, 2003. Milieu de dépôt et provenance des sédiments du Poudingue de Palassou dans la région de Chalabre (Aude). Encadrement à 50% avec J-C. Soula (MC, UMR 5563 LMTG).

Licence 3

— Julien Cordenos, 2010. Granulométrie et reconstitution paléohydraulique des séries continentales du piémont nord-pyrénéen du Paléocène à l'Oligocène. Encadrement à 100%.
— Etienne Pont, 2009. Conditions de la mise en mouvement de la charge de fond dans 2 rivières en tresses de la façade pacifique des Andes du Pérou. Encadrement à 100%.

Autres

— DESUPS - Lionel Viguié, 2004. Etude sédimentologique et paléomorphologique des molasses Eocènes au front du massif de Mouthoumet (Aude). Encadrement à 100%.
— Thèse d'ingénieur de l'Université Centrale d'Equateur. Michel Rosero, 1999. El néogeno de la Cuence Oriente. Encadrement à 50% avec patrice Baby (DR, IRD).

1.2.5 Activités de recherche - Publications

Je suis sédimentologue et géomorphologue, spécialiste des systèmes fluviaux. Je mène mes recherches au sein de l'UMR 5563 Géosciences Environnement Toulouse au sein du Thème Interaction Lithosphère Océan Atmosphère (LOA).
Mes activités de recherche portent sur la compréhension des processus fluviaux, les facteurs qui les contrôlent à diverses échelles de temps, leur identification dans l'enregistrement stratigraphique et leur influence sur l'architecture stratigraphique des systèmes fluviaux préservés dans les bassins sédimentaires. Ces dernières années, j'ai étudié les processus fluviaux en contexte aggradant à diverses échelles de temps (du phénomène instantané au million d'années). Ces dernières années, ce questionnement s'est porté sur :

— A l'échelle de l'année : le développement des morphologies fluviales anastomosées en relation avec la morphologie des levées naturelles, la mise en place de deltas et de crevasse et leur évolution vers une anabranche.
— A l'échelle du siècle : l'étude de l'influence respective du climat, de la sédimentation et de la tectonique sur le réajustement du cours d'un cours d'eau dans un contexte de piémont orogénique actif soumis aux *extrema* climatiques liés à l'ENSO.
— A l'échelle du millier d'années : la localisation, la fréquence et les facteurs de contrôle des avulsions qui ont mené à la construction d'un mégafan et à la compréhension de la transition tresses/méandres dans le contexte de la fin de la dernière glaciation. Ceci a permis de préciser les mécanismes liant l'hydrologie et la croissance de la végétation sur la stabilisation des méandres.
— A l'échelle du millions d'années : la naissance et l'évolution des systèmes fluviaux distributaires sur les piémonts orogéniques et leur potentiel de préservation dans l'enregistrement stratigraphique en fonction du contexte géodynamique.

Publications	Total	1er ou 2 ^{ème} auteur	Co-auteur
Rang A	21	9	12
Chapitres d'ouvrages	6	2	4
Autres (Rang B, cartes etc..)	7	2	5

Table 1.4 – Publications scientifiques

	Toutes	Depuis 2010
citations	367	201
indice h	12	7
indice i10	13	6

TABLE 1.5 – Bibliométrie (source Google Scholar au 26/09/2015)

Rang A

1. (*sous presse*) Monod, B., Regard, V., Carcone, J., **Christophoul, F.** - Weathered post-orogenic paleosurfaces in Central Pyrenees and associated tectonics. *Comptes Rendus Géosciences*
2. (*en révision*) **Christophoul, F.**, Burgos, J., Roddaz, M.,Antoine, P-O., Bernal, C., Baby, P. - Onset and development of a Distributive Fluvial System : stratigraphic architecture and potential of preservation. *Geological Society of London Special Publications*
3. (*en révision*) Ford, M., Hemmer, L., Vacherat, A., **Christophoul, F.** - Retrowedge foreland evolution along the eastern ECORS profile. A tectono-sedimentary record of the eastern pyrenean orogenesis. *Journal of the Geological Society of London.*
4. (*soumis*) **Christophoul, F.**, Regard, V., Martinod, J., Darrozes, J. - Morphodynamics of the Upper Pleistocene Garonne River (SW france) : conditions of the Braiding/meandering transition. *Geomorphology.* Ms. Ref. No. : GEOMOR-4935
5. Carretier, S., Regard, V., Vassallo, R., Aguilar, G., Riquelme, R., Martinod, J., **Christophoul, F.**, Charrier, R., Farias, M., Gayer, E., Audin, L., Lagane, C. (2015). Differences in ^{10}Be concentrations between river sand, gravels and pebbles along the west side of the Central Andes. *Quaternary Geochronology*, 27 :33-51, doi :10.1016/j.quageo.2014.12.002
6. Carretier, S., Regard, V., Vassallo, R., Martinod, J., **Christophoul, F.**, Gayer, E., Audin, L., Lagane, C.(2015) A note on ^{10}Be-derived mean erosion rates in catchments with heterogeneous lithology : examples from the western Central Andes. *Earth Surface Processes and Landforms*, doi : 10.1002/esp.3748
7. Mouthereau, F., Vacherat, A., Pik, R., Lacombe, O., Fellin, M., Castelltort, S., **Christophoul, F.**, Masini, E., 2014. Placing limits to shortening evolution in the Pyrenees : role of margin architecture and implications for the Iberia/Europe convergence. *Tectonics*.doi : 10.1002/2014TC003663
8. Baby, P., Rivadeneira, M., Barragán, R., **Christophoul, F.**, 2013. Thick-skinned tectonics in the Oriente foreland basin of Ecuador. In Nemcock, M., (ed.), Thick-Skin-Dominated Orogens : From Initial Inversion to full accretion. *Geological Society of London Special Publications* 377, doi 10.1144/SP377.1.
9. Bernal, C., **Christophoul, F.**, Laraque, A., Bourrel, L., Soula, J-C., Guyot, J-L., Baby, P., 2013. Crevassing and capture by floodplain as a cause of avulsion and anastomosis (lower Rio Pastaza, Peru). *Journal of South American Earth Sciences.* doi 10.1016/j.jsames.2012.11.009 [*Citations :1*]
10. Nguyen A.T., Darrozes, J., Soula, J-C., Saillard, M., **Christophoul, F.**, Guerrero, N., Courjault-Radé, P., 2013. Slope Stability of Continental Megalandslide. *Landslide Science and Practice*, 5 : 305-313. doi 10.1007/978-3-642-31427-8_39
11. Bernal, C., **Christophoul, F.**, Soula, J-C., Darrozes, J., Bourrel, L., Laraque, A., Bes de Berc, S., Baby, P., Burgos, J., 2012. Gradual avulsions of the Rio Pastaza in the Ecuadorian piedmont of the Andes from 1906 to 2008 : role of tectonics, deposition and ENSO events. *International Journal of Earth Sciences.* 101 : 1913-1928. doi 10.1007/s00531012-07529. [*Citations :1*]
12. Roddaz, M., **Christophoul, F.**, Burgos Zambrano, J.D., Baby, P., 2012. Provenance of late Oligocene to quaternary sediments of the Ecuadorian Amazonian foreland basin as

inferred from major and trace element geochemistry and NdeSr isotopic composition. *Journal of South American Earth Sciences*, 37 : 136-153. doi :10.1016/j.jsames.2012.02.008. [*Citations :2*]

13. Bernal, C., **Christophoul, F.**, Darrozes, J., Soula, J-C., Baby, P., Burgos, J., 2011, Late Glacial and Holocene avulsions of the Rio Pastaza Megafan (Ecuador-Peru) : frequency and controlling factor, *International Journal of Earth Sciences*. 100 : 1759-1782. doi 10.1007/s00531-01005559. [*Citations :14*]
14. Laraque, A., Bernal C., Bourrel, L., Darrozes, J., **Christophoul, F.**, Armijos, E., Fraizy, P., Pombosa, R., Guyot, J-L., 2009, Sediment budget of the Napo river, Amazon Basin, Ecuador and Peru. *Hydrological Processes*, 23, 3509-3524. doi 10.1002/hyp.7463 [*Citations :18*]
15. Bès de Berc, S., Soula, J.-C., Baby, P., Souris, M., **Christophoul, F.**, Rosero, J., 2005, Geomorphic evidence of active deformation and uplift in a modern continental wedge-top - foredeep transition : example of the eastern Ecuadorian Andes, *Tectonophysics*, v. 399, no. 1-4, p. 351-380. doi 10.1016/j.tecto.2004.12.030. [*Citations :41*]
16. **Christophoul, F.**, Soula, J-C., Brusset, S., Elibana, B., Roddaz, M., Déramond, J., Bessière, G., 2003, Time, place and mode of propagation of foreland basin systems as recorded by the sedimentary infill : examples of the Late Cretaceous and Eocene retro-foreland basins of the north-eastern Pyrenees. In McCann, T and Saintot A. (eds) Tracing Tectonic Deformation Using the Sedimentary Record. *Geological Society of London Special Publication*, 208, 229-252. doi : 10.1144/GSL.SP.2003.208.01.11
17. Roddaz,M., Brusset,S., Soula,J-C., Béziat,D., Ben Abbou,M., Debat,P., Driouch,Y. **Christophoul, F.**, Ntarmouchant, A., Déramond, J., 2002. Foreland basin magmatism in the Western Moroccan Meseta and geodynamic inferences,*Tectonics*, 21, 7-1 - 7-23. doi : 10.1029/2001TC901029 [*Citations :14*]
18. **Christophoul, F.**, Baby, P., Soula, J-C., Rosero, M., Burgos, J., 2002, Les ensembles fluviatiles néogènes du bassin subandin d'Equateur et implications dynamiques. *Comptes Rendus Géosciences*, 399, 1-4, 1029-1037. doi 10.1016/S16310713(02)018254 [*Citations :17*]
19. **Christophoul, F.**, Baby, P., Dávila, C., 2002, Stratigraphic responses to a major tectonic event in a foreland basin : the Ecuadorian Oriente from Eocene to Oligocene times, *Tectonophysics*, v. 345, p. 281-298. doi 10.1016/S00401951(01)002177 [*Citations :48*]
20. Soula, J-C., Debat, P., Brusset, S., Bessière, G., **Christophoul, F.**, Déramond, J., 2001, Thrust-related, diapiric, and extensional doming in a frontal orogenic wedge : example of the Montagne Noire, Southern French Hercynian Belt, *Journal of Structural Geology*, v. 23, 11, p 1677-1699. doi 10.1016/S01918141(01)000219 [*Citations :33*]
21. Ben Abbou, M., Soula, J-C., Brusset, S., Roddaz, M., N'Tarmouchant, A., Driouch, Y., **Christophoul, F.**, Bouabdelli, M., Majesté, C., Béziat, D., Debat, P., Déramond, J., 2001, Contrôle tectonique de la sédimentation dans le système de bassins d'avant-pays de la Meseta marocaine.*Comptes Rendus de l'Académie de Sciences - Series IIa - Earth and Planetary Science*, 332 : 703-709.doi 10.1016/S12518050(01)015907

Chapitres d'ouvrages

1. **Christophoul, F.**, Burgos, J., Baby, P., 2014. Dinamica de la Cuenca de ante-pais oriental desde el Paleogeno. in P. Baby, M., Rivadeneira and R. Barragan (eds.) La Cuenca Oriente : Geología y Petroleo ($2^{\text{ème}}$ édition).
2. Roddaz, M., Hermoza, W., Mora, M., Baby, P., Parra, M., **Christophoul, F.**, Brusset, S. and Espurt, N., 2010, Cenozoic sedimentary evolution of the Amazonian foreland basin system, in C. Hoorn and F. Wesselingh (eds.), Amazonia, Landscape and Species Evolution : A Look into the Past, Wiley, p 61-88. doi 10.1002/9781444306408.ch5. [*Citations :25*]
3. Diaz, M., Baby, P., Rivadeneira, M., **Christophoul, F.**, 2004, El pre-Aptense dela Cuenca Oriente Ecuatoriana, in P. Baby, M., Rivadeneira and R. Barragan (eds.), La cuenca Oriente : Geologia y Petroleo. Travaux de l'Institut Français des Etudes Andines, V. 144, 23-45.

4. **Christophoul, F.**, Burgos, J., Baby, P., Soula, J-C., Bes de Berc, S., Davila, C., Rosero, M., Rivadeneira, M., 2004. Dinamica de la Cuenca de ante-pais oriental desde el Paleogeno. in P. Baby, M., Rivadeneira and R. Barragan (eds.), La cuenca Oriente : Geologia y Petroleo. Travaux de l'Institut Français des Etudes Andines, V. 144, 93-114.
5. Burgos, J., Baby, P., **Christophoul, F.**, Soula, J-C., Rochat, P., 2004. Cuantificacion de las erosiones terciarias en la parte sur de la Cuenca Oriente. El pre-Aptense dela Cuenca Oriente Ecuatoriana, in P. Baby, M., Rivadeneira and R. Barragan (eds.), La cuenca Oriente : Geologia y Petroleo. Travaux de l'Institut Français des Etudes Andines, V. 144, 115-130.
6. Bes de Berc, S., Baby, P., Rosero, J., Souris, M., Soula, J-C., **Christophoul, F.**, Vega, J., 2004. La superficie Mera-upano : marcador geomorfologico de la incision fluviatil y del levantamiento tectonico de la zona subandina, in P. Baby, M., Rivadeneira and R. Barragan (eds.), La Cuenca Oriente : Geología y Petroleo. Travaux de l'Institut Français des Etudes Andines, V. 144, 153-168.

Autres

1. Monod, B., de Saint Blanquat, M., Aretz, M., Bilotte, M., **Christophoul, F.**, Debroas, E-J., Denèle, Y., Faure, M., Laumonier, B., Lézin, C., Nardin, E., Olivier, P., Regard, V., 2014. GARVEMIP, carte géologique numérique de Midi-Pyrénées à 1/250 000. BRGM, Orléans.
2. **Christophoul, F.**, 1999. Discrimination des influences eustatiques et tectoniques dans les basssins associés à des zones de convergence : exemples du bassin subandin d'Equateur. Thèse de l'Université Toulouse III, Paul Sabatier, 282p.
3. Baby, P., Rivadeneira, M., Davila C., **Christophoul, F.**, 1999. La Cuenca Oriente : estilo tectonico, etapas de deformacion y caracteristicas geologicas principales de los principales campos de Petroproduccion. Petroproduccion/IRD, Quito, Equateur, 88p.
4. Davila, C., **Christophoul, F.**, 1999. Revision del model sedimentologico del Campo Cuyabeo-Sansahuari, informe previo a la simulacion matematica de calculo de réservas. Rapport interne IR-Petroproduccion, Quito - Equateur. 40p.
5. Baby, P., Bernal, C., **Christophoul, F.**, Valdez, A., 1998. Modelo estructural y ciclos tectono-sedimentarios en la Cuenca Oriente, version 1.0. Rapport interne IRD-Petroproduccion, Quito-Equateur, 77p.
6. **Christophoul, F.**, 1998. Geologia del pre-Aptense de la Cuenca oriental. Rapport interne IRD-Petroproduccion, 45p.
7. **Christophoul, F.**, Baby, P., Rivadeneira, M., Davila, C., 1998. Sintesis tectono-estratigrafica del ciclo Tiyuyacu-Orteguaza. Rapport interne IRD-Petroproduccion, 56p.
8. Rivadeneira, M., Baby, P., **Christophoul, F.**, 1998. Analisis de algunas formaciones cretacicas y terciarias del Subandino Norte y de la zona de Nuevo Rocafuerte sintesis geologica y nuevas ideas. Rapport interne IRD-Petroproduccion, 28p.

Communications

Communications	Total	1er ou 2 ^{ème} auteur	Co-auteur	Oral	Poster
Nationaux	17	8	9	5	12
Internationaux	34	19	15	14	20
Conférences invitées	2	2	/	2	/

Table 1.6 – Communications scientifiques

1. **Christophoul, F.**, 2015. Fluvial to Alluvial systems of the north-pyrenean foothill since Miocene : from DFS to contributive drainage. Alluvial Fans 2015, November 30th - December 4th, Christchruch, New Zealand.

2. **Christophoul, F.**, Regard, V., Martinod, J., Darrozes, J, 2015. morphodynamics of the Upper Pleistocene Garonne River (SW france) : conditions of the Braiding/meandering transition. 15$^{\text{ème}}$ Congrès de l'ASF, Chambéry, 10-13 Octobre 2015. (Poster)
3. Ngombi Mavoungou, L., Ford, M., **Christophoul, F.**, 2014. Evolution du rétro-prisme Nord Pyrénéen : études tectonique et stratigraphique le long d'une coupe NNE-SSO (bassins de Comminges ouest - Mirande). Réunion des Sciences de la Terre (RST), Pau, 27-31 Octobre 2014. (Poster)
4. Rougier, G., Ford, M., Bader, A-G., **Christophoul, F.**, 2014. Etudes sédimentologique et tectonique du Bassin Aquitain central : contraindre l'histoire de la subsidence et de la déformation d'un rétro-bassin d'avant-pays. Réunion des Sciences de la Terre (RST), Pau, 27-31 Octobre 2014. (Poster)
5. Hemmer, L., Ford, M., **Christophoul, F.**, 2014. Evolution tectono-sédimentaire du rétro-bassin d'avant pays aquitain le long du profil ECORS : réalisation d'une coupe équilibrée et études de la subsidence. Réunion des Sciences de la Terre (RST), Pau, 27-31 Octobre 2014. (Poster) .
6. Grool, A., Vergès, J., Ford, M., **Christophoul, F.**, 2014. Pro-versus retro-foreland evolution : A case study of the Eastern Pyrenees. Réunion des Sciences de la Terre (RST), Pau, 27-31 Octobre 2014. (Poster).
7. Ford, M., **Christophoul, F.**, Prevost, M., Vacherat, A., 2014. Amount, timing and kinematics of deformation along a section through in the retrowedge of the Eastern Pyrenees, inversion of a highly extended, salt-rich rift system. Réunion des Sciences de la Terre (RST), Pau, 27-31 Octobre 2014. (Poster).
8. **Christophoul, F.**, Ford, M., Grool, A., Rougier, G., Hemmer, L., Ngombi-Mavoungou, L., 2014. Evolution tectono-stratigraphique du bassin d'avant-pays nord-Pyrénéen. Réunion des Sciences de la Terre (RST), Pau, 27-31 Octobre 2014. (Poster).
9. Vacherat, A.,Mouthereau, F., Pik, R., Paquette, J-L., **Christophoul, F.**, Tibari, B., 2014. Relations sources - bassins au Nord des Pyrénées contraintes par thermochronologie détritique. Réunion des Sciences de la Terre (RST), Pau, 27-31 Octobre 2014. (Poster).
10. **Christophoul, F.**, Bonnet, S., Carretier, S., Regard, V., 2014. Evolution post-orogénique du piémont Nord-Pyrénéen. Réunion des Sciences de la Terre (RST), Pau, 27-31 Octobre 2014. (Poster).
11. Bonnet, S., Carretier, S., **Christophoul, F.**, Regard, V., 2014. Dynamique des réseaux hydrographiques et morphologie du piedmont nord-pyrénéen. Réunion des Sciences de la Terre (RST), Pau, 27-31 Octobre 2014.
12. Ford, M., Grool, A., **Christophoul, F.**, Saura, E., Vergès, J., 2014. The role of salt tectonics in the evolution of the northeastern Pyrenees. Réunion des Sciences de la Terre (RST), Pau, 27-31 Octobre 2014.
13. Carretier, S., Regard, V., Vassallo, R., Aguilar, G., Martinod, J., Riquelme, R., **Christophoul, F.**, Charrier, R., Gayer, E., Farías, M., Audin, L., Lagane, C., 2014. Grain size effect in ^{10}Be concentrations and derived erosion rates along the western side of the Central Andes. Réunion des Sciences de la Terre (RST), Pau, 27-31 Octobre 2014.
14. Cauuet, B., Oriol Olesti, M., Tamas, C., Boussicault, M., **Christophoul, F.**, Garcia Pulido, J-L., 2014.New reasearch approach for identifying the mining landscapes : the exploration of Au alluvial deposits in Cerdagne and Sn in Morvan. VIII Congreso Internacional sobre mineria y metalurgia historicas en el sudoeste de Europa, Granada, Spain, 11-14 June 2014. (Oral)
15. Bernal, C., **Christophoul, F.**, Darrozes J., Laraque, A. , 2013. Channel Pattern variability along the Pastaza River (Ecuador and Northern Peru), 8 $^{\text{th}}$ International Conference on Geomorphology, Paris, France, 27-30 August 2013. (Poster)

16. **Christophoul, F.**, 2013. Structuration du Piémont nord-pyrénéen entre le miocène et le quaternaire : morphologie et topographie. 14 ème Congrès de l'ASF, Paris, Cité des sciences, 5-7 Novembre 2013. (poster).
17. **Christophoul, F.**, Regard, V., Darrozes, J., Martinod. J., 2013. Evolution du style fluvial de la Garonne lors du dépôt de la dernière terrasse. 14ème Congrès de l'ASF, Paris, Cité des sciences, 5-7 Novembre 2013. (oral).
18. **Christophoul, F.**, Regard, V., Darrozes, J., Martinod. J., 2013. Changes of fluvial styles of the Garonne (southwest of France) contemporary to the formation of its youngest terrace. 10th International Conference of Fluvial Sedimentology, 14-19 July 2013, Leeds, UK. (Poster).
19. **Christophoul, F.**. The post-foreland fluvial systems of the north-pyrenean foothill (Aquitaine Basin, France). 10 th International Conference of Fluvial Sedimentology, 14-19 July 2013, Leeds, UK. (Oral).
20. **Christophoul, F.**, Bernal C., 2012. Sediment volumes preserved in megafans : insight of a morphologic approach. Alluvial Fans 2012, Ras al Khaima, UAE, December 1-6th 2012. (Oral).
21. **Christophoul, F.**, 2012. Context of alluvial placers of the north eastern pyrenees (Cerdagne basin and Roussillon plain, France). Alluvial Fans 2012, Ras al Khaima, UAE, December 1-6th 2012. (Oral).
22. Bernal, C., **Christophoul, F.**, Darrozes, J., Laraque A., Bourrel, L., Guyot, J-L., Baby, P., 2011. Crevassing and capture by floodplain as a cause of avulsion and anastomosis (lower Pastaza, Peru). 4th Hybam Scientific Meeting, September 4-6th 2011, Lima-Peru. (Oral).
23. Baby, P., Roddaz, M., Brusset, S., Louterbach, M., Eude, A., Calderon, Y., Hermoza, W., Darrozes, J., **Christophoul, F.**, Soula, J-C., Guyot, J-L., Bolaños, R., 2011. Tectonic control on sédiment budget in western amazonia. 4th Hybam Scientific Meeting, September 4-6th 2011, Lima-Peru. (Oral).
24. Grimaud, J-L., Chardon, D., Beauvais, A.,**Christophoul, F.**, 2011. Cenozoic drainage evolution of West Africa : Spatial and temporal constraints from the lateritic record. Geophysical Research Abstracts Vol. 13, EGU2011-4308-3, 2011 EGU General Assembly 2011
25. **Christophoul, F.**, Bernal, C., Darrozes, J., Soula, J-C., Burgos, J.D., 2008. Progressive avulsion of the rio Pastaza as a response to topographic uplift and backtilt of the Ecuadorian Subandean Zone. 7th International Symposium on andean Geodynamics (ISAG 2008, Nice), extended abstracts, 140-143. (Poster).
26. Maisonnave, C., **Christophoul, F.**, Soula, J-C., 2008. Downstream paleofluvial morphology changes in a compressive foothill : case from the Eocene molasses of the north pyrenean foreland basin. SRef-ID : 1607-7962/gra/EGU2008-A-10770. (Poster).
27. Roddaz, M., **Christophoul, F.**, Soula, J-C., Burgos, J.D., Baby, P., Déramond, J., 2008. Subduction control on chemical composition of oligocene to Quaternary sediments of Ecuadorian Amazonian foreland basin from major and trace elements and Nd-Sr isotopes. 7th International Symposium on andean Geodynamics (ISAG 2008, Nice), extended abstracts, 454-457. (Oral).
28. Vassallo R., Pépin, E., Regard, V., Guyot, J-L., Carretier, S., Gayer, E., Audin, L., **Christophoul, F.**, Riquelme, R., Ordonez, J.J., Caceres, F.E., 2008. Climatic impact on the erosive dynamics of Pacific Central Andes revealed by cosmogenic and hydrological records of river sediments, 7th International Symposium on andean Geodynamics (ISAG 2008, Nice). (Poster).
29. Vassallo R., Pépin, E., Regard, V., Carretier, S., Gayer, E., Audin, L., **Christophoul, F.**, Riquelme, R., Guyot, J-L., Ordonez, J.J., 2008. Historical and millennial geomorphic evolution of Pacific Central Andes : coupling hydrological and cosmogenic records, European Geosciences Union, Vienna, Poster EGU2008-A-06914. (Poster).

30. Bourrel L., Darrozes J. , Guyot J.L., **Christophoul, F.**, Bondoux F., Mailler S., DeGenot V., 2007. Correlation between river slope and meandering variability (obtained by DGPS data) and morphotectonics for two Andean tributaries of the Amazon river : the case of Beni (Bolivia) and Napo (Ecuador-Peru) rivers. AGU Fall meeting, San Francisco, USA. (Poster).
31. **Christophoul, F.**, Soula, J.C., Bourrel, L., Bernal, C., Darrozes, J., 2007. Controlling factors of avulsion in an intertropical fluvial megafan (Pastaza megafan, Ecuador-Peru). Alluvial fans 2007, June 18-22, 2007, Banff, Canada. (Oral).
32. **Christophoul, F.**, Soula, J-C., Brusset, S., Viguier, L., Sutra, A., 2005. Response of hydrographic network to foreland basin development : case from the Eocene Molasses of the North Pyrenean Foreland Basin. 5th International Congress of Fluvial Sedimentology, August 9-11, Delft, the Netherlands). (Oral).
33. **Christophoul, F.**, Seyler, F., Fraizy, P., Calmant, S., Frappart, F., Filizola, N., 2005. Upstream accretion of mid-channel sandy Islands (Rio, Branco, Roraima State, Brazil). 5th International Congress of Fluvial Sedimentology, August 9-11, Delft, the Netherlands). (Oral).
34. Burgos, J.D., **Christophoul, F.**, Baby, P., Antoine, P.O., Soula, J-C., Good, D., Rivadeneira, M., 2005. Dynamic evolution of Oligocene - Neogene sedimentary series in a retro-foreland basin setting : Oriente Basin, Ecuador. 6th International Symposium of Andean Geodynamics (ISAG 2005, Barcelona), extended abstracts, 127-130. (Poster).
35. Burgos, J.D., **Christophoul, F.**, Soula, J-C., Baby, P., Bes de Berc, S., Rivadeneira, M., 2003. Alluvial Fan development in fothill context : Example of the Ecuadorian Subandean basin., 23rd Meeting of the International Association of Sedimentology, September 15-17th, Coimbra, Portugal. (Poster).
36. Baby, P. ; Gil, W. ; Hermoza, W. ; Roddaz, M. ; Bès de Berc, S. ; Brusset, S. ; Christophoul, F. ; Soula, J.-C. ; **Christophoul, F.**, 2003. North-south evolution of the subandean deformation from Bolivia to Ecuador : climatic or paleogeographic control ? EGS - AGU - EUG Joint Assembly, Nice, France, 6 - 11 April 2003, abstract 6266. (Poster).
37. **Christophoul, F.**, Soula, J-C., Brusset S., Déramond, J., 2003. Réponse d'un système fluviatile à la mise en place d'un anticlinal de propagation de chevauchement. 9ème Congrès de l'ASF, Bordeaux. (Oral).
38. **Christophoul, F.**, Burgos, J.D., Bes de Berc, S., Soula, J-C., Baby, P., 2003. Fluvial styles and drainage pattern of successive alluvial fans in the Ecuadorian Subandean Basin. 3rd Latin American Congress of Sedimentology, Belém, Brésil, 8-11 juin 2003. (Poster).
39. **Christophoul, F.**, Baby, P., Soula, J-C., Rosero, M., 2002. Contrôle du drainage par la surrection dans un contexte de de raccourcissement faible : exemple du Basin Subandin d'Equateur au Néogène., RST 2002 session E1, Nantes, France. 2p. (Oral).
40. Hermoza W., Baby P., Brusset S., **Christophoul, F.**, Gil W., 2002. Foreland basin system dynamics evolution of the peruvian Andes : new insights from mass balance computation, 5th ISAG, Toulouse, 2002. 5th Internati onal Symposium on andean Geodynamics (ISAG 2002, Toulouse), extended abstracts. (Poster).
41. **Christophoul, F.**, Baby, P., Alluvial to fluvial sediments as witenesses of structural events in the neogene of the Ecuadorian Subandean Basin. 4th International Congress of Fluvial Sedimentology, University of Nebraska, Lincoln, USA. (Poster).
42. **Christophoul, F.**, Soula, J-C., Elibana, B., Brusset, S., Déramond, J., 2001. Geometry and Timing of Cretaceous to Eocene Compresional Structures on the Northern Flank of the Eastern Pyrenées. EGU XI, April 8-12 2001, Strasbourg, OS04 : SUpm37 : G8. (Oral).
43. Baby, P., Rivadeneira, M., Barragan, R., **Christophoul, F.**, Bès de Berc, S., Deniaud, Y., Vega, J., Davila, C., Bernal, C., Diaz, M., Galarraga, M., Leon, E., Rosero, J., Rosero, M., Valdez, A ., 2001. Estructura y dinamica sedimentaria de la Cuenca Oriente. Jornadas de Ciencias de la Tierra. Escuela Politecnica Nacional, Quito, Equateur. (Oral).

44. **Christophoul, F.**, Baby, P., Déramond., J., 2000. Modification des signaux stratigraphiques d'origine tectonique à l'ordre 2 : à l'échelle locale et à l'échelle du bassin d'avant-pays. 18ème RST, 27-31 Avril 2000. Cité des Sciences et Technique, Paris. (Oral).
45. **Christophoul, F.**, Davila, C., Baby, P., Rivadeneira M., 1999. Descriminitaion of Eustatic and tecton influences in the ecuadorian Oriente Basin from Aptian to Oligocene Times. 4th International Symposium on Andean Geodynamics (4th ISAG 1999, Göttingen 4-6/10/99). (Poster).
46. Baby, P., Rivadeneira, M., **Christophoul, F.**, Barragán, R., 1999. Style and timing of deformation in the Oriente of Ecuador. 4th International Symposium on Andean Geodynamics (4th ISAG 1999, Göttingen 4-6/10/99). (Poster).
47. Baby, P., Guyot, J-L., Deniaud, Y., Zubieta, D., **Christophoul, F.**, Rivadeneira, M., Jara, F., 2000. The High Amazon basin : tectonic control and mass balance. Manaus 99', Hydrological and geochemical Processes in Large Scale River Basins. Manaus, Brésil. (Oral).
48. Baby, P., Gil Rodriguez, W., **Christophoul, F.**, Barragan, R., Bernal, C., 1999. Structural style and timing of hydrocarbon entrapment in the Oriente-Marañon foreland basin. INGEPET 1999, Lima, Pérou. (Oral).
49. Tambareau, Y., Hottinger, L., Crochet, B., **Christophoul, F.**, 1999. Shallow benthic foraminifera at the Cretaceous/Tertiary passage, western end of the Petites Pyrénées, southern France. IGCP 393 4th Meeting, University of the West Indies, Kingston, July 12-17 1999. (Poster).
50. Perret-Mirouse, M-F., **Christophoul, F.**, Vachard, D., Bessière, G., Brusset, S., Déramond, J., Guerrero, N., Sanz, J., 1999. The tectono-sedimentary evolution around the western meditterranean during Carboniferous. IGCP 421 meeting / subcommission on carboniferous stratigraphie, Errachidia, Maroc. (Poster).
51. Baby, P., Rivadeneira, M., Bernal, C., **Christophoul, F.**, Dávila, C., Galárraga, M., Marocco, R., Valdez, A., Vega, J., Barragán R., 1998. Structural Style and Timing of Hydrocarbon Entrapments in the Ecuadorian Oriente Basin. ABGP/AAPG International Conference and Exhibition November 8-11, 1998, Rio de Janeiro, Brazil. 82 (10),1 889. (Poster).

Conférences invitées

1. Ajustements morphologiques d'un cours d'eau en réponse aux forçages climatiques (la Garonne à la fin de la dernière glaciation), 2014, *Centre de Recherches Pétrographiques et Géochimiques, Nancy.*
2. Evolution du Bassin d'avant-pays Nord-Pyrénéen entre le Crétacé supérieur et l'Eocène (Corbières, Est du Bassin Aquitain), 2012, *Laboratoire des Fluides Complexes - Réservoirs, Pau.*

1.2.6 Projets et programmes scientifiques

— Depuis 2015 - OROGEN, projet TOTAL-BRGM-INSU, co-encradrement de thèses et post-doc. Collaboration, M. Ford (ENSG), H. Sinclair (Univ. Edimbourg).
— 2012-2016 - ANR (blanc) Minemet (PI : B. Cauuet, UMR TRACE, UT2), coordonnateur partenaire. Au sein de ce projet, je suis chargé d'établir le contexte géomorphologique et sédimentologique de placers alluviaux aurifères (Cerdagne et Roussillon) et stannifère (Morvan).
— 2012- 2016 -ANR (blanc) Pyramid (PI : Pr. M. Ford, ENSG, Nancy), coordonnateur partenaire. Porteur de sous-tâche. Dans le projet Pyramid, je suis impliqué dans différentes tâches. Je suis notamment chargé de construire l'architecture 3D du remplissage synorogénique du bassin d'avant-pays nord-pyrénéen. Je pilote une sous-tâche qui a pour but de comprendre les paramètres influent sur la dynamique post-orogénique du piémont post-foreland.
— 2008-2012 - Interreg SUDOE DO-SMS (PI : J. Darrozes, UMR LMTG Toulouse), participant.

— 2007-2011 - ANR (JC) Andes (PI : S. Carretier, UMR LMTG, Toulouse), participant. Au sein de ce projet, j'ai étudié la morphologie des rivières de la façade Pacifique du Pérou afin de mettre au point les stratégies d'échantillonnage pour les analyses ^{10}Be.
— 2003 - BQR (UFR SVT, Univ. Toulouse 3, Paul Sabatier), Co-PI avec Pr. J. Martinod (UMR LMTG).
— 1999 - 2002 - INSU PNSE (PI : P. Baby et J-L. Guyot IRD), participant.

1.2.7 Animations scientifiques

— 2015-2017 - Membre du comité d'organisation de 36$^{\text{th}}$ annual meeting de l'International Association of Sedimentologists et 16$^{\text{ème}}$ Congrès Français de Sédimentologie (IMS 2017), Toulouse, 10-12 Octobre 2017.
— 2014- Co-Porteur de la session Pyrénées, Réunion des sciences de la Terre (RST), Pau, 27-31 Octobre 2014.
— 2014 - Membre du comité scientifique de la Réunion des sciences de la Terre, Pau, 27-31 Octobre 2014.

1.2.8 Evaluation, expertise scientifique et activité éditoriale

— 2014 - Evaluateur de projets pour l'ANR AAP Générique.
— 2014 - Evaluateur de pré-projets pour l'ANR AAP Générique.
— 2013 - Expertise de dossiers de candidatures pour le programme de mobilité post-doctorale « Fernand BRAUDEL-IFER de la Fondation Maison des Sciences de l'Homme.
— Depuis 2013 - Membre du jury de l'appel d'offre « Innovation Pédagogique en Licence » et "Masters pluridisciplinaires" de l'DEX de Toulouse.
— 2012 - Evaluation de demande de financement de projets de recherche pour un appel d'offre de l'OSUG (Grenoble).
— 2008-2012 - Evaluation Biennale et quadriennale de l'activité des chercheurs dans le cadre du CoNRS section 18.
— 2010 - Evaluation de demandes de financements dans le cadre de l'accompagnement des campagnes à la mer (INSU-OA).

Reviews régulières pour le :
— *Journal of South American Earth Sciences,*
— *Journal of the Geological Society of London,*
— *International Journal of Earth Sciences (ex-Geologische Rundschau),*
— *Geomorphology,*
— *Comptes-Rendus Géosciences,*
— *Bulletin de la Société Géologique de France.*

1.2.9 Tâches et responsabilités d'intérêt collectif

Responsabilités pédagogiques
— Depuis 2014 - Membre du jury du concours d'entrée dans les écoles d'ingénieur "Géosciences Eau Environnement" (G2E), interrogateur pour les épreuves orales de géologie pratique.
— Depuis 2013 - Référent adjoint du champ disciplinaire « Sciences de la Terre et Environnements » du collège Biologie et Géosciences de l'Université Toulouse 3, Paul Sabatier.
— Depuis 2007 - Responsable de l'UE « Ressources Naturelles, risques et Environnement » de 1ère année de Master BGSTU (UE supprimée dans le cadre de l'accréditation du Master MEEF depuis la rentrée 2013).
— Depuis 2007 - Responsable de l'UE « Géologie sédimentaire et Camps de terrain » 3$^{\text{ème}}$ année de Licence « Réorientation en Sciences de la Terre et Environnement » (L3 RéoSTE).
— 2004 - 2008 - Responsable pédagogique de la L3 RéoSTE.
— 2004 - 2008 - Coordonnateur des échanges ERASMUS pour les Sciences de la terre et de l'Environnement.

— 2003 - 2007 - Responsable de l'UE « Pétrographie » de 1ère année de Licence mention Science Terre (L1 ST).

Responsabilités nationales
— 2008-2012 - Membre élu du Comité National de la Recherche Scientifique, collège B2, section 18.
— 2011-2012 - Membre nommé du jury d'admissibilité pour l'attribution de la Prime d'Excellence Scientifique en section 18 du CNRS.

Responsabilités locales
— Depuis 2012 - Membre de la commission communication de l'UMR 5563 GET.
— Depuis 2012 - Rédacteur de la lettre d'information (the diGEsT) de l'UMR 5563 GET.
— Depuis 2012 - Membre élu du Conseil des Etudes et de la Vie Universitaire (CEVU) de l'Univ. Toulouse 3, Paul Sabatier.
— 2012 - Membre de Comité de sélection MCU-Chaire CNRS à l'Université de Pau et des Pays de l'Adour.
— 2009 - Membre de comité de sélection MCU, Univ. de Chambéry.
— 2009 - Membre de jury de recrutement d'Assistant Ingénieur, Univ. de Pau et des Pays de l'Adour.
— 2006 - 2008 - Membre élu de la CSE 36 de l'Univ. Toulouse 3, Paul Sabatier.
— 2006 - 2008 - Membre suppléant nommé de la CSE 35-36 de l'Univ. de Pau et des Pays de l'Adour.
— 2003 - 2011 - Membre élu du Conseil de l'UFR des Sciences de la Vies et de la Terre de l'Univ. Toulouse 3, Paul Sabatier.

1.2.10 Formation continue et diffusion des connaissances

— Décembre 2012 - Article : "une collection paléobotanique inconnue : la collection Pierre Vetter et le Musée Régional de Géologie de Decazeville (Aveyron)" dans le bulletin du Groupe Français du Paléozoïque.
— Octobre 2012 - Sortie de terrain "les métamorphoses de la Garonne" dans le cadre de Novela, le festival de tous les savoirs (Org. Mairie de Toulouse) organisée par V. Regard et S. Bonnet.
— 2012 - "Quelles ressources naturelles pour demain ? Hydrocarbures conventionnels et non-conventionnels". Conférence / Débat de l'association "Débattonzen", Toulouse, 12 Mars 2012.
— 2009 - Conférence. "Henri Fayol et la Théorie des Deltas : un pionnier de la sédimentologie continentale et expérimentale". Musée Régional de Géologie Pierre Vetter, Decazeville.
— 2008 - 2010 - Formation continue des enseignants du second degré : Stage "Géologie de la Région Toulousaine" (F. Christophoul et P-O. Antoine).
— 2001 - Sortie de terrain. "Environnements de dépôts continentaux du Bassin Stéphanien de Decazeville". Association des Professeurs de Biologie-Géologie de la Marne (APBG 51).
— 2001 - Conférence. "Pierre Vetter et la Géologie du Stéphanien du Massif Central". 25 ans du Musée Vetter. Musée Régional de Géologie Pierre Vetter, Decazeville.

Chapitre 2

Bilan d'Activités et Projet de Recherches

2.1 Bilan d'activités de recherches

2.1.1 Résumé

Mes activités de recherche portent sur la compréhension des processus fluviaux, les facteurs qui les contrôlent à diverses échelles de temps, leur identification dans l'enregistrement sédimentaire et leur influence sur l'architecture stratigraphique des systèmes continentaux préservés dans les bassins sédimentaires.

Ces dernières années, j'ai étudié les processus fluviaux en régime de préservation à diverses échelles de temps (du phénomène instantané au million d'années). A partir d'une approche en termes de sédimentologie de faciès, d'architecture stratigraphique de cartographie des réseaux fluviaux et de bases de données géographiques, mes recherches ont porté successivement sur :

- A l'échelle de la dizaine d'années : le développement des morphologies fluviales anastomosées en relation avec la morphologie des levées naturelles, la mise en place de deltas et de crevasse et leur évolution vers une anabranche.
- A l'échelle du siècle : l'étude de l'influence respective du climat, de la sédimentation et de la tectonique sur le réajustement du cours d'un cours d'eau en contexte de piémont orogénique soumis aux *extrema* climatiques liés à ENSO. Plus spécifiquement :
  - la localisation, la fréquence et les facteurs de contrôle des avulsions qui ont mené à la construction d'un mégafan andin depuis le Dernier Maximum Glaciaire.
  - La mise en évidence de la chronologie des cycles incision/aggradation sur les terrasses alluviales de la Garonne, précisant ainsi le rôle des interactions hydrologie/végétation.
- A l'échelle du million d'années : l'étude de l'architecture stratigraphique du piémont des Andes d'Equateur depuis le Miocène en lien avec la mise en place d'un "Distributive Fluvial System" (DFS).

Ces travaux permettent de contraindre l'expression faciologique des forçages tectoniques, climatiques ainsi que le fonctionnement autocyclique dans les séries fluviales. Les résultats acquis trouvent des applications dans la structuration des réservoirs et l'aménagement des plaines alluviales.

2.1.2 Contexte

Suite à une thèse consacrée au relations tectonique/sédimentation dans le bassin rétroarc des Andes équatorienne (Christophoul, 1999), j'ai été recruté en 2002 sur un poste de "sédimentologie continentale". J'ai débuté ma carrière par des études sur des systèmes anciens (Christophoul et al., 2002a,b, 2003; Diaz et al., 2004; Christophoul et al., 2004). J'ai successivement mené mes recherches au sein de l'équipe Géodynamique de l'UMR 5563 Laboratoire des Mécansimes de Transfert en Géologie (LMTG) et au sein des thèmes Couplages Lithosphère Océan Atmosphère (LOA) à l'UMR 5563 Géosciences Environnement Toulouse (GET).

A partir de 2005, afin d'affiner les interprétations basées les observables dans l'enregistrement sédimentaire anciens à partir d'exemples actuels, j'ai entamé une conversion thématique vers la géomorphpologie fluviale. Cette conversion fut l'occasion de collaborer avec les hydrologues de l'ORE HyBam (Observatoire de Recherche en Environnement IRD/INSU rattaché à l'UMR 5563 GET). Cette collaboration s'est concrétisée par le co-encadrement d'une thèse (Carolina Bernal, financement Union Européenne, soutenue en 2009). A cette occasion, j'ai été amené à m'intéresser à des objets récents et à des phénomènes actuels (Laraque et al. (2009); Bernal et al. (2011, 2012, 2013).

A l'heure actuelle, je poursuis mes recherche :

- dans le domaine de la sédimentologie et des relations tectonique / sédimentation fluviale dans l'ancien.
- et en géomorphologie fluviale, à la fois sur des objets subactuels (Mégafans amazoniens, Terrasses de la Garonne) que sur les processus fluviaux (transition tresse/méandres) avec une volonté de changement d'échelle spatiale. En effet après m'être intéressé aux phénomènes à échelle locale (avulsions, mise en place et développement d'un "Distributive Fluvial System"), je souhaite développer mes recherche dans la compréhension de la distribution de ces objets

à l'échelle d'un piémont orogénique en liaison avec la subsidence à court et long terme dans les bassins sédimentaires où ils sont documentés.

Mon implication actuelle dans le Projet ANR Pyramid (PI : M. Ford, ENSG/CRPG Nancy) est l'occasion d'orienter mes recherches sur les séries synorogéniques marines ou fluviatiles du remplissage du bassin d'avant-pays nord-pyrénéen. Ces travaux me permettent également de valoriser mon expérience en géomorphologie fluviale afin de comprendre les processus qui contrôlent le fonctionnement d'un piémont post-orogénique avec le piémont post-foreland nord-pyrénéen.

Mon profil mixte Sédimentologue / Géomorphologue est atypique en France où les communautés de la sédimentologie et de la géographie physique sont séparées. Il est en revanche tout à fait dans le ligne des pratiques anglo-saxonnes où les chercheurs impliqués dans la compréhension des processus fluviaux dans l'ancien et l'actuel relève de la même communauté (faite de sédimentologues, géomorphologues, hydrauliciens et spécialistes de l'aménagement des cours d'eau).

2.1.3 Problématique Générale

Durant les dernières années, mes activités de recherches ont eu pour but d'améliorer la connaissance des forçages internes et externes contrôlant la dynamique des systèmes fluviaux. Dans les bassins sédimentaires, les séries fluviatiles constituent une part importante du remplissage, quel que soit le contexte tectonique du bassin sédimentaire considéré. Dans les rifts, les séries fluviales se rencontrent essentiellement durant le stade syn-rift (Einsele, 1992; Miall, 1996) alors que dans les bassins en compression (bassin d'avant-pays), les séries fluviales sont caractéristiques du stade tardif suralimenté et correspondent aux séries "molassiques" (Homewood et al., 1986; Sinclair, 1997).

Ces séries, quel que soit le contexte tectonique, se déposent en régime d'aggradation fluviale. Dans ce contexte, un cours d'eau va s'écouler sur ses propres sédiments et surélever son lit en réponse à la subsidence du bassin et/ou au forts apports en sédiments depuis l'amont. La surélévation du lit génère des rides alluviales instables, car montrant un gradient de pente latéral (vers la plaine d'inondation) parfois supérieur à leur gradient longitudinal, qui peuvent amener au déplacement brusque (de quelques heures à quelques jours) d'un cours d'eau abandonnant totalement ou partiellement son cours précédent ou "avulsion" (Jones and Schumm, 1999; Slingerland and Smith, 2004) (Fig.2.1).

Afin de combler l'espace disponible lié à la subsidence créée dans les bassins sédimentaires, l'aggradation des cours d'eau n'est pas suffisante et implique le déplacement du cours d'eau au cours du temps de manière à distribuer les sédiments de façon homogène dans la zone soumise à la subsidence. Ces déplacements peuvent se faire par déplacement graduel des rides alluviales (déplacement de barres de méandres par exemple), mais aussi, et plus efficacement, par avulsions successives. Ces avulsions sont le résultat cyclicités propre au fonctionnement du système fluvial et alluvial (Schumm et al., 1987; Pépin et al., 2010) mais aussi de forçages climatiques et tectonique.

A des échelles de temps plus courtes ($10^4/10^5$ ans), l'aggradation du lit d'un cours d'eau peut se produire dans le cadre de cycles de courte durée tels que le cycles glaciaires où l'aggradation sera limitée à la vallée incisée créée lors des incisions interglaciaires.

La compréhension des phénomènes d'avulsion, des paramètres qui les contrôlent et leur identification dans l'enregistrement sédimentaire sont un enjeu important du point de vue académique, afin d'améliorer le déchiffrage et la façon d'interpréter les archives sédimentaires dans les séries fluviales. D'un point de vue appliqué, la compréhension des avulsions, leur identification dans l'enregistrement stratigraphique sont d'un grand intérêt dans la compréhension de la structuration des réservoirs. L'étude et la compréhension des avulsions modernes et récentes ont une importance capitale dans la gestion des grandes plaines alluviales soumises à une forte pression anthropique.

Dans ce contexte général, je me suis attaché à comprendre les facteurs contrôlant l'aggradation fluviale du bassin d'avant-pays rétro-arc des Andes sur leur versant amazonien. Si les forçages externes s'expriment dans les séries aggradantes, ils s'expriment aussi sous la forme de changement morphologiques se produisant lors des périodes pléniglaciaires du Quaternaire. Afin d'extraire les paramètres contrôlant l'aggradation liée aux cycles glaciation / déglaciation rapides caractéristiques du Quaternaire, j'ai ensuite étudié la Garonne lors de la dernière déglaciation sur le piémont post-orogénique septentrional des Pyrénées.

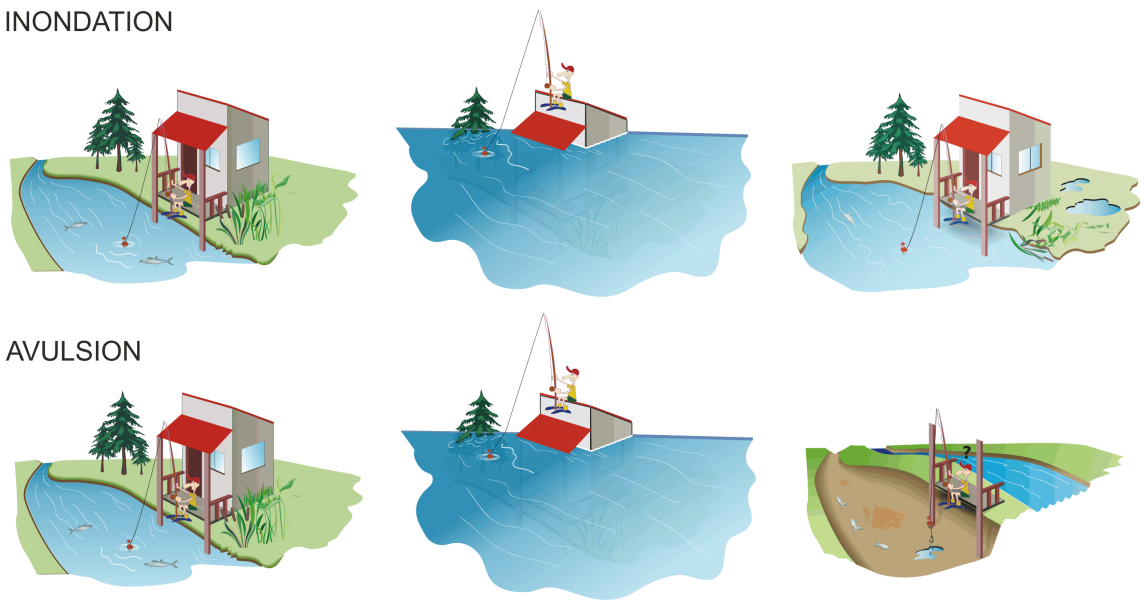

FIGURE 2.1 – Schéma montrant les différences entre une inondation et une avulsion. Suite à une inondation, le cours d'eau regagne son lit. Dans le cas d'une avulsion, il occupe un nouveau lit dans l'ancienne plaine d'inondation. Lors de l'avulsion décrite ici, le déclencheur de l'avulsion est une crue. D'autres phénomènes peuvent déclencher une avulsion (voir texte). Dessin C. Cavaré-Hester.

2.1.4 Contrôle des phénomènes d'avulsion

la Fig. 2.1 illustre la différence entre une inondation et une avulsion. Les causes d'avulsion sont très variées (Jones and Schumm, 1999; Stouthamer and Berendsen, 2000; Makaske, 2001). Cependant, ces causes peuvent être divisées en deux catégories, suivant qu'elles impliquent des processus à court (de l'échelle de l'heure à la journée) ou plus long terme (de l'échelle de l'année jusqu'à 10^4 ans). C'est la différence que font Jones and Schumm (1999) entre :

— "Setup" (contexte) : il met en jeu des processus qui contribuent à augmenter le rapport entre le pente en long du cours d'eau existant (Se) et la pente du futur chenal après avulsion (Sa). L'augmentation du rapport Se/Sa peut se faire soit par une diminution de Se ou une augmentation de Sa. Parmi ces processus conduisant à une diminution de Se, on trouve : l'augmentation de la sinuosité (rivières à méandres), l'augmentation de la longueur des drains (cas de cours d'eau alimentant un delta), le soulèvement tectonique (de la partie aval). Les processus induisant une augmentation de Sa peuvent être : l'aggradation des levées naturelles, l'aggradation d'un cône alluvial ou d'un delta (augmentation de la convexité du profil en long des curs d'eau), basculement tectonique latéral (Leeder and Alexander, 1987; Leeder and Jackson, 1993; Schumm et al., 2000). Tout ces processus vont mener le cours d'eau dans un équilibre instable et l'avulsion sera déclenchée par :

— "Trigger" (déclencheur) : une crue (déclencheur le plus courant, Fig. 2.1), l'augmentation du taux de sédimentation dans le chenal, la mise en place de barrages naturel (végétation, glace, rupture de surface d'une faille active, croissance d'un anticlinal). (Törnqvist, 1994; Stouthamer and Berendsen, 2000; Holbrook et al., 2006).

Il résulte du contexte et du déclencheur, l'ouverture d'un chenal dans les berges. Il s'agit d'un chenal de crevasse menant à une avulsion qui sera totale (abandon du chenal préexistant) ou partielle (avec la mise en place d'une anabranche Fig. 2.4). Les facteurs contrôlant l'avulsion totale ou partielle ont été modélisés par Slingerland and Smith (2004). Ces auteurs mettent en évidence le rôle de profondeur du chenal de crevasse et son élévation par rapport à la plaine d'inondation comme facteur discriminant d'une avulsion totale ou partielle. En pratique, le chenal de crevasse doit atteindre une profondeur suffisante pour garantir un débit suffisant lors de la chute de la crue ayant déclenché l'avulsion. Si le chenal de crevasse est assez profond, la contrainte cisaillante basale

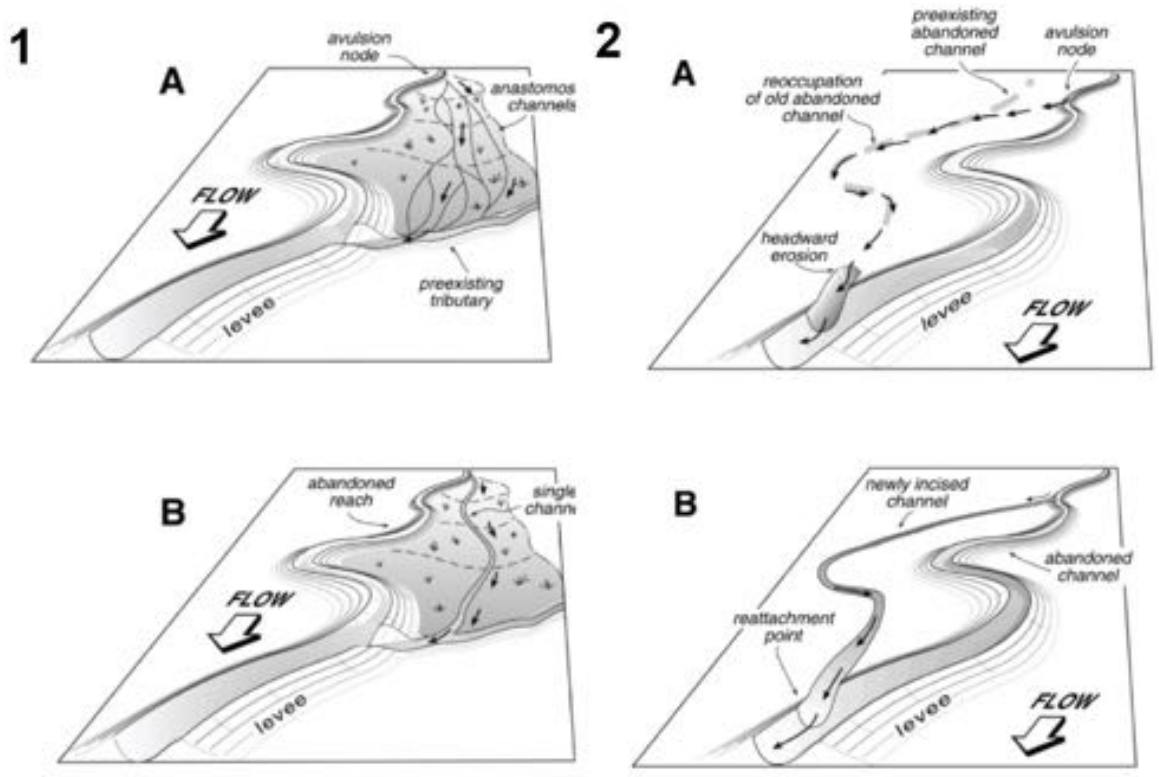

FIGURE 2.2 – Modèles d'avulsions par aggradation et incision
(Mohrig et al., 2000) 1 : modèle d'avulsion par aggradation. A : début de l'avulsion, le cours d'eau parent a abandonné un tronçon de son cours et s'écoule dans la plaine d'inondation. B : Plus tard, les chenaux en tresses du delta de crevasse ou crevasse splay se réunissent en un seul cours d'eau qui érode localement les dépôts du crevasse splay. L'avulsion est terminée. 2 : Modèle d'avulsion par incision. A : début de l'avulsion, le cours d'eau parent a abandonné un tronçon de son cours et s'écoule dans la plaine d'inondation où il annexe un cours précédemment abandonné. L'incision se fait par érosion régressive depuis le point de jonction avec le cours d'eau parent ("reattachment point" sur Fig. 2B). B : Stade terminal, le chenal est complètement incisé dans la plaine d'inondation.

("shear stress") parviendra à maintenir une érosion suffisante pour entretenir une anabranche. Un autre facteur contrôlant le type d'avulsion est le drainage de la plaine d'inondation . A partir d'exemples anciens, Mohrig et al. (2000) a proposé deux types d'avulsions liés aux caractéristiques de la plaine d'inondation, "bien" et "mal" drainée (Fig. 2.2).

— Avulsion par aggradation (Fig. 2.2-1) : Après ouverture d'un chenal au travers les levées naturelles, une aggradation rapide se produit dans la plaine d'inondation provocant la mise en place d'un delta progradant à réseau de drainage distributif (crevasse splay). Vers l'aval de ce dispositif les réseaux distributifs se reconcentrent en un seul chenal qui se connecte au réseau de drainage préexistant de la plaine d'inondation. L'avulsion est alors compète.

— Avulsion par incision (Fig. 2.2-2) : Après ouverture d'un chenal dans les levées naturelles, l'anabranche en cours de formation réannexe un chenal préexistant dans la plaine d'inondation qui rejoint le cours d'eau principal vers l'aval. Cette connexion provoque une vague d'érosion régressive depuis le point de confluence entre le chenal issu de l'avulsion et le chenal parant. Cette vague d'érosion régressive se déclenche en conséquence au nouveau niveau de base imposé par la confluence en aval. Une fois la vague d'érosion régressive remontée au point de bifurcation en amont, l'anabranche est complètement incisée dans la plaine d'inondation et est stabilisée.

L'étude du cours inférieur du Rio Pastaza (Fig. 2.3, 2.4) été l'occasion d'illustrer des phénomènes d'avulsion impliqués dans le développement d'une morphologie anastomosée à partir d'un cours d'eau à chenal unique. Ce type d'avulsions n'était pas décrit jusque là dans le bassin de l'Amazone.

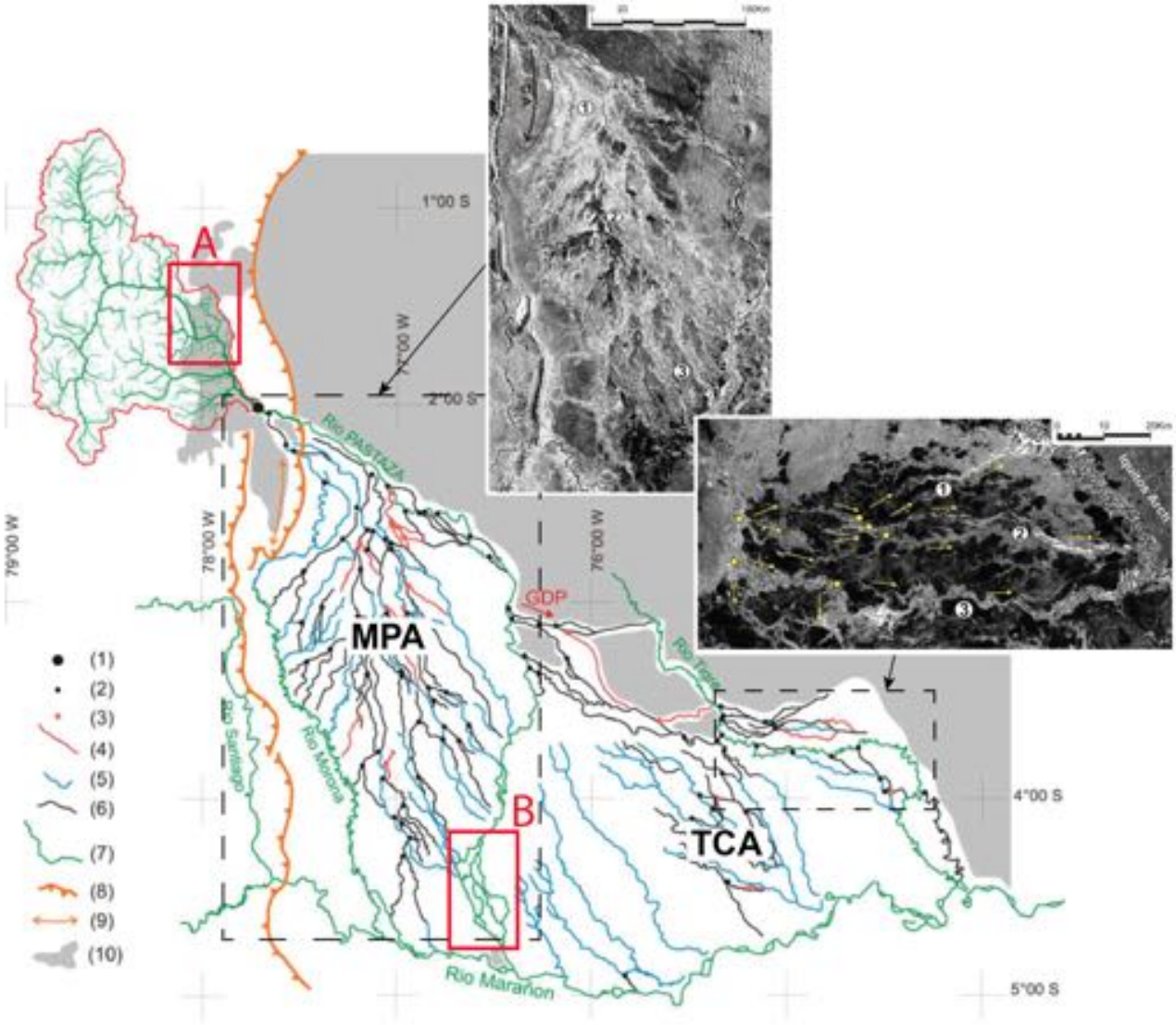

FIGURE 2.3 – Carte des cours successifs suivis par le Rio Pastaza depuis le LGM (Bernal et al., 2011). En rouge : bassin versant du Rio Pastaza dans les Andes d'Equateur (réseau hydrographique extrait du MNT SRTM), 1 : apex actuel du megafan du Rio Pastaza, 2 : sites d'avulsions, 3 : sites d'avulsions supposées, 4 cours supposés, 5 : cours réannexés, 6 : cours abandonnés, 7 : cours actuels, 8 : Front de chevauchement subandin, 9 : axe anticlinal, 10 : surface de Mera-Upano (Pré LGM), MBA : Zone Morona Pastaza occupée avant 9 200 ans Cal BP, TCA : Zone Tigre Corrientes, occupée après 9 200 ans Cal BP. A : Avulsion du bas Pastaza (paragraphe 2.1.4), B : Avulsion de Puyo (paragraphe 2.1.5)

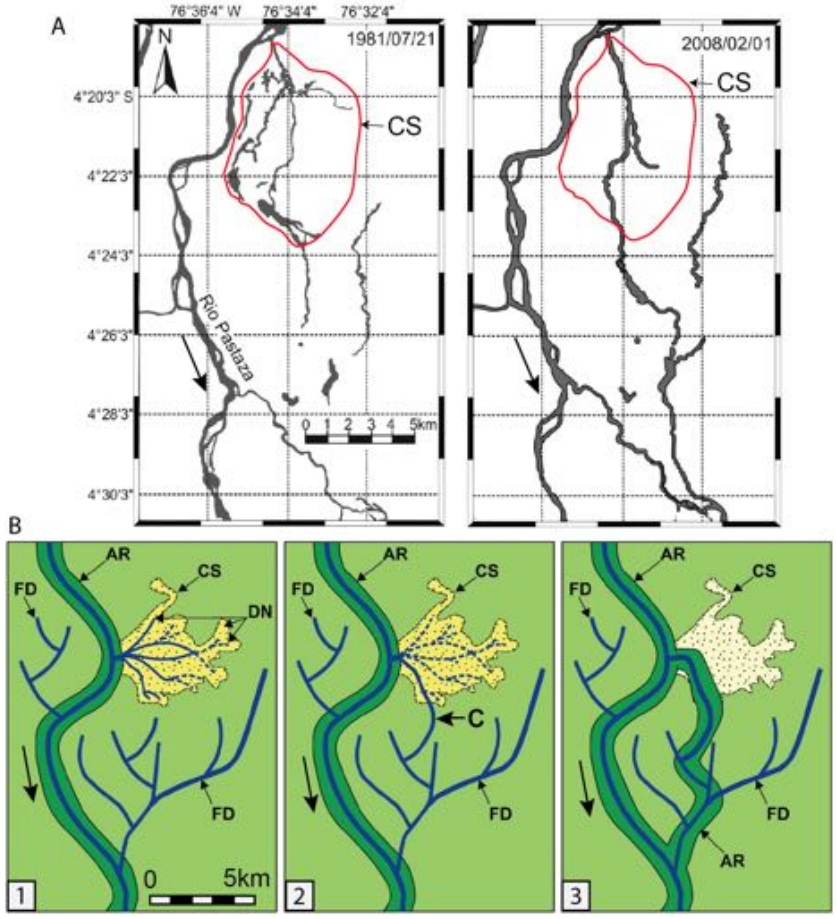

FIGURE 2.4 – Exemple de mise en place et modèle évolutif de mise en place d'une anabranche à partir d'un crevasse splay et de sa capture par drain dans la plaine d'inondation. A : évolution du réseau de drainage d'un crevasse splay en rive droite du Rio Pastaza entre 1981 et 2008. B : modèle évolutif de mise en place d'une anabranche. Avec AR : ride alluviale, CS : crevasse splay, DN : réseau distributaire, FD : drain de la plaine d'inondation, C : capture (Bernal et al., 2013).

A partir de séries temporelles d'images satellites, trois exemples d'avulsion liés à la mise en place d'une morphologie anastomosée sur le cours inférieur du Rio Pastaza (Nord Pérou) ont pu être illustrés. Ces trois exemples mettent en avant le rôle important des drains de la plaine d'inondation en tant qu'initiateur des anabranches. La Figure 2.4 B résume le déroulement de ces avulsions :

1. Ouverture d'une brèche dans les levées naturelles et progradation d'un crevasse splay dans la plaine d'inondation.
2. Connexion d'un drain du crevasse splay avec un drain de la plaine d'inondation, déclenchement d'une vague d'érosion régressive provocant l'abandon des autres drains du crevasse splay.
3. Remontée de la vague d'érosion régressive jusqu'au point d'avulsion initial, fin du rééquilibrage du profil en long de l'anabranche et stabilisation d'une nouvelle ride alluviale.

Le type d'avulsions illustré par les trois exemples étudiés se rapproche du modèle d'avulsion par aggradation de Mohrig et al. (2000). La Fig.2.4 A présente un de ces trois exemples, on peut constater que la progradation du crevasse splay dans la plaine d'inondation n'atteint pas le point de confluence de la future anabranche avec le cours d'eau principal et que la connexion de cette anabranche avec les drains de la plaine d'inondation se fait dans la plaine d'inondation. Il en résulte que le le profil de l'anabrache ; lors de sa connexion avec le drain de la plaine d'inondation va présenter un knickpoint entre le front du crevasse splay et le drain de la plaine d'inondation. Dans ces conditions, la stabilisation de l'anabranche ne peut se faire qu'en faisant intervenir une vague d'érosion régressive qui va inciser le crevasse splay à partir du niveau de base de la plaine d'inondation et non pas celui imposé par la confluence avec les chenal parent en aval. Dans ce cas, on se rapproche du modèle d'avulsion par incision de Mohrig et al. (2000). L'étude des avulsions du cours inférieur du Rio Pastaza met donc en évidence que les deux modèles d'avulsions proposés par Mohrig et al. (2000) ne représentent que deux extrêmes et que chaque avulsion sera un intermédiaire entre les deux en fonction de la taille du crevasse splay et de sa capacité à combler ou non l'espace disponible dans la plaine d'inondation.

Les données hydrométéorologiques disponibles sur la période étudiée ne permet pas de lier l'ouverture des chenaux de crevasse avec les épisodes d'El Niño extrêmes documentés sur cette période (1983, 1997). Il semble donc que le niveau des crues ne soit pas discriminant en tant que déclencheur des avulsions. Cette conclusion rejoint le postulat de Jones and Schumm (1999) qui indique que ce n'est pas le niveau d'une crue qui déclenche une avulsion, mais qu'à partir du moment ou le "setup" atteint une valeur seuil, n'importe quelle crue, quel que soit son niveau, déclenchera une avulsion. La nature du "setup" est difficile à contraindre dans ce cas. En l'absence de motif typique d'un contrôle tectonique (avulsions toutes localisées du même côté, abandon préférentiel dans une direction, alignement des points d'avulsion sur un linéament), il semblerait que le "setup" soit dans ce cas l'aggradation des levées naturelles.

2.1.5 à l'échelle du Siècle

L'étude des modifications du réseau de drainage est un outil classique pour déterminer les déformations de surface (Gaudemer et al., 1989; Leeder and Alexander, 1987; Leeder and Jackson, 1993; Ouchi, 1985; Schumm et al., 2000), (Fig. 2.5). Ces modifications peuvent porter sur la morphologie fluviale en réponse à des zones de surrections ou de subsidence (Ouchi, 1985; Schumm et al., 2000), sur la direction des drains en réponse aux jeux des failles en surface (Gaudemer et al., 1989) ou a des abandons progressifs liés à des basculement (Leeder and Alexander, 1987; Leeder and Jackson, 1993).

A côté des distorsions de marqueurs morphologiques dues à la tectonique, les cônes alluviaux se formant au débouchés des reliefs sont aussi des jauges des déformations actives (Bull, 1964; Bull and McFadden, 1977; Pinter and Keller, 1995; Horton and DeCelles, 2001; Keller and Pinter, 2002).

L'ensemble de ces modèles montrent que pour plusieurs types de faille et de mouvements de surface associés on peut obtenir une réorganisation du réseau de drainage au sein de cônes alluviaux similaires.

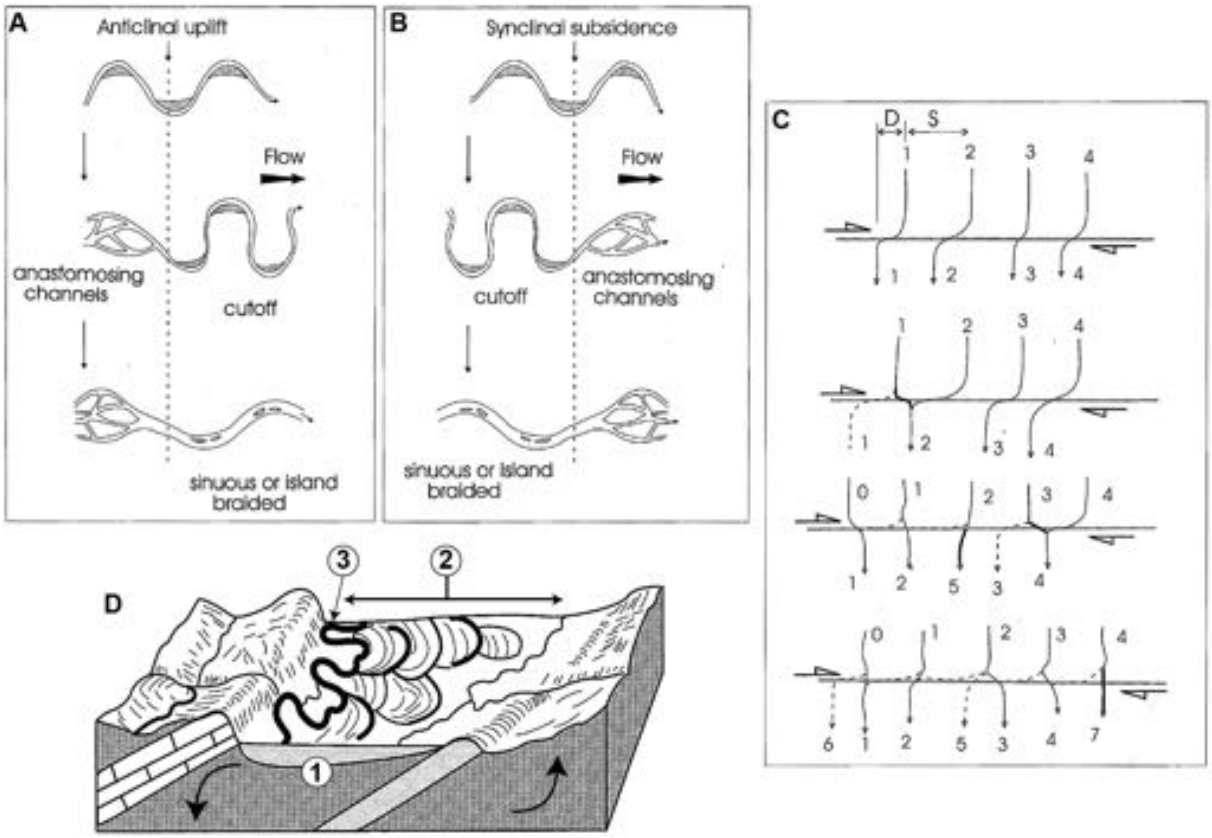

FIGURE 2.5 – Marqueurs fluviaux des déformations de surface.
A et B Ajustements morphologique des cours d'eau à divers contextes tectoniques (Ouchi, 1985),A : ajustement à la croissance d'une crête anticlinale, partant d'un cours d'eau méandriforme C : Décalage et captures de cours d'eau par une faille décrochante (Gaudemer et al., 1989; Huang, 1993), D : Abandon dissymétrique de méandres en réaction à un basculement latéral (Schumm et al., 2000), 1 : vallée dissymétrique, 2 : abandon de méandres majoritairement localisés sur une rive du cours d'eau, 3 : Lit du cours d'eau dissymétrique

L'étude d'un tronçon de quelques kilomètres du Rio Pastaza (Equateur) au débouché de la Cordillère Orientale à permis d'illustrer un exemple d'interaction complexes entre la déformation de surface liée à la tectonique active, la sédimentation d'un cône alluvial et le climat de la région dominé par les épisodes d'El Niño.

Le Rio Pastaza prend sa source dans les Andes d'Equateur. Son bassin versant s'étend sur la Cordillère Occidentale, la Dépression Interandine et la Cordillère Orientale (Fig.2.6B). La confluence de deux drains longitudinaux nord-sud donne naissance au Rio Pastaza qui traverse perpendiculairement la Cordillère Orientale par une vallée fortement incisée (jusqu'à 2000 m de profondeur). Le Rio Pastaza débouche sur un plateau (Surface de Mera-Upano,(Bès de Berc et al., 2005)) qui constitue la surface topographique à faible relief de la Zone Subandine (Fig. 2.6 B et C). Ce plateau correspond à un pédiment formé avant le dernier maximum glaciaire (LGM) (Bès de Berc et al., 2005) sur la surface sommitale du cône de piémont du Napo-Pastaza. (Bernal et al., 2012; Bès de Berc et al., 2005; Christophoul et al., 2002b). Il constitue une surface repère, qui là où elle n'a pas été incisée, montre une très faible relief. En franchissant le front topographique de la Cordillère Orientale, la vallée s'élargit brusquement et le Rio Pastaza y édifie un cône alluvial (se superposant à la partie apicale du cône du Napo-Pastaza précédent. Sur ce cône alluvial, le Rio Pastaza décrit un brusque virage à Droite, vers le sud. C'est sur ce tronçon que que le Rio Pastaza a subi plusieurs avulsions au cours du dernier siècle.

A partir de la compilation de documents cartographiques, de photographies aériennes et d'imagerie satellitaire, il a été possible de reconstituer les divers cours du Rio Pastaza. La Figure 2.6 montre le cours du Rio Pastaza en 1906 et 2002. Sur une durée d'un siècle, le Rio Pastaza s'est déplacé, effectuant une rotation de rotation horaire de 80°. L'analyse de séries temporelles à permis de préciser les stades intermédiaires. En plus de ces avulsions successives, le Rio Pastaza, initialement confluent avec le le Rio Puyo a été capturé par par un tributaire s'écoulant vers N160E confluant vers le sud avec le Rio Llushin (Fig. 2.6 C et D).

L'analyse de la topographie basée sur un MNT réalisé sur ENVI 4.7 à partir de bandes stéréoscopiques d'image satellite Aster (bande 3B et 3N), recalées sur des données cartographiques et GPS, permet de mettre en évidence les déformations de surface de la région. Ces déformations sont de deux types :

- La surface de Mera-Upano montre un basculement vers l'Ouest de 0,6 à 0,9°. Le plateau de Puyo se situant au toit du chevauchement Subandin, ce basculement est interprété comme un basculement au toit de ce dernier (Fig. 2.6 E). Les valeurs de basculement obervées sont minimales car la surface était initialement inclinée vers l'est (surface du cône du Napo-Pastaza).
- Les profils parallèles à la Cordillère Orientale montrent une structure anticlinale (d'axe est-ouest) à grande longueur d'onde et faible amplitude (Fig. 2.6 E). Le Rio Pastaza s'écoule sur son flanc sud.

Il semble donc que le Rio Pastaza se soit adapté à une topographie évolutive.

L'analyse des données hydrométéorologiques sur la période récente de l'intervalle 1906-2008 (1964-2008) permet de lier les avulsions du Rio Pastaza aux évènements extrêmes d'El Niño. Classiquement, les fortes précipitations et les crues dans le réseau hydrographique s'expriment surtout sur la façade Pacifique des Andes d'Equateur et sont peu enregistrées sur le versant amazonien. Cependant, le Rio Pastaza prenant sa source sur la Cordillère Occidentale, il apparaît que la partie haute de son bassin versant enregistre les évènements hydrologiques d'El Niño et les transmet sous forme d'ondes de crues vers l'aval. Ce résultat semble paradoxal, alors que dans le paragraphe précédent (2.1.4), le contrôle des avulsions du bas Pastaza le rôle déclencheur d'avulsion d'El Niño n'a pas pu être mis en évidence.

En conclusion, l'étude du Rio Pastaza au débouché de la cordillère orientale des Andes d'Equateur, sur une zone subandine tectoniquement active permet de hiérarchiser les paramètres influant sur les réorganisation du réseau de drainage :

- La déformation active de la zone subandine créée un "setup" par 2 types de déformations de surface :
  - un basculement vers l'Ouest au toit du front de Chevauchement Subandin, imposant une

composante est-ouest à son déplacement par avulsion.
  - la formation d'un pli anticlinal à grande longueur d'onde et faible amplitude, imposant une composante nord-sud à son déplacement.
- Le climat, sous la forme de crues liées au phénomène El Niño sert de déclencheur des avulsions.

A l'échelle régionale (Fig. 2.6 B), la diversion vers le sud du Rio Pastaza, qui pourrait être, à première vue interprétée comme résultant d'une capture due à un décrochement dextre (2.5 C), est en fait le résultat d'interactions entre la sédimentation d'un cône alluvial sur une surface en cours de basculement créant une pente vers l'ouest et vers le sud (flanc sud d'un pli à axe est-ouest) dont les avulsions et captures sont déclenchées par le climat.

2.1.6 à l'échelle du millier d'années

La réponse des systèmes alluviaux aux forçages tectoniques et climatiques peut s'exprimer de manière tout à fait différente suivant les contextes. Le Quaternaire est la période privilégiée pour évaluer l'empreinte des forçages climatiques dans l'enregistrement fluvial. En effet, le climat quaternaire est caractérisé par l'augmentation de la fréquence des fluctuations de réchauffement/refroidissement et par l'augmentation de l'amplitude de ces cycles menant à la mise en place de cycles glaciaires/interglaciaires (Tiedemann et al., 1994; Lisiecki and Raymo, 2005). Au cours des dernières années, j'ai pu étudier la réponse de systèmes fluviaux pour la même période de la fin du Pléistocène et de l'Holocène sur deux objets situés dans des contextes tectoniques et climatiques radicalement différents : La Garonne lors de la formation de sa dernière terrasse et le mégafan du Rio Pastaza, sur le piémont des Andes.

La Garonne pléistocène J'ai tout d'abord étudié l'évolution morphologique de la Garonne contemporaine de la formation de sa dernière terrasse (terrasse würmienne, transition pléniglaciaire/tardiglaciaire, pléistocène supérieur/holocène, Hubschman (1975d,a)). La Garonne possède un important réseau de terrasses dissymétriques (Fig. 2.9) composé de six niveaux principaux (Hubschman, 1975e). Ces niveaux de terrasses sont datés de manière relative en fonction de leur position dans l'emboîtement en référence au modèle de géomorphologie climatique quaternaire de (Penck, 1910). Les plus hautes sont attribuées au Donau et Günz (T6 et T5 sur la Figure 2.9), les niveaux intermédiaires (T4 à T2) au Mindel et Riss. La seule terrasse pour laquelle des datations sont disponibles est la dernière (T1) (Bourgeat et al., 1984; Bruxelles and Jarry, 2011; Carozza et al., 2013, 2014a; Stange et al., 2014), définie, selon les auteurs comme la "terrasse Würmienne" ou la "basse plaine" (Hubschman, 1975e).

La formation des grands réseaux de terrasses alluviales en lien avec les cycles glaciaires durant le Quaternaire est connu depuis les travaux de Penck and Brückner (1901) et de Penck (1910), (Fig.2.7). Ces travaux sont à l'origine d'un modèle conceptuel de "géomorphologie climatique" de formation des terrasses alluviales en lien avec les cycles glaciaires. Ce modèle a été raffiné au cours du temps (Büdel, 1977; Vandenberghe and Maddy, 2001; Vandenberghe, 2002, 2008; Vandenberghe et al., 1994; Vandenberghe and Maddy, 2000; Bridgland and Westaway, 2008) Les grandes lignes de ce modèle peuvent-être résumées de la manière suivante :

- Durant les périodes pléniglaciaires, l'érosion des sols est limitée et la charge de fond des cours cours d'eau provient des éléments grossiers résultants de l'abrasion glaciaire. La capacité des cours d'eau à transporter une importante charge de fond est faible. Avec la réduction de la pente du cours d'eau vers l'aval, cette capacité chute encore, provoque le dépôt de la charge de fond et l'aggradation du lit fluvial. Ce lit a tendance à s'élargir et à se déplacer latéralement (formant le remplissage d'une future terrasse alluviale).
- en période interglaciaire,l'érosion des sols dans le bassin versant augmente, le débit augmente (fonte des glaciers et précipitations non stockées dans le bassin versant sous forme de glace), la capacité des cours d'eau à déplacer la charge de fond augmente et provoque l'incision du lit du cours d'eau et la formation d'une terrasse alluviale.

Si l'on considère la formation d'une terrasse, l'abandon de la terrasse sera contemporain d'un interglaciaire, alors que l'aggradation sur cette terrasse sera contemporaine du pléniglaciaire (Büdel,

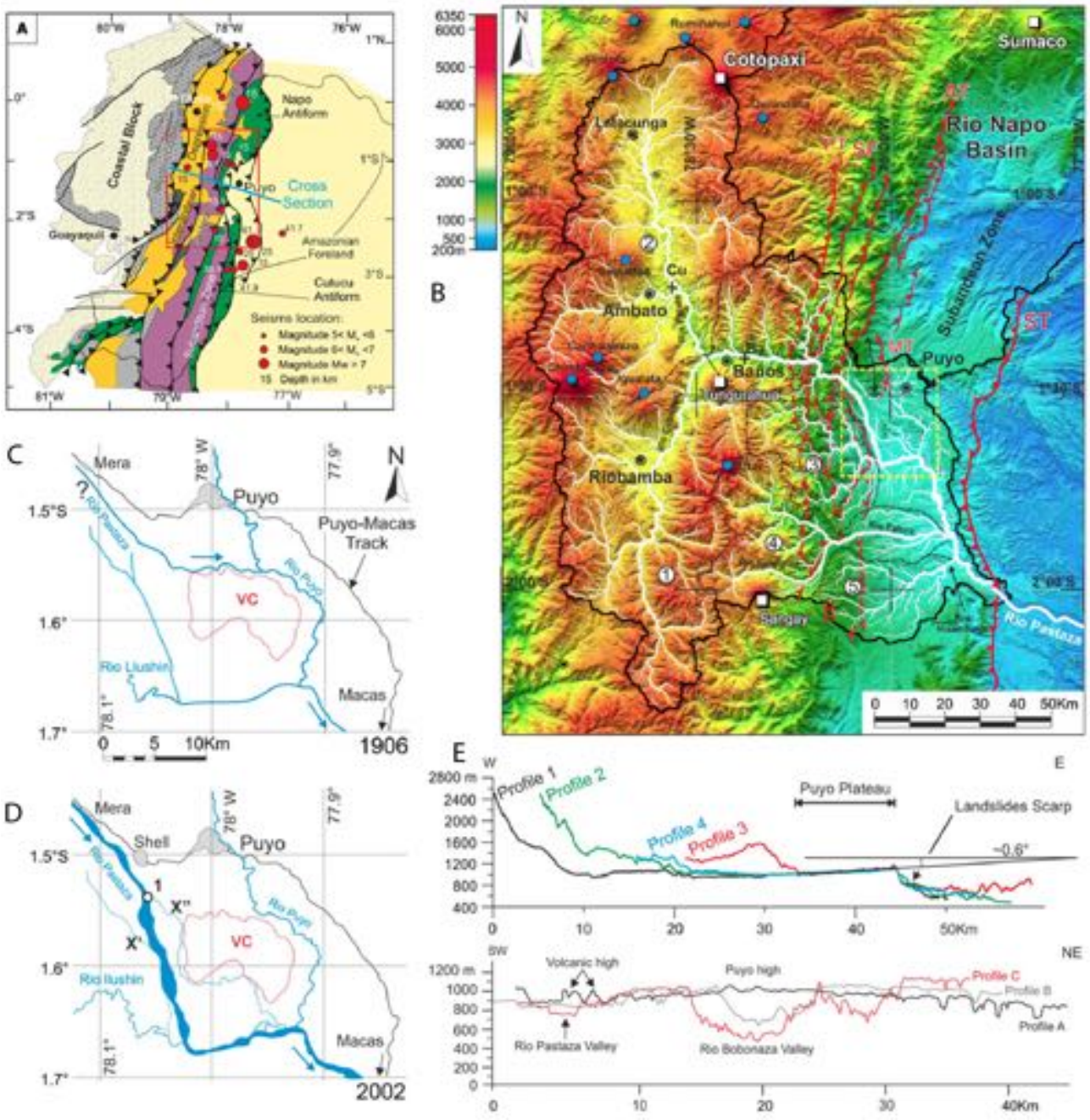

FIGURE 2.6 – Avulsions successives du Rio Pastaza entre 1906 et 2002
A : Localisation de la zone d'étude et foyers des principaux séismes. B : MNT des Andes d'Equateur et de la Zone Subandine. en blanc : cours d'eau, en noir : bassin versant du Rio Pastaza, en rouge : principales failles avec SF : Faille Subandine, PT : Chevauchement de Pallatanga, MT : chevauchement de Mirador, AT : Chevauchement d'Abitagua, ST : Chevauchement Subandin, carrés blancs : Volcans actifs, cercles bleus : édifices volcaniques éteints, 1 à 5 : principaux sous-bassins versants. C : cours du Rio Pastaza au Débouché de la Cordillère Orientale en 1906. D : *idem* en 2002, 1 : point de bifurcation, X' et X" : tronçons actifs en aval de la bifurcation, VC : relief d'un édifice volcanique. E : Profils topographiques est-ouest (profil 1 au nord, profil 4 au sud dans l'encadré pointillé jaune) et NE-SO de la zone subandine, notez le basculement vers l'ouest au toit du front de chevauchement subandin, (Bernal et al., 2012).

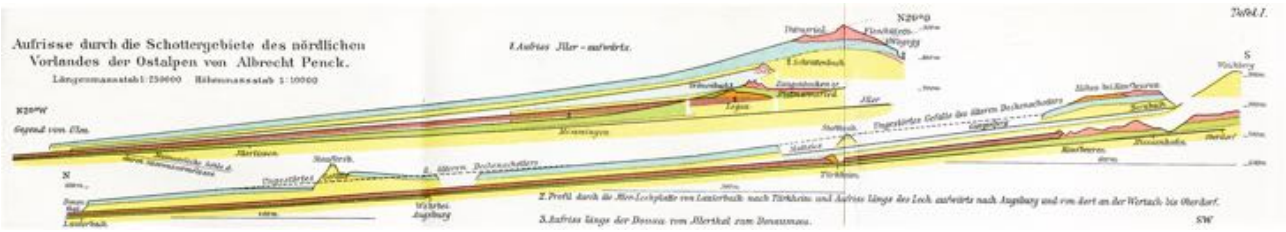

FIGURE 2.7 – Coupe au travers des épandages de galets sur le piémont nord des Alpes Orientales par Albrecht Penck. Il s'agit des profils des terrasses des affluents de la rive droite du Danube. En haut : Profil des terrasses le long de la vallée de l'Iller, en bas : Profil le long de la vallée du Lech jusqu'à Augsburg et le long du Wertach en amont (Penck and Brückner, 1901).

1977).

L'émergence, à partir des années 1960 d'une conception du fonctionnement du système fluvial basé sur les processus fluviaux (Leopold et al., 1964; Schumm, 1977; Métivier and Barrier, 2012) a largement remis en cause ce modèle de géomorphologie climatique.

Au-delà du modèle climatique qui invoque le rôle du climat dans l'abandon des terrasses alluviales lors des périodes de déglaciation. Les cours d'eau subissent de profondes modifications dont les témoins sont préservés dans le remplissage des terrasses. La figure 2.8 montre l'évolution de la morphologie d'un cours d'eau entre le Pléniglaciaire et l'Holocène (Huisink, 2000). Dans cette étude, on remarque que le pléniglaciaire est associé à une morphologie anastomosée ou en tresse, alors que le tardi-glaciaire se traduit par une morphologie à méandre. L'épisode froid du Younger Dryas (11-10 Ka) amène à un retour de la morphologie en tresse et à partir du début de l'holocène, on constate de nouveau une morphologie méandriforme. De nombreuses études similaires ont permis de préciser les changements de style fluviaux en Europe du nord-ouest (Antoine, 1993; Antoine et al., 2003; Cordier et al., 2006, 2012; Gargani et al., 2006; Huisink, 2000; van Huissteden, 2001; Kozarski, 1983; Mol et al., 2000; Mol, 1997; Vandenberghe et al., 1994; Stouthamer and Berendsen, 2000). On retrouve dans toutes ces études, des points commune, notamment la présence de morphologies en tresses lors du pléniglaciaire. Par contre, à partir de l'entrée dans le tardiglaciaire, les styles successifs adoptés par les rivières étudiées sont différents. Le seul point commun qui persiste est la chronologie des changements observés. Il apparaît donc qu'au premier ordre, le climat exerce un contrôle sur la morphologie des cours d'eau, mais la réponse des cours d'eaux va être différente d'une rivière à l'autre en fonction d'autres facteurs tels que la latitude, la position du tronçon observé dans le bassin (zones amonts proche des fronts glaciaires associées à des pentes fortes, zones avales soumises au niveau de base marin et présentant des pentes plus faibles *etc.*).

Dans ce cadre général de contrôle climatique des cycles incision/aggradation, une autre problématique plus spécifique s'est révélée intéressante à explorer : la compréhension de la transition tresse/ méandre. C'est une question ancienne qui intéresse une vaste communauté de sédimentologues, géomorphologues, hydrauliciens et aménageurs de cours d'eau. Cette question abordée depuis une cinquantaine d'années a permis d'écarter de nombreux paramètres supposes jouer un rôle dans le contrôle de la morphologie des cours d'eau. On peut citer : la granulométrie des sédiments transportés, la pente, le débit.... Au cours du temps, deux paramètres se sont imposés comme étant prépondérants : la présence de matériaux cohésifs sur le berges Smith (1998) et la présence de végétation (Andrews, 1984; Hey and Thorne, 1986; Huang and Nanson, 1997; Davies and Gibling, 2010; Gibling and Davies, 2012; Corenblit et al., 2014b,b). cependant permis d'isoler des paramètres jouant un rôle important dans la transition tresses méandres. (Carson, 1984), par des modélisations analogiques à pu montrer l'importance de la présence de matériaux cohésifs en tant que facteur de stabilisation des méandres par une consolidation des berges. De la même manière, les modélisations analogiques de (Tal and Paola, 2007, 2010) ont permis de mettre en évidence l rôle de la végétation dans la stabilisation des méandres. L'étude de l'évolution de la morphologie de la Garonne durant la dernier glaciation permet de proposer de nouvelles hypothèses quant aux relations climat/morphologie.

La Garonne à la fin de la dernière glaciation se situe dans un contexte particulier par rapport

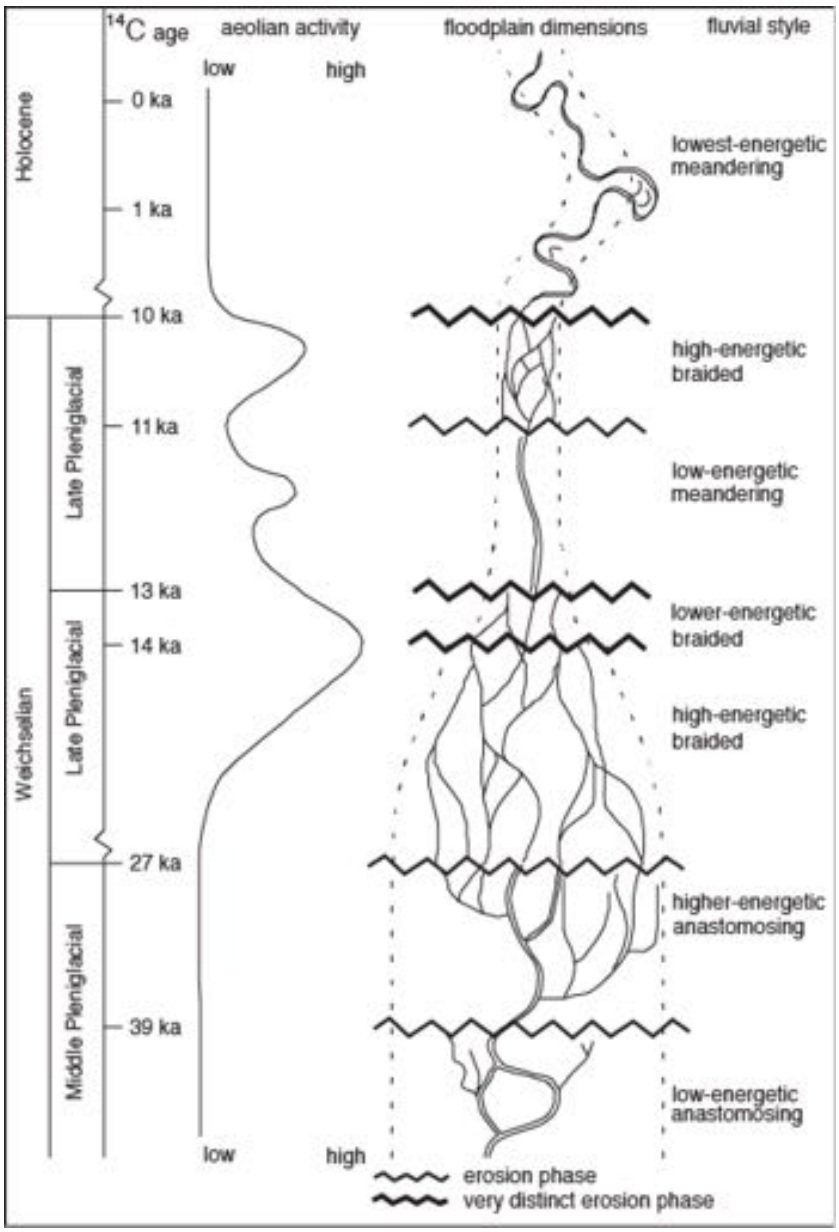

FIGURE 2.8 – Compilation des changements de styles fluviaux dans la Vallée de La Vecht du Pléniglaciaire moyen à l'Holocène intégrant les phases d'érosion et l'activité éolienne (Vandenberghe (2003), adapté de Huisink (2000)).

aux autres cours d'eau décrits pour la même période en Europe du nord-ouest pour la même période (Antoine, 1993; Antoine et al., 2003; Huisink, 2000; Mol et al., 2000; Mol, 1997; Gargani et al., 2006; Pastre et al., 2003; Vandenberghe, 2003). Du point de vue climatique, le bassin versant de la Garonne enregistre, par ses marqueurs morphologiques et l'évolution de la végétation, les effets du retrait glaciaire dès 31 ka BP (Andrieu-Ponel et al., 1993, 1988; Delmas et al., 2011; Jalut et al., 1992; Jalut and Turu i Michels, 2006). Contrairement aux plus hautes latitudes (Mol, 1997; Huisink, 2000; Mol et al., 2000; Pastre et al., 2003; Vandenberghe, 2003),le LGM est peu marqué dans le bassin de la Garonne (Fig. 2.10) alors que le Younger Dryas se traduit par des changements de végétation importants (Andrieu-Ponel et al., 1988, 1993). Du point de vue du contexte géodynamique, la Garonne se situe sur un piémont "passif" qui s'est installé sur le versant nord des Pyrénées à partir du Miocène.

L'étude des changements morphologiques de la Garonne du Pléistocène supérieur à l'Holocène a a été réalisée à partir d'une cartographie des chenaux préservés dans le remplissage de la dernière terrasse par traitement de photographies aériennes (Fig. 2.9). La Fig. 2.10 montre l'évolution de la morphologie de la Garonne lors de la dernière glaciation en regard des changements de végétation, du climat et des taux de sédimentation dans le lac glaciaire de Barbazan. La Fig. 2.11 résume cette évolution. Le pléniglaciaire est associé, comme dans la majorité des rivières nord-ouest européennes à une morphologie en tresse. La transition tresse/méandres est difficile à dater, mais est antérieure à 14 Ka Cal BP (Stange et al., 2014). Cette transition est donc contemporaine du tardi-glaciaire. Elle aboutira à la mise en place d'un cours d'eau méandriforme "gravel meandering" à faible sinuosité (1,4, MB1 sur Fig. 2.9, Fig. 2.10). Après cet transition tresse/méandre, la Garonne voit son style fluvial changer par une forte augmentation de sa sinuosité (2,0, MB2 sur Fig. 2.9, Fig. 2.10) toujours associée à une charge de fond grossière. Cette transition est mieux datée, Bourgeat et al. (1984) montrent que MB2 est contemporaine du Younger Dryas. Par conséquent, l'abandon final de la terrasse T1 (incision du lit actuel atteignant plus de 10 m dans la zone amont du secteur d'étude) (Fig. 2.9) est postérieur à MB2 et marque donc le début de l'Holocène.

A côté de cette chronologie, il apparaît que la transition tresse/méandre, contrairement à la majorité des cas exposés dans la littérature, se fait sans changement majeur de granulométrie de la charge de fond et la transition tresse/méandre se fait entre des cours d'eau de type "Gravel Bed Braided" et "Gravel Meandering" (Miall, 1985, 1996). La réduction de la charge de fond est une cause reconnue du déclenchement de la transition Tresse/ Méandre (Marston et al., 1995) et a été souvent évoquée comme la cause de la méandrisation durant le tardi-glaciaire (Antoine, 1993; Mol, 1997; Huisink, 2000). Dans une récente synthèse sur la transition tresse/méandre dans les cours d'eau à charge de fond grossière ("gravel braided" et "gravel meandering"), Métivier and Barrier (2012) montrent que dans le cas spécifique de ce type cours d'eau, un changement de granulométrie dans la charge de fond n'a pas d'effet sur la morphologie rejoignant ainsi les conclusions de Brierley and Hickin (1991). L'origine de la transition tresse/méandre pour la Garonne est donc autre. En l'absence de matériel cohésif sédimentant sur les berges, la croissance de la végétation pionnière permet d'augmenter la cohésion des sédiments par l'ancrage des racines dans les sédiments Corenblit et al. (2014a). En retour, la végétation en période de hautes eaux va réduire localement le shear stress et permettre l'aggradation des corps sédimentaires.

D'autre part, si l'ensemble des dépôts de galets contemporains des tresses et méandres sont recouvert de dépôts sableux et limoneux, ces derniers sont postérieurs à la mise en place des tresses et méandres (Christophoul et al., subm; Carozza et al., 2014b). Ils n'ont donc pas la capcité de renforcer la cohésion des berges au moment de l'activité des tresse et méandres. Il semble donc que l'installation de la végétation soit le paramètre prépondérant dans la transition tresses/méandres.

Lors du pléniglaciaire, on peut raisonnablement supposer que le régime hydrologique de la Garonne était de type glaciaire avec un pic de hautes eaux en Août et qu'il est devenu, progressivement de type pluvio-nival comme l'actuel, caractérisé par un pic de hautes eaux en Avril-Mai. Le pic de hautes eaux en Août et donc de recouvrement des corps sédimentaires pendant la période de croissance de la végétation est peu propice à la colonisation de ces derniers, alors qu'un pic de hautes eaux en avril laissera les corps sédimentaires à découvert pendant la période de croissance de la végétation, rendant la colonisation et la stabilisation des barres plus probable.

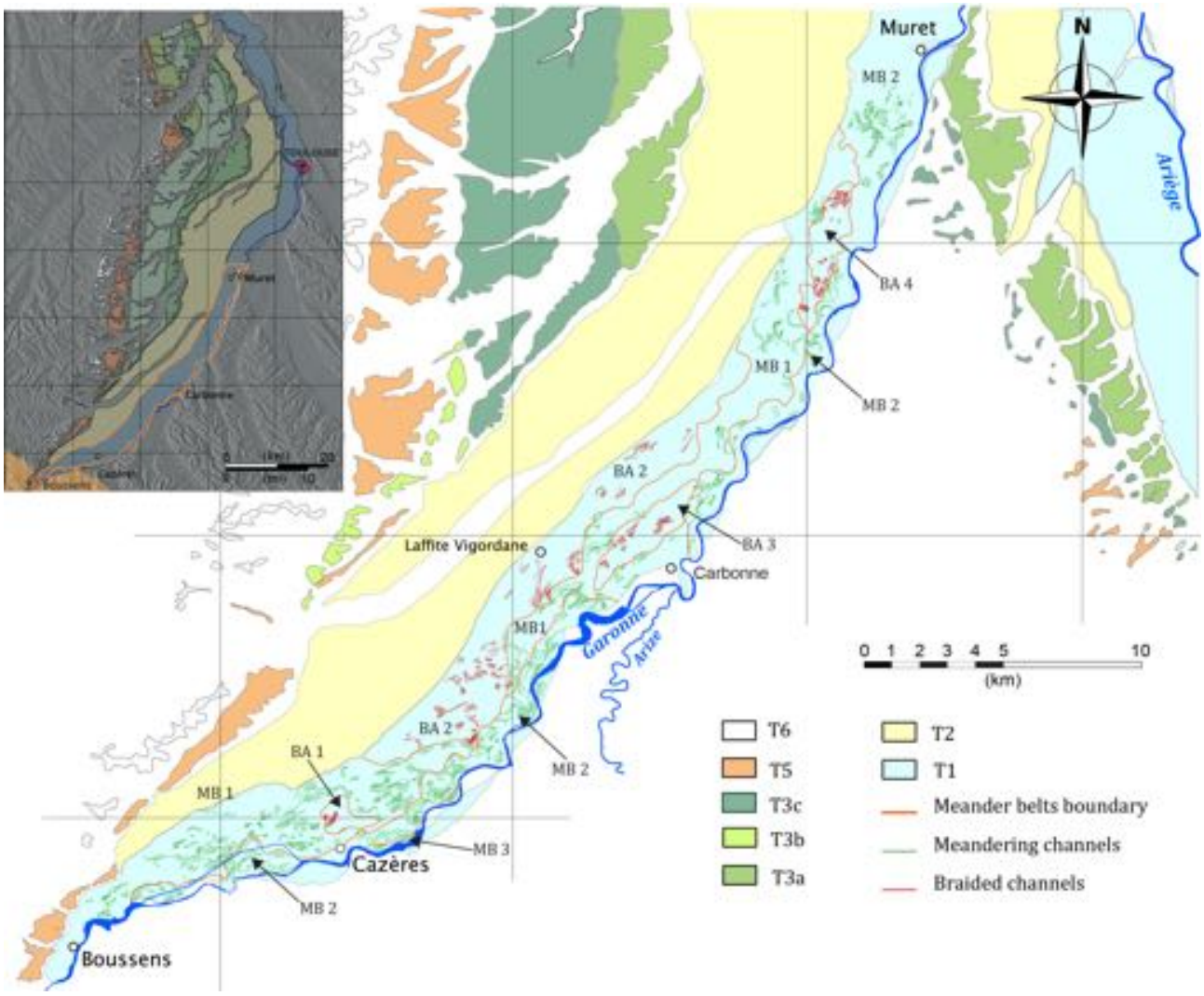

FIGURE 2.9 – Carte des chenaux successifs de la Garonne constituant le remplissage de la terrasse würmienne
T1 à T6 : Terrasses de la Garonne, BA1 à 4 : zone de préservations de chenaux en tresses, MB 1 à 3 : ceintures de méandres (différenciées en fonction de leur sinuosité). (Christophoul et al., subm).

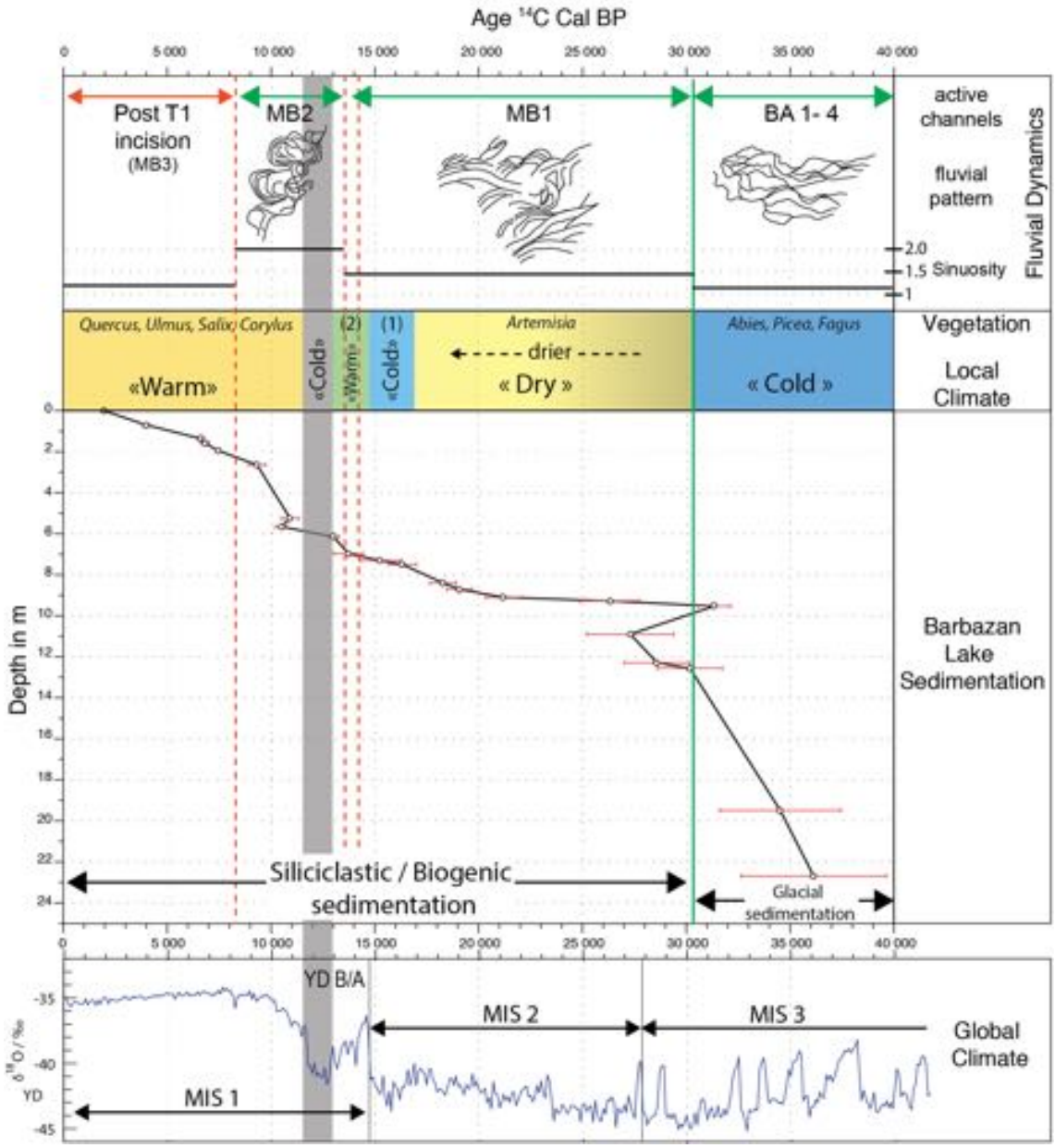

FIGURE 2.10 – Evolution du climat, de la végétation et de la morphologie de la Garonne lors de la dernière déglaciation.

(Christophoul et al., subm). Corrélation entre la sédimentation dans le lac glacaire de Barbazan (modifié de Stange et al. (2014)). Courbe de δ^{18}O d'après (Lisiecki and Raymo, 2005), (Martinson et al., 1987). B/A : Bolling/Allerod, YD : Younger Dryas. Ages ^{14}C calibrés avec CalPal2007online (Danzeglocke et al., 2007). Caractéristiques de la végétation et du climat d'après(Reille and Andrieu-Ponel, 1995; Jalut and Turu i Michels, 2006; Rius et al., 2012; Carozza et al., 2014a). (1) Végétation entre 16 900-14 700 yrs Cal BP : *Artemisia, Juniperus.* (Jalut and Turu i Michels, 2006), (2) Végétation entre 14 700 ? 12 895 yrs Cal BP : *Abies, Betula, Quercus* (Jalut and Turu i Michels, 2006). BA1 à 4 et MB 1 à 3 : chenaux représentés sur la Fig. 2.9

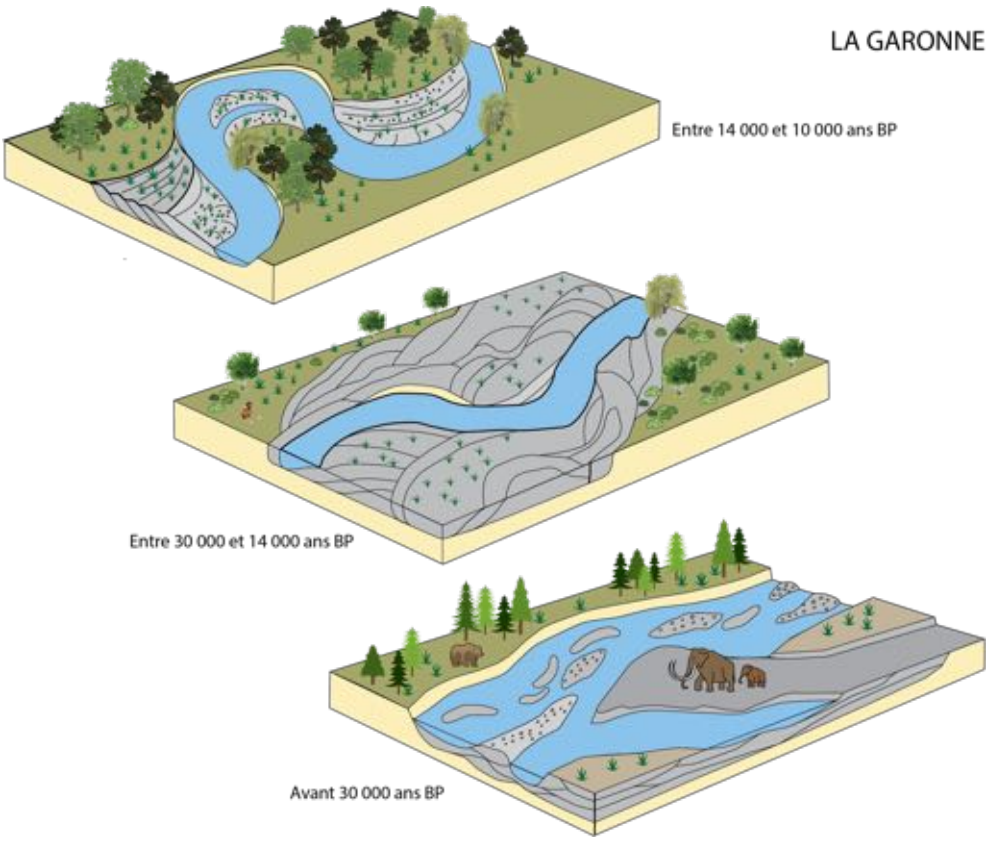

FIGURE 2.11 – Evolution de la morphologie de la Garonne durant la dernière déglaciation. Avant 30 000 ans BP : rivière en tresses, entre 30 000 et 14 000 ans BP : rivière méandriforme à faible sinuosité, de 14 000 à 10 000 ans BP : rivière méandriforme à forte sinuosité (d'après Christophoul et al. (subm).

On peut donc émettre l'hypothèse d'un contrôle hydrologique de la transition tresses/méandres faisant intervenir la végétation comme agent principal de stabilisation du lit fluvial. Cette hypothèse sera développée dans mon projet recherche (paragraphe 2.2.6)

Le Rio Pastaza depuis le Dernier Maximum Glaciaire Sur le piémont amazonien des Andes d'Equateur, le contexte est totalement différent. D'un point de vue climatique, le Pléistocène supérieur / Holocène du piémont des Andes d'Equateur enregistre les évènements climatiques de manière différente. Le Dernier Maximum Glaciaire (LGM) est plus marqué alors que la présence du Younger Dryas est faiblement marquée dans la morphologie et la végétation. L'occurence du Younger Dryas aux basses latitudes est d'ailleurs un débat toujours ouvert (Heine, 1994; Heine and Heine, 1996; Heine, 2000; Liu and Colinvaux, 1985). Du point de vue géodynamique, le piémont amazonien des Andes d'Equateur se situe à l'articulation entre le prisme orogénique actif du bassin retroarc andin et le foredeep du bassin d'avant-pays amazonien. Dans la Zone Subandine (prisme orogénique), de nombreuses failles actives sont connues, des mouvements verticaux rapides à l'échelle historique y ont été identifiés (Bès de Berc et al., 2005) et la zone est le siège d'une forte sismicité (Legrand et al., 2005). La partie amont de son bassin versant se situe dans l'arc volcanique andin et de nombreux volcans actifs y sont connus (Barberi et al., 1988).

Le Rio Pastaza débouche sur la zone Subandine (Fig. 2.3, 2.6) avant de traverser un nouveau tronçon incisé, au toit du Chevauchement Subandin. Sortant de ce tronçon, au niveau du front topographique actuel de la Zone Subandine, il débouche sur la plaine amazonienne. Après un tronçon de 200 km sur lequel ils s'écoule vers le sud-est, la rivière décrit une large courbe vers le sud jusqu'à sa confluence avec le Rio Marañon 2500 km plus au sud (Fig. 2.3).

Autour du LGM le piémont des Andes d'Equateur se caractérise par la formation d'un pédiment constituant une surface marqueur connue comme surface de Mera-Upano (Bernal et al., 2011; Bès de

Berc et al., 2005), (Fig.2.3). La mise en place de ce pédiment semble indiquer que le LGM correspond à un épisode sec. Après le LGM, le Rio Pastaza a laissé les traces de ses cours successifs sous forme de rides alluviales abandonnées ou réannexées par des cours d'eau de petite taille (underfit). Ces rides alluviales peuvent être aisément cartographiées du fait de leur réponse spectrale particulière mettant en évidence des contrastes de végétation. A partir de photos satellites, la cartographies des cours successifs du Rio Pastaza révèle la présence très nombreux cours abandonnés séparés par des points d'avulsions (au nombre de 108). Cette cartographie met en évidence un large éventail de forme triangulaire couvrant 60 000 km^2 décrivant un réseau hydrographique de type distributif caractéristique d'un mégafan ou au sens de Weissmann et al. (2010) un "Distributive Fluvial System" (DFS). L'ensemble de cet éventail se superpose à la surface de Mera-Upano qui, a été réincisé depuis le LGM. Cet éventail peut-être divisé en deux partie :

— Une première, située à l'ouest, de forme losangique, située entre le cours actuel du Rio Pastaza à l'est et le Rio Morona à l'ouest (Morona Pastaza Area ou MPA, Fig. 2.3, Bernal et al., 2011) faite d'une forte concentration de rides alluviales méandriformes montrant un schéma en éventail et un sens d'écoulement parallèle au front de chevauchement subandin. Les datations ^{14}C indiquent que ces rides alluviales ont été actives entre le LGM et 9 200 ans Cal BP.

— A l'est, une zone de forme rectangulaire faite d'une plus faible concentration de rides alluviales étroites et rectilignes montrant des directions d'écoulements vers le sud-est (Tigre Corrientes Area ou TCA, 2.3, Bernal et al., 2011). Dans la partie la plus orientale (Rio Tigre actuel) ces rides alluviales abandonnées montrent un schéma anastomosé (Bernal et al., 2011). L'occupation de cette partie du mégafan/DFS du Rio Pastaza s'est faite autour d'un site d'avulsion situé sur le cours actuel du Rio Pastaza. Cette avulsion est à l'origine de la Grande Diversion du Rio Pastaza (GDP sur la Figure 2.3). Les datations ^{14}C, indiquent que ces rides ont été actives après 9 200 ans Cal BP.

Le cours actuel du Rio Pastaza résulte de l'abandon de la TCA suite à une dernière avulsion dont le site se situe en aval du GDP (Fig. 2.3). L'âge de cette avulsion est mal contraint, mais est antérieure à 1691.

La cartographie des cours successif du Rio Pastaza ainsi que les datations disponibles permettent de calculer la fréquence des avulsions. Dans la MPA, les avulsions se sont produites tous les 200 ans en moyenne alors que cette fréquence est de une avulsion / 400 ans dans la TCA (voir détails dans Bernal et al., 2011).

Si la migration de l'apex du DFS du Rio Pastaza est en lien direct avec la croissance du Front de chevauchement subandin (Bernal et al., 2011), cette différence de fréquence d'avulsions peut s'expliquer par l'organisation du système fluvial de piémont. Comme mentionné dans le paragraphe précédent, dans la MPA, les rides alluviales méandriformes, sont plus nombreuses et plus larges alors que dans la TCA elles sont plus étroites et associées à une morphologie anastomosée (fig. 2.3). Il semble donc que dans la MPA, zone située plus près de l'apex, l'aggradation du système fluvial soit plus importante, maintenant au cours du temps les cours d'eau près du seuil de déclenchement des avulsions alors que dans la TCA, zone située en position plus distale l'aggradation est moins importante et le seuil de déclenchement des avulsions est atteint moins souvent. Il apparaît donc que dans la MPA, près de l'apex du mégafan/DFS il y ait beaucoup moins d'espace disponible, du fait de la forte aggradation que dans la partie distale (TCA). Cette réduction de l'espace disponible progressif, de l'apex vers les zones distales semble être une caractéristique classique des DFS qui se traduit sur le long terme par une progradation du système fluvial (Weissmann et al., 2013).

Comparé au cas de la Garonne, l'étude d'un cours d'eau amazonien depuis le LGM montre de grandes différences. Là où la Garonne montre des cycles aggradation/incision, le Rio Pastaza, depuis le LGM reste continuellement en aggradation. L'expression des évènements climatiques de la transition Pléistocène supérieur/holocène (Younger Dryas) n'ont pas de signature dans la géomorphologie. Cette observation semble confirmer une intensité plus faible du Younger Dryas au basses latitudes voire son absence. Par contre, le LGM est un épisode beaucoup plus marqué par une réduction de l'activité des cours d'eau et la mise en place d'un pédiment. Au delà des différences de contexte climatique, les différences de contextes géodynamiques montrent aussi leur importance :

— dans le cas de la Garonne, le piémont nord-pyrénéen est peu impacté par la tectonique. La période quaternaire se traduit par l'incision généralisée, par cycles glaciaires / interglaciaires successifs, d'un piémont préexistant.
— sur le piémont amazonien, la subsidence du bassin d'avant-pays a maintenu une aggradation constante du système fluvial au moins depuis le LGM.

2.1.7 à l'échelle du million d'années

Depuis quelques années, un débat est né dans la communauté des sédimentologues fluviatilistes autour de la notion de "big river", l'intérêt étant que ces grandes rivières, dans l'enregistrement sédimentaire constituent d'excellents réservoirs d'hydrocarbures. Deux visions des systèmes fluviaux s'opposent : les tenants des systèmes "distributifs" (Distributive Fluvial Systems ou DFS) (Hartley et al., 2010; Weissmann et al., 2010, 2013) et ceux des systèmes "contributifs" (Fielding et al., 2012; Sambrook Smith et al., 2010) :

— Le modèle "contribtutif" est le modèle traditionnel d'organisation du réseau hydrographique, organisé en cours d'eau confluent vers l'aval, augmentant progressivement la taille des cours d'eau et structurant des grands bassins versants se jetant dans les océans (Horton, 1945; Fielding et al., 2012; Sambrook Smith et al., 2010).
— Le modèle "distributif" est né d'un article de (Hartley et al., 2010) qui s'appuie sur un inventaire à échelle mondiale des zones alluviales montrant un réseau distributif, c'est à dire montrant des bifurcations ou des anabranches. Ces zones rassemblent des objets géomorphologiques tels que les cônes alluviaux, les mégafans, les plaines alluviales et les zones d'anastomose. Toutes ce zones ont en commun de montrer des diffluences menant à une diminution de la taille de chenaux vers l'aval.

La principale conclusion de Hartley et al. (2010) est que les DFS, constituent, à l'heure actuelle une part non négligeable des systèmes fluviaux et que ces objets et les modèles de faciès qui leur sont particuliers (Fisher et al., 2007), devraient être pris en compte dans l'enregistrement stratigraphique alors que la plupart des modèles de faciès utilisés pour identifier les différents type de cous d'eau (Miall, 1996, 1985) est basée sur des exemples actuels pris dans des systèmes contributifs. L'enjeu principal de ces deux conceptions des systèmes fluviaux est l'amélioration de la compréhension de la continuité et la connectivité dans les réservoirs fluviaux d'hydrocarbures. En effet, dans la vision "distributive" des systèmes fluviaux, la taille de chenaux se réduit vers l'aval suite aux bifurcation et points d'avulsions créant le système distributif (Fisher et al., 2007; Hartley et al., 2010; Weissmann et al., 2013). Au contraire dans un système contributif, la taille des chenaux (et donc des réservoirs potentiels) s'accroit vers l'aval. On comprend aisément les conséquences de ces deux modèle en termes d'exploration et de modélisation des réservoirs.

Si les différents acteurs de ce débat s'accordent sur l'existence des deux types de systèmes fluviaux à la fois à l'actuel et dans l'enregistrement sédimentaire, l'état actuel du débat en est à chercher à savoir lequel des deux types constitue la "norme" dans l'enregistrement sédimentaire (Fielding et al., 2012). Il est donc d'un grand intérêt d'identifier, dans l'enregistrement sédimentaire les caractéristiques des systèmes fluviaux.

Ces deux modèles sont basés sur une observation exhaustive des systèmes fluviaux actuels par le biais d'imagerie satellite (Hartley et al., 2010; Fielding et al., 2012). Cependant, l'imagerie satellitaire nous permet d'observer des objets actifs mais aussi les traces d'évolution ancienne (Bernal et al., 2011). Blum and Aslan (2006) montrent qu'une l'imagerie doit être observée et interprétée comme une carte géologique, tous les objets observés n'ayant pas le même âge. On peut donc se poser la question de savoir ce que l'on observe réellement : des objets actuels ou anciens ? L'observation des objets actuels ou quaternaires supérieur est-elle aussi pertinente en tant qu'analogue de l'enregistrement stratigraphique ? En effet, comme indiqué dans le paragraphe 2.1.6, les systèmes fluviaux quaternaires enregistrent et réagissent à des fluctuations climatiques sous forme de cycles glaciaires/interglaciaire à haute fréquence. Ces systèmes ne sont donc pas forcément transposables à des périodes où le caractéristiques du climat étaient toutes autres.

Dans ce contexte, l'étude de la mise en place et de l'évolution du système fluvial du piémont subandin d'Equateur, contemporain du remplissage du bassin d'avant-pays subandin se révèle d'un

grand intérêt (Bernal et al., 2011; Christophoul et al., 2014). Depuis le début du Néogène, le bassin évolué en un seul dépocentre, du fait du faible taux de raccourcissement associé à la croissance du prisme orogénique d'avant-pays,(Baby et al., 2013). Ce dépocentre préserve plus de 3000 m de séries fluviatiles au sein desquelles on peut noter une ingression "marine" s'échelonnant entre le Miocène inférieur et le Pléistocène (Fig. 2.12). L'ensemble de ces séries décrivent

Par rapport au modèle "distributif" il ressort de l'étude de l'évolution récente du système fluvial du piémont des Andes d'Equateur (Bernal et al., 2011) qu'un DFS n'apparaît pas forcément en tant que tel à un instant "t" (avec des bifurcations et plusieurs cours actifs) mais doit être conçu comme un objet dynamique. Observé aujourd'hui, le Rio Pastaza est une composante du réseau contributif du bassin de l'Amazone. Cependant envisagé sur les derniers 20 000 ans, en balayant plus de 60 000 km2, le Rio Pastaza délimite en effet un DFS. Une telle remarque a été adressée par Fielding et al. (2012) à Hartley et al. (2010) concernant la plaine Indo-Gangétique arguant du fait que le réseau est au premier ordre contributif. Cette plaine comporte néanmoins deux exemples de DFS (la Kosi et la Tista) sur lesquels un seul cours d'eau est actif à l'heure actuelle (Chakraborty and Ghosh, 2010; Wells and Dorr, 1987) mais dont l'évolution récente en tant que système distributif est particulièrement bien contrainte (sur 300 ans).

La conclusion de de l'analyse ci-dessus est qu'un réseau hydrographique, sur les zones de piémont, n'est définitivement ni contributif, ni distributif. Ces deux types d'organisation du réseau de drainage correspondent à un instantané dans des contextes particuliers au sein d'un objet dynamique qu'est le système fluvial soumis à des cycles d'aggradation/incision. Cette conclusion peut-être étendue à d'autres objets comme le piémont nord-pyrénéen (Christophoul, 2013). Cet aspect sera développé dans mon projet de recherche (voir paragraphe 2.2.5).

2.1.8 Conclusions

Sur les dernières années, mes travaux axés sur la compréhension des systèmes alluviaux à différentes échelles de temps ont permis de mieux comprendre les phénomènes de courte durée (instantané à quelques centaines d'années) afin d'améliorer leur identification dans le registre fossile.

A l'échelle du phénomène d'avulsion (quelques heures à quelques jours ou cumulé sur un siècle), l'étude des avulsions du Rio Pastaza ont permis de mettre en évidence leur importance dans le développement des morphologies anastomosées et des systèmes distributifs actuels en lien avec l'aggradation fluviale sur le piémont andin et au sens large sur les piémonts orogéniques.

L'étude des changements morphologiques des cours d'eau à l'échelle du millier d'années notamment dans le cadre de l'étude de la Garonne à la transition Pléistocène supérieur/Holocène a permis de mettre en évidence le rôle des forçages climatiques et de proposer un scénario original quant à l'influence du type de régime hydrologique et ses conséquences sur le rôle de la végétation dans le cadre de la transition tresses/méandres.

L'étude du DFS du Rio Pastaza depuis le LGM montre que les zones de piémonts lors des périodes d'aggradation sont favorable au développement des systèmes distributifs.

Enfin, ces résultats appliqués à des systèmes qui se sont développés sur plusieurs millions d'années (piémont andin d'Equateur depuis le Néogène) permettent de mettre en évidence la prépondérance du contrôle tectonique (subsidence flexurale à long terme dans un bassin d'avant chaine) dans le controle de l'aggradation fluviale, le potentiel de développement et de préservation des DFS dans un tel contexte.

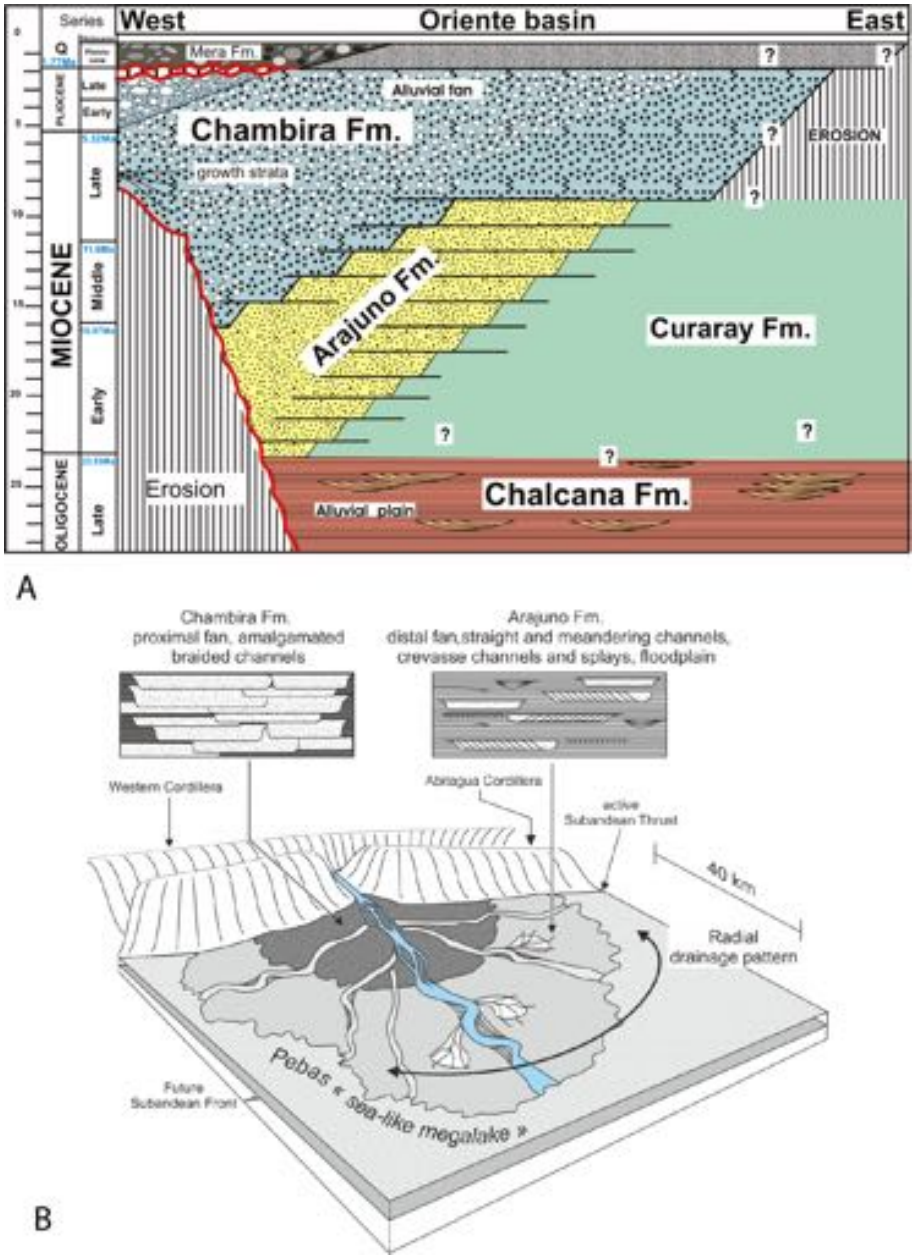

FIGURE 2.12 – Architecture stratigraphique des formations néogènes du bassin Subandin d'Equateur (Christophoul et al., 2014). A : Schéma temps espace du néogène du bassin Subandin d'Equateur, B : Reconstitution schématique du piémont subandin d'Equateur au Miocène Moyen/Supérieur.

2.2 Projet de Recherches

2.2.1 Résumé

Mon projet de recherches concerne les interactions tectonique/climat/érosion/sédimentation sur les piémonts orogéniques et post-orogéniques. Il a pour but d'améliorer la compréhension des mécanismes contrôlant l'aggradation fluviale sur les piémonts dans différents contextes : les piémonts actifs où la tectonique des bassins d'avant-chaîne est le facteur de contrôle prépondérant et les piémonts passifs où les forçages climatiques sont plus à même de s'exprimer. Ce projet a pour but de répondre aux questions suivantes :

1. Comment se traduisent les forçages tectoniques dans l'architecture stratigraphique d'un rétro-bassin d'avant-pays durant son stade synorogénique ?
2. Quelle est l'influence respective des forçages tectoniques et climatiques dans l'enregistrement sédimentaire sur les piémonts post-orogéniques ?
3. Quels facteurs contrôlent le développement de certains types de morphologies fluviales sur les piémonts orogéniques ?

Ces problématiques seront appliquées sur des objets, actuels ou anciens tels que les séries syn-foreland du Bassin d'Aquitaine, le piémont post-orogénique nord-pyrénéen et le piémont amazonien des Andes.

Ces questions structurent les axes de mon projet de recherche. Ces axes s'échelonnent entre le court terme (Axe 4, paragraphe 2.2.6), des échéances intermédiaires (Axe 1, paragraphe 2.2.3 et Axe 3, paragraphe 2.2.5) et le long terme (Axe 2, paragraphe 2.2.4). Ce projet de recherche s'appuiera sur des collaboration locales, nationales et internationales.

Les axes 1 et 3 sont en cours. Ils correspondent aux tâches au sein desquelles je suis impliquée dans le cadre du projet ANR Blanc 2012-2016 PYRAMID et du projet OROGEN (TOTAL-BRGM-INSU), le financement pour leur mise en œuvre est acquis. Les axes 2 et 4 feront l'objet de demandes de financement dans les années à venir.

2.2.2 Problématique

Au passage du front topographique, un cours d'eau débouchant sur un piémont peut adopter deux dynamiques différentes en termes de relations érosion/ sédimentation :

— Déposer tout ou partie de sa charge sédimentaire et construire son lit sur ses propres sédiments. On parlera donc d'aggradation.

— Eroder le substratum par érosion verticale, horizontale ou une composée des deux. On parlera de piémont en incision.

Sur les piémonts en aggradation, les cours d'eau sont en équilibre instable et sont soumis à des fréquentes avulsions, modifiant leur cours et permettant la dispersion des sédiments qu'ils transportent sur d'importantes surfaces. Les piémonts en aggradation, du fait de l'important alluvionnement et des ressources en eaux disponibles, génère des terres arables particulièrement fertiles et fortement peuplées mais dont instabilité de cours d'eau et leur fréquentes avulsions soumettent les populations à des risques d'inondations, de destructions d'habitat et d'infrastructures. Deux exemples récents illustrent cette instabilité et ses conséquences : l'avulsion partielle de la Kosi sur le piémont himalayen (Chakraborty et al., 2010) qui a causé plus de 300 000 sinistrés et les inondations/avulsion des années 1930 du Fleuve Jaune (Li and Finlayson, 1993) (Fig. 2.13) qui fut à l'origine de 1 300 000 morts (Fig.2.13).

Du fait de l'importance de ces instabilités de la morphologie des cours d'eau et leur conséquences en matières d'aménagement il est important de comprendre les facteurs qui contrôlent ces dynamiques. Sur les piémonts des chaînes de montagne, la dynamique des des cours d'eau peut-être contrôlée par des processus autocycliques, mais aussi par des forçages externes tel que climatiques. Dans le cas d'un piémont orogénique, les forçages tectoniques viennent se rajouter aux forçages climatiques. Ces forçages peuvent s'exprimer à l'échelle locale (associés à un faille active par exemple) ou à échelle régionale par l'intermédiaire de moteurs à grande longueur d'onde tels que la flexure des

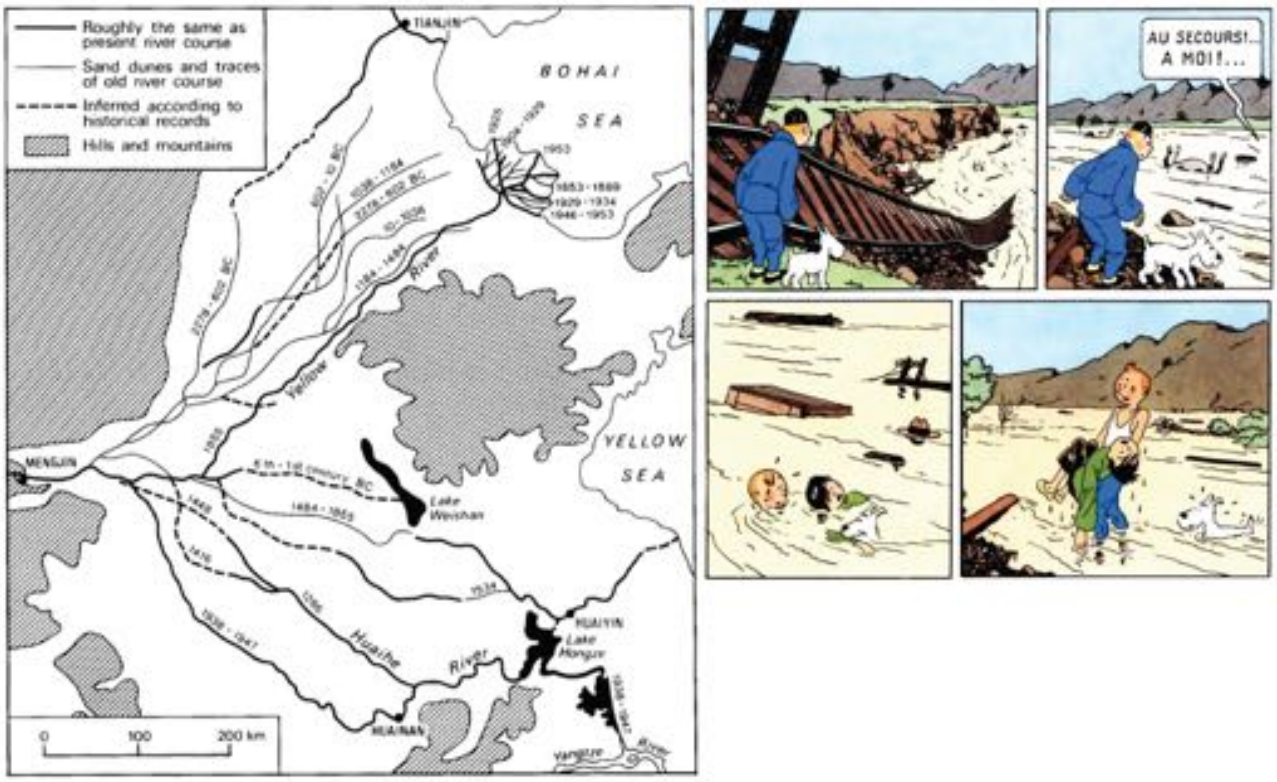

FIGURE 2.13 – Avulsions du Fleuve Jaune.
A gauche : cours successifs du Fleuve Jaune depuis le 2276 Av. J.C. (modifié de Li and Finlayson, 1993). A droite : les inondations/avulsions du Fleuve Jaune des années 30 telles qu'illustrées par Hergé dans "le Lotus Bleu" (Hergé, 1946).

plaques lithosphériques liées à l'orogène ou des mouvement verticaux à l'échelle de la chaîne dans son ensemble (réajustement isostatique consécutif à l'érosion de la chaîne ou "orogenic unloading").

L'évolution d'une chaîne de montagne et celle des bassins d'avant-chaîne qui lui sont associés va être à l'origine de cycles aggradation/incision qui vont s'enregistrer dans le remplissage sédimentaire des bassins ainsi que par une signature particulière dans la géomorphologie des piémonts associés au chaines de montagne.

Les piémonts vont donc, suivant la dynamique prépondérante des cours d'eau qui le parcourent montrer un réseau de drainage au géométrie différentes. Les piémonts en incisions, se caractérisent par un réseau hydrographique de type contributif alors que les piémonts aggradants, du fait des fréquentes avulsions qui s'y produisent se caractérisent par un réseau hydrographique de type distributif. Dans le paragraphe 2.1.7, j'ai exposé l'état du débat sur la prépondérance des réseau de type distributif par rapport aux réseaux de type contributifs et leur importance dans l'enregistrement sédimentaire (Sambrook Smith et al., 2010; Weissmann et al., 2010; Fielding et al., 2012; Weissmann et al., 2013).

En conséquence, il semble pertinent de chercher à savoir comment s'expriment les cycles aggradation/incision dans l'enregistrement stratigraphique. Et comment les phases d'incision vont recouper les systèmes distributifs et comment ils vont influer sur les propriétés d'éventuels réservoirs qui peuvent en résulter.

On peut donc se demander :

1. Comment se traduisent les forçages tectoniques dans l'architecture stratigraphique d'un piémont orogénique associé à un rétro-bassin d'avant-pays durant son stade synorogénique ?
2. Quelle est l'influence respective des forçages tectoniques et climatiques dans l'enregistrement sédimentaire sur les piémonts post-orogéniques ?
3. Quels facteurs contrôlent le développement de certains types de morphologies fluviales sur les piémonts orogéniques ?

Afin de répondre à ces questions, mon projet de recherche se structure en quatre axes de recherches. Les prochains paragraphes détaillent chacune de ces questions, leur problématique propre, l'objet d'étude le plus approprié à apporter des réponses significatives ainsi que les méthodes pertinentes à mettre en œuvre.

2.2.3 Axe 1 : Séries synorogéniques du bassin d'avant-pays nord-pyrénéen

Problématique La chaîne des Pyrénées (Fig. 2.14)résulte de la collision de de l'Ibérie et de l'Eurasie entre le crétacé supérieur et l'Oligocène. Il en résulte une chaîne de montagne structurée autour d'un prisme orogénique à double vergence. La charge topographique exercée par ce prisme orogénique sur les deux plaque lithosphérique ibérique et eurasienne est à l'origine de deux bassins flexuraux (bassin de l'Ebre au sud et la bordure sud du bassin d'Aquitaine au nord, constituant le bassin d'avant-pays nord-pyrénéen.

Depuis les travaux de Riba (1976), les discordances progressives (ou structures de croissance ou growth strata) sont les objets privilégiés pour tracer la déformation sur les fronts de chaines plissées et l'évolution tectono-sédimentaire dans les bassins d'avant-pays. Ces structures de croissances ont été identifiées en grand nombre dans le bassin d'avant-pays sud-pyrénéen(Riba, 1976; Puigdefabregas and Souquet, 1986; Déramond et al., 1993; Ford et al., 1996) permettant de mettre en évidence la propagation du prisme de chevauchement sud-pyrénéen entre le crétacé supérieur et l'Oligocène. Dans le bassin d'avant-pays nord-pyrénéen, de telles structures sont peu décrites (Tambareau et al., 1995; Christophoul et al., 2003) (Fig. 2.15). Le bassin d'avant-pays nord-pyrénéen étant positionné en position de retro-foreland, cette absence de discordances progressives peu apparaître comme l'expresssion d'une propagation moindre du prisme orogénique, induisant des taux de raccourcissement plus faibles ayant comme conséquence des dépocentres successifs superposés limitant le développement de structures de croissances ou les limitant spatialement.

On peut donc se demander si il existe une spécificité des retro-bassins d'avant-pays dans leur évolution tectono-stratigraphique (Naylor and Sinclair, 2008). Comment se disposent les dépocentres successif dans ce contexte ? Quelle est la chronologie de la déformation dans ce contexte particulier ?

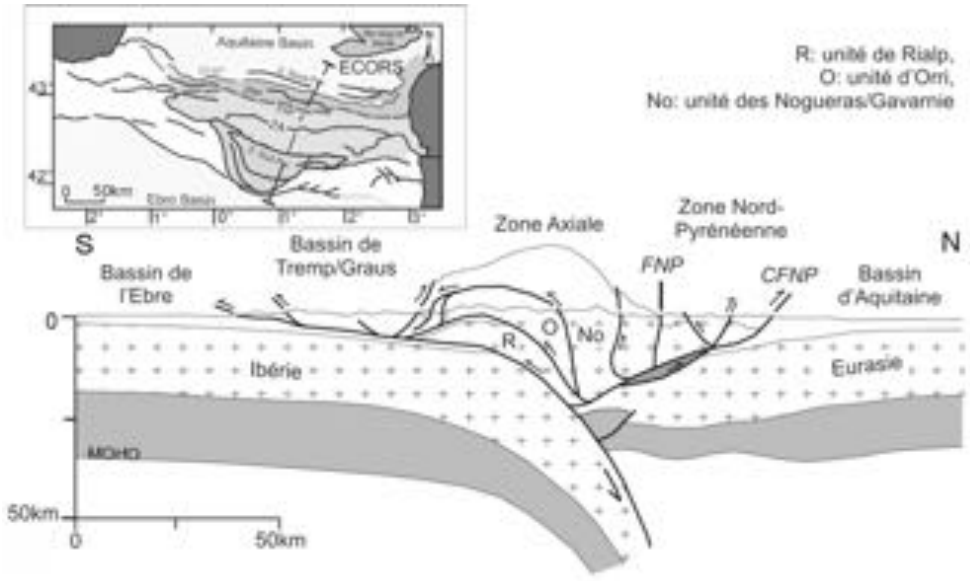

FIGURE 2.14 – Coupe structurale des Pyrénées le long du profil ECORS (modifié de Muñoz (1992) ; Filleaudeau (2011))

Mise en œuvre Afin de contraindre le cadre stratigraphique de l'évolution du bassin d'avant-pays, nord-pyrénéen, il est nécessaire de synthétiser la nombreuse littérature disponible sur le bassin d'Aquitaine, réviser les âges stratigraphique et réinterpréter les nombreuses données de puits d'exploration (disponible dans les bases de données du BRGM) ainsi que des données de sismique réflexion afin d'établir les schémas chronostratigraphiques permettant de visualiser l'architecture stratigraphique du bassin. Ces schémas seront construits le long de coupes structurales nord-sud mais aussi le long de profils est-ouest afin de mettre en évidence la composante parallèle à la chaine de l'évolution des systèmes sédimentaires au cours du temps. L'interprétation des lignes sismique sera l'occasion de mettre en évidence des structures de croissances jusque là ignorée permettant de préciser le timing et la cinématique de la déformation entre la zone Nord-pyrénéenne et la zone sous-pyrénéenne.

A côté de cette synthèse, l'acquisition de données de terrain (sédimentologie, paléocourants) ainsi que de la thermochonologie basse température et de traçage de sources permettra de contraindre les zones d'apport et l'organisation du système sédimentaire au cours du temps en relation avec l'exhumation de la chaîne.

Cet axe de recherche constitue la tâche 2 de l'ANR Pyramid. Il se base sur des collaborations nationales (BRGM, M. Ford, Nancy). Ce point est en cours d'avancement, un premier article (Ford et al., Rev) est en révision. Cet axe se prolongera, pour l'étude des stades précoces du bassin d'avant-pays par un post-doc dans le cadre du Projet TOTAL-BRGM-INSU "OROGEN"

2.2.4 Axe 2 : Contrôle de l'aggradation fluviale sur le piémont amazonien des Andes

Cet axe de recherche est le prolongement de mes travaux sur la compréhension des processus fluviaux sur le piémont amazonien des Andes. Après des études qui se sont focalisées sur l'identification des processus d'avulsion à grande échelle : à l'échelle de l'anabranche (Bernal et al., 2013), d'un tronçon de rivière (Bernal et al., 2012) ou d'un mégafan (Bernal et al., 2011), je souhaite comprendre les processus de construction des piémonts à plus petite échelle : celle d'un piémont orogénique dans sa globalité afin de mettre en évidence quels phénomènes à grande longueur d'onde contrôlent l'aggradation fluviale sur un piémont.

Problématique Dans le concept du Sediment routing system (Allen, 2008)(Fig. 2.16), les sédiments transportés des reliefs vers les océans ("source to sink") peuvent suivre des trajectoires

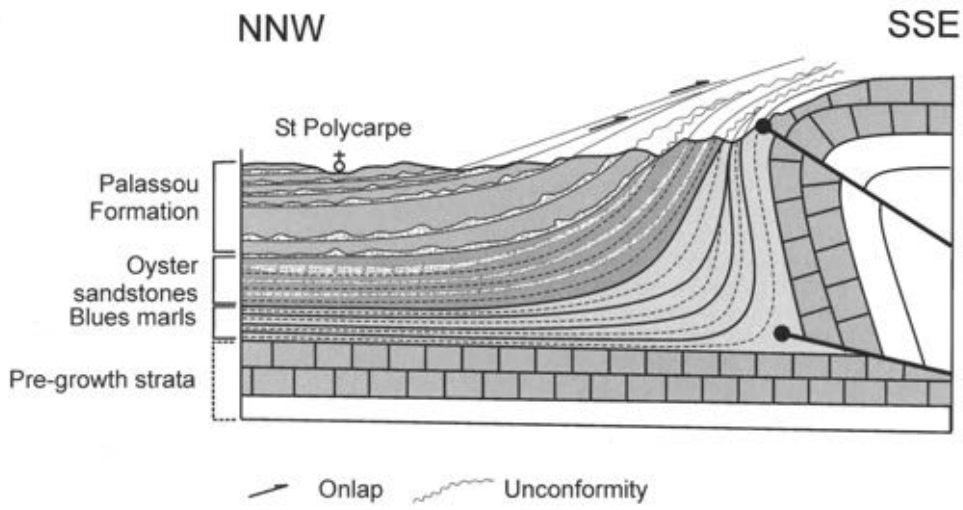

FIGURE 2.15 – Coupe au front du Massif de Mouthoumet
montrant le dispositif en discordance progressive des séries éocènes (Christophoul et al., 2003).

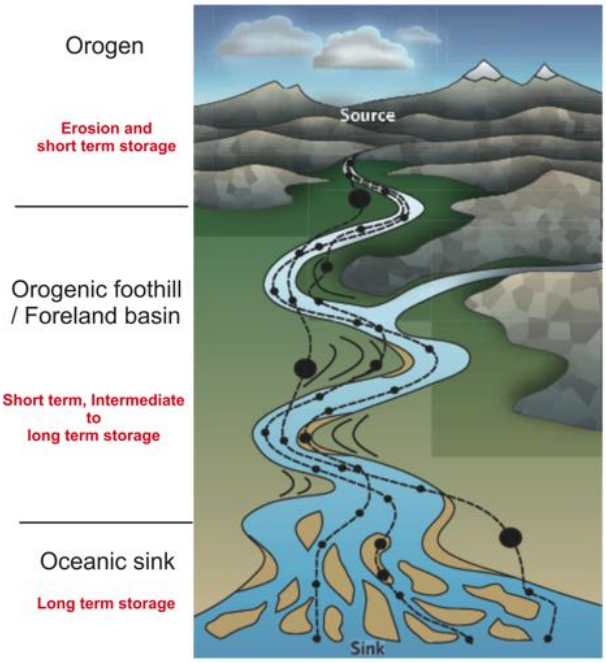

FIGURE 2.16 – Modèle conceptuel de "sediment routing system"
(modifié de Allen (2008))

courtes ou longues suivant qu'ils restent dans le lit mineur ou qu'ils sont temporairement stockés dans la plaine d'inondation. Le réseau fluvial joue dans ce cas un rôle de tampon entre le relief et les marges océaniques (Castelltort and Van Den Driessche, 2003). Si on applique ce concept de "sediment routing system" à un bassin d'avant-pays DeCelles and Giles (1996); Catuneanu (2004), le "foredeep" du bassin va :

1. Préserver temporairement les sédiments, jusqu'à ce que la propagation du front de chevauchement intègre la partie proximale du "foredeep" dans le prisme orogénique et provoque leur érosion ou :
2. Préserver de manière beaucoup plus définitive les sédiments déposés, à l'échelle des temps géologiques, dans les bassins sédimentaires où on peut encore les observer à l'heure actuelle, dans le bassin d'avant-pays sud-pyrénéen (e.gDéramond et al. (1993); Puigdefabregas and Souquet (1986); Homewood et al. (1986)),

Dans ce contexte, se pose la question des volume de sédiments préservés dans les bassins d'avant-chaine et sur quelle échelle de temps ces sédiments vont etre préservés avant d'etre remobilisés par l'érosion avant d'etre transportés vers un "sink" océanique "définitif". Sur le piémonts en aggradation, ces sédiments sont majoritairement préservés dans des DFS (voir paragraphe 2.1.7), on peut donc se demander quel est le volume de sédiments préservés dans les "Distributives Fluvial Systems"? Classiquement, la détermination des volumes de sédiments préservés dans les bassins sédimentaires se fait par le biais d'un cubage basé sur l'interprétation de sismique réflexion (Clift, 2006; Clift et al., 2008; Rouby et al., 2009) Cependant, ce type d'études ne peut être entreprise que sur des longues périodes de temps ou des marges océaniques océaniques ou la préservation des sédiments exportés des continents est meilleure. Mener ce type d'étude sur des objets subactuels et actuels en domaine continental n'est pas envisageable avec des données de sismique réflexion. En effet, ces objets correspondent aux premières millisecondes des coupes sismiques, souvent bruitées, ou les réflecteurs sont peu continus et difficilement corrélables. Il est donc nécessaire d'envisager le calcul des volumes préservé dans les DFS et au sens large sur les piémonts actifs par des méthodes alternatives.

La sédimentation sur les piémont orogénique est souvent concentrée dans des cônes alluviaux, fluviaux (mégafans) et au sens large dans des "Distributive Fluvial Systems" ou "DFS" (Hartley et al., 2010; Leier et al., 2005; Weissmann et al., 2013) comme on peut le constater sur le piémont sud-himalayen(plaine Indo-Gangétique avec les cônes de la Tista et de la Kosi (Wells and Dorr, 1987; Chakraborty and Ghosh, 2010) ou sur le piémont amazonien des Andes avec les cônes des Rio Pilcomayo, Beni, Parapeti (Horton and DeCelles, 2001; Barnes and Heins, 2009) ou du Rio Pastaza (Bernal et al., 2011).

Sur les piémonts orogéniques, les DFS se forment au débouché du front topographique et jouent un rôle majeur dans la dispersion des sédiments et la localisation des zones de sédimentation dans les bassins d'avant-pays suralimentés (Hartley et al., 2010; Leier et al., 2005). De part leur taille, leur pente moyenne, ils contituent des unités géomorphologiques à part entière. Là où les cônes alluviaux se construisent par la superposition et la juxtaposition de lobes successifs dominé par des processus gravitaires (Schumm et al., 1987; Blair and McPherson, 1994), la sédimentation dans les mégafans est dominée par des processus de bifurcations et d'avulsions d'un cours d'eau principal.

La présence des DFS et des cours d'eau à morphologie anastomosée est à l'origine d'interprétations automatiques : "si il y a anastomose, c'est qu'il y a de l'aggradation et si il y a de l'aggradation c'est qu'il y a de la subsidence". Ces interprétations rapides ne prennent pas en compte de nombreux paramètres qui peuvent générer une morphologie anastomosée. Smith (1986) a proposé que les morphologies anastomosées soient liées à la subsidence, mais en faisant allusion à une subsidence locale et pas à l'échelle du bassin. Cependant, les causes d'avulsion et donc de mise en place d'anabranches n'est pas nécessairement due à la subsidence flexurale du bassin Jones and Schumm (1999); Makaske (2001). Un piémont se construit par aggradation et cette aggradation se fait en domaine continental. Une aggradation fluviale sur un piémont peut donc se faire sans la moindre subsidence.

La question sous-entendue ci-dessus est donc : Le développement de morphologies anastomosées dans les bassins d'avant pays est elle un indicateur de subsidence régionale (flexurale dans le cas

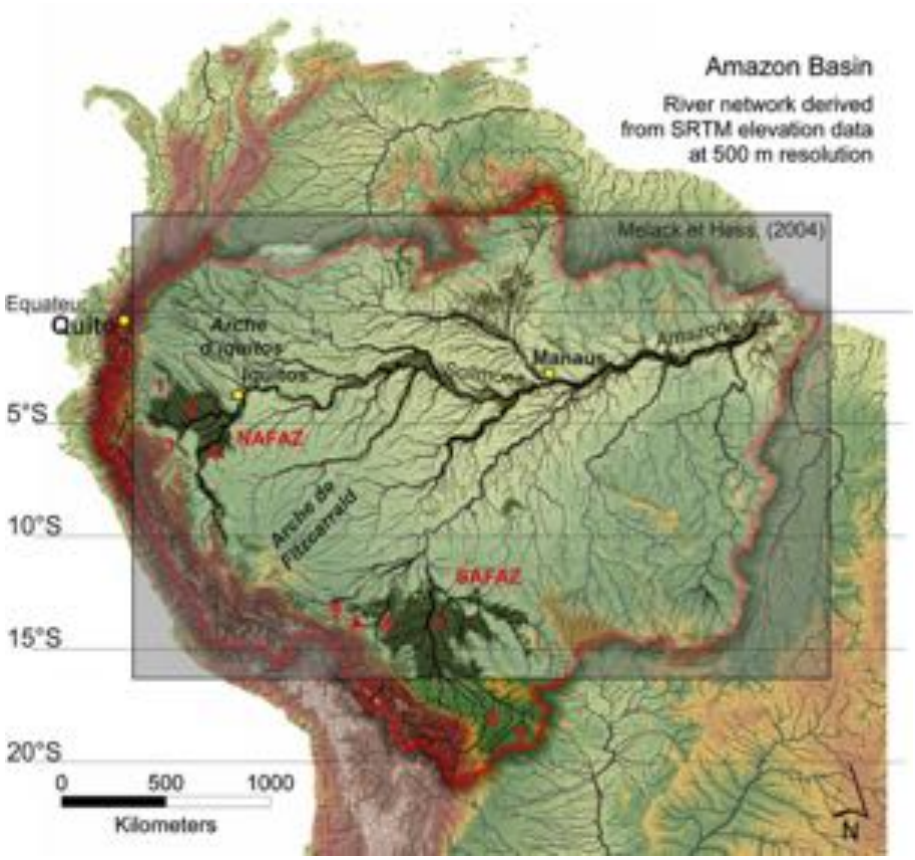

FIGURE 2.17 – Bassin de l'Amazone et morphologie du piémont subandin.
En noir : réseau hydrographique (épaisseur croissante avec l'ordre de Stralher). En superposition : carte des zones de plaine d'inondation dans le bassin de l'Amazone Mellack and Hess (2004), les zones en vert olive sont les zones de plaine d'inondation. Zones d'agradation fluviale : au nord : NAFAZ (North Amazonian Fluvial Aggradation Zone) avec : 1 : Rio Pastaza, 2 : Rio Marañon, 3 : Rio Huallaga, 4 : cours inférieur du Rio Ucayali ; au sud : SAFAZ : South Amazonian Fluvial Aggradation Zone, incluant : 5 : Rio Grande, 6 : 7 : Rio Mamoré, 8 : Rio Beni, 9 : Rio Ixiamas. D'après Roddaz et al. (2005); Regard et al. (2009); Martinez and Le Toan (2007); Wilkinson et al. (2010).

de ces bassins) ou le reflet de réponses du réseau hydrographique à des contextes locaux ?

Objet d'étude Afin de répondre aux questions posées dans le paragraphe précédent, le piémont amazonien des Andes est un bon cas d'étude. Du point de de l'organisation du réseau fluvial, le piémont Amazonien des Andes (Fig. 2.17) présente, du nord au sud, une alternance de zones d'aggradation fluviale (NAFAZ et SAFAZ, Fig.2.17 et de zones en incision (Arche d'Iquitos et Arche de Fitzcarrald, Fig.2.17). Les deux zones d'aggradation fluviale peuvent être mise en évidence par la cartographie des plaines d'inondation (Mellack and Hess, 2004; Martinez and Le Toan, 2007). A nord, l'Arche d'Iquitos constitue la partie exhumée du bourrelet périphérique du Bassin d'Avant-pays Nord-Amazonien (Roddaz et al., 2005, 2010). Le relief positif de l'Arche de Fitzcarrald est l'expression en surface de la subduction de la ride de Nazca sous la chaîne des Andes et son avant-pays. Ce relief est du à la faible densité de la ride, imposant une subduction plane et provocant une déformation de surface de la plaque subductée (Espurt et al. (2007); Regard et al. (2009)). La NAFAZ La sédimentation dans l'avant-pays est contrôlé à la fois par la subsidence flexurale du bassin à l'échelle de l'histoire de l'avant-pays Roddaz et al. (2005, 2010) et à l'actuel : le piémont des Andes assure une grande partie du piégeage des sédiments exporté depuis les Andes(Aalto et al., 2003; Baby et al., 2009). Cependant, on peut se poser la question de savoir sice piégeage est le fait de la subsidence flexurale du bassin ou de la dispersion "à l'horizontale" des sédiments du fait des

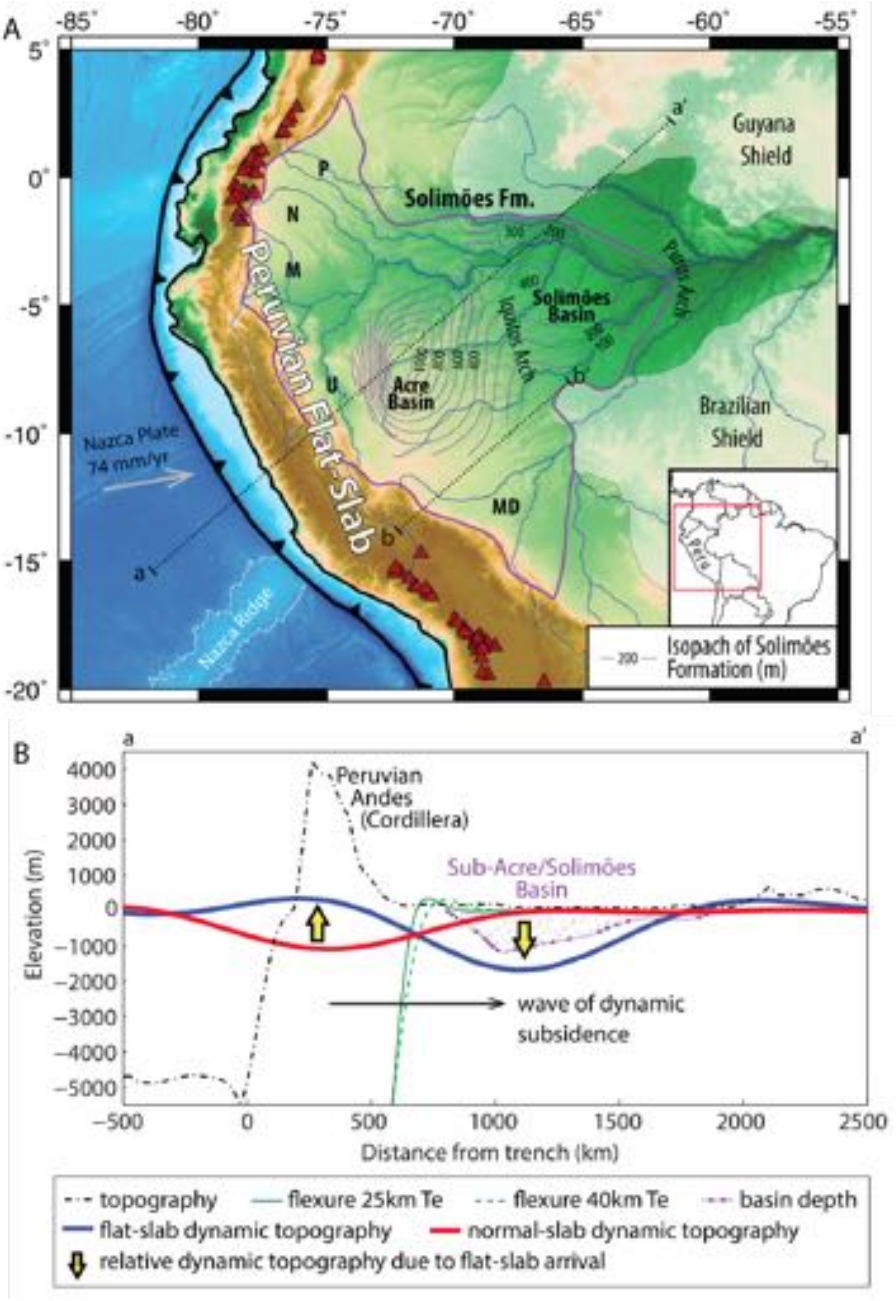

FIGURE 2.18 – Contexte tectonique de la subduction plate du Perou
A :Sous-bassins : P : Putumayo, N : Napo, M : Marañon, U : Ucayali, MD : Madre de Dios. Limites de la Formation Solimões en violet, isopaques en blanc. Triangles rouges : volcans. B : Profils illustrant les différentes contributions à la topographie totale dans le bassin Amazonien. (Eakin et al., 2014)

fréquentes avulsions des cours d'eau.

Depuis les dernières années, la géodynamique de la subduction andine et l'origine du déversement de l'Amazone dans l'Océan atlantique a généré plusieurs interprétations Eakin et al. (2014); Espurt et al. (2007); Sacek (2014); Shephard et al. (2010, 2012) Toutes ces études s'accordent sur un rôle prépondérant de la subsidence flexurale dans la localisation des dépocentres successifs dans le bassin (Eakin et al., 2014), (Fig. 2.18). Cependant, ces études sont basées sur des profils 2D et ne permettent pas d'expliquer la répartition actuelle des zones d'aggradation fluviales actuelles ni la variation latérale de la distribution des dépocentres au cours du temps.

Mise en œuvre Ce projet s'articule autour de 2 chantiers :

1. Calcul des volumes de sédiments préservés dans les DFS du piémont Amazonien.

   Compte tenu de l'étendu des DFS du piémont amazonien des Andes et de la diversité des contextes climatiques dans lesquels ils se développent (entre 0° et 20° de latitude sud) (Fig. 2.17), il est nécessaire de s'intéresser à au moins un exemple dans chaque zone d'aggradation fluviale du piémont. Dans la zone d'aggradation nord amazonienne (NAFAZ, Fig. 2.17), deux objest se prête particulièrement à cette approche : le DFS du Rio Pastaza que j'"tudie depuis de nombreuses années (Bernal et al. (2011, 2012, 2013); Christophoul et al. (2014)) et le cours inférieur du Rio Ucayali (Fig. 2.19). Dans la zone d'aggradation sud amazonniene (SAFAZ, Fig. 2.17), le DFS du Rio grande en Bolivie présente des caractéristique morphologiques différentes à même d'illustrer l'expression d'un contexte climatique et hydrologique différent de ceux de la NAFAZ.

   Chacun de ces objets fera l'objet d'une cartographie morphologique. Cette cartographie sera complétée par des datations (^{14}C, ^{10}Be) des différents éléments architecturaux (plaine d'inondation, levées) afin de contraindre les taux de sédimentation. La morphologie des rides alluviales et notamment leur épaisseur sera contrainte par imagerie géophysique (tomographie électrique, Ground Penetrating Radar).

   A partir de cette cartographie et des datations des rides alluviales et des taux de sédimentation, le calcul des volumes se fera en prenant en compte chaque composant autour de la ride alluviale (Fig. 2.20) chenal, levées naturelles et la zone de plaine d'inondation alimentée par la ride. Le volume global est la somme des volumes piégés par chaque ride alluviale.

   La quantification des volumes préservés sur le piémont, comparés aux flux exportés depuis les Andes à diverses échelles de temps (Aalto et al. (2006, 2003); Baby et al. (2009); Barnes and Heins (2009); Barnes and Pelletier (2006)) permettra de quantifier le rôle de tampon du piémont dans les transferts de sédiments vers le "sink" que constitue le cône de l'Amazone.

   Cet aspect sera mis en œuvre à partir de collaborations locales (V. Regard, J. Darrozes, M. Llubes, GET, Toulouse) et internationales (S. Bernal, EPN, Quito, Equateur, G. Weissman, Univ. New Mexico, Albuquerque).

2. Modélisation 3D de la subsidence sur le piémont Amazonien des Andes

   Afin de quantifier et de localiser les zones de subsidence actuelle dans le bassin retroarc subandin des Andes, il est nécessaire de reconstituer l'histoire de subsidence du bassin en 3D, prenant en compte la géométrie non cylindrique (nombreuses virgations) de la chaine andine et ses variations de largeur (1 000 km en Bolivie, 100 km en Equateur) qui vont influer sur la charge tectonique exercée sur la plaque sud-américaine.

   Cet aspect sera basé sur une compilation des données concernant les propriétés de la lithosphère de la plaque sud-américaine (composition, rigidité) ainsi que des isopaques des séries sédimentaires préservées dans les bassins subandins. Ces données sont disponibles dans la litérature ou inédites et accessibles via des collaborations internationales.

   La modélisation 3D de la subsidence sra effectuée sous Flex 3D.

   Cette tache de compilation et de modélisation 3D de la subsidence le long du piémont andin se basera sur des collaborations locales (A. Robert, D. Rouby et P. baby, GET, toulouse).

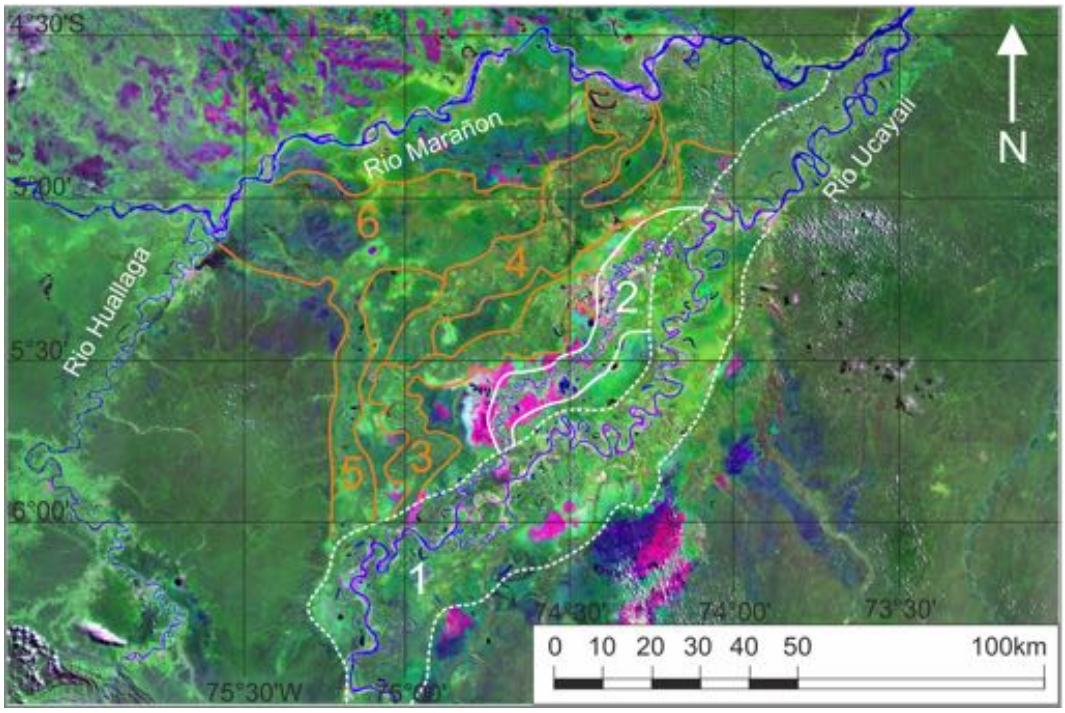

FIGURE 2.19 – Cartographie des rides alluviales du cours inférieur du Río Ucayali (nord Pérou)
1 : ride active, 2 : ride ré-annexée, 3 to 6 : rides abandonnées

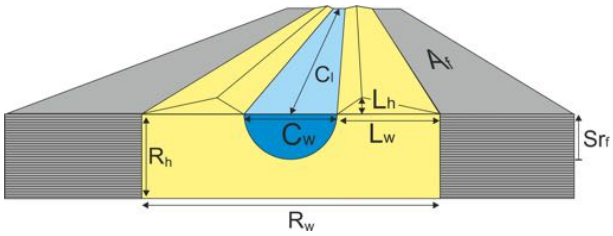

FIGURE 2.20 – Volumes préservés dans une ride alluviale à partir de la géométrie des éléments architecturaux
Avec R_w : largeur de la ride alluviale, R_h : hauteur de la ride, C_l : longueur de chenal, C_w : largeur de chenal, L_w : largeur de levée, L_h : hauteur de levée, A_f : surface de la plaine d'inondation, Sr_f : taux de sédimentation dans la plaine d'inondation.

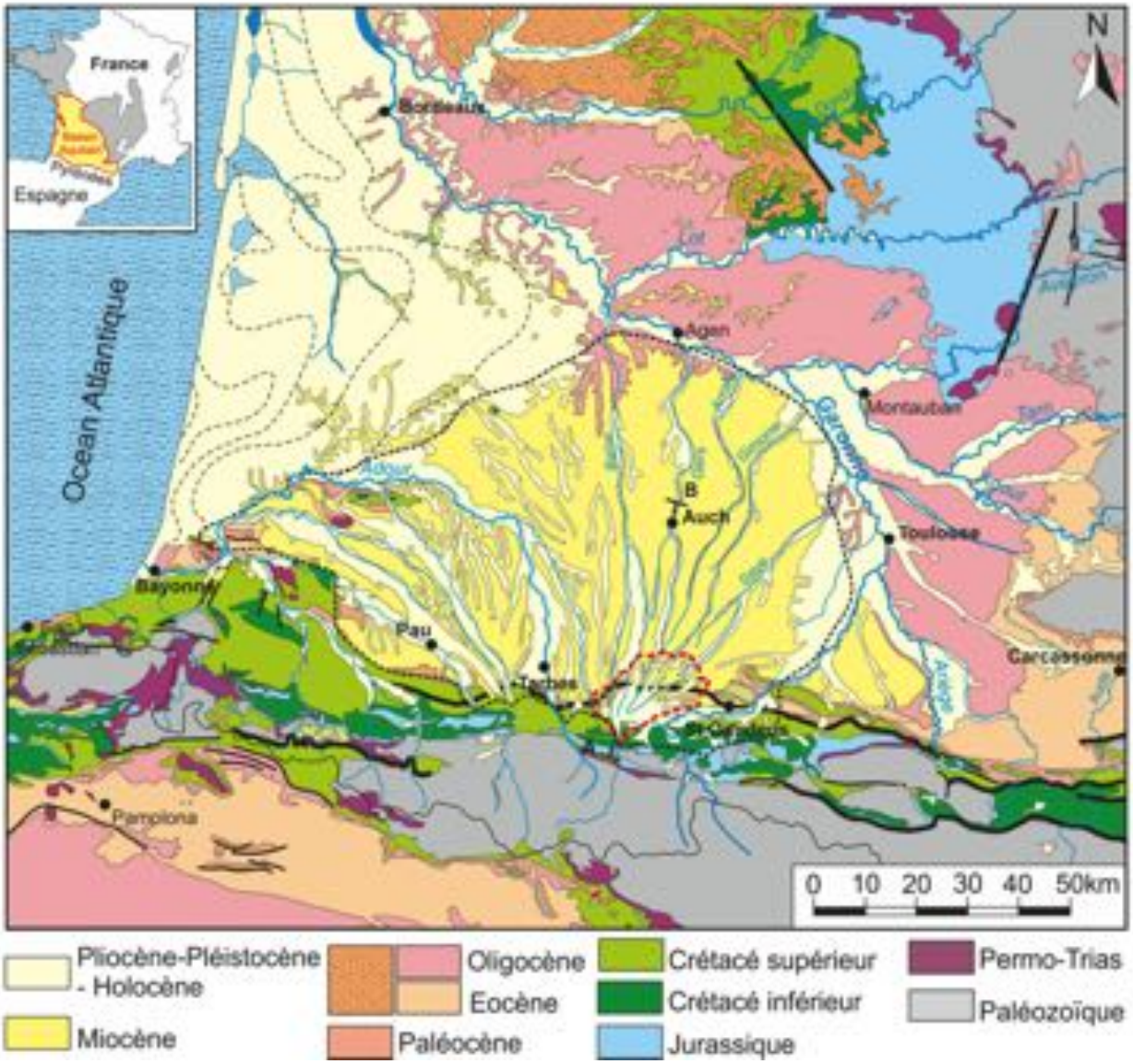

FIGURE 2.21 – Carte géologique des Pyrénées et du Bassin Aquitain (modifié de B.R.G.M. et al. (1974)).

2.2.5 Axe 3 : Un piémont orogénique "post-foreland" : le piémont nord-pyrénéen

Problématique Si l'étude des bassins d'avant-pays est à l'origine d'une littérature importante (voir paragraphe 2.2.3), les stades post-foreland on peu retenu l'attention. A côté de l'exemple des séries des Pyrénées synorogéniques et du Piémont Amazonien actuel des Andes où les forçages tectoniques sont prépondérants et afin de s'affranchir d'un trop forte expression de ce forçage dans la l'architecture stratigraphique et la morphologie du piémont, il est nécessaire de s'intéresser à des cas où le forçage tectonique est moins prépondérant ou s'exprime à plus grande longueur d'onde. L'étude d'un piémont "passif" est le lieu privilégié pour examiner l'architecture stratigraphique propre à un système dominé par des forçages externes (climatiques).

Objet d'étude Dans ce contexte, le piémont nord pyrénéen post-foreland (Fig.2.21) est un cas intéressant. Les études récentes ont montré que depuis le Miocène, les principaux chevauchement dont le raccourcissement accommode la convergence Ibérie/Eurasie cessent de fonctionner (Ortuno et al., 2008; Filleaudeau, 2011; Ortuno et al., 2013), montrant que les bassins d'avant-pays liés à l'orogène pyrénéen passe d'un stade syn-foreland à un stade post-foreland. A l'heure actuelle le

moteur de la sismicité des Pyrénées est lié à une déformation crustale superficielle à l'origine de mécanisme aux foyers essentiellement normaux Vernant et al. (2013).

Le piémont post-foreland nord-pyrénéen s'est développé au pied des relief et occupe à l'heure actuelle la majeure partie de la partie sud du Bassin d'Aquitaine. Ce piémont, à l'heure actuelle montre un réseau hydrographique en éventail (Fig. 2.21). Ce dispositif en éventail est nommé "cône de Lannemezan". Au sens strict, le "cône de Lannemezan" Alimen (1964); Icole (1969a,b, 1973) est limité au débouché de la Vallée des Nestes et n'occupe que le "Plateau de Lannemezan" (en pointillé rouge sur la Fig. 2.21 (Icole, 1969b, 1973). Il s'agit d'une formation détritique grossière (certains blocs sont de taille métrique, Icole (1969b, 1982))à matrice argilo-sableuse affleurant mal et affectée par un profil d'altération (Alimen, 1964; Icole, 1973) rendant la caractérisation de son organisation faciologique originelle difficile. Ce "cône de déjection" n'est pas le seul et trois édifices similaires (cône de Ger, cône de l'Adour et Cône de Lannemezan) constituent le piémont pliocène nord-Pyrénéen. Ce système des cônes alluviaux se superpose aux molasses miocènes d'Aquitaine(Crouzel, 1957). Ces molasses sont un assemblages complexe de conglomérats, de grès et de sables et de calcaires. Le matériel détritiques est en partie issu des Pyrénées mais aussi du Massif Central (Dubreuilh et al., 1995).

Par comparaison, le piémont sud-pyrénéen a été beaucoup plus étudié (Garcia-Castellanos et al., 2003; Babault et al., 2005). Ce deux piémonts, même si ils sont lié à la même chaîne de montagne, sont totalement différents. Le piémont sud-pyrénéen s'est édifié dans un contexte de bassin endorhéique (Garcia-Castellanos et al., 2003) qui a permis une agradation importante qui a recouvert en onlap les reliefs de la chaine jusqu'à des altitudes élevée (1800m). A l'opposé, le piémont nord-pyrénéen n'a pas connu d'épisode endorhéique et est resté, tout au long de son histoire sous le contrôle combiné de son bassin versant et du niveau de base marin de l'Océan Atlantique. Ce deux contextes différents laissent supposer une évolution sédimentologique et géomorphologique du piémont nord-pyrénéen radicalement différente de celle du versant sud.

D'un point de vue régional on peut donc se poser la question de la nature du piémont nord-pyrénéen : est-ce un ou plusieurs DFS ré-incisés durant le quaternaire ou bien une simple forme d'érosion résultant de l'incision d'un piémont rectiligne ? D'un point de vue plus général, existe-t-il une architecture stratigraphique caractéristique d'un piémont post-orogénique et si oui, en quoi se différencie-t-elle de celle des série synorogéniques ?

Mise en œuvre Afin de répondre à ces question, dans un premier temps, il est nécessaire d'établir l'architecture stratigraphique (distribution des faciès, définition de gradients proximaux-distaux, motif d'empilement des faciès) à partir de la nombreuse littérature ancienne sur le sujet (Alimen (1964); Crouzel (1957); Hubschman (1975e,d,a,b,c); Icole (1973, 1969b,a, 1982)) et de données de terrain notamment des données de paléocourants, absentes dans la littérature. Cette architecture sera contrainte du point de vue chronostratigraphique par la synthèse des nombreuses datations biostratigraphiques obtenues dans les vingts dernière années notamment à partir des grand mammifères (Richard (1948); Duranthon (1991); Antoine et al. (1997)). Cette architecture stratigraphique sera complétée par une étude des provenances sédimentaires (pétrographie des éléments figurés, minéraux lourds, isotopie de la fraction fine) dans le but de mettre en évidence la contribution des sources pyrénéenne et du Massif Central ainsi que pour définir quelles zones du piémont était sous influence pyrénéenne et du Massif Central(Fig. 2.22).

Cette étude sera complétée par des simulations numériqaues des processus de piémont (code CIDRE, S. Carretier) qui permettront d'examiner différents scénarios de relief initial et d'intensité de forçage quyi seront comparés à l'architecture stratigraphique observée et l'évolution morhologique du piémont qui en sera déduite.

Ce projet est en cours de réalisation. La problématique exposée ci-dessus correspond à la sous-tâche 3.2.1 "évolution post-orogénique du piémont nord-pyrénéen" du Projet ANR Pyramid. Il est basé sur des collaborations locales (V. Regard, S. Carretier, S. Bonnet, M. Roddaz) et nationales (P. Van der Beek, M. Mouchené, ISTerre, Grenoble).

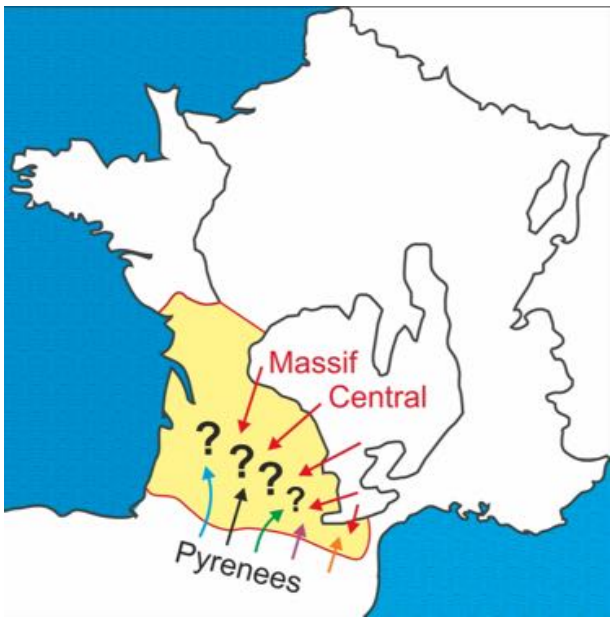

FIGURE 2.22 – Hypothèses de provenance des sédiments du piémont nord-pyrénéen.

2.2.6 Axe 4 : Processus fluviaux de piémont : la transition tresses/méandres

Cet axe de recherche constitue la suite du projet mené sur la compréhension de la mise en place des terrasses de la Garonne (Christophoul et al., subm). Un des éléments de discussion de cette étude propose une hypothèse quant aux relations hydrologie/végétation dans le cadre de la transition tresses/méandres dans les cours d'eaux à graviers. La vérification de cette hypothèse est l'occasion de proposer un projet réalisable à court terme basé sur des collaborations locales.

Problématique En géomorphologie fluviale, l'identification des paramètres contrôlant la transition tresses/ méandres est un vieux débat qui trouve ses applications aussi bien dans l'aménagement des cours d'eau (Walter and Merritts, 2008), la caractérisation des réservoirs d'hydrocarbures mais peut aussi servir d'outil prédictif pour l'évolution des cours d'eau dans un contexte de changement global. Depuis plus de 50 ans (Lane, 1957), les communautés de sédimentologues, géomorphologues et hydrauliciens ont examiné l'influence de nombreux paramètres sans pouvoir mettre en évidence de critère discriminant (van den Berg, 1995; Lewin and Brewer, 2001; Métivier and Barrier, 2012). Un synthèse exhaustive de l'évolution des concepts a été publiée récemment par Métivier and Barrier (2012) dressant un état de l'art sur la transition tresses/méandre dans la cours d'eau à charge de fond grossière en tresse et à méandres "gravel bed braided" and gravel meandering" rivers (Miall, 1985, 1996) De nombreux paramètres hydrauliques et morphologiques ont été tour à tour évoqués :

1. la pente en long du cours d'eau.van den Berg (1995), à partir d'une base de données de cours d'eau démontre qu'il existe une valeur seuil,au-delà de laquelle une rivière en tresse passe à une morphologie à méandres. Quelques années, plus tard, à partir de la même base de données, implémentée, Lewin and Brewer (2001) montre que cette valeur seuil n'existe pas et que les résultats de van den Berg (1995) sont la conséquence d'un base de données incomplète ou comportant des valeurs érronées.
2. le débit liquide : Le débit liquide influe sur le rayon hydraulique. Le changement de débit liquide tend à modifier ce rayon et donc les dimensions du chenal (largeur et profondeur) mais ne semble pas présenter de valeur seuil de débit provocant le passage d'une morphologie en tresse à méandriforme (Leopold and Maddock, 1953; Métivier and Barrier, 2012).
3. la charge de fond : Un changement brusque de la granulométrie et des flux transportées par charge de fond peut induire des changement morphologiques importants par une modification du critère de stabilité de Parker (Parker, 1976) et modifier le rapport d'aspect du chenal. Cependant, un changement important de la granulométrie transportées par charge

de fond ne va que marginalement modifier le rapport d'aspect du chenal et de manière insuffisante pour provoquer un changement morphologique majeur (Métivier and Barrier, 2012). Même si une modification des flux transportés par charge de fond peut conduire à des changements substantiels dans les valeurs des paramètres contrôlant la morphologie (Mackin, 1948), une des particularités des gravel-bed rivers" est d'avoir un transport par charge de fond faible (Schumm, 1963, 1977; Yalin and Da Silva, 2001; Parker et al., 2007). Brierley and Hickin (1991) propose d'ailleurs que les gravel meandering rivers ne soit que le résultat du remaniement *in-situ* des dépôts transportés par des cours d'eaux en tresse antérieurs et que le transport par charge de fond y soit presque nul. On peut donc supposer que dans les "gravel-bed rivers" le transport, par charge de fond étant faible, il ne va pas influer sur la morphologie du cours d'eau.

Néanmoins, depuis une trentaine d'années, deux paramètres retiennent l'attention : la présence de matériaux cohésifs sur les berges Carson (1984) et la végétation Tal and Paola (2007, 2010); Gibling and Davies (2012). Si ces paramètres semblent influer sur la morphologie des cours d'eau, les mécanismes les reliant sont encore peu connus. Il semble que les caractéristiques du régime hydrologique et notamment la position, dans l'année, de la période de hautes eaux par rapport à la période de croissance de la végétation puisse jouer un rôle Christophoul et al. (subm). Lors de la dernière déglaciation (débutée vers 34 ka Delmas et al. (2011) ou 30 Ka Andrieu-Ponel et al. (1988)) la Garonne voit sa morphologie passer de tresses à méandres (Christophoul et al., subm), (Fig. 2.11). Ce changement morphologique s'effectue en deux étapes, par une transition tresse/ méandre à faible sinuosité suivie d'une augmentation de la sinuosité

Or, vers 30 ka, on peut supposer que le régime hydrologique de la Garonne était de type glaciaire à l'image, par exemple, de nombreux cours d'eau actuels des Alpes Suisse (Fig.2.23). Dans ce type de régime hydrologique, le pic de hautes eaux dans les cours d'eau est atteint en Août (période de fonte maximale du glacier suivant le pics de températures estivales) et la période de basses eaux intervient en hiver (pas de fonte des glaciers et rechargement par les chutes de neige). La montée des basses vers les hautes eaux se produit au printemps. La période de germination et de croissance de la végétation se fait au printemps et en été (les dates exactes sont fluctuantes en fonction du climat local et de l'altitude). Il en résulte que durant la période de croissance de la végétation, le cours d'eau affiche un débit important et la probabilité pour que les barres de graviers dans le lit mineur soit recouvertes par les eaux est importante. La possibilité de colonisation des bancs de graviers par la végétation est donc réduite.

A l'occasion de l'étude des changements de morphologie fluviale enregistrés dans le remplissage de la basse terrasse de la Garonne (Christophoul et al., subm), j'ai été amené à me poser la question des relations existant entre le régime hydrologique de la Garonne, la colonisation par la végétation et leurs conséquences en terme de changement morphologique.

En Effet, au cours de la déglaciation, le régime hydrologique de la Garonne s'est modifié vers un régime hydrologique de type pluvio-nival (régime actuel de la Garonne). Sur la Figure 2.23, on remarque que le pic de hautes eaux se produit durant le printemps et la baisse vers les basses eaux a lieux entre le printemps et l'été, période de germination et de croissance de la végétation. Il en résulte que lors de la période de croissance de la végétation, la probabilité pour que les barres de graviers, dans le lit mineur, soient découvertes est plus importante que dans le cadre d'un régime hydrologique de type glaciaire.

En conséquences, il apparaît que si la végétation joue un rôle prépondérant sur la stabilisation des bancs dans le lit mineur et sur les berges, cela n'est rendu possible que par un contexte hydrologique favorable caractérisé par un pic de hautes eaux se produisant en phase, au cours du cycle hydrologique, avec la période de croissance de la végétation (Christophoul et al., subm). Dans ce cas, il apparaît donc que l'interaction entre l'hydrologie du cours d'eau et la végétation est à l'origine de la transition tresses/méandres.

Mise en œuvre La Figure 2.23 illustre cette hypothèse établie sur l'exemple ancien de la Garonne durant le Pléistocène supérieur doit être vérifiée dans l'actuel. Afin de tester cette hypothèse, plutôt que de s'intéresser à des exemples ponctuels illustrant des contextes particuliers, l'approche la plus

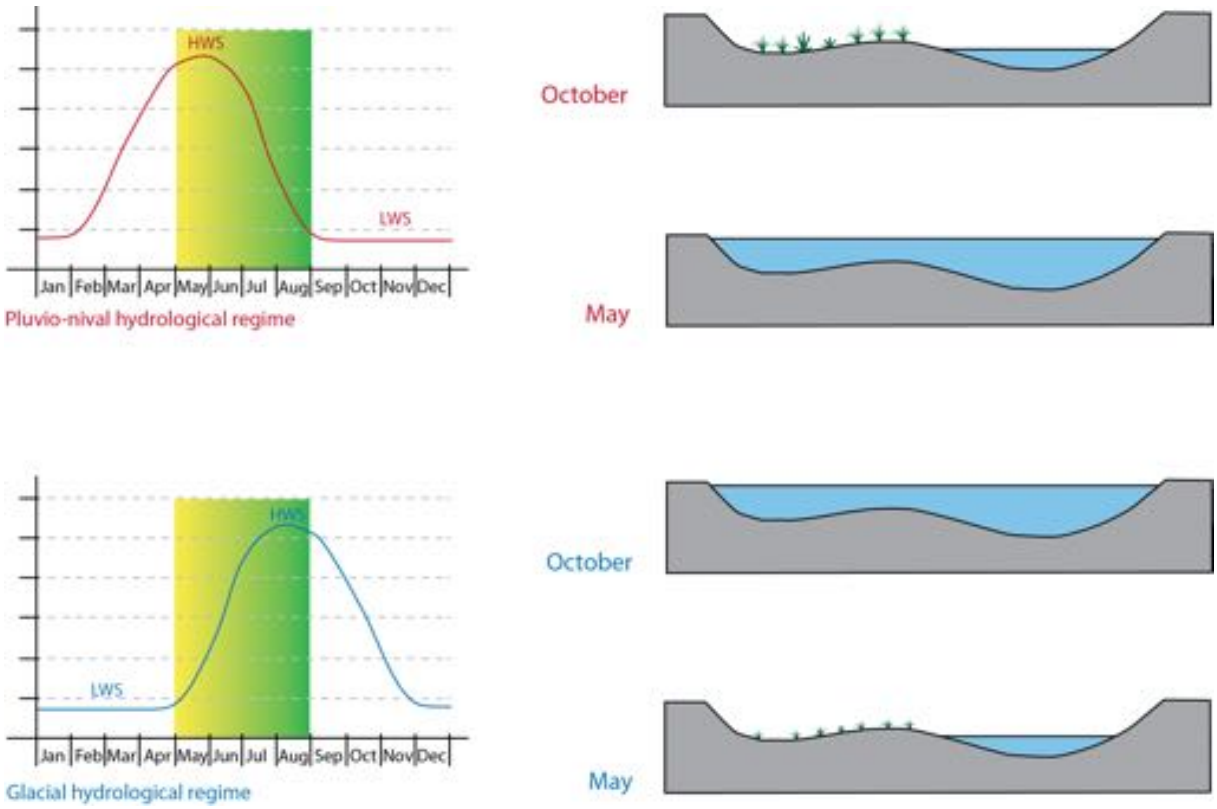

FIGURE 2.23 – Interactions régime fuvial / croissance de la végétation.
Hypothèse sur le rôle de la position de la période de hautes eaux (HWS) dans l'année par rapport à la période de croissance de la végétation (dégradé jaune/vert) sur la stabilisation des bancs dans le lit mineur d'un cours d'eau (d'après Christophoul et al. (subm)).

pertinente,

Si les bases de données concernant la morphologie et l'hydrologie des cours d'eau sont nombreuses (Osterkamp and Hedman, 1982; Church and Rood, 1983; Parker et al., 2007; Métivier and Barrier, 2012), peu d'entre-elles intègrent des données concernant la végétation (Andrews, 1984; Hey and Thorne, 1986; Huang and Nanson, 1997; Rowntree and Dollar, 1999). Cependant, ces bases de données intègrent la végétation en tant qu'agent physique de la stabilisation des berges et pas sa dynamique de croissance.

Dans un premier temps, il est donc nécessaire d'implémanter une base de données à partir des bases existantes (Osterkamp and Hedman, 1982; Church and Rood, 1983; Andrews, 1984; Hey and Thorne, 1986; Huang and Nanson, 1997; Rowntree and Dollar, 1999; Parker et al., 2007; Métivier and Barrier, 2012) comportant les caractéristiques physiques des cours d'eau (largeur, profondeur, rapport d'aspect, granulométrie de la charge de fond, pente en long, style fluvial). Ces données seront ensuite géoréférencées afin de pouvoir extraire, en fonction de la latitude et de la topographie les caractéristiques générales du climat local.

Dans un deuxième temps, les caractéristiques du régime hydrologique des cours d'eau sera intégré à partir de bases de données locales ou mondiales disponibles. Les caractéristiques de la végétation seront intégrées à partir de données bibliographiques (type de végétation, période de croissance dans l'année...).

A partir de cette base de données, une série de tests statistiques permettront de vérifier la représentativité de la base de données aussi bien du point de vue de la distribution des données en fonction des contextes climatiques que des répartitions saisonnières des pics de débit au sein du régime hydrologique.

Perspectives Cette question, à l'interface entre la géomorphologie, l'hydrologie et l'écologie fera l'objet, dans un premier temps, d'une proposition de sujet de Master 2 pour les Master Terre et Planètes et H2SE afin de mettre en place la base de donnée et de d'effectuer des tests statistiques, en co-encadrement avec Vincent Regard (MCU,Géomorphologue, GET) et Elise Nardin (CR, Traitement statistique, GET). A plus long terme, cette question pourrait se poursuivre par une thèse de doctorat en collaboration avec des spécialistes en écologie (Eco-Lab, Toulouse) et de biogéomorphologie (Dov Corenblit, MCU, Univ. Descartes, Clermont-Ferrand).

Bibliographie

Aalto, R., Dunne, T., and Guyot, J.-L. (2006). Geomorphic controls on andean denudation rates. *The Journal of Geology*, 114(1) :85–99.

Aalto, R., Maurice-Bourgoin, L., Dunne, T., Montgomery, D., Nittrouer, C., and Guyot, J.-L. (2003). Episodic sediment accumulation on amazonian flood plains influenced by el niño/southern oscillation. *Nature*, 425(6957) :493–497.

Alimen, H. (1964). Le quaternaire des pyrénées de la bigorre. In *Mémoire du service de la Carte Géologique de la france*, page 394. Service de la carte Géologique de la france.

Allen, P. (2008). From landscapes into geological history. *Nature*, 451(7176) :274–276.

Andrews, E. D. (1984). Bed-material entrainment and hydraulic geometry of gravel-bed rivers in colorado. *Geological Society of America Bulletin*, 95(371-378).

Andrieu-Ponel, V., Eicher, U., and Reille, M. (1993). La fin du dernier pléniglaciaire dans les pyrénéees (france) : donnéees polliniques, isotopiques et radiométriques. *Comptes rendus de l'Académie des sciences. Série II. Mécanique, physique, chimie, sciences de l'univers, sciences de la terre*, 316. Multilingue.

Andrieu-Ponel, V., Hubschman, J., Jalut, G., and Hérail, G. (1988). Chronologie de la dégladation des pyrénées françaises. dynamique de sédimentation et contenu pollinique des paléolacs ; application à l'interprétation du retrait glaciaire. *Bulletin de l'Association française pour l'étude du quaternaire*, 25(2) :55–67.

Antoine, P. (1993). Le système des terrasses du bassin de la somme : modèle d'évolution morpho-sédimentaire cyclique et cadre paléoenvironnemental pour le paléolithique. *Quaternaire*, 4(1) :3–16.

Antoine, P., Munaut, A.-V., Limondin-Lozouet, N., Ponel, P., Dupéron, J., and Dupéron, M. (2003). Response of the selle river to climatic modifications during the lateglacial and early holocene (somme basin-northern france). *Quaternary Science Reviews*, 22(20) :2061–2076.

Antoine, P.-O., Duranthon, F., and Tassy, P. (1997). L'apport des grand mammifères (rhinocérotidés, suoïdés, proboscidiens) à la connaissance des gisements du miocène d'aquitaine. In Aguilar, J.-P., Legendre, S., and Michaux, J., editors, *Biochrom' 97*, volume 21 of *Mémoire des travaux de l'EPHE, Institut de Montpellier*, pages 581–590.

Babault, J., Van Den Driessche, J., Bonnet, S., Castelltort, S., and Crave, A. (2005). Origin of the highly elevated pyrenean peneplain. *Tectonics*, 24 :TC2010, doi :10.1029/2004TC001697.

Baby, P., Guyot, J.-L., and Hérail, G. (2009). Tectonic control of erosion and sedimentation in the amazon basin of bolivia. *Hydrological Processes*, 23(22) :3225–3229.

Baby, P., Rivadeneira, M., Barragan, R., and Christophoul, F. (2013). Thick-skinned tectonics in the oriente foreland basin of ecuador. *Geological Society, London, Special Publications*, 377 :18.

Barberi, F., Coltelli, M., Ferrara, G., Innocenti, F., Navarro, J.-M., and Santacroce, R. (1988). Plio-quaternary volcanism in ecuador. *Geological Magazine*, 125(1) :1–14.

Barnes, J. and Heins, W. (2009). Plio-quaternary sediment budget between thrust belt erosion and foreland deposition in the central andes , southern bolivia. *Basin Research*, 21 :91–109.

Barnes, J. and Pelletier, J. (2006). Latitudinal variations of denudation in the evolution of the bolivian andes. *American Journal of Science*, 306 :1–31.

Bernal, C., Christophoul, F., Darrozes, J., Laraque, A., Bourrel, L., Soula, J.-C., Guyot, J.-L., and Baby, P. (2013). Crevassing and capture by floodplain drains as a cause of partial avulsion and anastomosis (lower rio pastaza, peru). *Journal of South American Earth Sciences*.

Bernal, C., Christophoul, F., Darrozes, J., Soula, J.-C., Baby, P., and Burgos, J. (2011). Late glacial and holocene avulsions of the rio pastaza megafan (ecuador–peru) : frequency and controlling factors. *International Journal of Earth Sciences*, 100(7) :1759–1782.

Bernal, C., Christophoul, F., Soula, J.-C., Darrozes, J., Bourrel, L., Laraque, A., Burgos, J., Bès de Berc, S., and Baby, P. (2012). Gradual diversions of the rio pastaza in the ecuadorian piedmont of the andes from 1906 to 2008 : role of tectonics, alluvial fan aggradation, and ENSO events. *International Journal of Earth Sciences*, 101(7) :1913–1928.

Bès de Berc, S., Soula, J., Baby, P., Souris, M., Christophoul, F., and Rosero, J. (2005). Geomorphic evidence of active deformation and uplift in a modern continental wedge-top–foredeep transition : Example of the eastern ecuadorian andes. *Tectonophysics*, 399(1-4) :351–380.

Blair, T. C. and McPherson, J. G. (1994). Processes and forms of alluvial fans. In Abrahams, A. and Parsons, A., editors, *Geomorphology of desert Environments*, pages 354–402. Chapman and Hall, London.

Blum, M. and Aslan, A. (2006). Signatures of climate vs. sea-level change within incised valley-fill successions : Quaternary examples from the texas gulf coast. *Sedimentary Geology*, 190(1) :177–211.

Bourgeat, F., Icole, M., and Revel, J. C. (1984). Les terrasses alluviales dans les petites-pyrénées et l'avant-pays molassique : les conditions de leur mise en place. *Bulletin de l'Association française pour l'étude du quaternaire*, 21(1) :60–66.

B.R.G.M., E.L.F.-R.E., ESSO-R.E.P., and S.N.P.A. (1974). *Géologie du Bassin d'Aquitaine*. B.R.G.M, Orléans.

Bridgland, D. R. and Westaway, R. (2008). Climatically controlled river terrace staircases : A worldwide quaternary phenomenon. *Geomorphology*, 98(3-4) :285–315.

Brierley, G. J. and Hickin, E. J. (1991). Channel planform as a non-controlling factor in fluvial sedimentology : the case of the squamish river floodplain, british columbia. *Sedimentary Geology*, 75(1-2) :67–83.

Bruxelles, L. and Jarry, M. (2011). Climatic conditions, settlement patterns and cultures in the paleolithic : The example of the garonne valley (southwest france). *Journal of Human Evolution*, 61(5) :538–548.

Büdel, J. (1977). *Klima-Geomorphologie*. Gebrüder Bornträger, Berlin.

Bull, W. B. (1964). Geomorphology of egmented alluvial fans in western fresno county, california. *United States Geological Survey, Professionnal Paper*, (352-E) :89–128.

Bull, W. B. and McFadden, L. D. (1977). Tectonic geomorphology north and south of the garlock fault, cailfornia. In Doerhing, D., editor, *Geomorphology in Arid Regions*, pages 115–138. 8th Annual Geomorphology Symposium, Binghampton, New York State University at Binghampton.

Carozza, J.-M., Carozza, L., Valette, P., Llubes, M., Py, V., Galop, D., Danu, M., Ferdinand, L., David, M., Sévègnes, L., Bruxelles, L., Jarry, M., and Duranthon, F. (2014a). The subfossil tree deposits from the garonne valley and their implications on holocene alluvial plain dynamics. *Comptes Rendus Geoscience*, 346(1-2) :20–27.

Carozza, J.-M., Philippe, V., Laurent, C., Muriel, L., Laurie, F., Serge, E. O., and Laurent, S. (2013). L'architecture morpho-sédimentaire de la basse plaine de la moyenne garonne en aval de toulouse : premiers résultats. 24(4) :397–406. Français.

Carozza, J.-M., Valette, P., Carozza, L., Llubes, M., Ferdinand, L., Edou Obame, S., and Sévègnes, L. (2014b). L'architecture morpho-sédimentaire de la basse plaine de la garonne moyenne en aval de toulouse : premiers résultats. *Quaternaire*.

Carson, M. (1984). The meandering-braided river threshold : A reappraisal. *Journal of Hydrology*, 73(3-4) :315–334.

Castelltort, S. and Van Den Driessche, J. (2003). How plausible are high-frequency sediment supply-driven cycles in the stratigraphic record ? *Sedimentary Geology*, 157(1-2) :3–13.

Catuneanu, O. (2004). Retroarc foreland systems—-evolution through time. *Journal of African Earth Sciences*, 38(3) :225–242.

Chakraborty, T. and Ghosh, P. (2010). The geomorphology and sedimentology of the tista megafan, darjeeling, himalaya : Implications for megafan building processes. *Geomorphology*, 115 :252–266.

Chakraborty, T., Kar, R., Ghosh, P., and Basu, S. (2010). Kosi megafan : Historical records, geomorphology and the recent avulsion of the kosi river. *Quaternary International*, 227 :143–160.

Christophoul, F. (1999). *Discrimination des influences tectoniques et eustatiques dans les bassins liés à des zones de convergence : exemples du bassin subandin d'Equateur*. PhD thesis, Université Toulouse 3, Paul Sabatier.

Christophoul, F. (2013). the post-foreland fluvial systems of the north pyrenean foothill (aquitaine basin, france). In *ICFS 10*. International Conference of Fluvial sedimetnology, 14-19 July 2013, University of Leeds, UK.

Christophoul, F., Baby, P., and Dávila, C. (2002a). Stratigraphic responses to a major tectonic event in a foreland basin : the ecuadorian oriente basin from eocene to oligocene times. *Tectonophysics*, 345(1-4) :281–298.

Christophoul, F., Baby, P., Soula, J.-C., Rosero, M., and Burgos, J. (2002b). The neogene fluvial systems of the ecuadorian foreland basin and dynamic inferences. *Comptes Rendus Geoscience*, 334(14) :1029–1037.

Christophoul, F., Burgos, J., Baby, P., Soula, J.-C., Bes de Berc, S., Davila, C., Rosero, M., and Rivadeneira, M. (2004). Dinamica de la cuenca de ante-pais oriental desde el paleogeno. *Travaux de l'Institut Français des Etudes Andines*, 144(93-114).

Christophoul, F., Burgos Zambrano, J., Roddaz, M., Bernal, C., Antoine, P.-O., Soula, J.-C., and Baby, P. (2014). Onset and development of a distributive fluvial system in the amazon basin (neogene of the oriente basin of ecuador). *Geological society of London Special Publication*, XXX :XXX–XXX.

Christophoul, F., Regard, V., Martinod, J., and Darrozes, J. (subm.). Morphodynamics of the upper pleistocene garonne river (SW france) : conditions of braiding/meandering transition. *Geomorphology*. GEOMOR-4935.

Christophoul, F., Soula, J.-C., Brusset, S., Elibana, B., Roddaz, M., Bessiere, G., and Deramond, J. (2003). Time, place and mode of propagation of foreland basin systems as recorded by the sedimentary fill : examples of the late cretaceous and eocene retro-foreland basins of the north-eastern pyrenees. *Geological Society, London, Special Publications*, 208(1) :229–252.

Church, M. and Rood, K. (1983). *Catalogue of alluvial river channel regime data*. The University of British Columbia, Department of Geography.

Clift, P. (2006). Controls on the erosion of cenozoic asia and the flux of clastic sediment to the ocean pd clift. *Earth and Planetary Science Letters*, 241(3) :571–580.

Clift, P. D., Hodges, K. V., Heslop, D., Hannigan, R., VanLong, H., and Calvès, G. (2008). Correlation of himalayan exhumation rates and asian monsoon intensity. *Nature Geoscience*, 1(12) :875–880.

Cordier, S., Harmand, D., Frechen, M., and Beiner, M. (2006). Fluvial system response to middle and upper pleistocene climate change in the meurthe and moselle valleys (eastern paris basin and rhenish massif). *Quaternary Science Reviews*, 25(13-14) :1460–1474.

Cordier, S., Harmand, D., Lauer, T., Voinchet, P., Bahain, J.-J., and Frechen, M. (2012). Geochronological reconstruction of the pleistocene evolution of the sarre valley (france and germany) using OSL and ESR dating techniques. *Geomorphology*, 165-166 :91–106.

Corenblit, D., Davies, N. S., Steiger, J., Gibling, M. R., and Bornette, G. (2014a). Considering river structure and stability in the light of evolution : feedbacks between riparian vegetation and hydrogeomorphology : CONSIDERING RIVER STRUCTURE AND STABILITY IN THE LIGHT OF EVOLUTION. *Earth Surface Processes and Landforms*, pages n/a–n/a.

Corenblit, D., Steiger, J., González, E., Gurnell, A. M., Charrier, G., Darrozes, J., Dousseau, J., Julien, F., Lambs, L., Larrue, S., Roussel, E., Vautier, F., and Voldoire, O. (2014b). The biogeomorphological life cycle of poplars during the fluvial biogeomorphological succession : a special focus on *Populus nigra* l. : THE BIOGEOMORPHOLOGICAL LIFE CYCLE OF POPLARS. *Earth Surface Processes and Landforms*, 39(4) :546–563.

Crouzel, F. (1957). *Le Miocène continental du bassin d'Aquitaine*. PhD thesis, Faculté des Sciences de Toulouse, France.

Danzeglocke, U., Jöris, O., and Weninger, B. (2007). CalPal-2007online.

Davies, N. S. and Gibling, M. R. (2010). Cambrian to devonian evolution of alluvial systems : The sedimentological impact of the earliest land plants. *Earth Science Reviews*, 98(3-4) :171–200.

DeCelles, P. G. and Giles, K. A. (1996). Foreland basin systems. *Basin Research*, 8(2) :105–123.

Delmas, M., Calvet, M., Gunnell, Y., Braucher, R., and Bourlès, D. (2011). Palaeogeography and 10be exposure-age chronology of middle and late pleistocene glacier systems in the northern pyrenees : Implications for reconstructing regional palaeoclimates. *Palaeogeography, Palaeoclimatology, Palaeoecology*, 305(1-4) :109–122.

Déramond, J., Souquet, P., Fondecave, M.-J., and Specht, M. (1993). Relationships between thrust tectonics and sequence stratigraphy surfaces in foredeeps : model and examples from the pyrenees (cretaceous-eocene, france, spain). *Geological society of London Special Publication*, 71(193-219).

Diaz, M., Baby, P., Rivadeneira, M., and Christophoul, F. (2004). El pre-aptense dela cuenca oriente ecuatoriana. *Travaux de l'Institut Français des Etudes andines*, 144 :23–45.

Dubreuilh, J., Capdeville, J.-P., Farjanel, G., Karnay, G., Platel, J.-P., and Simon-Coinçon, R. (1995). Dynamique d'un comblement continental néogène et quaternaire : l'exemple du bassin d'aquitaine. *Géologie de la france*, 4(1) :3–26.

Duranthon, F. (1991). Biozonation des molasses oligo-miocènes de la région toulousaine par l'étude des mammifères. apports à la connaissance du bassin d'aquitaine (france). *Comptes Rendus de l'Académie des Sciences - Series II*, 313 :965–970.

Eakin, C. M., Lithgow-Bertelloni, C., and Dávila, F. M. (2014). Influence of peruvian flat-subduction dynamics on the evolution of western amazonia. *Earth and Planetary Science Letters*, 404 :250–260.

Einsele, G. (1992). *Sedimentary Basins : evolution, facies and sediment budget*. Springer, Berlin, Heidelberg.

Espurt, N., Baby, P., Brusset, S., Roddaz, M., Hermoza, W., Regard, V., Antoine, P.-O., Salas-Gismondi, R., and Bolaños, R. (2007). How does the nazca ridge subduction influence the modern amazonian foreland basin ? *Geology*, 35(6) :515.

Fielding, C. R., Ashworth, P. J., Best, J. L., Prokocki, E. W., and Sambrook Smith, G. H. (2012). Tributary, distributary and other fluvial patterns : What really represents the norm in the continental rock record ? *Sedimentary Geology*, 261-262 :15–32.

Filleaudeau, P.-Y. (2011). *Croissance et dénudation des Pyrénées du Crétacé Supérieur au Paléogène : Apports de l'analyse de bassin et thermochronométrie détritique*. PhD thesis, UPMC, Paris, FRANCE.

Fisher, J. A., Nichols, G. J., and Waltham, D. A. (2007). Unconfined flow deposits in distal sectors of fluvial distributary systems : Examples from the miocene luna and huesca systems, northern spain. *Sedimentary Geology*, 195 :55–73.

Ford, M., Hemmer, L., Vacherat, A., and Christophoul, F. (Rév.). Retrowedge foreland evolution along the eastern ecors profile. a tectono-sedimentary record of the eastern pyrenean orogenesis. *Journal of the Geological Society of London*.

Ford, M., Williams, E. A., Artoni, A., Vergès, J., and Hardy, S. (1996). Progressive evolution of a fault related fold pair from growth strata geometries, sant llorenç de morunys, SE pyrenees. *Journal of structural Geology*, 19 :413–441.

Garcia-Castellanos, D., Vergés, J., Gaspar-Escribano, J., and Cloetingh, S. (2003). Interplay between tectonics, climate, and fluvial transport during the cenozoic evolution of the ebro basin (ne iberia). *Journal of Geophysical Research*, 108 :doi : 10.1029/2002JB002073.

Gargani, J., Stab, O., Cojan, I., and Brulhet, J. (2006). Modelling the long-term fluvial erosion of the river somme during the last million years : Long-term river erosion modelling. *Terra Nova*, 18(2) :118–129.

Gaudemer, Y., Tapponier, P., and Turcotte, D. (1989). River offsets across active strike-slip faults. *Annales Tectonicae*, 3 :55–76.

Gibling, M. R. and Davies, N. S. (2012). Palaeozoic landscapes shaped by plant evolution. *Nature Geoscience*, 5(2) :99–105.

Hartley, A. J., Weissmann, G. S., Nichols, G. J., and Warwick, G. L. (2010). Large distributive fluvial systems : Characteristics, distribution, and controls on development. *Journal of Sedimentary Research*, 80(2) :167–183.

Heine, K. (1994). The mera site revisited : Ice-age amazon in the light of new evidence. *Quaternary International*, 21 :113–119.

Heine, K. (2000). Tropical south america during the last glacial maximum : evidence from glacial, peri-glacial and fluvial records. *Quaternary International*, 72 :7–21.

Heine, K. and Heine, J. (1996). Late glacial climatic fluctuations in ecuador. glacier retreat during the younger dryas time. *Arctic and Alpine Research*, 28 :596–501.

Hergé (1946). *Le Lotus Bleu*. Casterman.

Hey, R. D. and Thorne, C. R. (1986). Stable channels with mobile gravel beds. *Journal of Hydraulic Engeneering*, 112 :671–689.

Holbrook, J. M., Autin, W. J., Rittenour, T. M., Marshak, S., and Globe, R. J. (2006). Stratigraphic evidence for millennial-scale temporal clustering of earthquakes on a continental-interior fault : Holocene mississippi river floodplain deposits, new madrid seismic zone, usa. *Tectonophysics*, 420 :531–454.

Homewood, P., Allen, P. A., and Williams, C. D. (1986). Dynamics of the molasse basin of western switzerland. *Special Publication of the International Association of Sedimentologists*, 8 :199–217.

Horton, B. K. and DeCelles, P. G. (2001). Modern and ancient fluvial megafans in the foreland basin system of the central andes, southern bolivia : Implications for drainage network evolution in fold-thrust belts. *Basin Research*, 13 :43–63.

Horton, R. E. (1945). Erosional development of streams and their drainage basins. *Geological Society of America Bulletin*, 56 :275–370.

Huang, H. Q. and Nanson, G. C. (1997). Vegetation and channel variation ; a case study of four small streams in southeastern australia. *Geomorphology*, 18 :237–249.

Huang, W. (1993). Morphologic patterns of stream channels on the active yishi fault, southern shandong province, eastern china : implication for repeated earthquakes in the holocene. *Tectonophysics*, 219 :283–304.

Hubschman, J. (1975a). Conclusion : Evolution pédo-géochimique et interprétation paléobioclimatique de piémont quaternaire garonnais. *Bulletin de l'Association française pour l'étude du quaternaire*, 12(3) :211–216.

Hubschman, J. (1975b). Le plateau de lannemezan. *Bulletin de l'Association française pour l'étude du quaternaire*, 12(3) :207–209.

Hubschman, J. (1975c). Les terrasses récentes de la garonne et leur évolution. *Bulletin de l'Association française pour l'étude du quaternaire*, 12(3) :137–147.

Hubschman, J. (1975d). L'évolution des nappes alluviales antérissiennes de la garonne, dans l'avant-pays molassique. *Bulletin de l'Association française pour l'étude du quaternaire*, 12(3) :149–169.

Hubschman, J. (1975e). *Morphogénèse et pédogénèse quaternaires dans le piémont des Pyrénées garonnaises et ariégeoises*. PhD thesis, Université de Toulouse - Le Mirail.

Huisink, M. (2000). Changing river styles in response to weichselian climate changes in the vecht valley, eastern netherlands. *Sedimentary Geology*, 133(1-2) :115–134.

Icole, M. (1969a). Age et nature de la formation dite de lannemezan. *Revue de Géographie Pyrénéenne et du Sud-Ouest*, 40(2) :157–170.

Icole, M. (1969b). Le plateau de lannemezan. In *Livret Guide excursion A6*, pages 31–37. 8éme congrès de l'INQUA, Paris.

Icole, M. (1973). *Géochimie des altérations dans les nappes d'alluvions du piémont occidental nord-pyrénéen*. PhD thesis, Sciences, Paris.

Icole, M. (1982). La formation de lannemezan, formation villafranchienne du piémont central des pyrénées françaises. In *Actes du Colloque "Le Villafranchien Méditérranéen"*, pages 187–199. Université des Sciences et technbiques de Lille, 9-10 Décembre 1982.

Jalut, G., Marti, J., Fontugne, M., Delibrias, G., Vilaplana, J., and Julia, R. (1992). Glacial to interglacial vegetation changes in the northern and southern pyrénées : Deglaciation, vegetation cover and chronology. *Quaternary Science Reviews*, 11(4) :449–480.

Jalut, G. and Turu i Michels, V. (2006). La végétation des pyrénées françaises lors du dernier épisode glaciaire et durant la transition glaciaire interglaciaire (last termination). In *Els Pireneus i los areescircumdants durant el tardiglacial. Mutacions i filiacions tecnoculturals, evolucio paleoambiental. Homenatge Georges Laplace. XIV Col.loqui internacional d'arquelogia de Puigcerda, 10-11 November 2006. Institut d'Estudis Ceretans.* Fullola, J.M., Valdeyron, M., Langlais, M. (eds.).

Jones, L. S. and Schumm, S. A. (1999). Causes of avulsion : An overview. In Smith, N. D. and Rogers, J., editors, *Fluvial Sedimentology VI*, pages 169–178. Blackwell Publishing Ltd., Oxford, UK.

Keller, E. A. and Pinter, N. (2002). *Active Tectonics : earthquakes, uplift and landscapes.* Prentice Hall, Upper Saddle River, New Jersay, 07458.

Kozarski, S. (1983). River channel changes in the middle reach of the warta valley, great poland lowland. *Quaternary Studies in Poland*, 4 :159–169.

Lane, E. (1957). A study of the shape of channels formed by natural streams flowing in erodible materials. In *Missouri River Division Sediment Series*, number 9 in United States Army Corps of Engineers. Missouri River Division, Omaha, NB.

Laraque, A., Bernal, C., Bourrel, L., Darrozes, J., Christophoul, F., Armijos, E., Fraizy, P., Pombosa, R., and Guyot, J. L. (2009). Sediment budget of the napo river, amazon basin, ecuador and peru. *Hydrological Processes*, 23(25) :3509–3524.

Leeder, M. R. and Alexander, J. (1987). The origin and tectonic signficance of assymetrical meanderbelts. *Sedimentology*, 32 :217–226.

Leeder, M. R. and Jackson, J. A. (1993). The interaction between normal faulting and drainage in active extensionalo basinswith examples form the western united states and central greece. *Basin Research*, 5 :79–102.

Legrand, D., Baby, P., Bondoux, F., Dorbath, C., Bès De Berc, S., and Rivadeneira, M. (2005). The 1999– 2000 seismic experiment of macas swarm (ecuador) in relation with rift inversion in subandean foothills. *Tectonophysics*, 395 :67–80.

Leier, A. L., DeCelles, P. G., and Pelletier, J. D. (2005). Mountains, monsoons, and megafans. *Geology*, 33(4) :289.

Leopold, L. B. and Maddock, T. J. (1953). The hydraulic geometry of stream channel ans some physiographic implications. *Unites States Geological Survey Professionnal Paper*, 252.

Leopold, L. B., Wolman, M. G., and Miller, J. P. (1964). *Fluvial processes in geomorphology.* W. H. Freeman and Company, San Francisco.

Lewin, J. and Brewer, P. A. (2001). Predicting channel patterns. *Geomorphology*, 40(3-4) :329–339.

Li, S. and Finlayson, B. L. (1993). Flood management on the lower yellow river : hydrological and geomorphological perspectives. *Sedimentary Geology*, 85 :285–296.

Lisiecki, L. E. and Raymo, M. E. (2005). A pliocene-pleistocene stack of 57 globally distributed benthic δ^{18}o records : Pliocene - pleistocence benthic stack. *Paleoceanography*, 20(1) :PA1003.

Liu, K. and Colinvaux, P. A. (1985). Forest changes in the amazon basin during the last glacial maximum. *Nature*, 318(556-557).

Mackin, J. H. (1948). Concept of the graded river. *Geological Society of America Bulletin*, 59 :463–512.

Makaske, B. (2001). Anastomosing rivers : a review of their classification, origin and sedimentary products. *Earth Science Reviews*, 53 :149–196.

Marston, R. A., Girel, J., Pautou, G., Piégay, H., Bravard, J.-P., and Arneson, C. (1995). Channel metamorphosis, floodplain disturbance and vegetation development : Ain river, france. *Geomorphology*, (121-131).

Martinez, J. and Le Toan, T. (2007). Mapping of flood dynamics and spatial distribution of vegetation in the amazon floodplain using multitemporal SAR data. *Remote Sensing of Environment*, 108(3) :209–223.

Martinson, D., Hays, J., Imbrie, J., Moore, T., and Shackleton, N. (1987). Age dating and orbital theory of the ice ages : Development of a high-resolution 0 to 300,000-year chronostratigraphy. *Quternary Research*.

Mellack, J. M. and Hess, L. L. (2004). Remote sensing of wetlands on a global scale. *SIL News*, 42 :1–5.

Métivier, F. and Barrier, L. (2012). Alluvial landscape evolution : What do we know about metamorphosis of gravel-bed meandering and braided streams ? In Church, M., Biron, P. M., and Roy, A., editors, *Gravel-Bed Rivers*, chapter 34, pages 474–501. John Wiley & Sons, Ltd, Chichester, UK.

Miall, A. D. (1985). Architectural-element analysis : a new method of facies analysis applied to fluvial deposits. *Earth Science Reviews*, 22 :261–308.

Miall, A. D. (1996). *The Geology of Fluvial Deposits : Sedimentary Facis, Basin Analysis and Petroleum Geology*. Springer Verlag, Berlin.

Mohrig, D., Heller, P. L., Paola, C., and Lyons, W. J. (2000). Interpreting avulsion process from ancient alluvial sequences : Guadalope-matarranya system, northern spain and wasatch formation, western colorado. *Geological Society of America Bulletin*, 112 :1787–1803.

Mol, J. (1997). Fluvial response to weichselian climate changes in the niederlausitz (germany). *Journal of Quaternary Science*, 12(1) :43–60.

Mol, J., Vandenberghe, J., and Kasse, C. (2000). River response to variations of periglacial climate in mid-latitude europe. *Geomorphology*, 33(3-4) :131–148.

Muñoz, J. A. (1992). Evolution of a continental collision belt : ECORS-pyrenees crustal balanced cross-section. In *Thrust Tectonics*, pages 235–246. K.R. Mc Klay. Chapman and Hall.

Naylor, M. and Sinclair, H. D. (2008). Pro- vs. retro-foreland basins : Pro- vs. retro-foreland basins. *Basin Research*, 20(3) :285–303.

Ortuno, M., Marti, A., Martin-Closas, C., Jimenez-Moreno, G., E., M., and Santanach, P. (2013). Paleoenvironments of the late miocene pruedo badsin : implications for the uplift of the central pyrenees. *Journal of the Geological Society of London*, 170 :79–92.

Ortuno, M., Queralt, P., Marti, A., Ledo, J., Masana, E., Perea, H., and Santanach, P. (2008). The north maladeta fault (spanish central pyrenees) as the vielha 1923 eartquake seismic source : Recent activity revealed by geomorphology and geophysical research. *Tectonophysics*, 453 :246–262.

Osterkamp, W. R. and Hedman, E. R. (1982). Perennial stream-flow characteristics related to channel geometry and sediment in missouri river basin. volume 1242.

Ouchi, S. (1985). Response of alluvial rivers to slow active movement. *Geological Society of America Bulletin*, 96 :504–515.

Parker, G. (1976). On the cause anc characteristics scales of meandering and braiding in rivers. *Journal of Fluid Mechanics*, 76 :457–480.

Parker, G., Wilcock, P., Paola, C., Dietrich, and Pitlick, J. (2007). Physical basis for quasi-universal relations describing bankfull hydraulic geometry of singl-thread gravel bed rivers. *Journal of Geopysical Research - Earth Surface*, 112 :F04005.

Pastre, J.-F., Limondin-Lozouet, N., Leroyer, C., Ponel, P., and Fontugne, M. (2003). River system evolution and environmental changes during the lateglacial in the paris basin (france). *Quaternary Science Reviews*, 22(20) :2177–2188.

Penck, A. (1910). Versuch einer klimaklassifikation auf physiographische grundlage. *Preussiche Akademie der Wissenschaften. Sitz der Phys.-Mth.*, K1(12) :236–246.

Penck, A. and Brückner, E. (1901). *Die Alpen im Eiszeitalter.* Taunitz, Leipzig.

Pépin, E., Carretier, S., and Hérail, G. (2010). Erosion dynamics modelling in a coupled catchment–fan system with constant external forcing. *Geomorphology*, 122 :78–90.

Pinter, N. and Keller, E. A. (1995). Geomorphic analysis of neotectonic deformation, northern oowens valley, california. *Geologische Rundschau*, 84 :200–212.

Puigdefabregas, C. and Souquet, P. (1986). Tectonosedimentary cycles and depositional sequences of the mesozoic znd tertiary from the pyrenees. *Tectonophysics*, 129 :173–203.

Regard, V., Lagnous, R., Espurt, N., Darrozes, J., Baby, P., Roddaz, M., Calderon, Y., and Hermoza, W. (2009). Geomorphic evidence for recent uplift of the fitzcarrald arch (peru) : A response to the nazca ridge subduction. *Geomorphology*, 107(3-4) :107–117.

Reille, M. and Andrieu-Ponel, V. (1995). The late pleistocene and holocene in the lourdes basin, western pyrénées, france : a new pollen analytical and chronological data. *Vegetation History and Archebotany*, 4 :1–21.

Riba, O. (1976). Syntectonic unconformities of the alto carderner, spanish pyrenees : a genetic interpretation. *Sedimentary Geology*, 15 :213–233.

Richard, M. (1948). Contribution à l'étude du bassin d'aquitaine. les gisements mammifères tertiaires. In *Mémoire de la Société Géologique de France*, page 380. Société Géologique de France.

Rius, D., Vannière, B., and Galop, D. (2012). Holocene history of fire, vegetation and land use from the central pyrenees (france). *Quaternary Research*, 77(1) :54–64.

Roddaz, M., Hermoza, W., Mora, A., Baby, P., Parra, M., Christophoul, F., Brusset, S., and Espurt, N. (2010). Cenozoic sedimentary evolution of the amazonian foreland basin system. In Hoorn, C. and Wesselingh, F. P., editors, *Amazonia : Landscape and Species Evolution*, pages 61–88. Wiley-Blackwell Publishing Ltd., Oxford, UK.

Roddaz, M., Viers, J., Brusset, S., Baby, P., and Hérail, G. (2005). Sediment provenances and drainage evolution of the neogene amazonian foreland basin. *Earth and Planetary Science Letters*, 239(1-2) :57–78.

Rouby, D., Bonnet, S.and Biancotto, F., Guillocheau, F., Braun, J., Dauteuil, O., Robin, C., and Gallagher, K. (2009). Sediment supply to the orange sedimentary system over the last 150 ma : an evaluation from erosion/sedimentation balance. *Marine and Petroleum Geology*, 26 :782–794.

Rowntree, K. M. and Dollar, E. S. J. (1999). Vegetation controls on channel stability in the bell river, eastern cape, south africa. *Earth Surface Processes and Landforms*, 24 :127–134.

Sacek, V. (2014). Drainage reversal of the amazon river due to the coupling of surface and lithospheric processes. *Earth and Planetary Science Letters*, 401 :301–312.

Sambrook Smith, G. H., Best, J. L., Ashworth, P. J., Fielding, C. R., Goodbred, S. L., and Prokocki, E. W. (2010). Fluvial form in modern continental sedimentary basins : Distributive fluvial systems : Comment. *Geology*, 38(12) :e230.

Schumm, S. A. (1963). A tentative classification of alluvial river channels. *United States Geological Survey Circular*, (477).

Schumm, S. A. (1977). *The fluvial system*. Blackburn Press, Caldwell, N.J.

Schumm, S. A., Dumont, J.-F., and Holbrook, J. M. (2000). *Active tectonics and alluvial rivers*. Cambridge University Press.

Schumm, S. A., Mosley, M. P., and Weaver, W. E. (1987). *Experimental fluvial geomorphology*. Wiley, New York.

Shephard, G. E., Liu, L., Müller, R. D., and Gurnis, M. (2012). Dynamic topography and anomalously negative residual depth of the argentine basin. *Gondwana Research*, 22(2) :658–663.

Shephard, G. E., Müller, R. D., Liu, L., and Gurnis, M. (2010). Miocene drainage reversal of the amazon river driven by plate–mantle interaction. *Nature Geoscience*, 3(12) :870–875.

Sinclair, H. D. (1997). Tectonostratigraphic model of underfilled peripheral foreland basins : An alpine perspective. *Geological Society of America Bulletin*, 109 :323–347.

Slingerland, R. L. and Smith, N. D. (2004). River avulsions and their deposits. *Annual Review of Earth and Planetary Sciences*, 32(257-285).

Smith, C. E. (1998). Modeling high sinuousity meanders in a small flume. *Geomorphology*, 25(19–30).

Smith, D. G. (1986). Anastomosing river deposits, sedimentation rates and basin subsidence, magdalena river, northwestern colombia, south america. *Sedimentary Geology*, 46 :177–196.

Stange, K. M., van Balen, R. T., Kasse, C., Vandenberghe, J., and Carcaillet, J. (2014). Linking morphology across the glaciofluvial interface : A 10be supported chronology of glacier advances and terrace formation in the garonne river, northern pyrenees, france. *Geomorphology*, 207 :71–95.

Stouthamer, E. and Berendsen, H. (2000). Factors controlling the holocene avulsion history of the rhine–meuse delta (the netherlands). *Journal of Sedimentary Research*, 70(5) :1051–1064.

Tal, M. and Paola, C. (2007). Dynamic single-thread channels maintained by the interaction of flow and vegetation. *Geology*, 35(4) :347.

Tal, M. and Paola, C. (2010). Effects of vegetation on channel morphodynamics : results and insights from laboratory experiments. *Earth Surface Processes and Landforms*, 35(9) :1014–1028.

Tambareau, Y., Crochet, B., Vilatte, J., and Déramond, J. (1995). Evolution tectono-sédimentaire du versant nord des pyrénées centre-orientales au paléocène et l'eocène inférieur. *Bulletin de la Socitété Géologique de France*, 166(4) :375–387.

Tiedemann, R., Sarnthein, M., and Shackleton, N. J. (1994). Astronomic timescale for the pliocene atlantic d18o and dust flux records of ocean drilling program site 659. *Paleoceanography*, 9(6) :619–638.

Törnqvist, T. E. (1994). Middle and late holocene avulsion history of the river rhine (rhine meuse delta, netherlands). *Geology*, 22 :711 714.

Twain, M. (1883). *Life on the Mississipi*. Dover.

van den Berg, J. H. (1995). Prediction of alluvial channel pattern of perennial rivers. *Geomorphology*, 12(4) :259–279.

van Huissteden, J. (2001). Detection of rapid climate change in last glacial fluvial successions in the netherlands. *Global and Planetary Change*, 28(1-4) :319–339.

Vandenberghe, J. (2002). The relation between climate and river processes, landforms and deposits during the quaternary. *Quaternary International*, 91(1) :17–23.

Vandenberghe, J. (2003). Climate forcing of fluvial system development : an evolution of ideas. *Quaternary Science Reviews*, 22(20) :2053–2060.

Vandenberghe, J. (2008). The fluvial cycle at cold–warm–cold transitions in lowland regions : A refinement of theory. *Geomorphology*, 98(3-4) :275–284.

Vandenberghe, J., Kasse, C., Bohncke, S., and Kozarski, S. (1994). Climate-related river activity at the weichselian-holocene transition : a comparative study of the warta and maas rivers. *Terra Nova*, 6(5) :476–485.

Vandenberghe, J. and Maddy, D. (2000). The significance of fluvial archives in geomorphology. *Geomorphology*, 33(3-4) :127–130.

Vandenberghe, J. and Maddy, D. (2001). The response of river systems to climate change. *Quaternary International*, 79(1) :1–3.

Vernant, P., Hivert, F., Chery, J., Steer, P., Cattin, R., and Rigo, A. (2013). Erosion-induced isostatic rebound triggers extension in low convergent mountain ranges. *Geology*, 41(4) :467–470.

Walter, R. C. and Merritts, D. J. (2008). Natural streams and the legacy of water-powered mills. *Science*, 319 :299–304.

Weissmann, G. S., Hartley, A. J., Nichols, G. J., Scuderi, L. A., Olson, M., Buehler, H. A., and Banteah, R. (2010). Fluvial form in modern continental sedimentary basins : Distributive fluvial systems. *Geology*, 38(1) :39–42.

Weissmann, G. S., Hartley, A. J., Scuderi, L. A., Nichols, G. J., Davidson, S., Owen, A., Atchley, S., Bhattacharya, P., Chakraborty, T., Ghosh, P., Nordt, L., Michel, L., and Tabor, N. (2013). *Prograding distributive fluvial systems - geomorphic models and ancient examples*, pages 131–147. Number 104. SEPM Special Publication.

Wells, N. and Dorr, J. (1987). Shifting of the kosi river, northern india. *Geology*, 15 :204–207.

Wilkinson, M. J., Marshall, L. G., Lundberg, J. G., and Kreslavsky, M. H. (2010). Megafan environments in northern south america and their impact on amazon neogene aquatic ecosystems. In Hoorn, C. and Wesselingh, F., editors, *Amazonia : landscape and species evolution, a look into the past.*, pages 162–184. Oxford : Wiley Blackwell.

Yalin, M. and Da Silva, A. (2001). *Fluvial processes*. Delft, International Association of Hydraulic Engineering and Research Monograph.

Chapitre 3

Sélection de cinq articles

Les cinq articles présentés dans cette troisième partie illustrent le titre de ce mémoire « Réponse des systèmes alluviaux aux forçages tectoniques et climatiques à diverses échelles de temps : du phénomène d'avulsion à l'architecture stratigraphique des bassins sédimentaires ». Ils en suivent la logique. Les quatre premiers sont des études géomorphologiques s'intéressant respectivement à des processus actuels, à l'échelle séculaire et du quaternaire récent. Le dernier, est une étude sédimentologique et des relations tectonique/sédimentation menée sur un exemples ancien à actuel à l'échelle du million d'années.

Le premier article (Bernal et al., 2013) décrit un phénomène d'avulsion actuel (évènements suivis sur une durée de 30 ans) impliqué dans la mise en place d'une morphologie fluviale anastomosée. Il illustre le fonctionnement autocyclique d'un système alluvial en l'absence apparente de forçage externe.

Le deuxième (Bernal et al., 2012) montre l'ajustement du cours d'eau dans un contexte de piémont orogénique actif. Il illustre les relations complexes entre tectonique/climat/sédimentation. Cette étude permet cependant de mettre en évidence le rôle respectif de la tectonique locale en tant que « favorisant » (setup) le déplacement du cours d'eau et celui du climat (événements extrêmes liés à ENSO) en tant que déclencheur des avulsions amenant au déplacement du cours d'eau.

Le troisième (Christophoul et al., subm) aborde la question des paramètres contrôlant la morphologie fluviale et notamment ceux impliqués dans la transition tresses/méandres.Cette étude, basée sur une cartographie fine du style fluvial des chenaux préservés dans le remplissage de la terrasse würmienne de la Garonne nous permet, avec des datations et des palynologiques de montrer les modalités du contrôle climatique des style fluviaux mais surtout de proposer un modèle de relations climat/végétalisation/méandrisation jusque là supposé.

Le quatrième (Bernal et al., 2011) montre les résultat d'avulsions successives à l'échelle de la dizaine de milliers d'années (sur la période post-LGM). Il met en évidence la signature particulière des avulsions en fonction du facteur de contrôle prépondérant. Il met aussi en évidence des fréquences d'avulsions différentes dans le temps et dans l'espace mettant là-aussi en évidence des facteurs de contrôle différents.

Le cinquième (Christophoul et al., en révision) illustre l'évolution d'un système fluvial de piémont contrôlé par la croissance du prisme orogénique subandin durant la croissance topographique des Andes équatorienne au Miocène. Cette étude sédimentologique met en évidence les caractéristiques des chenaux et de la plaine d'inondation dans un gradient proximal/distal ainsi que la migration du système alluvial/fluvial au cours du temps. Elle permet de mettre en évidence l'architecture stratigraphique d'un Disbributive Fluvial System et de discuter le potentiel de préservation des ces objets dans l'enregistrement stratigraphique en fonction du contexte tectonique du bassin dans lesquels ils se mettent en place.

Annexe A

Bernal, C., Christophoul, F., Darrozes, J., Laraque, A., Bourrel, L., Soula, J-C., Guyot, J-l., Baby, P. (2013)
Journal of South American Earth Sciences

Cet article, issu des travaux de thèse de C. Bernal, présente un exemple de développement d'une morphologie fluviale de type anastomosé sur le cours inférieur du Rio Pastaza au Pérou. Cette étude précise le mécanisme à l'origine du développement d'une morphologie de type anastomosée. Il met en avant le rôle des crevasses splays comme initiateurs des anabranches se développant le long du cours inférieur du Rio Pastaza.

Résumé :

Le phénomène d'avulsion est le principal processus impliqué dans le développement des cours d'eau à morphologie anastomosée (Smith & Morozova, 2000 ; Southamer & Berendsen, 2000). Cette étude illustre trois exemples d'avulsions découlant de la mise en place de deltas de crevasse (crevasse splay) conduisant à la formation de chenaux anastomosés le long du cours inférieur du Rio Pastaza, une rivière tropicale prenant sa source dans les Andes d'Equateur et s'écoulant dans l'avant-pays amazonien. Sur son cours inférieur, le Rio Pastaza s'écoule dans un plaine alluviale sans tectonique notable. Le régime pluviométrique local montre une distribution régulière au cours de l'année.

A partir de l'analyse d'images satellites couvrant la période 1977-2008, trois cas ont été étudiés.

Le premier débute en 1990 par l'ouverture d'un chenal de crevasse dans la levée naturelle située en rive droite du Rio Pastaza. Ce chenal annexe un cours d'eau préexistant, drainant la plaine d'inondation. Un crevasse-splay se met en place au débouché de ce chenal et décapite la partie amont du drain dans la plaine d'inondation. La partie aval annexée devient alors une anabranche du Rio Pastaza.

En aval, deux autres avulsions partielles ont conduit à la mise en place de chenaux anastomosés suite à la progradation de crevasses splays dans la plaine d'inondation. Dans les deux cas, un des distributaire du crevasse splay a été capturé par un drain antécédent de la plaine d'inondation. La vague d'érosion régressive consécutive à cette capture permet la déconnexion des autres distributaires du crevasse splay et concentre les écoulements dans un seul tributaire. Ce tributaire issu de la jonction du tributaire du crevasse splay en amont et de l'ancien drain de la plaine d'inondation vers l'aval génère un chenal anastomosé.

Journal of South American Earth Sciences 44 (2013) 63–74

Contents lists available at SciVerse ScienceDirect

Journal of South American Earth Sciences

journal homepage: www.elsevier.com/locate/jsames

Crevassing and capture by floodplain drains as a cause of partial avulsion and anastomosis (lower Rio Pastaza, Peru)

Carolina Bernal [a,1], Frédéric Christophoul [a,*], José Darrozes [a,2], Alain Laraque [b,3], Luc Bourrel [c,4], Jean-Claude Soula [a,5], Jean-Loup Guyot [d,6], Patrice Baby [e,7]

[a] UMR 5563 GET, Université de Toulouse – CNRS – IRD – CNES, 14 Av., Edouard Belin, F-31400 Toulouse, France
[b] UMR 5563 GET, Université de Toulouse – CNRS – IRD – OMP – CNES, 14 Avenue Edouard Belin, 31400 Toulouse, France
[c] UMR 5563 GET, Université de Toulouse – CNRS – IRD – OMP, 14 Avenue Edouard Belin, 31400 Toulouse, France
[d] IRD Brasil, CP 7091 – Lago Sul 71619-971 – Brasilia (DF), Brazil
[e] IRD, 14 Av. Edouard Belin, F-31400 Toulouse, France

ARTICLE INFO

Article history:
Received 6 December 2011
Accepted 19 November 2012

Keywords:
Crevasse splay
Avulsion
Anastomosis
Amazonian basin
Floodplain
Pastaza

ABSTRACT

Avulsion is the main process at the origin of anastomosing rivers. This study illustrates 3 examples of avulsions resulting from crevasse splays evolving in anastomosed channels along the Rio Pastaza, a tropical humid river sourced in the Ecuadorian Andean Cordillera and flowing into the Amazonian foreland. The Lower Pastaza flows in an alluvial plain, with no tectonic influence and an average monthly rainfall equally distributed throughout the year.

Based on the analysis of satellite image recorded over the period 1977–2008, three cases have been studied. The first one began in 1990 with crevassing of natural levees of the right bank of the Pastaza main channel and the formation of a small channel linking up with a pre-existing tributary to this main channel. A splay formed at the confluence beheaded the tributary which became an anabranch of the main river. Downstream, two other avulsions developed from crevasse splays on a low gradient floodplain. In both cases, capture of one of the distributary channels flowing on the splay by a pre-existing drain of the floodplain and consecutive headward erosion arrives to disconnect the other drains and capture their flow into a single-thread channel. As this channel rejoins the Pastaza main channel downstream, this process gives rise to the larger-scale anastomosing system which characterizes the lower reach of the Rio Pastaza.

1. Introduction

Avulsion is the process whereby a channel belt shifts relatively abruptly from one location in the floodplain surface to another in favour of a steeper gradient (Slingerland and Smith, 2004; Mohrig et al., 2000; Bridge, 2003; Stouthamer, and Berendsen, 2007). Avulsions may result in a new channel belt (Makaske, 2001).

Avulsions can take place in a variety of alluvial environments, including alluvial fans, braided river floodplains, meandering river floodplains, anastomosed rivers and delta plains (Törnqvist, 1994; Jones and Harper, 1998; Morozova and Smith, 2000; Makaske, 2001; Jain and Sinha, 2005; Leier et al., 2005; Assine, 2005; Sarma, 2005; Sinha et al., 2005). Avulsions are primarily features of aggrading floodplains (Slingerland and Smith, 2004) where they constitute the main cause of anastomosing channel initiation (Makaske, 2001).

River avulsion setup is a long-term process in which the river aggrades over tens to thousands of years and becomes poised for avulsion. Several mechanisms have been proposed as being responsible for important aggradation rates including increased sediment load relative to capacity, change in peak water discharge, or decrease in channel gradient owing to sinuosity increase, delta extension, base level perturbation, downstream tectonic uplift (Jones and Schumm, 1999; Stouthamer and Berendsen, 2000; Slingerland and Smith, 2004). The trigger is a short-term event

* Corresponding author. Tel.: +33 (0) 5 61 55 26 70; fax: +33 (0) 5 61 33 25 60.
E-mail addresses: chavelacarola@yahoo.com.mx (C. Bernal), christo@get.obs-mip.fr (F. Christophoul), darrozes@get.obs-mip.fr (J. Darrozes), alain.laraque@ird.fr (A. Laraque), bourrel@get.obs-mip.fr (L. Bourrel), soula@get.obs-mip.fr (J.-C. Soula), jean-loup.guyot@ird.fr (J.-L. Guyot), patrice.baby@ird.fr (P. Baby).
[1] Tel.: +33 (0) 5 61 55 26 21; fax: +33 (0) 5 61 33 25 60.
[2] Tel.: +33 (0) 5 61 55 26 65; fax: +33 (0) 5 61 33 25 60.
[3] Tel.: +33 (0) 5 61 55 26 41; fax: +33 (0) 5 61 33 25 60.
[4] Tel.: +33 (0) 5 61 55 26 39; fax: +33 (0) 5 61 33 25 60.
[5] Tel.: +33 (0) 5 61 55 26 50; fax: +33 (0) 5 61 33 25 60.
[6] Tel.: +55 61 32 48 53 23; fax: +55 61 32 48 53 78.
[7] Tel.: +33 (0) 5 61 55 26 72; fax: +33 (0) 5 61 33 25 60.

0895-9811/$ – see front matter © 2012 Elsevier Ltd. All rights reserved.
http://dx.doi.org/10.1016/j.jsames.2012.11.009

which immediately provokes the avulsion. Triggers are most frequently floods, but may also be processes as varied as abrupt tectonic movements, ice jams, log dams; vegetative blockages, debris dam, beaver dams, hippopotami trails, or other bank failures and downstream migration of bars that temporarily block the throat of a branch (Stanistreet et al., 1993; Jones and Schumm, 1999; Mohrig et al., 2000; Slingerland and Smith, 2004).

It has been suggested that two end-members of the avulsion series could be (1) incisional avulsion characterized by an early incision and then infilling by migrating bar and (2) aggradational avulsion beginning with aggradation followed by integration of streams into a single downcutting channel (Smith et al., 1989). Mohrig et al. (2000) proposed that the type of avulsion is strongly influenced by whether or not the adjacent floodplain is well drained.

Several numerical models of avulsion have been proposed in order to understand mechanics and sedimentary architecture of alluvial plains, deltas, and fans (Slingerland and Smith, 2004; Jerolmack and Paola, 2007). However, these models do not include some aspects of the fluvial environment (e.g., vegetated levees and floodplains) that may play a key role in avulsion dynamics (Mohrig et al., 2000). Indeed avulsions although infrequent (Smith et al., 1989; Morozova and Smith, 2000) can best be studied by direct observation.

The present study focuses on the lower Río Pastaza (Ecuadorian and northern Peruvian Amazonia) which drains one of the largest tropical alluvial megafans: the Pastaza megafan (Räsänen et al., 1990; Bernal et al., 2011). Recently, substantial attention has been paid to the construction of the Pastaza megafan (Christophoul et al., 2002; Bes de Berc et al., 2005; Burgos, 2006; Bernal et al., 2011, 2012). In the present study, an attempt is made to depict recent avulsions in the Lower Rio Pastaza, near its confluence with the Rio Marañon and to discuss their nature and their role in the construction of floodplain. This study is based on the analysis of the evolution of the fluvial morphology using satellital images and supported by the hydro-pluviometric data yet recorded in the region.

2. Geologic and geomorphologic context

The Río Pastaza drains the eastern Ecuadorian Andes and the upper Amazonian Basin (Fig. 1). The Ecuadorian Andes are characterized by recently active volcanoes, two of them, the Tungurahua (5020 m a.s.l.) and the Sangay (5230 m a.s.l.) having had eruptions throughout the 20th century. Fluvial aggradation started in the Amazonian foreland around 22 Ma with sediments derived from the west (Christophoul et al., 2002; Roddaz et al., 2005, 2010; Burgos, 2006). This sedimentation corresponds to the deposits of the Neogene Napo-Pastaza megafan *sensu lato*. The megafan apex migrated forward as a result of thrust fault propagation (Bès de Berc et al., 2005) but no tectonic influence has been detected in the study area except flexural subsidence originated as a result of thrust

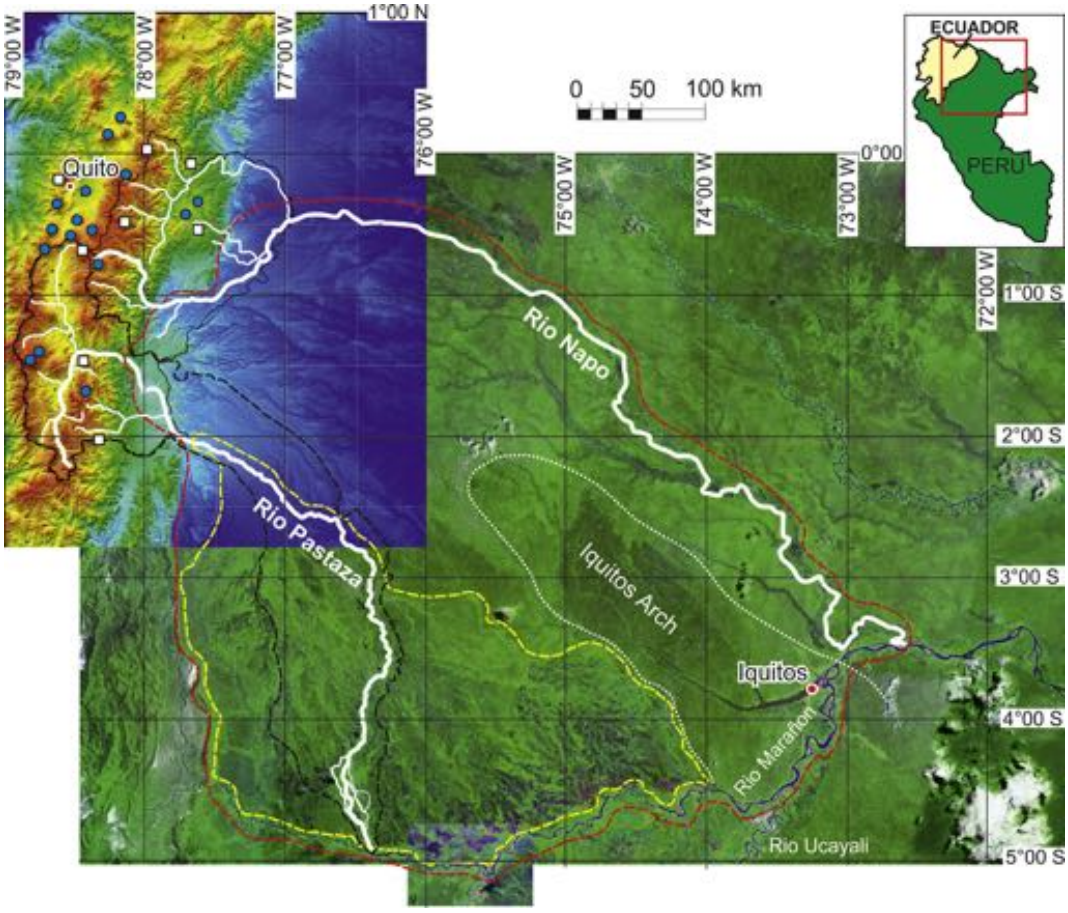

Fig. 1. Mosaic of digital elevation model and Landsat image of Napo-Pastaza Megafan. The watershed is represented in black lines and the modern river network, in white. White squares represent active volcanoes (*Reventador Volcano*, *RV*; *Tungurahua Volcano*, *TV*; *Sangay Volcano*, *SV*) and blue spots represents active volcanoes. Black dashed line: boundary of the Rio Pastaza river basin. Red dashed line is the boundary of the Napo-Pastaza megafan (Bes de Berc et al., 2005). Yellow dashed line represents the post-LGM Pastaza Megafan (Bernal et al., 2011). (For interpretation of the references to colour in this figure legend, the reader is referred to the web version of this article.)

stacking in the cordilleras (Roddaz et al., 2005). The most recently active part of the Pastaza megafan (Räsänen et al., 1990, 1992; Zapata et al., 1998; Bernal et al., 2011) is located in the southeast of the Neogene megafan, in the subsiding area between the Pastaza – Marañon – Ucayali confluence and the Iquitos Arch. The Rio Pastaza is 710 km long and its drainage basin covers 39,000 km^2. The modern course of the Rio Pastaza in the Amazonian plain is the result of numerous avulsions (more than 100), which occurred since the Last Glacial Maximum (Bernal et al., 2011, 2012). The last major avulsion of the Rio Pastaza in the Amazonian plain is older than AD 1691 (Bernal et al. 2011).

3. The Rio Pastaza basin

The Rio Pastaza rises to the rear of the Eastern cordillera from the confluence of two longitudinal rivers flowing in the inter andean depression and sourced in the western cordillera (Fig. 1). It crosses the Eastern Cordillera along a deeply incised (>2000 m) and narrow valley (Fig. 1). Its tributaries form a treillis drainage network with a predominance of the transverse segments on the left (north) bank and a predominance of longitudinal segments on the right (south) bank. Along this reach, the Rio Pastaza exhibits a low meandering single channel pattern its width never exceed 100 m.

In the subandean zone, the Pastaza valley become much wider and shallow and exhibit mainly degradational terraces (Bès de Berc et el., 2005). Several re-orientations with diversion angles of 90°(e.g. reach A in Figs. 1 and 2) to 60° are observed. There, the Rio Pastaza exhibits a braided planform (Bernal et al., 2012) and its width increases and reaches 3.6 km (Fig. 2).

The valley deepens and narrows where crossing the Subandean front (Bernal et al., 2012, reach B in Fig. 2) acquiring a meandering pattern. Then, it widens in the Amazonian plain while its slope regularly decreases downstream (Fig. 2, reaches C, D and E). Fluvial style changes with slope abatement. The upper part (reach C on Fig. 2) has a $2.0 \cdot 10^{-3}$ slope. There, the Rio Pastaza, although clearly individualized, exhibit a multi-channel pattern with a high braiding parameter. Its width reaches 2.5 km. The middle part (reach D on Fig. 2) has a $3.0 \cdot 10^{-4}$ slope (reach D on Fig. 2). The morphology of the Rio Pastaza is there that of a single channel low sinuosity meandering stream. The channel width is around 450 m. The lower part of the Rio Pastaza consists in a huge floodplain made of open water and forest covered areas with a $2.0 \cdot 10^{-4}$ river slope. In this part the Rio Pastaza exhibits an anastomosing pattern (Fig. 2, reach E).

4. Hydrometeorological data

A previous study of the pluviometry and discharge in Ecuadorian streams (Laraque et al., 2009) has shown that rainfall and discharge regimes are highly variable in space and show a strong orographical control. The pluviometric and hydrologic regimes of the Río Pastaza in various parts of its drainage basin have been established using data issued from three pluviometric and two hydro-sedimentological stations (location on Fig. 2) over the period 1964–2005. The data issued from the stations situated in the range (Cusubamba and Baños

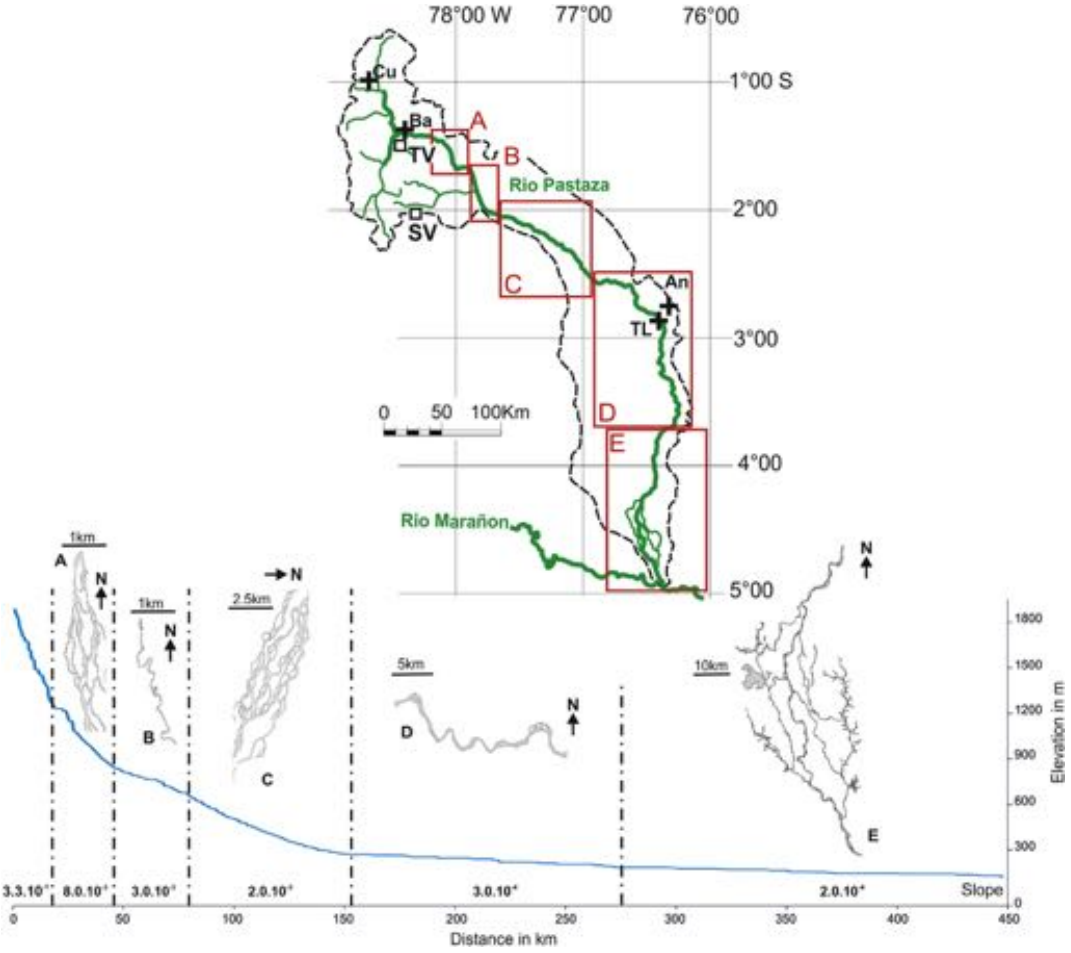

Fig. 2. The Rio Pastaza, drainage basin, hypsometric profile of the Rio Pastaza and associated channel patterns (reaches A to E). White squares: active volcanoes with TV: Tungurahua and SV: Sangay. Black crosses: (*Cusubamba St.*, *Cu*; *Baños St.*, *Ba*; *Andoas St.*, *An*; *Teniente López St.*, *TL*).

pluviometric stations, Baños hydrologic station) are highly dependant upon their situation. In the proximity of the study area, it is practically impossible to get any data because of isolation and insecurity (Laraque et al., 2009). However, the stations of the middle Pastaza basin also situated in the Amazonian wetland can be considered to be representative of the lower Pastaza basin.

At the Teniente Lopez meteorological station (230 m a.s.l.), the average annual rainfall is 2579 mm and is distributed roughly evenly throughout the year (7–10% each month, Fig. 3). The minimum and maximum values of average monthly rainfall are 188.6 mm (March) and 252.8 mm (April), respectively (Espinoza et al., 2009). At the Andoas hydrological station (Fig. 2) 150 km upstream of the study area water discharge has been recorded for 5 years (1997–2002), with an average annual discharge of 910 $m^3 s^{-1}$. The highest average monthly discharge (Fig. 4) occurs in May (1222 $m^3 s^{-1}$) and the lowest in September (674 $m^3 s^{-1}$).

Remote sensing analyses of the hydrology of the Amazonian wetland show that the lower Pastaza is like the rest of Amazonia affected by annual floods invading the whole floodplain. At high water stage, the entire floodplain of the distal part of the Pastaza megafan and as consequence, the lowermost Pastaza is covered by water (Mellack and Hess, 2004; Martinez and Le Toan, 2007). In contrast with the range and the immediate piedmont, we have no data showing the impact of ENSO events.

5. Data and methods

This study was based on the integration of available hydro-sedimentological and geological information with new morphologic and topographic data obtained from satellite and/or aerial images and a digital elevation model.

5.1. Satellite images

Spatial variations of channel pattern as well as avulsion occurrences were traced over the past 31 years using ASTER and Landsat time series satellite imagery (MSS, TM, ETM+, 1977–2002), and CBERS (China-Brazil Earth Resources Satellite, 2008) for Ecuador-Peru. We selected the less cloudy images for approximately the same hydrological period (June–July), except the 2008 satellite image.

The selected images were orthorectified using the software ENVI 4.8; and projected to UTM Zone 18 S. Images were georeferenced and orthorectified by mean of a Geographic Information System (GIS, Arc View 9.1). However one of the main problems was the discrimination between open water and land. In order to solve this we used the wavelengths in the near and middle-infrared ranges (740–2500 nm; Jensen, 2000). In order to extract river channels and unforested floodplain, near and middle infrared bands were gray-level thresholded and then binarized. Binarized images were then vectorized and projected in the GIS. Channels widths were extracted from the binarized images. Channel lengths were extracted from the vectorized images coupled with topographic data. The Amazonian piedmont of the Peru Andes remains very cloudy at any time and optical/IR image acquisitions remain uncertain therefore the temporal coverage is weak.

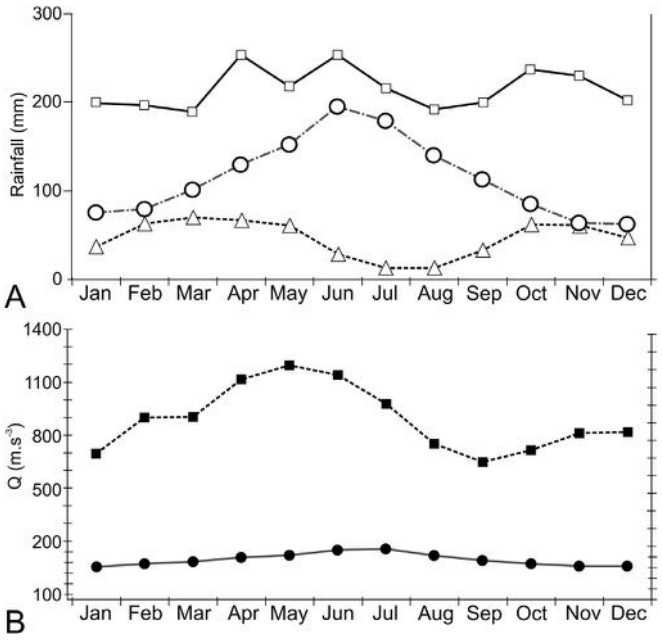

Fig. 3. Hydro-pluviometric regimes of the Rio Pastaza basin (modified from Laraque et al., 2009). (A) Monthly average rainfall (mm) at Cusubamba, Baños and Teniente Lopez. (B) Monthly average water discharge (Q in $m^3 s^{-1}$) in Baños and Andoas stations. Location of stations on Fig. 2.

5.2. Topographic data

Topographic data used in this study are those of the SRTM-3 V4 DEM (Jarvis et al., 2008). Suitability of SRTM-3 data for geomorphological studies even in low relief areas has been shown by Coltelli et al. (1996), Farr et al. (2007) and Valeriano et al. (2006). These data are based on radar interferometry (INSAR) in the C band. Pixel size at the equator is 90 m and slightly increases with the latitude. According to Rodriguez et al. (2005), error in height, in the studied part of the Amazonian lowland is ~5 m.

The SRTM DEM for our study area was reprocessed with ENVI 4.8 using elevation data from topographic maps of the Ecuadorian and Peruvian geographic surveys. DEM SRTM V4 data are shown in Fig. 4. In order to check the coherence of elevation data provided by the SRTM V4 DEM, we extracted a long profile along the left bank of the main channel of the lowermost Pastaza (Fig. 4). Indeed, open water bodies (channels, lakes or unforested floodplain) provoke a loss of coherence in radar response and their elevation in the DEM results from interpolation with surrounding data. In the case of an alluvial river such as the lower Pastaza it seems reasonable to assume that river bank slope and river slope are similar, even though this is not necessarily the case in incising rivers. In fact, the slope computed from the elevation data is $2.5 \cdot 10^{-4}$ (Fig. 4) and that extracted from topographic maps is $2.0 \cdot 10^{-4}$ (Fig. 2).

The topographic data extracted from the SRTM DEM are strongly influenced by vegetation. Indeed, radar waves penetrate the vegetation. As a consequence, the height value on a SRTM Cell (90 × 90 m) is neither the elevation of the canopy nor the elevation of the ground, but an intermediate value. This value corresponds to the "mean scattering phase center height" (Kellndorfer et al., 2004). In accordance with the density and the height of the local vegetation, the mean scattering phase center height varies all over the study area. Nevertheless, the vegetation map on Fig. 4C (CDC-UNALM, 2002) shows the vegetation is quite homogeneous on the three crevasse splays studied. In the areas of homogeneous vegetation we can think the long wave length variations in height reflect the ones of the topography while the sharp changes in height depict change in the type of vegetation.

6. Image and topography analyses

Comparing satellite images allowed us to define three areas of interest along the lower Pastaza (Fig. 2 reach E). The first example is located in the right bank of the Rio Pastaza (1 on Fig. 5) and is

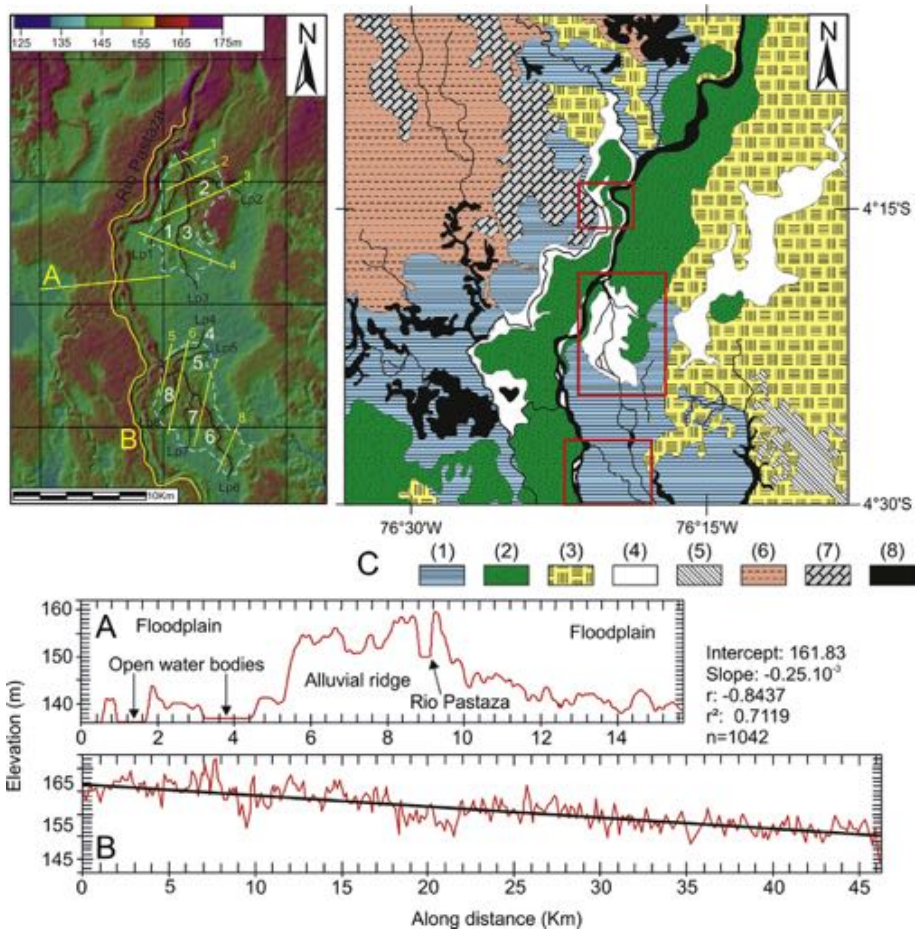

Fig. 4. SRTM V4 DEM of the lower Rio Pastaza and topographic profiles. This DEM shows the topography of the Modern Rio Pastaza alluvial ridge and its associated floodplain. On the left bank of the Rio Pastaza, two crevasse splays can be observed. They correspond respectively to the crevasse splay 2 and 3 on Fig. 3. The crevasse splays are bounded by a light blue dashed lines. Yellow solid lines 1 to 8 and black solid lines Lp1 to Lp6 corresponds to the topographic profiles exhibited on Figs. 8 and 9. A and B: topographic profiles with A: topographic profile across the Rio Pastaza alluvial ridge, and B: topographic profile of the Rio Pastaza alluvial ridge extracted along the Rio Pastaza right bank. White numbers 1 to 8 corresponds to the alluvial ridge identified and featured on Figs. 8 and 9. C: map of the vegetation of the study area (modified from CDC-UNALM, 2002). (1): Herbaceous swamp, (2): Dense flooded forest dominated by palmtree ("Aguajal"), (3): Mixed flooded forest, (4): Riparian forest, (5): Forest of high terrace, (6): Forest of intermediate terrace, (7): Forest of low terrace, (8): Channels and lakes. (For interpretation of the references to colour in this figure legend, the reader is referred to the web version of this article.)

concerned with opening of a channel joining the Rio Pastaza and one of its tributaries, the Rio Huangana. The second example is located downstream, to the left of the Rio Pastaza (2 on Fig. 5), and illustrates the evolution of a crevasse splay into an anastomosed channel. The third example is an ancient crevasse splay further evolved than the preceding one having given rise to a larger-scale anabranch downstream of the formers (3 on Fig. 5).

Despite the scarcity of cloud-free images 10 scenes showing a marked change for the fluvial morphology were found for the period 1977–2008 for the first example (Rio Pastaza-Rio Huangana junction), and 8 for the second. No optical images showing morphological changes have been found for the third example, but this lack was supplied by a topographic analysis allowed by the SRTM DEM.

6.1. Splay 1, the Rio Huangana crevasse splay

Six of the ten available images of the area are shown on Fig. 6 (1981, 1989, 1990, 1994, 2001 and 2008). The initial 1981 image (Fig. 6) shows the Río Pastaza and the Río Huangana flowing almost parallel to each other. The Río Huangana is separated from the Pastaza by a large natural levee but will rejoin the Pastaza downstream. 1989 images (Fig. 6) show a progressive reduction of channel width of the Rio Huangana (Fig. 6). The 1990 image (Fig. 6) shows a small diverging stream "A" issued from the outer bend of the Rio Pastaza and breaching the levee to join the Rio Huangana downstream. At the diverging point of the Stream "A", the Rio Pastaza elevation is 152 m a.s.l. while the floodplain downstream is at 144 m a.s.l.

The 1994 image (Fig. 6) show a slow but constant widening of the stream "A" (<30 m in 1990, 60 m in 1994 and 90–100 m in 2001). As a consequence, there is an increase in water volume inducing the development of a crevasse splay by the "A" channel (2001, Fig. 6) at the confluence with the Huangana, associated with the creation of a marsh between the Pastaza's western levee and the floodplain. This marsh may have been a result of the formation of the crevasse splay damming the upper reach of the Huangana already situated at a lesser elevation than the Pastaza main channel). The crevasse splay issued from the stream "A" covers 1.9 km^2 in 2001 and 5.3 km^2 in 2008. The crevasse splay starts developing around seven narrow channels (15–30 m wide for the distributive channel and 50 m wide for the annexed Huangana downstream reach) debouching in the floodplain on the right bank of the Rio Huangana. The 2008 image shows the Huangana River beheaded (Fig. 6). The distributive channels forming the crevasse splay evolved into an anastomosing network of five main channels

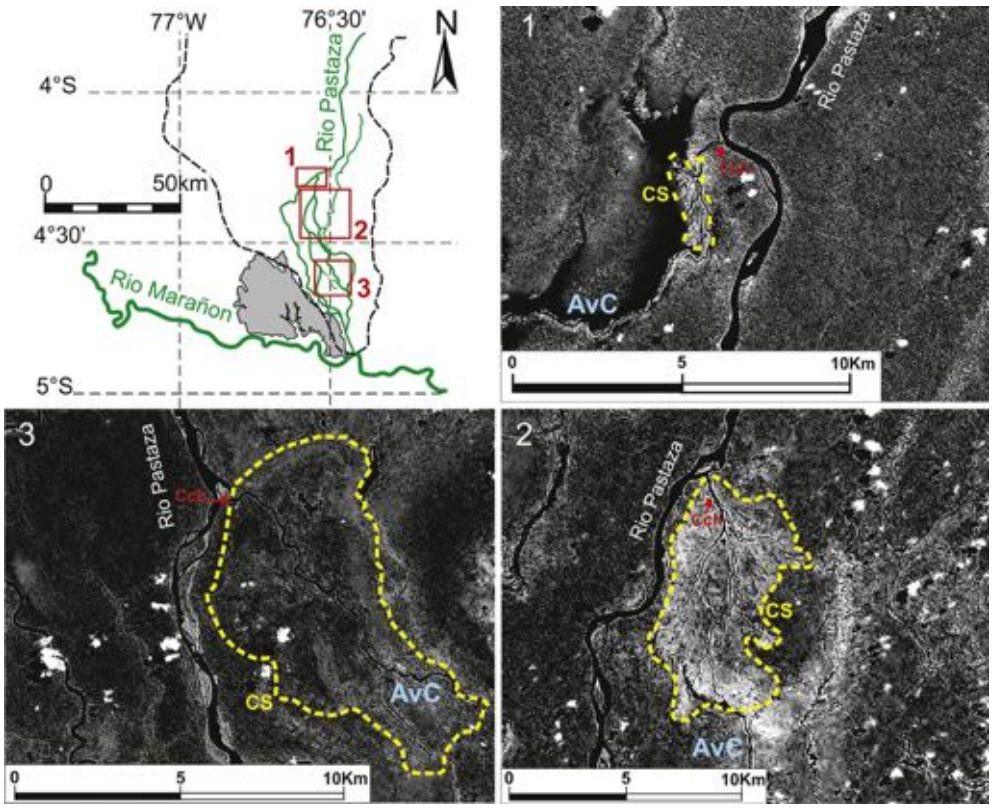

Fig. 5. Location and satellite images of the 3 crevasses splays and anastomosing channels detailed in this study (Landsat TM, VNIR band). Black dashed line: boundary of the Rio Napo drainage basin, green solid line: active channels. 1) Rio Huangana crevasse splay, 2) Splay 2, left bank of the Rio Pastaza, 3) Splay 3, Southern left bank of the Rio Pastza. Yellow dashed line: boundary of crevasse splays. CS: crevasse splay, CCh: Crevasse Channel, AvC: Anastomosing channel. (For interpretation of the references to colour in this figure legend, the reader is referred to the web version of this article.)

(30–60 m wide) rejoining the Rio Pastaza along the downstream course of the Rio Huangana.

6.2. Splay 2, left bank of the Rio Pastaza

Fig. 5.2 shows a 26.16 km^2 large crevasse splay made up of three lobes formed from three alluvial ridges. The 1981 image (Fig. 7) shows a well-developed crevasse splay with a distributive network prograding into the floodplain. The 1987, 1989 and 1994 images (Fig. 7) show these flooded areas have disappeared and the trunk channel bifurcating downstream, leading to active channels organized in a distributary pattern. In 1989 (Fig. 7) the trunk channel joins the Pastaza. Between 1991 and 2008 the network becomes simpler with the progressive consolidation of a single trunk channel (Fig. 7).

The topography of this crevasse splay is shown in Fig. 4. Four transverse and four river/alluvial ridge long profiles were extracted from the DEM (Fig. 8). Profile 1 (Fig. 8) is close to the apex of the crevasse splay and reveals a 1.7 km wide alluvial ridge culminating at 158 m a.s.l. above a low relief area with a mean elevation between 142 and 147 m. Profile 2 (Fig. 8) is located in the area where the initial alluvial ridge starts dividing into two and then 3 s order alluvial ridges. The ridge as a whole is now 2.9 km wide and culminates at 155 m a.s.l. Profile 3 (Fig. 8) exhibits the 3 s order ridges. Each of these ridges is around 1 km wide and culminate at 155 m a.s.l. Profile 4 crosses the two south-western lobes of the crevasse splay which are wider (2 and 3.2 km) and less elevated (147 and 149 m a.s.l.) than the upstream ridges, whereas the floodplain is at 136 m a.s.l. A V-shaped depression is observed between the eastern second order ridges. This depression is interpreted as the non-vegetated active channel (lighter green colour in the Landsat image, Fig. 5.2). A smaller but similar depression appears in the western second order ridge (profile 4, Fig. 8, left). This would indicate that the channels widen downstream within the alluvial ridges. As a whole, the relief of the alluvial ridges is impressively high. The mean height of these alluvial ridge would be 10–12 m. The highest fluvial levees known are those of the Mississippi (10 m high, Brierley et al., 1997). The width of the channels supposed to have origined these levees is only some tenth meters. In our mind, these heights are greatly enhanced by the difference of vegetation between the top of the levees and the floodplain. Though the vegetation map of Fig. 4C shows a common vegetation type between the ridges and the surrounding floodplain, we suppose the vegetation at the top of the levees (higher in altitude, with less moist soils) is made of higher and more concentrated palmtrees than the floodplain. As a consequence the elevation of the SRTM cells on the levees is much higher than it is really (close to height of the canopy) while the elevation in the floodplain is closer to the one of the ground. These differences make the elevation of the levees impossible to precise.

Profiles Lp1 to Lp4 are long profiles of the alluvial ridges (Fig. 8). The upper enveloping line of the westernmost profile Lp1 shows a gentle downstream slope. This shape is globally convex up with a slope increasing downstream. The mean slope is $1.64 \cdot 10^{-3}$ that is an order of magnitude higher than the slope of the Rio Pastaza ($0.2 \cdot 10^{-3}$, see Fig. 5A). Profile Lp2 is that of the central lobe of the crevasse splay (Fig. 5). Its overall shape is similar to that of Lp1 and its mean slope is $1.22 \cdot 10^{-3}$. We can quote a sharp abatement in elevation at 11 km along Lp2. Compared to the Map of the vegetation (Fig. 4C) it corresponds to the transition between the riparian

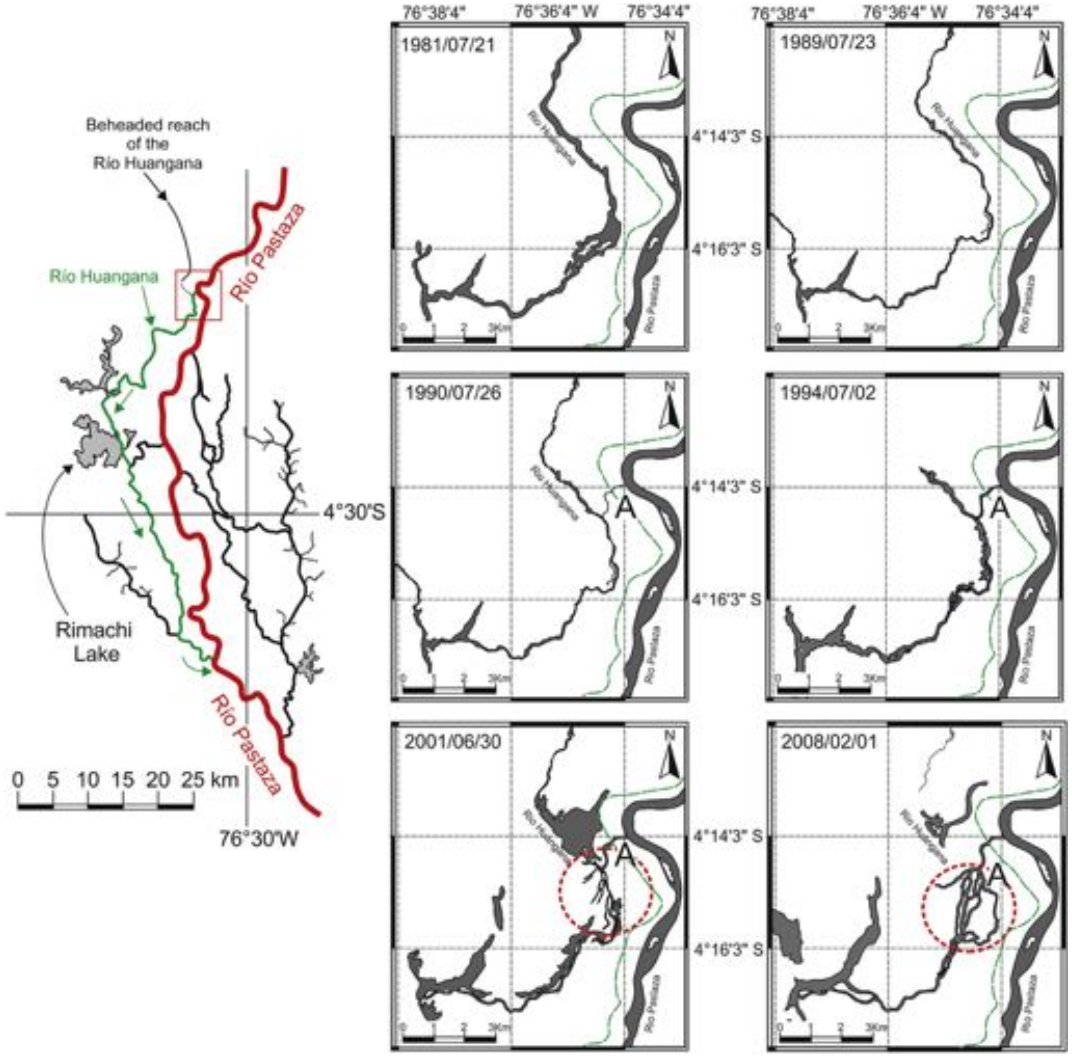

Fig. 6. - Time series of satellite images (Landsat Band 5 – Band 4 – CBER) recording the avulsion and crevasse splay evolution of the Rio Huangana crevasse splay on the right bank of the Rio Pastaza. Green dashed line corresponds to the boundary of the right bank levee of the Rio Pastaza. On the left: map of the lowermost Rio Pastaza, exhibiting the Rio Huangana, its point of divergence with the Rio Pastaza (red box) illustrated by the time series on the right. Remark the downstream junction of the Rio Huangana with the Rio Pastaza through the Rimachi floodplain lake. (For interpretation of the references to colour in this figure legend, the reader is referred to the web version of this article.)

forest developed on the splay and the herbaceous swamp vegetation of the floodplain located downstream. Profile Lp3 is that of the eastern lobe of the crevasse splay. It is shorter than the other alluvial ridges of the splay (2.3 km) and has a steeper slope ($2.07 \cdot 10^{-3}$).

6.3. Splay 3, southern left bank of the Rio Pastaza

This crevasse splay (Fig. 5.3) and its structure are difficult to identify on satellite images because of its low contrast, which suggests that vegetation is quite homogeneous and higher (darker) all over the splay. In contrast, the SRTM DEM reveals very clearly the structure (Fig. 4). Four transverse topographic profiles (Profiles 5–8) and ridge long profiles (Lp4 to Lp8) are shown in Fig. 9. Profiles 5 to 8 depict a proximal-distal gradient within the crevasse splay. Profile 5 exhibits the same bell shape than profile 1 of Splay 2 and can similarly be interpreted as an alluvial ridge. The top of this alluvial ridge culminates at 157 m whereas the floodplain has an elevation of 136 m. Profile 6, located downstream in the crevasse splay, enables the identification of two alluvial ridges. The first one is 5 km wide and culminates at 155 m. The second is 1.7 km wide. Profile 7 is located farther downstream and crosses only one alluvial ridge 2 km wide and 16 m high). The same alluvial ridge 1.2 km wide and 12 m high is visible in Profile 8 where another ridge is observed. The alluvial ridge long profiles (Lp4 to Lp8 on Fig. 9) reveal the morphological characteristics of these splays. Profiles Lp4 and Lp5 (Fig. 9) follow short transverse ridges (~3.5 km) formed in the northern part of the splay (Fig. 5). These ridges are directly connected to the crevasse channel through the right bank levees of the Rio Pastaza main channel. They exhibit regularly decreasing slopes ($4.85 \cdot 10^{-3}$ and $6.28 \cdot 10^{-3}$, respectively) toward the floodplain. This slope is an order of magnitude higher as the Pastaza river gradient ($0.25 \cdot 10^{-3}$, Fig. 5). Lp6 (Fig. 9) follows the longest alluvial ridge of the splay. The first 12 km of the profile exhibit a low but constant decrease in elevation with a $0.66 \cdot 10^{-3}$ slope followed by an abrupt decrease in elevation in the last kilometre. This decrease in elevation is interpreted as a vegetation change from the alluvial ridge to the floodplain like observed on Lp2. Lp7 and Lp8 are along longitudinal ridges/channels bifurcating from the Lp6 ridge/channel in the southern lobes of the splay. Lp7 is 3.8 km long. Its slope is $3.27 \cdot 10^{-3}$. Lp8 is 5.5 km long and has a $1.24 \cdot 10^{-3}$ slope.

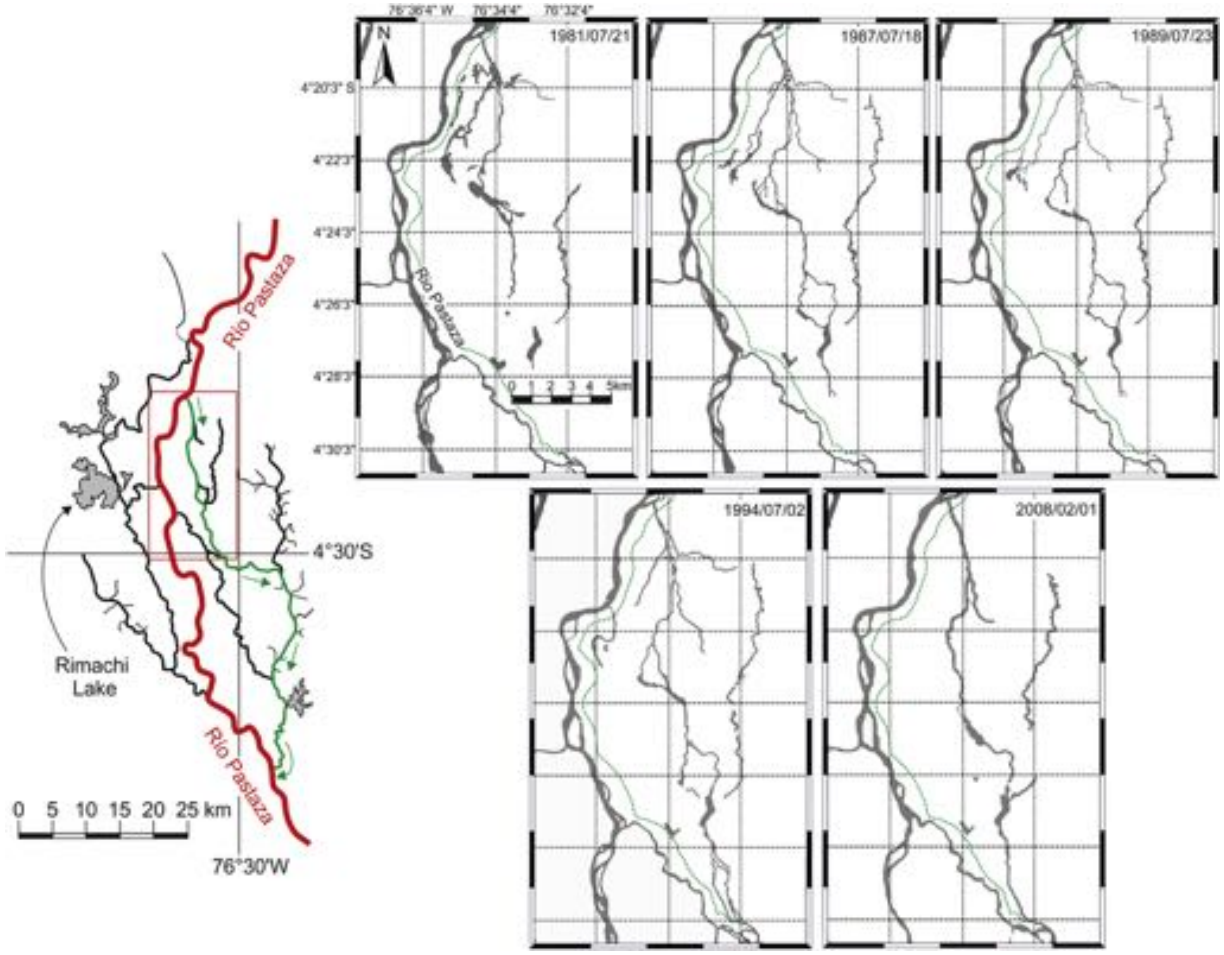

Fig. 7. Time series of satellite images (Landsat Band 5 – Band 4 – CBER) recording the avulsion evolution and crevasse splay evolution of the Splay 2 on the northern left bank of the Rio Pastaza. Green dashed line corresponds to the boundary of the left bank levee of the Rio Pastaza. (For interpretation of the references to colour in this figure legend, the reader is referred to the web version of this article.)

Satellite images reveal no evolution of the distributive drainage network of the crevasse splay through time. This apparent stability of the drainage network along with the well-developed vegetation suggest that this crevasse splay is older than the other crevasse splays described above and represents the terminal stage of evolution of a crevasse splay into an anabranch. The older age of this crevasse splay may explain why Lp6 ridge/channel (Fig. 9) has a lower slope than the other ridge/channels. It would suggests that the anastomosed channel tries to reach an equilibrium profile with a regular slope by smoothing the knickpoint initially created at the junction of the crevasse splay distributary and the floodplain drain it annexes. The lack of accurate topographic data and channel geometry this reasoning can only be hypothesize.

7. Discussion

7.1. History of avulsions

All the three avulsion sets analysed involve crevasse splays showing the same evolutional trend: (1) initial crevassing; (2) crevasse splay propagation in the floodplain; (3) capture of one of the splay channels by a pre-existing channel of the floodplain (or annexation) with headward erosion progressively reducing the initial channel slope. Because headward incision diminishes the elevation of the captured splay channel, the flow of the other distributaries of the splay is captured into this channel (Fig. 10) (see also Smith et al., 1989; Slingerland and Smith, 2004). In our study area, this process will then arrive to the formation of a diverging – rejoining channel being part of a larger-scale anastomosing system.

In detail, the long profiles of the alluvial ridges indicate that an alluvial ridge evolved into an anastomosing channel after having acquired a lower slope than the others (Lp6 on Fig. 9 and in a lesser extend in Lp2 on Fig. 8). Slingerland and Smith (2004) propose that gradient decrease by headward erosion be associated with avulsions by incision and did not mention (but did not reject) this process for avulsions by progradation and annexation. In our cases, the difference in elevation between the floodplain and the ridge containing the avulsed channel will produce profile readjustment in any case. In fact, the systems studied experienced incision, annexation and progradation at various stages in their evolutional history. Splay 1 (Rio Huangana) started as an incising channel, then annexing a pre-existing river, and finally forming a prograding splay (beheading the host river) as a result of increasing flow and sedimentary load. Splay 2 initiates as a progradational splay with one of the distributive channels being then captured by (or annexing) a small stream of the floodplain, implying incisional profile readjustment. Splay 3 likely initiated as a progradational splay, with a channel captured by (or annexing) a stream of the floodplain which would be then affected by incision.

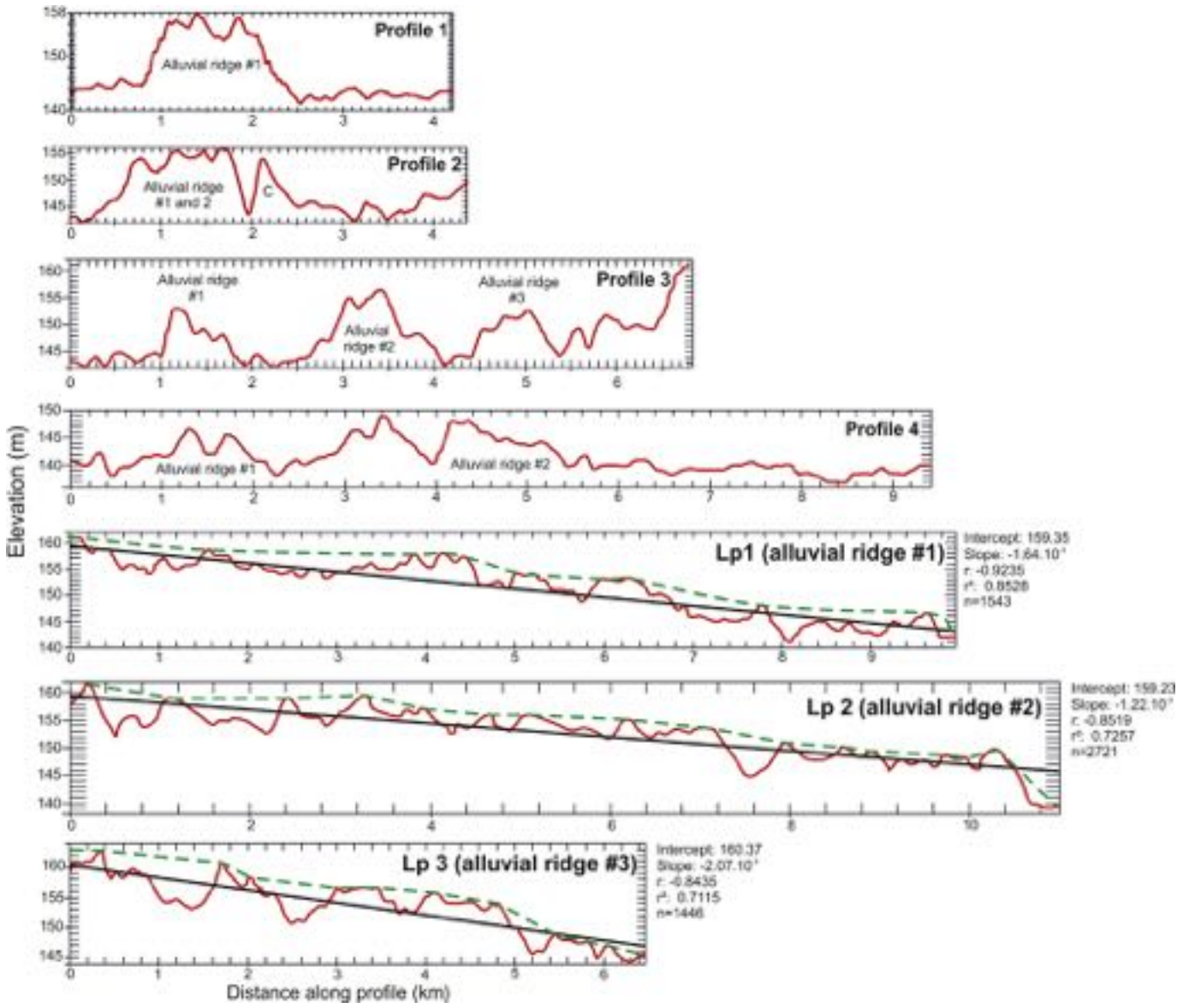

Fig. 8. Topographic profiles of the Splay 2 on the northern left bank crevasse splay. Location of profiles on Fig. 5. Profiles 1 to 4: topography across the crevasse splay. Profiles Lp1 to Lp3: along ridge profiles of the alluvial ridges of the crevasse splay (alluvial ridges #1 to 3 identified on Fig. 4). Green arrows point the location of the anastomosed channel. (For interpretation of the references to colour in this figure legend, the reader is referred to the web version of this article.)

7.2. Avulsions in the amazonian basin

Many of the largest rivers of the world are located in tropical areas together with some of the major areas of alluvial sédimentation by megafan systems (Latrubesse et al., 2005). In the amazon basin, modern or ancient avulsions are mainly known along the andean foothill and concentrated in two fluvial aggradation zones, in the north in Peru including the Lower Rio Pastaza, the Rio Marañon, the Rio Huallaga and the rio Ucayali (North Amazonian Fluvial Aggradation Zone, NAFAZ) and an other in the south in Bolivia and Brazil including the Rio Beni and the Rio Mamoré (South Amazonian Fluvial Aggradation Zone, SAFAZ). These areas can be easily identified because they correspond to extensive floodplain area (Mellack and Hess, 2004; Martinez and Le Toan, 2007; Wilkinson et al., 2010). Avulsions in these two area belong to megafans or alluvial plains (Dumont, 1991; Dumont and Fournier, 1994; Dumont, 1996; Horton and DeCelles, 2001; Bernal et al., 2011, 2012).

Though they are linked to megafan building, these avulsions occurred on very different kind of rivers. These avulsions are also different in terms of avulsion typology (Jones and Schumm, 1999).

Indeed, avulsions described by Horton and DeCelles (2001) in the SAFAZ, on the Bolivian foothill, are mainly nodal avulsions which occurred on low sinuosity sandy braided streams (Rio Parapeti, Pilcomayo and Rio Grande). The avulsion node is located at the topographic front of the Andes. These rivers channel are also highly variable in width, with a hectometric channel within a kilometer wide braidplain. The Rio Beni avulsions (Dumont, 1996) occurred on a high sinuosity sandy meandering stream (Gautier et al., 2007, 2010). The Rio Beni, in the area concerned with avulsions is 500 m wide and its alluvial ridge is 10 km in width. Unfortunately, there is no precise age of these avulsions.

In the NAFAZ, avulsions traces are known in the Rio Pastaza Megafan (Bernal et al., 2011, 2012). These avulsions occured since the LGM (Bernal et al., 2011). Avulsions in the Pastaza megafan occurred as the morphology of the Rio Pastaza changed through

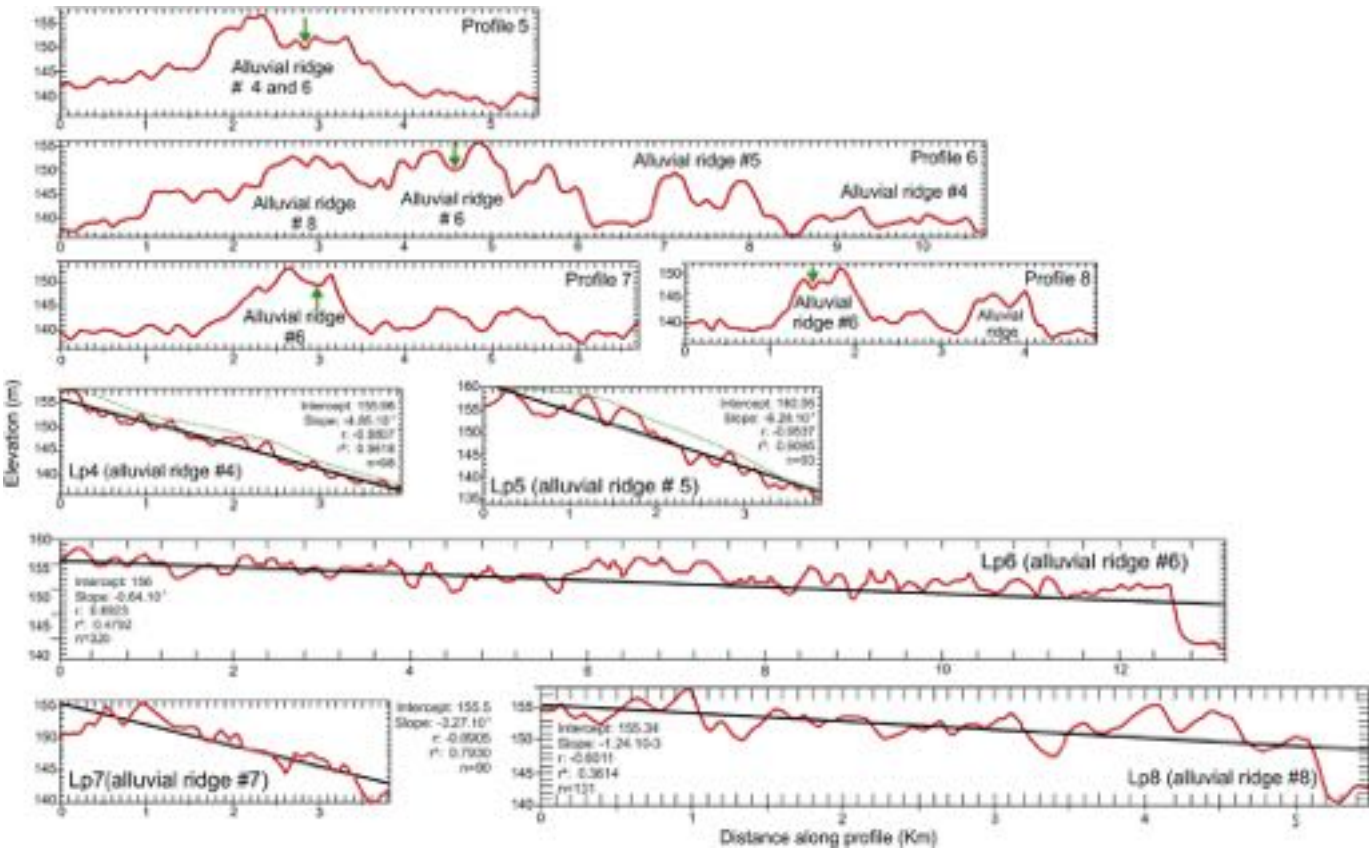

Fig. 9. Topographic profiles of the Splay 3, on the southern left bank crevasse splay. Location of profiles on Fig. 5. Profiles 5 to 8: topography across the crevasse splay. Profiles Lp4 to Lp8: along ridge profiles of the alluvial ridges of the crevasse splay (alluvial ridges #4 to 8 featured on Fig. 5). Green arrows point the location of the anastomosed channel. (For interpretation of the references to colour in this figure legend, the reader is referred to the web version of this article.)

time. These avulsions were nodal between 21, 160 and 9200 Cal years BP associated with wandering/meandering streams and then random avulsions related to straight to low sinuosity rivers since 9200 Cal years BP. The development of the anastomosing morphology presented in this study only occurred since 1691 AD (Bernal et al., 2011). Avulsions identified in the Lower Rio Ucayali (Dumont, 1996) occurred on a high sinuosity meandering river (600 m in width within a 20 km wide alluvial ridge). The modern Ucayali exhibits three major anastomosed channels.

On the Andean foothill avulsions only led to anastomosing morphologies in the NAFAZ, on the lower Rio Ucayali and Pastaza, Both are tributaries of the Rio Marañon. The Rio Marañon flows

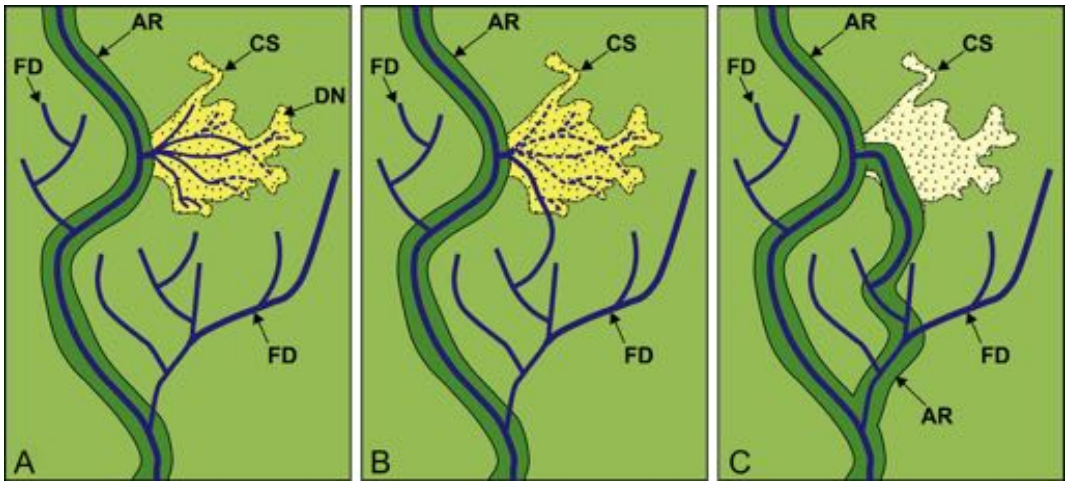

Fig. 10. Sketch map showing the evolution of the lower Pastaza crevasse splay into an anastomosing alluvial ridge. AR: Alluvial ridge (including channel and natural levees), CS: crevasse splay, DN: Distributary network, FD: Floodplain drainage. A: initial crevassing and progradation of the crevasse splay in the floodplain. B: crevasse splay channel capture by a pre-existing floodplain drain and abandonment of the crevasse splay channel after the capture. C: final abandonment of the crevasse splay channels end development of a new alluvial ridge joining the former crevasse splay drain upstream and the former floodplain drain downstream.

perpendicularly to the subandean topographic front of the Andes while the Rio Pastaza and Ucayali flow obliquely before joining the Rio Marañon. The Rio Marañon is moreover bigger than the Rio Pastaza and Ucayali. In the SAFAZ, the Rio Beni joins the Rio Solimoes in Brazil 1700 km downstream. The Rio Grande, Parapeti and Pilcomayo joins no other stream and disappear in the subandean basin by mean of terminal fans. Comparing the two areas, it appears the anastomosing reaches of rivers in the subandean foothill are related to the Rio Marañon. Due to its size, it seems to control the base level in the NAFAZ. Therefore it controls the river gradient in the lower course of its tributaries. In contrast, in the SAFAZ, there is no direct base level control exerted by a main drain and avulsions are mainly controlled by the tectonic context (Horton and De Celles, 2001). Unfortunately there are no data precising the aggradational dynamic of the Rio Marañon.

8. Conclusion

In spite of minor differences, the three examples studied in the present paper show the same evolutional history: (1) initial crevassing; (2) crevasse splay propagation in the floodplain; (3) capture of one of the splay channels by a pre-existing channel of the floodplain with headward erosion progressively reducing the initial channel slope; (4) change of this channel into a diverging – rejoining channel being part of a larger-scale anastomosing system. The main difference is concerned with the capturing (or annexed) floodplain stream. In example 1 (Rio Huangana) this stream is a tributary flowing parallel to the main channel for a rather long distance before being annexed and beheaded. The splay is rather distant from the main channel, relatively small, and immediately postdates the annexation. In examples 2 and 3, the splay forms where crevassing occurs, is relatively large, and develops a distributary network. Capture or annexation selects one of these drains to further become an anabranch of the future larger-scale anastomosing system. Crevassing and consecutive avulsions take advantage of the presence of meanders and this location seems to be at the origin of the rather regular anastomoses of the lower Pastaza.

Although the precipitation regime and discharges curves are rather regular, levees breaching and crevasse splay formation are likely to be results of annual floods which are present in this area as in the rest of Amazonia.

Acknowledgements

This investigation was supported by a doctoral Albαn fellowship of the European Union (n° E05D057404EC), IRD and Université Paul Sabatier grants. We are grateful to the HYBAM/Ecuador project and its partnership institutions, INAMHI and IRD; and to the 'Instituto Geofisico' of the 'Escuela Politecnica Nacional' of Quito – Ecuador. The Centre for Tropical Agriculture (CIAT) provided topographic data. The authors thank Bart Makaske and an anonymous reviewer for their constructive comments.

References

Assine, M., 2005. River avulsions on the *Taquari megafan*, Pantanal wetland, Brazil. Geomorphology 70, 357–371.

Bernal, C., Christophoul, F., Darrozes, J., Soula, J.-C., Baby, P., Burgos, J., 2011. Late glacial and holocene avulsions of the Rio Pastaza Megafan (Ecuador-Peru): frequency and controlling factors. International Journal of Earth Sciences (Geologische Rundschau) 100, 1759–1782. http://dx.doi.org/10.1007/s00531-010-0555-9.

Bernal, C., Christophoul, F., Soula, J.-C., Darrozes, J., Bourrel, L., Laraque, A., Burgos, J., Bès de Berc, S., Baby, P., 2012. Gradual diversions of the Rio Pastaza in the Ecuadorian piedmont of the Andes from 1906 to 2008: role of tectonics, alluvial fan aggradation and ENSO events. International Journal of Earth Sciences (Geologische Rundschau). http://dx.doi.org/10.1007/s00531-012-0752-9.

Bès De Berc, S., Soula, J., Baby, P., Souris, M., Christophoul, F., Rosero, J., 2005. Geomorphic evidence of active deformation and uplift in a modern continental wedge-top – foredeep transition: example of the eastern Ecuadorian Andes. Tectonophysics 399, 351–380.

Bridge, J., 2003. Rivers and Floodplains: Forms, Processes and Sedimentary Record. Blackwell Publishing, p. 491.

Brierley, G.J., Ferguson, R.J., Woolfe, K.J., 1997. What is a fluvial levee? Sedimentary Geology 114, 1–9.

Burgos, J., 2006. Genèse et progradation d'un cône alluvial au front d'une chaine active: exemple des Andes Equatoriennes au Néogene. Ph.D. thesis, Université Paul Sabatier, Toulouse, France, p. 282.

CDC-UNALM, 2002. Complejo de humedales del abanico del Rio Pastaza, Loreto-Peru. Centro de Datos para la Conservación – Universidad Nacional Agraria La Molina (CDC-UNALM), Lima Peru. http://cdc.lamolina.edu.pe/Descargas/eer/menu_eer.htm, p. 122.

Christophoul, F., Baby, P., Soula, J.-C., Rosero, M., Burgos, J., 2002. The Neogene fluvial systems of the Ecuadorian foreland basin and dynamic inferences. Comptes Rendus Géosciences 334, 1029–1037. http://dx.doi.org/10.1016/j.crte.2002.14.003.

Coltelli, M., Fornaro, G., Franceschetti, G., Lanari, R., Migliaccio, M., Moreira, J.R., Papathanassiou, K.P., Puglisi, G., Riccio, D., Schwabisch, M., 1996. SIR-C/X-SAR multifrequency multipass interferometry: a new tool for geological interpretation. Journal of Geophysical Research 101, 23127–23148.

Dumont, J.-F., 1991. Fluvial shifting in the Ucamara depression as related to the neotectonics of the Andean foreland Brazilian Craton Border (Peru). Géodynamique 6, 9–20.

Dumont, J.-F., Fournier, M., 1994. Geodynamic environment of Quaternary morphostructures of the Subandean foreland basins of Peru and Bolivia: characteristics and study methods. Quaternary International 21, 129–142.

Dumont, J.-F., 1996. Neotectonics of the Subandes-Brazilian Craton boundary using geomorphological data: the Marañon and Beni Basins. Tectonophysics 257, 137–151.

Espinoza, J.C., Ronchail, J., Guyot, J.L., Cochonneau, G., Filizola, N., Lavado, W., de Oliveira, E., Pombosa, R., Vauchel, P., 2009. Spatio-temporal rainfall variability in the Amazon Basin Countries (Brazil, Peru, Bolivia, Colombia and Ecuador). International Journal of Climatology 29, 1574–1594.

Farr, T.G., Rosen, P.A., Caro, E., Crippen, R., Duren, R., Hensley, S., Kobrick, M., Paller, M., Rodriguez, E., Roth, L., Seal, D., Shaffer, S., Shimada, m, Umland, J., Werner, M., Oskin, M., Burbank, D., Alsdorf, D., 2007. The shuttle radar topography mission. Review of Geophysics 45, RG2004. http://dx.doi.org/10.1029/2005RG000183.

Gautier, E., Brunstein, D., Vauchel, P., Roulet, M., Fuertes, O., Guyot, J.-L., Darrozes, J., Bourrel, L., 2007. Temporal relations between meander deformation, water discharge and sediment fluxes in the floodplain of the Rio Beni (Bolivian Amazonia). Earth Surface Processes and Landforms 32, 230–248. http://dx.doi.org/10.1002/esp.1394.

Gautier, E., Bunstein, D., Vauchel, P., Jouanneau, J.-M., Roulet, M., Garcia, C., Guyot, J.-L., Castro, M., 2010. Channel and floodplain sediment dynamics in a reach of the tropical meandering Rio Beni (Bolivian amazonia). Earth Surface Processes and Landforms 35, 1838–1853.

Horton, B.K., DeCelles, P.G., 2001. Modern and ancient fluvial megafans in the foreland basin system of the central Andes, southern Bolivia: implications for drainage network evolution in fold-thrust belts. Basin Research 13, 43–63.

Jain, V., Sinha, R., 2005. Response of active tectonics on the alluvial Baghmati River, Himalayan foreland basin, eastern India. Geomorphology 70, 339–356.

Jarvis, A., Reuter, H.I., Nelson, A., Guevara, E., 2008. Hole-filled Seamless SRTM Data V4. International Centre for Tropical Agriculture (CIAT). Available from: http://srtm.csi.cgiar.org.

Jensen, J.R., 2000. Remote Sensing of the Environment: An Earth Resource Perspective. Prentice Hall, Upper Saddle River, New Jersey, p. 592.

Jerolmack, D.J., Paola, C., 2007. Complexity in a cellular model of river avulsion. Geomorphology. http://dx.doi.org/10.1016/j.geomorph.2007.04.022.

Jones, L., Harper, J., 1998. Channel avulsions and related processes, and large – scale sedimentation patterns, Rio Grande, San Luis Valley, Colorado. Geological Society of America Bulletin 110, 411–421.

Jones, L., Schumm, S., 1999. Causes of avulsion: an overview. Special Publication of the International Association of Sedimentologists 28, 171–178.

Kellndorfer, J., Walker, W., Leland, P., Dobson, C., Fites, J.A., Hunsaker, C., Vona, J., Clutter, M., 2004. Vegetation height estimation from shuttle radar topography mission and national elevation datasets. Remote Sensing of Environment 93, 339–358. http://dx.doi.org/10.1016/j.rse.2004.07.017.

Laraque, A., Bernal, I.C., Bourrel, L., Darrozes, F., Christophoul, F., Armijos, E., Fraizy, P., Pombosa, R., Guyot, J.-L., 2009. Sediment budget of the Napo river (Amazon basin, Ecuador and Peru). Hydrological Processes 23, 3509–3524. http://dx.doi.org/10.1002/hyp.7463.

Latrubesse, E., Stevaux, J.C., Sinha, R., 2005. Tropical rivers. Geomorphology 70, 187–206. http://dx.doi.org/10.1016/j.geomorph.2005.02.005.

Leier, A., DeCelles, P., Pelletier, J., 2005. Mountains, monsoons and megafans. Geology 33, 289–292.

Makaske, B., 2001. Anastomosing rivers: a review of their classification, origin and sedimentary products. Earth-science Reviews 53, 149–196.

Martinez, J.M., Le Toan, T., 2007. Mapping of flood dynamics and spatial distribution of vegetation in the Amazon floodplain using multitemporal SAR data. Remote Sensing of Environment 108, 209–223.

Mellack, J.M., Hess, L.L., 2004. Remote sensing of wetlands on a global scale. SIL News 42, 1–5.

Mohrig, D., Heller, P.L., Paola, C., Lyons, W.J., 2000. Interpreting avulsion process from ancient alluvial sequences: Guadalope-Matarranya (Northern Spain) and Wasatch Formation (western Colorado). Geological Society of America Bulletin 112, 1787–1803.

Morozova, G., Smith, N., 2000. Holocene avulsion style and sedimentation patterns of the Saskatchewan River, Cumberland Marshes, Canada. Sedimentary Geology 13, 81–105.

Räsänen, M.E., Salo, J.S., Jungnert, H., Pittman, L.R., 1990. Evolution of the Western Amazon Lowland Relief: impact of Andean foreland dynamics. Terra Nova 2, 320–332.

Räsänen, M.E., Neller, R., Salo, J., Jungner, H., 1992. Recent and ancient fluvial deposition systems in the Amazonian foreland basin. Peru Geological Magazine 129, 293–306.

Roddaz, M., Baby, P., Brusset, S., Hermoza, W., Darrozes, J., 2005. Forebulge dynamics and environmental control in Western Amazonia: the case study of the Arch of Iquitos (Peru). Tectonophysics 399, 87–108.

Roddaz, M., Hermoza, W., Mora, A., Baby, P., Parra, M., Christophoul, F., Brusset, S., Espurt, N., 2010. Cenozoic sedimentary evolution of the amazonian foreland basin system. In: Hoorn, C., Wesselingh, F. (Eds.), Amazonia, Landscape and Species Evolution: a Look in the Past. Blackwell Publishing. http://dx.doi.org/10.1002/9781444306408.ch5.

Rodriguez, E., Morris, C.S., Belz, J.E., Chapin, E.C., Martin, J.M., Daffer, W., Hensley, S., 2005. An Assessment of the SRTM Topographic Products. Technical Report JPL D-31639. Jet Propulsion Laboratory, Pasadena, California, p. 143.

Sarma, J., 2005. Fluvial process and morphology of the Brahmaputra River in Assam, India. Geomorphology 70, 226–256.

Sinha, R., Jain, V., Prasad Babu, G., Ghosh, S., 2005. Geomorphic characterization and diversity of the rivers of the Gangetic plains. Geomorphology 70, 207–225.

Slingerland, R., Smith, N.D., 2004. River avulsion and their deposits. Annual Review of Earth and Planetary Sciences 32, 257–285.

Smith, N.D., Cross, T.A., Dufficy, J.P., Clough, S.R., 1989. Anatomy of an avulsion. Sedimentology 36, 1–23.

Stanistreet, I.G., Cairncross, B., McCarthy, T.S., 1993. Low sinuosity meandering river bedload rivers of the Okavongo Fan: channel confinement by vegetated levees without fine sediment. Sedimentary Geology 85, 135–156.

Stouthamer, E., Berendsen, H.J.A., 2000. Factors controlling the holocene avulsion history of the Rhine–Meuse delta (The Netherlands). Journal of Sedimentary Research 70, 1051–1064.

Stouthamer, E., Berendsen, H.J.A., 2007. Avulsion: the relative roles of autogenic and allogenic processes. Sedimentary Geology 198, 309–325.

Törnqvist, T.E., 1994. Middle and Late Holocene avulsion history of the river Rhine (Rhine-Meuse delta, Netherlands). Geology 22, 711–714.

Valeriano, M.M., Kuplich, T.M., Storino, M., Amaral, B.D., Mendes, J.R., Lima, D., 2006. Modeling small watersheds in Brazilian Amazônia with SRTM-90m data. Computer in Geosciences 32, 1169–1181.

Wilkinson, M.J., Marshall, L.G., Lundberg, J.G., Kreslavsky, M.H., 2010. Megafan environments in Northern South America and their impact on Amazon Neogene aquatic ecosystem. In: Hoorn, C., Wesselingh, F.P. (Eds.), Amazonia, Landscape and Species Evolution: a Look into the Past. Blackwell publishing. http://dx.doi.org/10.1002/9781444306408.ch10.

Zapata, A., Ticona, P., Atencio, E., 1998. Evolución del Abanico del Pastaza y su relación con los depósitos Ucamara, X Congreso Peruano de Geología, Lima – Perú, pp. 61–70.

Annexe B

Bernal, C., Christophoul, F., Soula, J-C., Darrozes, J., Bourrel, L., Laraque, A., Burgos, J., Bès de Berc, S., Baby, P. (2012)
International Journal of Earth Sciences (Geologische Rundschau)

Cet article, issu des travaux de thèse de C. Bernal présente un exemple d'avulsion, suivi à l'échelle historique, dans un contexte de tectonique active. Cette étude illustre les interactions complexes entre les paramètres climatiques (précipitations, débits), la déformation de surface (se réduisant, dans le cas étudié à un basculement) et la sédimentation dans une zone de transition entre un tronçon encaissé et déconfiné.

Résumé :

Les tracés successifs empruntés par le rio Pastaza sur le piémont des Andes d'Equateur ont pu être cartographiés grâce à la compilation de cartes historiques, de photographie aériennes Ainsi que par une analyse fine de la topographie et des profils en long et de données de terrain.

Le passage rapide du rio Pastaza d'un cours transverse à longitudinal s'est fait par deux avulsions partielles consécutives s'étant produites entre 1906 et 1976 au niveau d'un changement morphologique de la plaine alluviale (transition tresse - méandre). Ces avulsions sont liées à l'aggradation fluviale au pied d'un cône de piémont progradant sur la surface topographique du plateau de Puyo, inclinée à contrepente, résultant du basculement de la surface au toit du Chevauchement Frontal de la Zone Subandine.

Une première avulsion s'étant produite après 1906 se traduit par l'abandon de la branche nord du cours du Rio Pastaza. Une suivante, antérieure à 1976 mène à la coexistence de la branche post-1906 et d ?une nouvelle branche nord-sud. La branche post-1906 est par la suite progressivement abandonnée jusqu'à 2008.

Le basculement tectonique a renforcé l'aggradation à l'amont du nœud commun des trois avulsions décrites tout en favorisant le déplacement du cours d'eau le long de la cordillère des Andes en créant une pente locale vers l'ouest.

La corrélation entre les phénomènes ENSO extrêmes sur la période 1976-2008 suggère que le déclencheurs des avulsions sont les hauts débits de crues liés aux ENSO (plus exactement aux épisodes pluvieux de Niña consécutifs aux ENSO) qui contrastent très fortement avec les débits des crues annuelles, par ailleurs peu marqués par rapport à la distribution annuelle des débits du Rio Pastaza.

Int J Earth Sci (Geol Rundsch) (2011) 100:1759–1782
DOI 10.1007/s00531-010-0555-9

ORIGINAL PAPER

Late Glacial and Holocene avulsions of the Rio Pastaza Megafan (Ecuador–Peru): frequency and controlling factors

Carolina Bernal · Frédéric Christophoul · José Darrozes · Jean-Claude Soula · Patrice Baby · José Burgos

Received: 29 November 2008 / Accepted: 20 April 2010 / Published online: 6 June 2010

Abstract The geomorphological study by means of remote sensing imagery of the Rio Pastaza Megafan (Ecuador and northern Peru) reveals the traces of numerous avulsions. One hundred and eight avulsion sites have been defined. The location of these sites, the available radiocarbon ages as well as historical maps of the seventeenth century, enable us to propose an evolution history of the migration and avulsions of the Rio Pastaza since the Last Glacial Maximum. The first avulsions of the Río Pastaza occurred after the LGM in a zone close to and roughly parallel to the sudandean front, where the developed avulsion gave a distributive pattern to the ancient stream of the Río Pastaza in an area located between the modern Río Morona and Pastaza, where they caused the Rio Pastaza to develop a fan-like distributary pattern. This is interpreted as a response to thrust-related forelimb tilt, progressively shifting eastward the Rio Pastaza and the apex of the megafan. This sequence of events ended with the Great Diversion of the Rio Pastaza towards the modern Rios Corrientes and Tigre. Avulsions occurred in the Tigre-Corrientes Area between 9200 and 8,500 years Cal BP. Afterwards, the Río Pastaza was diverted to its present-day north–south course. This last significant avulsion occurred before AD 1691. In the area located between the modern Río Morona and Pastaza, avulsion frequency—probably overestimated—ranges between 100 and 200 years. In the Ríos Tigre and Corrientes area, avulsion frequency—probably underestimated—ranges from 300 to 400 years. Regional tectonics is likely to have triggered most of the avulsions in the Morona Pastaza area but its influence is restricted to this area. The factors controlling the avulsions in the Tigre-Corrientes area are less clear because the frequently described "hydrologic"-driven avulsion as observed in areas characterized by contrasted hydrologic cycles are inconsistent with the characteristics of the hydrologic cycles of the Rio Pastaza.

Keywords Avulsion · Megafan · Amazonia · Controlling factors · Post-LGM · Tectonics

C. Bernal · F. Christophoul (✉) · J. Darrozes · J.-C. Soula · P. Baby
Université de Toulouse, UPS (SVT-OMP), LMTG, 14 Av, Edouard Belin, 31400 Toulouse, France
e-mail: christo@lmtg.obs-mip.fr

C. Bernal
e-mail: bernal@lmtg.obs-mip.fr

J. Darrozes
e-mail: darrozes@lmtg.obs-mip.fr

J.-C. Soula
e-mail: soula@lmtg.obs-mip.fr

P. Baby
e-mail: patrice.baby@ird.fr

P. Baby
IRD, LMTG, 31400 Toulouse, France

J. Burgos
Petroamazonas, Av. Naciones Unidas E7-95 y Shyris, Quito, Ecuador, 4to piso, Quito, Ecuador
e-mail: jose_burgos@petroamazonas.ec

Introduction

Fluvial megafans form as rivers exit the topographic front of a mountain and play a major role in the dispersal of sediments and sedimentation in overfilled foreland basins (Leier et al. 2005).

Because of their size and mean slope, megafans constitute specific geomorphic units. Whereas smaller-sized alluvial fans involve deposition of successive lobes as the

main process of sediment accumulation (Blair and McPherson 1992; Schumm et al. 1987), sedimentation in megafans is dominated by avulsion and bifurcation of the main streams (Bridge and Karssenberg 2005). Style of avulsions (Slingerland and Smith 2004) in megafans as well as their frequency strongly influences the sedimentation rate and the stratigraphic architecture. Numerous studies have been carried out on the typology and frequency of avulsion and characteristics of anastomosis in deltas (Törnqvist 1994; Stouthamer and Berendsen 2000, 2001), and alluvial plains (Nelson 1970; Saucier 1994; Autin et al. 1991; Morozova and Smith 1999, 2000). Megafans have been less considered (Gole and Chitale 1966; Gohain and Parkash 1990; Singh et al. 1993; Assine 2005; Assine and Soares 2004). However, because of their size, slope and situation in the piedmont of mountain fronts, the question arises of the specificity of megafans in terms of causes and triggers of avulsion, and, in particular, the balance between tectonics and sedimentary/climatic events.

This study focuses on the Napo-Pastaza megafan in the northern Andes. This megafan is located on the Amazonian foothills of Ecuador and northern Peru, roughly between 2°00 and 5°00S and between 74°00W and 78°00W. It covers 51,400 km^2 (Fig. 1). This study is based on the mapping of the successive courses of the Rio Pastaza and its main tributaries, mainly from remote sensing and DEM analyses. The aim of this paper is to establish the relative chronology, the average frequency and the style of the avulsions in the past 20,000 years and to discuss the causes and triggers of these avulsions as functions of the different entities which have formed the megafan system. Dynamics of avulsion in the Pastaza megafan will be then compared with other areas known for frequent avulsions.

General setting

Geology and geomorphology

Structural organization

The part of the Ecuadorian Andes involved in the Amazonian drainage can be divided into 4 morphotectonic units which are, from west to east: the Western Cordillera, the Interandean depression, the Eastern Cordillera, the Subandean zone and the Amazonian foreland (Fig. 1).

The Western Cordillera and Interandean Depression are constituted by Upper Cretaceous-Paleogene formations, mainly andesitic (Reynaud et al. 1999; Lavenu et al. 1992; Kennerley 1980) unconformably overlain by neogene andesitic formations affected by late Miocene to early Pleistocene deformations (Lavenu et al. 1992; Barragann et al. 1996; Hungerbühler et al. 2002; Winkler et al. 2005) and Quaternary volcanic formations (Kennerley 1980; Barberi et al. 1988; Lavenu et al. 1992).

The Eastern Cordillera consists in Paleozoic through upper Cretaceous rocks, metamorphosed and deformed during late Cretaceous to Paleocene time (Pratt et al. 2005), eroded and then blanketed by late Miocene to Pliocene volcanic/volcanoclastic formations and Quaternary volcanics (Lavenu et al. 1992). Apatite fission track analyses and U-Th/He measurements indicate a moderate to slow uplift from the Miocene to the late Pliocene (Spikings et al. 2000; Spikings and Crowhurst 2004).

The Subandean zone is separated from the Eastern Cordillera by the west dipping Subandean Thrust fault. The Subandean zone comprises in the west the Abitagua Cordillera, and in the east two thrust-related antiformal thrust stacks (as defined by e.g., McClay 1992), locally known as the Napo and Cutucu "uplifts", involving Jurassic through Neogene formations. These antiformal stacks appear as axial culminations (in the sense of Ramsay 1967, p. 346, Ramsay and Huber 1987) separated by an axial depression known as the Pastaza depression. The Pastaza depression is filled with middle (?) through Upper Pleistocene piedmont deposits (Mera formation) which formed the apex of the Mera megafan (Tschopp 1953; Baby et al. 1999; Bes de Berc et al. 2005).

In front of the Subandean zone, the Amazonian basin preserves a sedimentary stack ranging from Paleozoic to Oligocene overlying the Brazilian shield. Fluvial aggradation occurred there since ~22 Ma accumulating sediments issued from the west (Christophoul et al. 2002; Burgos 2006) to build a very large megafan. This large megafan termed hereafter Neogene megafan corresponds to the present-day basins of the left-bank tributaries of the Rio Maranon (including the Rio Pastaza) and those of the right-bank tributaries of the Rio Napo. It can be shown that the apex of this fan migrated eastward from the early Miocene to now as a result of the forward propagation of the mountain front (Christophoul et al. 2002; Bes de Berc et al. 2005; Burgos 2006). In the east of the megafan, an elongated flat-topped topographic high striking N130°, interpreted to be the exhumed Upper Miocene forebulge (Iquitos Arch in Roddaz et al. 2005), appears as an area of no- or limited Neogene deposition. The active part of the megafan (the modern Pastaza megafan) is located in the south-western side of the Neogene megafan, including the left-bank tributaries of the Rio Morona-Santiago, the lower Rio Pastaza, and the right-bank tributaries of the Rios Tigre and Corrientes.

The Puyo Plateau

The 'Pastaza depression' appears as a very gentle arch dipping 0.4–0.5° west in its central part known as the Puyo

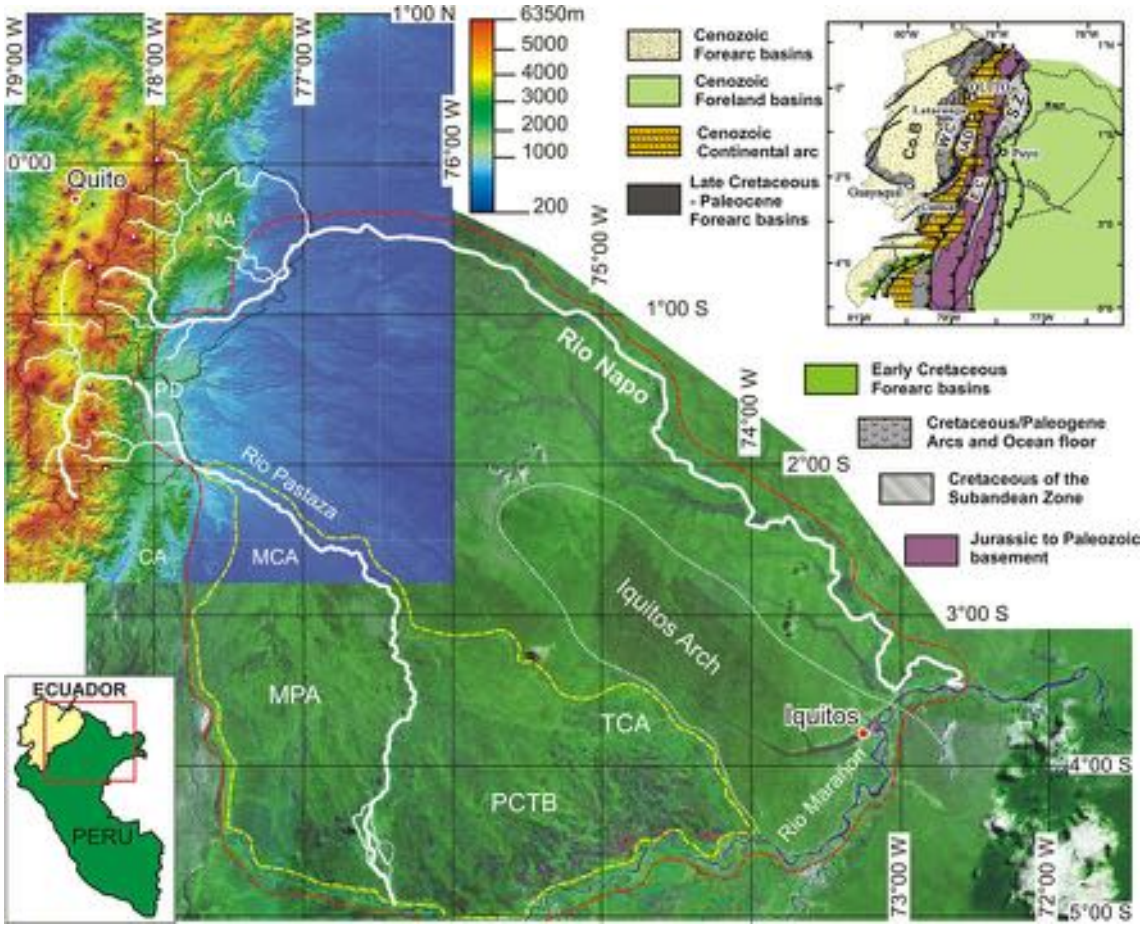

Fig. 1 Composite map of the Napo-Pastaza Megafan (DEM SRTM 3 resolution and Landsat 7). *Solid black lines* limits of the Napo and Pastaza catchments, *solid white lines* modern Rio Napo and Pastaza, *red dashed lines* limits of the Plio-Pleistocene Napo-Pastaza Megafan, *yellow dashed lines* post-LGM Pastaza Megafan. *Blue points* volcanoes, *white squares* actives volcanoes. *NA* Napo Antiform, *PD* Pastaza Depression, *CA* Cutucu Antiform, *MCA* Morona Cangaime Area, *MPA* Morona Pastaza Area, *TCA* Tigre-Corrientes Area, *PCTB* Pastaza-Corrientes Transition Band

plateau. The plateau surface appears as a low angle weathered and hardened surface cut through the uppermost Pleistocene Mera megafan (Mera surface, Heine 1994, 2000; Bes de Berc et al. 2005). The same surface is found in the upper Amazonian foreland (Villano surface, Figs. 1, 2) here it forms another but highly dissected plateau. Arching and backtilting of the Puyo plateau as consequences of the propagation of the Subandean Frontal Thrust (Bes de Berc et al. 2005) caused beheading or diversions of the transverse rivers—including the Pastaza River—which formerly flowed eastward into the Amazonian plain (Bes de Berc et al. 2005; Burgos 2006).The tectonic offset between the Puyo and Villano plateaus reaches ~450 m in the centre of the arch and decreases progressively sideways. The Mera erosional surface formed between ~23 and 24 ^{14}C ky BP which is the age of the younger sediment cut by the surface, and ~18 ^{14}C ky BP which is the age of the older deposits along rivers incising the surface (Bes de Berc et al. 2005). As this period corresponds to the time of deposition of the Last Glacial Maximum (LGM) terminal moraines (Heine 2000), the formation of the surface can be ascribed to the LGM. Therefore, arching and backtilting of this surface and the consecutive diversion of the Rio Pastaza were younger than the LGM.

The Rio Pastaza catchment upstream of the Amazonian domain

The Rio Pastaza forms by the confluence of two longitudinal rivers flowing in the Interandean Depression (Figs. 1, 2). Downstream of this confluence, the Rio Pastaza crosses the Eastern Cordillera along a deep (>2,200 m) and narrow transverse valley (Fig. 1). In the Subandean Fault zone and the western Puyo plateau, the Pastaza valley becomes much wider and shallow showing stepped degradational terraces (Bes de Berc et al. 2005). In the central Puyo plateau, the Rio Pastaza traverses a preserved Pliocene volcanic complex.

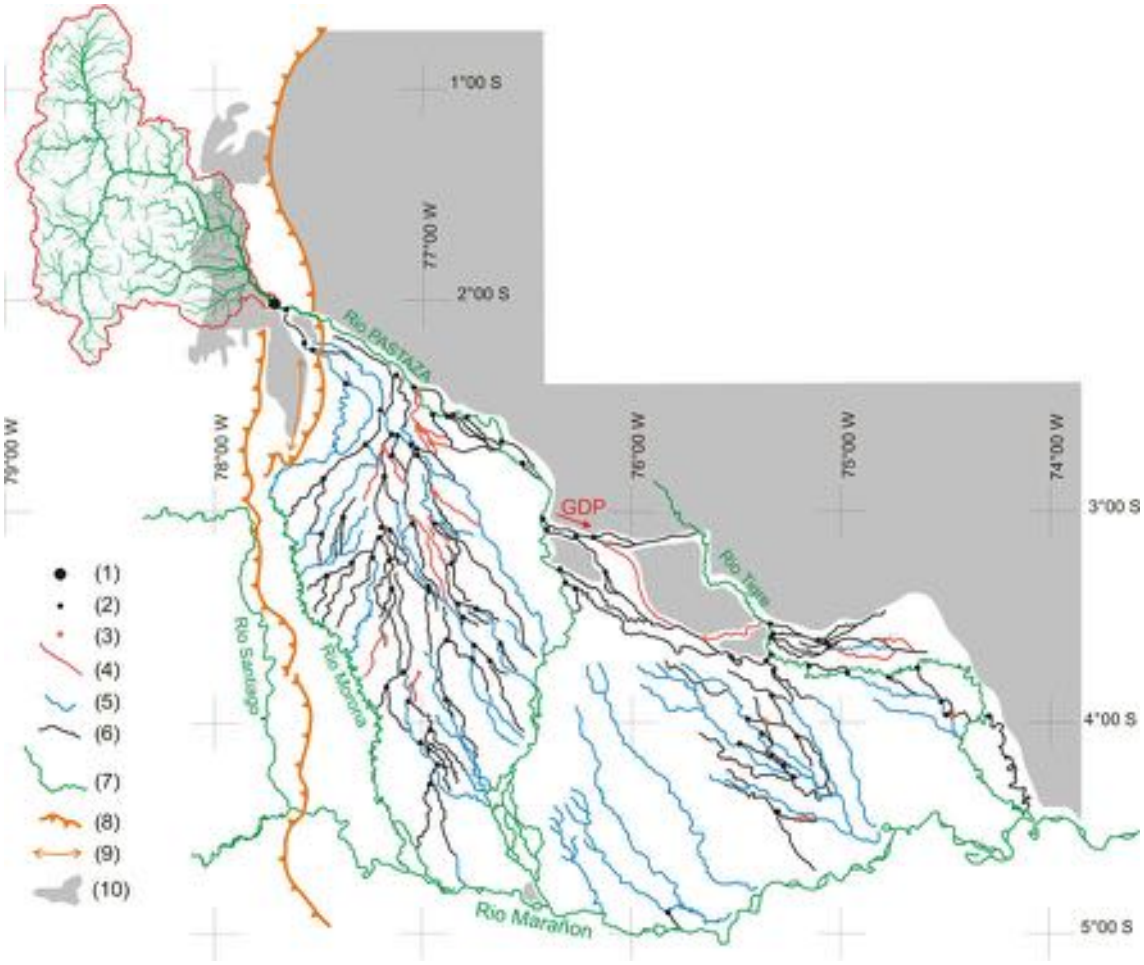

Fig. 2 Hydrographic network of the Rio Pastaza basin. To the northwest, with *red lines* catchment of the Rio Pastaza Megafan (extracted from the SRTM DEM). With *green lines* drainage network. Thickness of lines depends on the Stralher order of the streams. Thinnest lines correspond to order 3 streams. *1* Modern apex of the Pastaza Megafan, *2* avulsion sites, *3* supposed avulsion sites, *4* abandoned stream, *5* abandoned stream re-annexed by the modern drainage network, *6* supposed abandoned stream, *7* main modern streams, *8* eastern boundary of the subandean tectonic structures, *9* Cangaime anticline axis, *10* Puyo plateau and Villano surface

The overall flow direction is there towards the south-southeast. The area of the Pastaza catchment upstream of its debouchement in the Amazonian plain is 13,700 km^2. Measurements of vertical incision rates in the Eastern Cordillera since the LGM have given values ranging from 0.5 to 0.67 cm year^{-1}, increasing from the LGM to now, resulting from a rapid uplift, up to 1 cm year^{-1} in front of the Abitagua cordillera (Bes de Berc et al. 2005). The deep incision of the Eastern Cordillera by the Pastaza valley indicates that a rather rapid uplift of at least 2 mm year^{-1} succeeded the Miocene through middle Pliocene period of slow denudation and uplift evidenced by the Apatite fission tracks analyses and U-Th/He measurements of Spiking et al. (2000) and Spiking and Crowhurst (2004). Denudation rate, greater than $\sim$0.2 mm year^{-1} in average and locally as high as 0.4 mm year^{-1}, have been obtained in the Eastern Cordillera by Vanacker et al. (2007a, b) from cosmogenic radionuclide (^{10}Be) studies.

Climatic setting

Late Pleistocene and Holocene climate

Several authors (Hastenrath 1981; Hastenrath and Kutzbach 1985; Heine and Heine 1996; Heine 2000) consider the LGM to have been a cooler and more arid period responsible for the lack of sediment in the Brazilian lowland between 24 and 17 ky (Ledru et al. 1998) whereas Seltzer et al. (2002) indicate cool but wet conditions from 30 to 15 ky in the Peruvian Altiplano. In Ecuador, the LGM moraines are ^{14}C dated between 25 and 15 ky although the maximum extent of glaciers is inferred to have

occurred between 30 and 25 ^{14}C ky BP (Heine 2000). According to the latter author, the retreat of glaciers between 25 and 16 ^{14}C ky BP was due to glacier shrink because of increased aridity (increased insolation and decreased precipitations) and not to warming (Heine 2000). Increased aridity can explain the development of an erosion surface involving soil creeping and sheetflooding rather than fluvial incision and transport (e.g., Leeder et al. 1998). In the southern interandean depression, pollen analyses indicate that climate was cooler and moister than today during the late glacial period (17–11 Cal ky BP, Rodbell et al. 1999; Hansen et al. 2003). However, the vegetational changes in the Interandean Depression may have been influenced by winds from the west as well as from the east (Hansen et al. 2003), and these results are not necessarily applicable to the Amazonian basin much more influenced by the humid Atlantic winds.

For Clapperton et al. (1997), a significant re-advance of glaciers occurred during the Younger Dryas (11–10 ^{14}C ky BP) whereas for Heine and Heine (1996) and Heine (2000), this advance of glaciers took place at least 500 years later.

The climatic data for the Holocene have been inferred from vegetational changes in the Interandean Depression (Rodbell et al. 1999; Hansen et al. 2003) and in the northern side of the Neogene megafan (Yasuni National Park, northeast of Ecuador, Weng et al. 2002). Weng et al.'s (2002) palynological studies indicate that tropical rain forest has developed throughout the Holocene with minor climatic oscillations. According to these authors, severe droughts occurred in the period 8,700–5,800 Cal years BP, which should be correlated with other records from Amazonia, adjacent savannas and the Andes (Hastenrath and Kutzbach 1985; Frost 1988; Behling and Hooghiemstra 1998, 1999). This "dry" period was succeeded by more uniform and wetter conditions with alternating wetter and drier millennial-scale events (Weng et al. 2002).

The ENSO events

ENSO (El Nino Southern Oscillation) events have been recorded in Ecuador and neighbouring areas since the late Pleistocene. According to Keefer et al. (2003) studying deposits in the Pacific side of the Northern Peruvian Andes, 10 severe ENSO events occurred between 38,200 and 12,900 Cal years. In the southern Interandean Depression of Ecuador, Rodbell et al. (1999) and Moy et al. (2002) studying storm-induced lake deposits found that ENSO events became significant only after $\sim$5 ky BP, with highest spectral density and frequencies between $\sim$3.5 and 2.6 ky and during the last 660 years. The reduced ENSO activity should be correlated with the severe droughts of the period 8,700–5,800 Cal years BP inferred by Weng et al. (2002) whereas the increased ENSO activity should be correlated with the following wetter period. The seventeenth and twentieth centuries are also characterized by very strong ENSO events (Cobb et al. 2003; Keefer et al. 2003) and the last very severe events occurred in the years 1982–1983 and 1997–1998.

The recent and historical ENSO events generated floods and steep-sloping hillslope-toe landslides on the western slopes of the Western Cordillera, an area that is normally much less humid than the Eastern Cordillera and Amazon basin (Demoraes and d'Ercole 2001). In contrast, in eastern Ecuador continuously submitted to the humid Atlantic winds, no unusual floods were signalled during the 1982–1983 and 1997–1998 events. Similarly, no catastrophic floods have been registered for the seventeenth century events in the catalogue of major historical disasters in eastern Ecuador with the reserve that chronicles of that time seem to have been little concerned with eastern Ecuador.

Tectonic activity

Recent and active tectonics

In the Interandean Depression, late Miocene to early Pleistocene syntectonic deposits have been recognized and dated by means of K–Ar and U-Th/He measurements at 8.5–7.9 to 1 Ma (Lavenu et al. 1992; Kennerley 1980; Barberi et al. 1988; Barragann et al. 1996; Hungerbühler et al. 2002; Winkler et al. 2005).

In the Eastern Cordillera, the deformation affects the widespread volcanic and volcaniclastic Pisayambo formation aged of 9–10 to 6 Ma (Lavenu et al. 1992; Barberi et al. 1988), and lavas issued from volcano Altar aged of less than 3.5 Ma (Lavenu et al. 1992), which indicates that the deformation is younger than 3.5 Ma. Apatite fission track analyses and U-Th/He measurements in the western Eastern Cordillera indicate a slow to very slow (when compared with other active ranges) denudation rates from the Miocene to the late Pliocene/early Pleistocene (Spikings et al. 2000; Spikings and Crowhurst 2004). Since the Rio Pastaza has incised the eastern Cordillera more than 2,000 m (Fig. 1), these results support the interpretation that deformation and related uplift of the Eastern Cordillera was Pleistocene in age.

In the frontal Eastern Cordillera and the Subandean Zone, a tectono-sedimentary and geomorphic study supported by ^{14}C dating indicate a tectonic activity related to the propagation of a low angle thrust ramp from at least the middle Pleistocene to now (Bes de Berc et al. 2005).

Earthquakes

In the Harvard Catalogue, 30 earthquakes with magnitude Mw $\geq$ 5 were registered between 1976 and 1999 in eastern Ecuador, with two events $\geq$Mw7 (Mw7.1, 03/06/87; Mw7.0, 10/03/95), the latter being attributed to the activity of the Cutucu frontal thrust (Yepes et al. 1996). Thirty historical events with intensity $\geq$VIII have been recorded between AD1541 and AD 1995 (IGEPN 1999). One event of intensity XI has occurred in AD1797 (MsNOAA magnitude 8.30, NOAA Catalogue, U.S. Geological Survey, 2003), and two events of intensity X in AD1698 (MsNOAA magnitude 7.70) and AD1949 (MsNOAA magnitude 6.80). Most of these events are situated in the Eastern Cordillera and the Subandean Zone. The rare events situated under the Pastaza megafan were deep events which are likely to have had no influence on the drainage network.

Landslides

Earthquakes-triggered landslides were observed in the Eastern Cordillera such as those triggered by the 5 March 1987 M $\sim$7 event (Hall 1991). In eastern Ecuador, the major landslides not triggered by earthquakes were independent of the ENSO events (for example, the La Josefina landslide, the greatest known in Ecuador, occurred in 1993, Demoraes and D'Ercole 2001). Moreover, no landslides related to the severe and frequent seventeenth century ENSO events are registered in the catalogue of major historical disasters and no landslide formed during the 1982–1983 and 1997–1998 events (Demoraes and D'Ercole 2001). Whatever their trigger, the sediments delivered by these major landslides were incised and entirely removed by rivers a few days after the disaster (e.g., Hall 1991) with no avulsion observed downstream. In any event, no major landslides have been registered in the valleys of the Rio Pastaza and major tributaries, and a careful observation of satellite images and air photos has shown no well-characterized landslide scars in the upper Pastaza basin.

Volcanic eruptions

Ecuador is characterized by 20 active volcanoes (e.g., Hall 1977; Hall and Beate 1991; Hall et al. 2008). Four of the most important active or recently active volcanoes, Chimborazo, Cotopaxi, Tungurahua and Sangay, are within, or at the boundary of, the Pastaza drainage basin (Fig. 1).

Chimborazo volcano was active in the late Pleistocene (Hall and Beate 1991; Barba et al. 2008) and the Holocene (between about 8,000 and 1,000 years ago, Barba et al. 2008). The first two of the major Holocene events generated large pyroclastic deposits and thick lahars. Pyroclastic deposits are described for five other major eruptions occurring until the fifth to seventh centuries (Barba et al. 2008).

Cotopaxi volcano had numerous eruptions producing andesitic scoria and pumice ash flows, blocky lava flows and lahars ($\sim$30 eruptions since 1530, Hall 1977). At least four rhyolitic eruptions occurred during the past 10,000 years. A very large ($\sim$71,000 m^3) debris flow (lahar) occurring $\sim$4,500 years ago flowed >130 km east and south into the Rio Patate valley. The initial dry volume has been estimated to $\sim$2 km^3. The most distinctive lahar deposits of the historical period occurred in 1877 and in the eighteenth century. Since 1906, only small eruptions are signalled with limited ash falls or pyroclastic flows (IGEPN 2009) although renewed seismic activity has occurred since 2001 (Molina et al. 2008). Modelling of lahar flows indicate high discharge rates ($\sim$15,000 m^3 s^{-1}, Castro et al. 2006).

Tungurahua volcano has been active since at least the late Pleistocene. Tungurahua II, mainly composed of andesite lava flows younger than 14 ky BP, was partly destroyed by a collapse event, 2,955 $\pm$ 90 years ago, which produced a 8-km^3 avalanche on a distance of $\sim$20 km and a large lahar (Hall et al. 1999). The eruptive activity of the present volcano (Tungarahua III) commenced in the period $\sim$2,300–1,400 years BP (Hall et al. 1999). Lava extrusions and pyroclastic flows occurred since the fourteenth century, notably in 1773, 1886, 1916–1918 and 2006–2008 (LePennec et al. 2008; IGEPN 2009). During the 1916 and 1918 eruptions, large amounts of ashes and lapillis were transported by Pastaza's tributaries (IGEPN 2009). An ash layer of $\sim 6 \times 10^6$ m^3 was deposited in August 2001 near Baños and the Patate/Chambo confluence (LePennec et al. 2008).

Sangay volcano is the most active volcano in the Northern Vocanic zone of the Andes, and a permanent explosive activity has been observed since 1628 with an average recurrence time of large eruptions of less than 50 years. The early Sangay III lava flows are older than LGM moraines (Monzier et al. 1999). The activity is of a Strombolian type with block and ash explosions, ash falls, pyroclastic flows and lahars (see Monzier et al. 1999).

The direct impact of these eruptions on the Amazonian Pastaza system is difficult to appreciate. For example, the 4,500-year-old lahars generated at the Cotopaxi cap, although gigantic, are not observed downstream of the Patate—Chambo confluence. The lahars produced by the 3,000 years BP sector collapse of the Tungurahua have been observed in none of the terraces of the Rio Pastaza downstream of the immediate proximity of the volcano (Bes de Berc et al. 2005). The large historical pyroclastic

flows of the Tungurahua have been largely contained within the channel cut by a tributary to the Pastaza and did not reach this river (Stinton and Sheridan 2008). However, in the upper Pastaza valley, near Baños, the T2 terrace covered with a lava flow dated between ~2,200 and ~1,500 ^{14}C years BP (Hall et al. 1999) overlies fluvial deposits made of reworked volcanic material (Bes de Berc et al. 2005). Volcanic material reworked by fluvial transport has also been observed in a low terrace cut into the Middle Pleistocene volcanic hills of the Puyo plateau (Burgos et al., unpublished). Deposits from the eastern flank of Sangay III have been stocked in the Sangay fan (Monzier et al. 1999), and it is unlikely that more than a minor part of these deposits was introduced en masse into the Pastaza network after each eruption.

The volume of material input by the volcanic eruptions in the Pastaza network is more difficult to estimate because only the volume of exceptional or recent events has been calculated. The volumes of material for these exceptional events are ~<2 km^3 for the Chimborazo; 2.5 km^3 for the Cotopaxi giant lahar to which could be added a volume of ~4 km^3 representing the 4 rhyolitic eruptions signalled by Mothes et al. (1998); the ~3,000 years BP sector collapse of the Tungurahua II mobilized 8 km^3 to which could be added associated lahars. The numerous eruptions of lesser importance mobilized much smaller volumes of material. If we assume that each of these eruptions provided approximately the same quantity of material as the 2006 eruption (~5×10^{-3} km^3), and that the frequency of eruptions has remained similar to that of the historical ones, then the 30 eruptions have given no more than ~0.15 km^3. This gives a total volume of less than 20 km^3 to which must be added the volume of the Sangay deposits which have not been stocked in the Sangay fan.

Materials and methods

The avulsions in the Pastaza megafan have been studied by means of remote sensing image analysis because of its size and of the inaccessibility of the greatest part of the area. Moreover, the high density of the vegetation and the low topographic amplitude of alluvial ridges make field identification of abandoned fluvial morphologies difficult.

This study was performed using Landsat and ASTER images and SRTM DEM. The set of Landsat images used in this study is summarized in Table 1.

The MrSID^{TM} Landsat 7 images correspond to a mozaic of 58 images acquired on a period ranging from 1999 to 2001 (see Table 1). These mozaics extend north–south over 10 degrees of latitude and span east–west for the full width of the UTM zone.

These images are processed to change the Landsat spatial resolution (30 m) of the multispectral composition. First, TM7 Band (midle-infrared) is displayed as red, TM4 band, near-infrared band, is displayed as blue and TM2 band, green band, is displayed as green.

The initial pixel size of these bands (~30 m) is then reduced using cubic interpolation to the spatial resolution of the panchromatic band (TM8, ~15 m).

The process follows with calculation of the Hue-Saturation-Intensity schemes for the multispectral images. The multispectral image is reconstructed from the Hue-Saturation schemes, and the intensity scheme is replaced by the TM8 panchromatic band. The resulting sharpened image combines the spatial resolution of the panchromatic band (~15 m) with the radiometric characteristics of the 30 m data, which allows the preservation of high frequency details.

MrSID Landsat 5 images have a lower resolution of around 30 m. The mosaic corresponds to 78 images with a period ranging from 1986 to 1994 (Table 1).

For detection of soil moisture and vegetation changes, we used ASTER images that have higher accuracy. This sensor acquires four bands on VNIR spectral domain, 6 band on the short-wave infrared (SWIR) and 5 band on the Thermal domain (TIR). The spatial resolution of the sensor decreases with the wavelength: 15 m on VNIR domain, 30 m on SWIR and 90 m on thermal domain. As for

Table 1 MrSID Image database used for the studied area with their characteristics

Satellite	Landsat			
Years	1990		2000	
Mosaics	S-18-00	S-18-05	S-18-00 2000	S18-05- 2000
# of landsat images	40	38	30	28
UTM Zone	18	18	18	18
Upper Latitude	0°	5° South	0°	5° South
Period	1986/03/23 to 1994/06/30	1986/06/22 to 1994/07/14	1999/07/11 to 2001/10/02	1999/07/11 to 2001/09/20
Spatial resolution (m)	28.5	28.5	14,25	14.25
Spectral band used	(TM7, TM4, TM2) + TM8		TM7, TM4, TM2	
Datum	WGS 84			

Landsat 7 image, the SWIR and TIR resolution was improved using the same process of image sharpening using high spatial resolution of VNIR bands (i.e., 15 m).

The spectral response of vegetation is characterized by a high reflectance level in the near-infrared region (NIR from 700 to 1,400 nm, Baret and Guyot 1991). In western Amazonia, botanical studies have determined that changes in the abundance of vegetation (palm flora) are related to topography and soil drainage conditions (Montufar and Pintaud 2006).

Vegetational changes are organized in very bright, more or less sinuous, bands, ~1 km wide and 10–100 km long like those shown in Fig. 3. These narrow and sinuous bands are interpreted as abandoned streams along which vegetation is absent or recent. The absence or the recent development of vegetation may be a result of the recent abandonment. Vegetational changes may have also been caused by changes in the draining properties of soils due to the presence of coarser-grained sedimentary bodies such as channels and alluvial ridges.

We used also radar images which have interesting capabilities of vegetation penetration of the microwaves. This penetration capability increased with the wavelength, in our studied area ground penetration cannot occur due to soil moisture. In some case, when the gallery forest covers abandoned channels, we used JERS radar images which permit to evidence hidden fluvial channels for the optical (s.l.) Landsat and Aster images. Another interesting property of the radar wave penetration is its capacity to cross the clouds.

To supplement this study, we also used the Shuttle Radar Topography Mission DEM (SRTM V3 with three arc second of spatial resolution). Its vertical accuracy is around 10–15 m depending on topographic gradient, vegetation cover, tropospheric humidity (Welch and Marko 1981; Lang and Welch 1994).

Geomorphologic studies using SRTM data have demonstrated its efficiency (Potts et al. 2008; Zandbergen 2008; Guth 2006 and among others). For Amazonian morphology, Rosseti and Valeriano (2007) starting from the

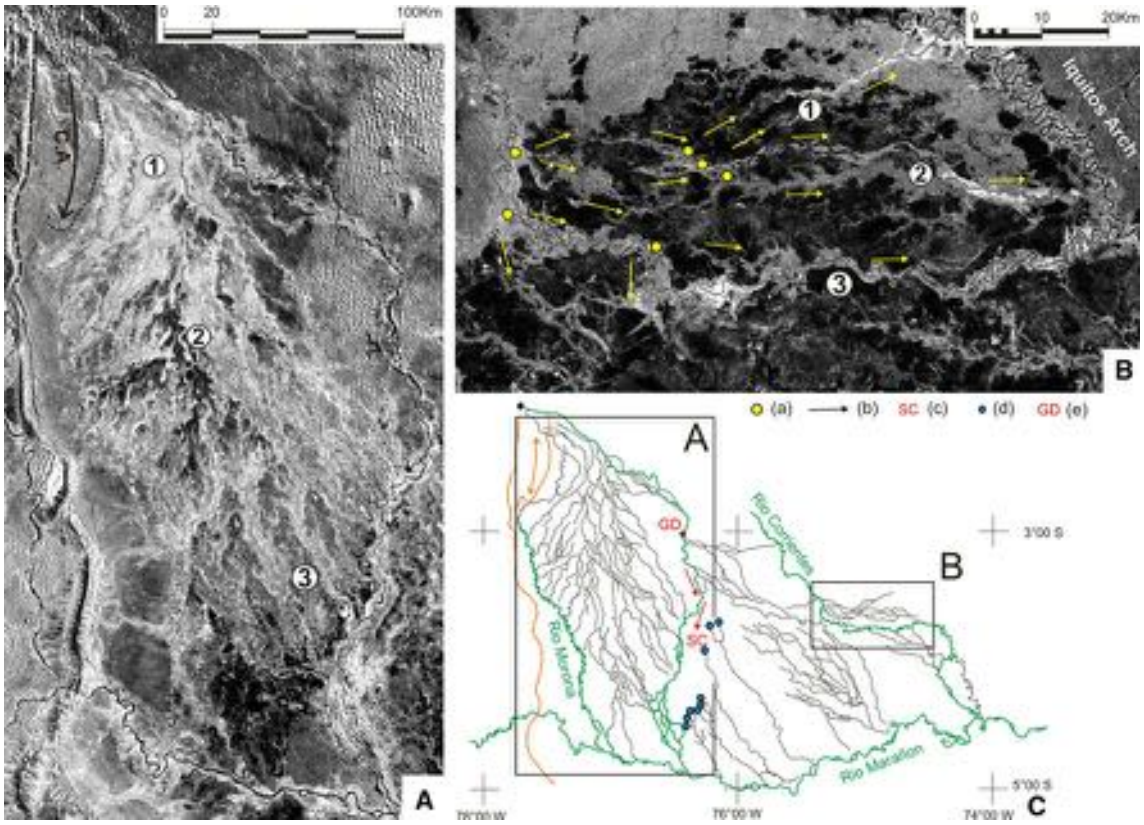

Fig. 3 Examples of successive courses and avulsion sites of the Rio Pastaza. ***A*** Morona Pastaza area (MPA), *CA* Axis of the Cangaime anticline, *1*, *2* and *3*, see text for explanation. ***B*** Northern part of the area of the Rio Tigre and Corrientes (TCA), (*a*) avulsion sites, (*b*) plaeocurrents in abandoned reaches, *1*, *2* and *3*, see text for explanation. ***C*** Location map of images *A* and *B* within the pastaza megafan. (*c*) Southern Curve of the Rio Pastaza resulting from the last significative avulsion of the Rio Pastaza (prior to 1691 AD), (*d*) Streams beheaded as a consequence of the avulsion which gave birth to SC, (*e*) GDP: avulsion site of the Great Diversion of the Rio Pastaza by mean of which the Rio Pastaza passed from the MPA to the TCA. Image Landsat 7

example of the Amazon estuary in Brazil demonstrate the pertinence of using SRTM DEMs for mapping abandoned streams and other geomorphic features in low relief, highly vegetated, low areas such as rain forests.

The modern Pastaza megafan complex

The present-day Pastaza megafan is situated in the southwest side of the Neogene megafan to the southeast of the Puyo plateau and covers 51,400 km^2, which is an area much larger than that of the catchment of the Rio Pastaza (13,700 km^2, see above). The Pastaza megafan appears as a marked topographic high within the Amazonian plain. In this respect, it is similar to the smaller-sized megafans identified in the Bolivian piedmont (Horton and DeCelles 2001) and differs from most of the distributary areas of the Amazonian lowlands such as the Rio Beni plain in Bolivia (Dumont 1996) which are depressed areas.

The modern megafan complex is bounded by the Rio Mangosiza/Morona to the west, the upper Rio Tigre valley and the Iquitos arch to the northeast, and the Rio Marañon to the south (Fig. 1). This megafan is formed by the left-bank tributaries of the Rio Mangosiza/Morona, the lower Pastaza basin, the lower Corrientes and lowermost Tigre basin (downstream of the Tigre—Corrientes confluence), and the tributaries to the Rio Marañon situated in the triangle between the Pastaza and Tigre/Corrientes basins.

The apex of the megafan complex is situated at the debouchement of the Rio Pastaza from the Puyo plateau (Fig. 1). The proximal part of the fan has a 3 m km^{-1} mean slope whereas, in the same area, the Rio Pastaza has a lower slope of 2 m km^{-1} (C in Fig. 4). There, the Rio Pastaza has an overall NW–SE direction and exhibits a multi-channel pattern with a high braiding parameter. In front of the Cutucu dome (Cangaime anticline), all the streams between the Rios Mangosiza and Cangaime, either tributaries to the Pastaza or to the Mangosiza/Morona, exhibit a more or less accentuated curved pattern. This region will be termed hereafter Mangosiza-Cangaime area (MCA) (Figs. 1, 2 and 4).

The middle part of the megafan system has a 0.5 m km^{-1} slope, and the Rio Pastaza has a 0.3 m/km slope (reach D on Fig. 6). The Rio Pastaza is there a single channel low sinuosity meandering stream flowing towards the south. The change in flow direction of the Rio Pastaza from southeast to south will be termed hereafter the "Great Diversion of the Rio Pastaza" (GDP) (Figs. 1, 8).

In this middle megafan complex, three regions may be distinguished. In the southwest, a parallelogram-shaped abandoned megafan well apparent in the Landsat images constitutes the present-day drainage divide between the Morona and Pastaza basins (Fig. 1). This region will be termed hereafter Morona Pastaza area (MPA). In the southeast, another system, partly abandoned, includes the present-day lower Corrientes/Tigre basins. This region will be termed Tigre-Corrientes area (TCA). Between the MPA and the TCA, a large WNW-ESE-trending abandoned flood plain join the upper southeast-flowing reach of the Rio Pastaza to the Rio Corrientes. This area will be termed Pastaza-Corrientes transition band (PCTB). The NW–SE section of the modern Pastaza valley having the same direction as this abandoned floodplain and showing similar abandoned alluvial ridges is to be included in the PCTB.

The distal part of the megafan complex consists in a huge floodplain made of swamps, forested areas and open water areas with a very low regional slope (0.3 m km^{-1}) and river slope (0.2 m km^{-1}). In this distal fan part, the Rio Pastaza exhibits an anastomosing pattern (Fig. 4, reach E). Its course is there markedly oblique to the general stream direction which is south-southeast to southeast. The lower order streams form anastomosed channels but remnants of former meandering reaches are frequently observed.

Avulsions in the Pastaza Megafan complex

Numerous avulsions have been recognized in the different areas defined in the modern Pastaza fan (Figs. 2).

Avulsion relics in the MPA

The MPA corresponds to the elongated abandoned megafan now forming the drainage divide between the Morona and Pastaza basins well apparent in the satellite images. The active streams that re-occupied some of the abandoned channels are still arranged as a low angle distributary pattern rising from the megafan ridge. The area of the abandoned alluvial fan is $\sim$13,750 km^2, greater than the well-known Kosi megafan, northern India, which is only $\sim$10,000 km^2. Volume estimate by means of an integration of transverse profiles yields a minimum value of 140 km^3. The MPA fan apex is situated in the north-northwest, at $\sim$30 km to the south of the modern Rio Pastaza in the area then occupied by the curved streams of the eastern MCA. In the northwest (Fig. 3A), paleochannels are amalgamated and difficult to distinguish in Landsat images and SRTM DEM unless where re-occupied by active streams. There, alluvial ridges appear quite rectilinear (3 on Fig. 3A). Meander loops are visible (2 on Fig. 3A) but their sinuosity is moderate (2 in Fig. 3A) and constant over the whole area (S $\sim$1.2).

In the median part of the MPA fan (3 on Fig. 3A), the paleochannels are not amalgamated, and the morphology of

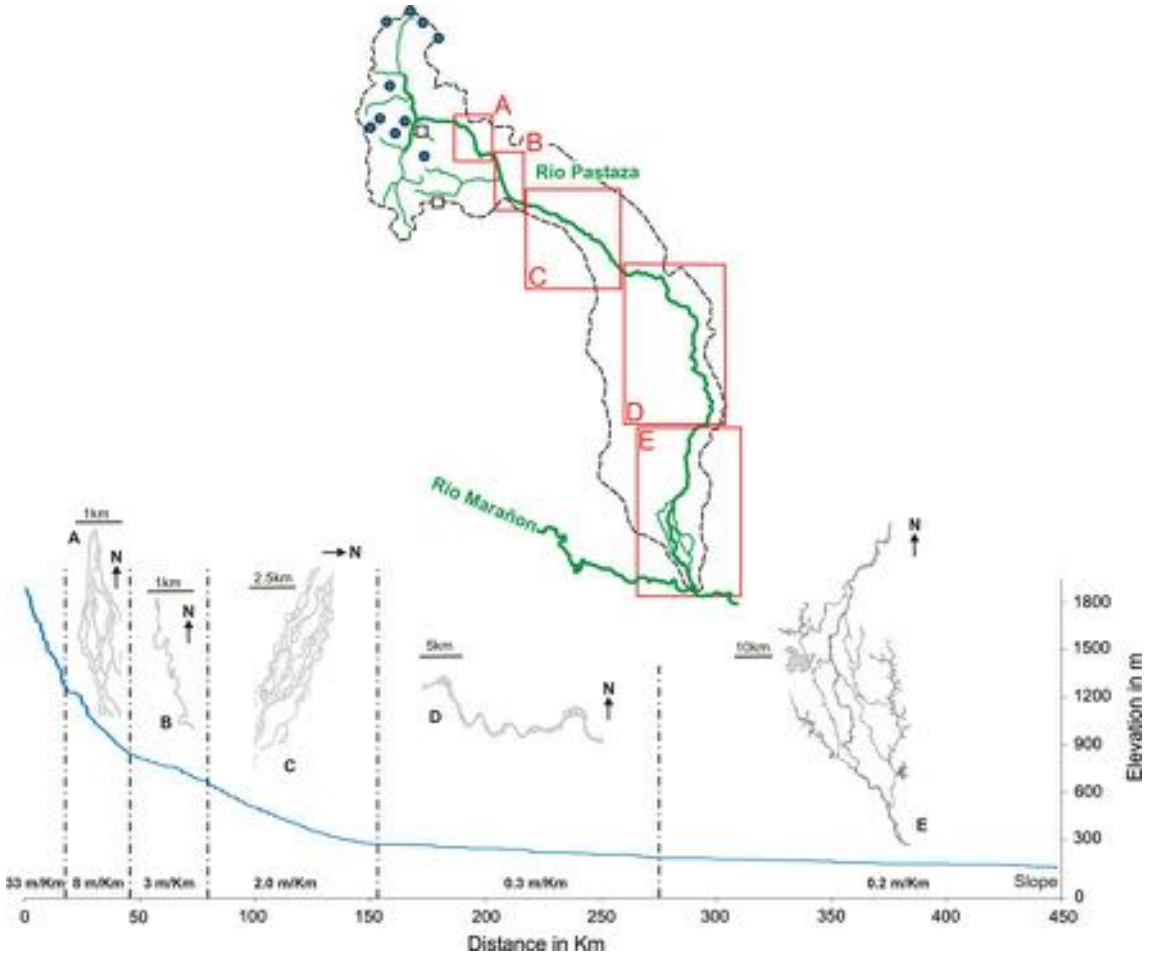

Fig. 4 Schematic map of the Rio Pastaza drainage basin, river profile, slope and associated channel pattern of the Rio Pastaza (profile extracted from the SRTM V3 DEM of the area)

alluvial ridges is much easier to characterize. Ancient streams display sub-parallel patterns and are frequently re-occupied by right-bank tributaries of the modern Pastaza and the left-bank tributaries of the modern Rio Morona (Fig. 1, 3C). Three types of reaches may be observed: (1) ancient reaches characterized by a reduced contrast between the valley and the forested floodplain; (2) recently abandoned reaches with a marked contrast between valley and floodplain; and (3) abandoned reaches re-annexed, entirely or partly, by present-day rivers. These channels/alluvial ridges have a moderate sinuosity (but the modern streams that re-occupy these channels are much more sinuous), and diverging channels are frequent and may have switched into adjacent ones (2 on Fig. 3A) as frequently observed in alluvial megafans (e.g., Wells and Dorr 1987, in the Kosi megafan). True rejoining channels (i.e., channels rejoining those channels from which they diverged see Slingerland and Smith 2004) are rare. Forty-four avulsion sites involving two recently abandoned reaches or involving recently abandoned and presently active reaches have been numbered in the MPA (Fig. 3). Avulsion sites between older reaches or difficult to locate are mapped as 'supposed avulsion sites'. Twelve of these 'supposed' avulsion sites have been numbered in the MPA.

In the south where slopes are shallower, diverging/rejoining channels forming anastomosed patterns are observed, in particular the lowermost Pastaza River. Swampy areas are frequent in this area except a topographically higher triangular plateau close to the Pastaza-Marañon confluence representing a remnant of the Villano surface.

Avulsion relics in the MCA

In this area, the abandoned channels of the Rio Pastaza are numerous and identified using radiometric contrasts in the vegetation. Ancient alluvial ridges have been re-annexed by underfit streams, which makes easier their identification in the SRTM DEM. Re-occupation of pre-existing channels by underfit stream has been described as characteristic of a

post-avulsion evolution of an abandoned reach (Bristow 1999).

The area to the east of the Cangaime anticline is characterized by a southward regional slope and a gently domed topography (Fig. 5). The principal rivers which appear as underfit streams having annexed ancient alluvial ridges describe a curved path around the forelimb of the anticline, those situated in the west incising the frontal dome and those in the east contouring it (1 on Figs. 3A, 6A). Incisions by these rivers are equal to or exceed 10 m (Fig. 5). The rivers in the south west are issued from the west or the northwest and traverse the Cangaime anticline through transverse water gaps. The rivers situated in the centre or in the west of the dome are issued from the north of the anticline, in the area separating the anticline from the Puyo plateau, near the debouchement of the Pastaza. Several abandoned paths of the Rio Pastaza have been recognized in this area. Path #1 (Fig. 6A, B) appears as a gentle convex to east curve parallel to the anticlinal front. This path is the oldest one, for it joins the highest terrace on the right bank of the Rio Pastaza. Its uppermost part cut the nose of the Cangaime fold through a water gap. This water gap is abandoned at the junction with the upper terrace where it is prolonged by a wind gap. Path # 1, except its uppermost part (the wind gap), is now re-occupied by the Rio Macuma which comes from the Eastern Cordillera after having formed a 180° loop at the tip of the western Cutucu dome (Bès de Berc 2003). Path #2 (Fig. 6) leaves path #1 immediately to the south (Fig. 6A) and forms a tighter valley rejoining path #1 ~30 km downstream. Path #3 is derived from path 1 through an avulsion site located upstream of the 1–2 site (a in Fig. 6A). Another avulsive branch leaves path #2 at point b to follow a new course which corresponds to a section of the present-day Rio Pastaza flowing towards the east-southeast (path # 4). Near point c, another abandoned stream is observed connecting the Pastaza and path #3 (path # 4). The present course of the Pastaza towards the southeast (path # 5) thus appears as a result of the last avulsion. In any event, avulsion 4 (point c) was younger than avulsions 1–3, for the bifurcation between paths #4 and #5 is observed on a lower terrace. Paths # 1, # 4 and # 5 follow meandering valleys whereas path # 3 forms a low sinuosity valley. This low sinuosity valley contrasts with the high sinuosity and the low amplitude of the meander loops of the underfit stream which re-occupied it. No wide valley seems to have been ever formed by path # 2 but a series of curved tributaries is observed in LANDSAT images suggesting repeated partial avulsions giving rise to short-lived avulsive streams. The wide meanders of path # 4 having amplitude and bed width of the same order of magnitude as the present channel but higher sinuosity are well apparent in the LANDSAT images and the SRTM DEM at the vicinity (~8 km) of the present course of the Pastaza (path # 5). Meander mosaics preserving preferentially meander loops convex to the west are observed locally in the west of path # 4 whereas a vegetated band free of meander (Fig. 1) remnants separates path # 4 and path # 5 (the present Rio Pastaza).

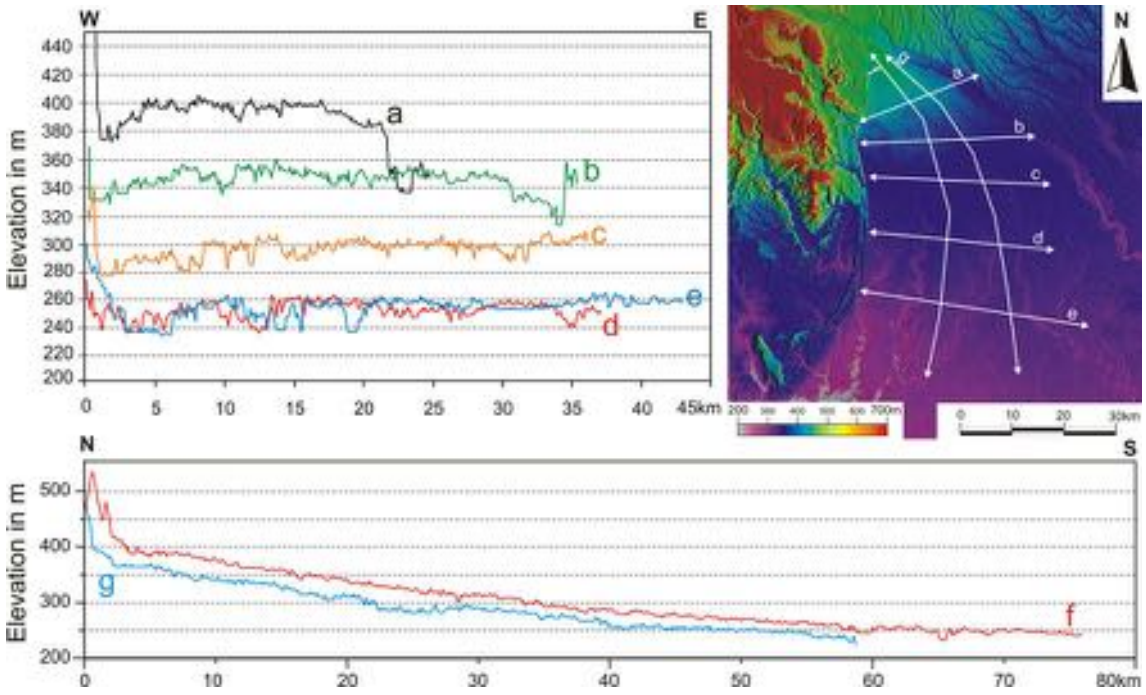

Fig. 5 Topographic profiles extracted from the SRTM DEM showing the topography of the upper part of the Pastaza Megafan

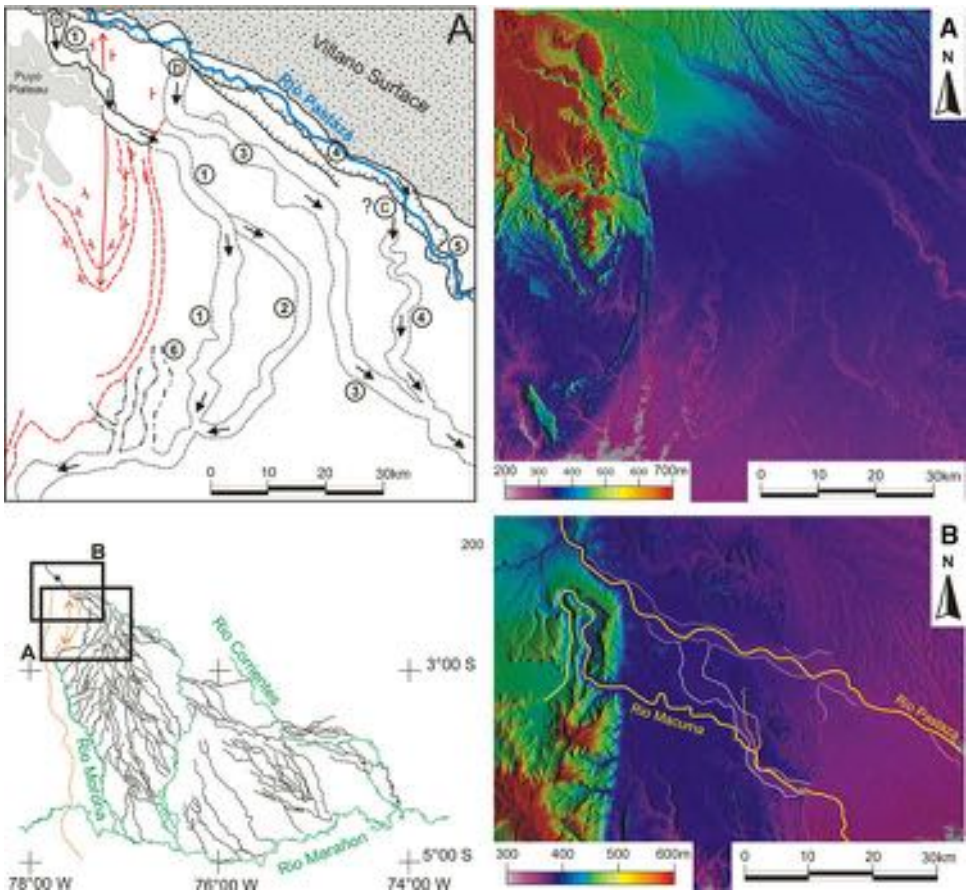

Fig. 6 To the *left* map of the successive streams of the Rio Pastaza in the MCA. Those streams are bounded by *pointed lines*. The *dashed-double pointed lines* correspond to superimposed streams. *Ticked lines* indicate terrace scarps. Successive streams of the Rio Pastaza are numbered following chronology. Stream #5 is the modern Rio Pastaza. To the *right* DEM SRTM V3. On the left bank of the Rio Pastaza the characteristic dendritic drainage network developed on top of the Villano surface. Some parts of this surface are also preserved on the right bank. At the *bottom* topographic profile across the Pastaza Megafan and the Villano surface, we can quote the strongly dissected aspect of the Villano surface

The avulsions in the PCTB and the Great Diversion of the Pastaza

Landsat images and the transverse profiles extracted from the SRTM DEM (Fig. 5) show that a large WNW-ESE-trending abandoned valley joins the upper southeast-flowing reach of the Rio Pastaza to the Rio Corrientes in continuation of the Pastaza valley. Downstream, i.e., south of the GDP (Figs. 2, 7), the Pastaza valley narrows significantly, which confirms the abandon of the former wide valley which assured the transition between the MPA/MCA and the TCA. As in the northern TCA, a succession of avulsions and channel rejoinings formed anastomosed channel patterns, now abandoned, in the present Pastaza floodplain as well as in the Pastaza-Corrientes abandoned valley. The multi-channel pattern shown by the present-day Pastaza in this area (downstream of the GDP) may represent the last expression of this process. Therefore, the PCTB including the NW–SE reach of the Pastaza can be considered as an avulsion belt (Slingerland and Smith 2004). It is worth nothing that the multi-channel pattern of the Pastaza disappears downstream of the abandon, and the Rio Pastaza resumes a meandering course for an along-valley distance of more than 150 km.

In the east of the PCTB, 8 avulsion sites including the 4 ones having led to the present-day course of the Pastaza have been defined. In the west, 7 avulsion sites have been defined. The present southward bend of the Pastaza (GDP) resulted from the last of these avulsions (Fig. 1).

Immediately downstream GDP, the 1990 Landsat image (Fig. 1) shows an oxbow-shaped swampy area appearing in a blue–green colour in the outer arc of the present-day bend, in geometrical continuity with the abandoned valley. This feature, less apparent in the 2000 image, suggests an ancient left-hand open curve cut through by the Pastaza. The SRTM DEM indicates that the bottom of the present Pastaza valley is there lower than the swampy area. A similar though smaller-sized feature is observed 25 km to the south (Fig. 1). There, the present Pastaza channel diverged from a convex-eastward loop appearing in a bright light green to form a convex-westward curve flowing close to the abandoned channel without rejoining it. In both cases, the Pastaza thus appears as having incised through its proper valley to achieve the avulsion (avulsion by incision after Slingerland and Smith 2004). It should be pointed out that downstream of the PCTB, the DEM profiles and the presence of swampy areas on both sides of the river bed indicate that the Rio Pastaza exhausted its bed

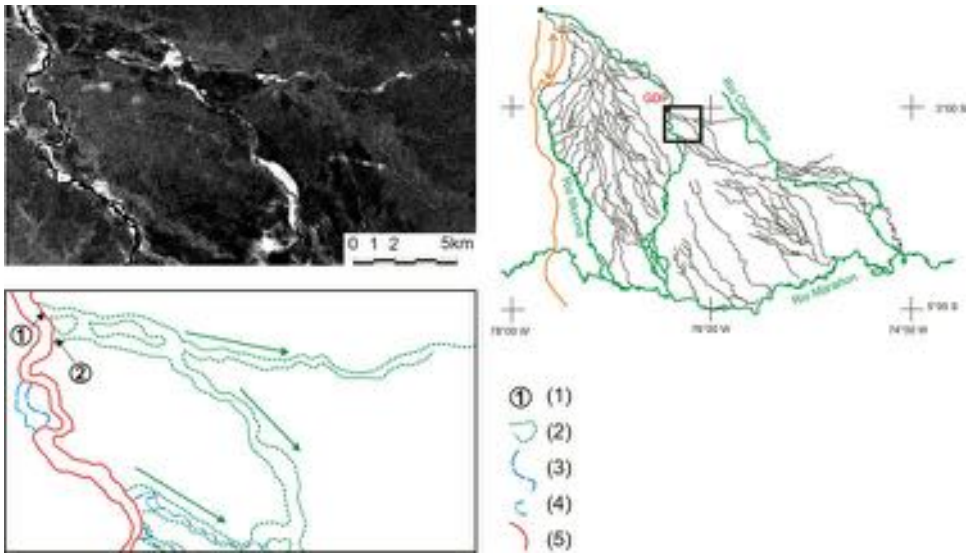

Fig. 7 Satellite Image and interpretative map of the Great Diversion of the Pastaza are. Observe the sharp contrast between alluvial ridges (even abandoned and the floodplain area). (*1*) points of avulsion, (*2*) abandoned alluvial ridges, (*3*) abandoned loop of the Rio Pastaza, (*4*) underfitted streams re-occupying abandoned reaches, (*5*) modern Rio Pastaza Channel

instead of incising it as in the north. This uplift of the Pastaza has for effect to separate the eastern portions of previous southeast-flowing rivers now dying out into the swampy fringes of the right side of the Pastaza alluvial ridge from their western counterpart now rising from the swamps of the left side of this ridge.

Avulsions in the TCA

The TCA is composed of two parts. The northern part (upper and middle Corrientes) shows distributary/rejoining alluvial ridges settled in a wide (up to ~70 km) floodplain, giving rise to anastomosing channels which characterize partial avulsions (see definitions and terminology in Slingerland and Smith 2004). The modern and ancient alluvial ridges are distinguished by contrasted spectral responses as shown by the example of the Rio Corrientes at the vicinity of the north-eastern boundary of the area (Fig. 3B). Abandoned alluvial ridges (1 and 2 in Fig. 3B) have in general a brighter response and sharp boundaries strongly suggesting that vegetation was younger and therefore, that the avulsions were younger, than in the MPA. The abandoned channels, however, have a more or less bright green response (indicating a more or less recent vegetation growth) which can be interpreted as a succession of abandonments and avulsions. The alluvial ridges in the TCA are linear as in the MPA but the sinuosity of the ancient channels seems to have been higher (~1.7). Recent meandering streams such as the modern Rio Corrientes may reoccupy the larger abandoned channels (3 in Fig. 3B). Eighteen avulsions sites have been numbered in this northern part of the TCA. In the middle part of the TCA, two avulsion belts may be distinguished: the lowermost Rio Corrientes belt trending west-east in the northeast and the Cuinico belt trending northwest—southeast in the southwest.

The southern part of the TCA is fan shaped showing modern and ancient distributaries joining the Rio Marañon or the lowermost Rio Tigre. Landsat images show two interfering fans well apparent in the arrangement and shape of the numerous swamps of this region (Fig. 1). This pattern is less obvious, however, when only the alluvial ridges and well-defined channels are considered (Figs. 1, 3).The modern and abandoned channels are mostly parallel, even though more sinuous channels are observed in the upper part. Well-characterized avulsions are less frequent than in the north (9 avulsion sites) even though some of the channels are anastomosed.

Chronology, age and frequency of avulsions

The observations above may arrive to a relative chronology of the major avulsions. The radiocarbon ages available in the literature (Räsänen et al. 1990, 1992; Bes de Berc et al. 2005) help us to constrain the ages of the avulsions in the areas of the Megafan. In the entire Pastaza megafan complex, 108 avulsion sites have been identified, representing an avulsion frequency of 0.51 ± 0.06/100 years and an average recurrence time of ~200 years (196 ± 2 years and 240 ± 3 years if we except the 'supposed' avulsion sites) (Table 2). However, as shown earlier, the type and origin of avulsions are quite different in the areas we have distinguished, and this value is only indicative.

Avulsions in the MCA/MPA and western PCTB

The first entity to have developed was the MPA megafan (Fig. 8A) where the channels, though re-annexed, were abandoned a long time ago as shown by their subdued spectral response. The brighter spectral response of the

Table 2 Ages, conversions 14C ages/Calendar ages and computing of avulsions recurrence of the Rio Pastaza

Scenario		Time interval	Interval duration (years)			All Avulsions	Recurrence (years)		Most reliable	Recurrence of most reliable (years)	
1	Avulsions since 17920 years BP and 1691 AD	Between 17920 ± 70 BP and 1691 AD (Bes de Berc et al. 2005; Fritz in Gomez 1994)	(21,162 ± 261)—(1950–1691)	21,164(1)		108	195		88	240	
				20,903	20,903 ± 261	108	193	193 ± 2	88	237	237 ± 3
				20,642(2)		108	191		88	234	
2	Avulsions between 17920 and 8180 years BP	Between 17920 ± 70 BP and 8180 ± 120 BP (Bes de Berc et al. 2005; Räsanen et al. 1992)	(21,162 ± 261)—(9198 ± 200)	12,425(1)		84	148		67	185	
				11,964	11,964 +/461	84	142	142 ± 6	67	179	179 ± 7
				11,503(2)		84	137		67	172	
3	Avulsions between 17920 and 7650 years BP	Between 17920 ± 70 BP and 7658 ± 120 BP (Bes de Berc et al. 2005; Räsänen et al. 1992)	(21,162 ± 261)—(8476 ± 112)	13,059(1)		84	155		67	195	
				12,686	12,686 ± 373	84	151	151 ± 4	67	189	189 ± 6
				12,313(2)		84	147		67	184	
4	Avulsions between 8180 years BP and 1691 AD	Between 8180 ± 120 BP and 1691 AD (Räsänen et al. 1992; Fritz in Gomez 1994)	(9,198 ± 200)—(1950–1691)	9,139(1)		24	381		21	435	
				8,939	8,939 ± 200	24	372	372 ± 9	21	426	426 ± 10
				8,739(2)		24	364		21	416	
5	Avulsions between 7650 years BP and 1691 AD	Between 7658 ± 120 BP and 1691 AD (Räsänen et al. 1992; Fritz in Gomez 1994)	(8,476 ± 112)—(1950–1691)	8,329(1)		24	347		21	397	
				8,217	8,217 ± 112	24	342	342 ± 5	21	391	391 ± 6
				8,105(2)		24	338		21	386	

Conversions 14C ages/Calendar ages were done following the INTCAL04 (Reimer et al. 2004). Columns "All avulsions" and "Global recurrence" take in account all the avulsions sites identified in the area (see Fig. 4) while columns "Most reliable" and "Recurrence of most reliable" do not take in account the "supposed sites of avulsion" of Fig. 2

(1) upper limit value, (2) lower limit value

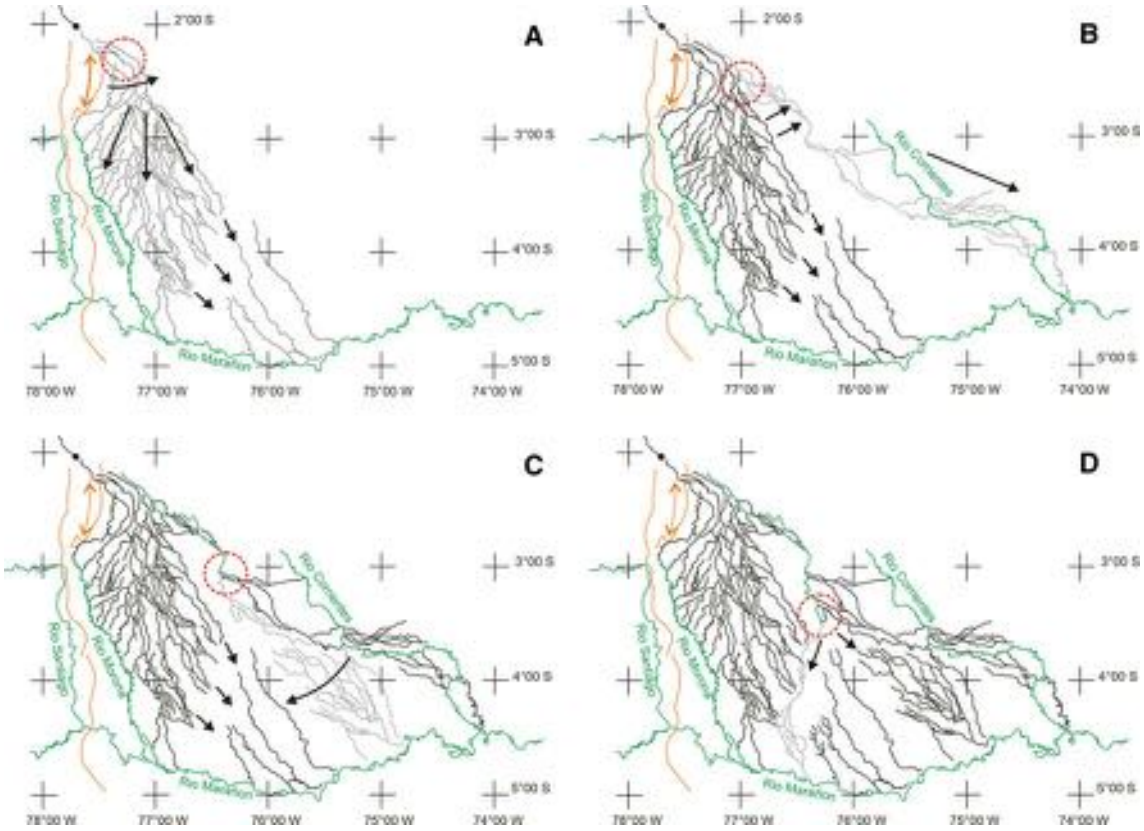

Fig. 8 Maps of the migrations of the Rio Pastaza through times. **a** Beginning of the avulsions in the Pastaza Megafan. These avulsions occurred after 21,160 ± 260 years Cal BP, **b** Great Diversion of the Rio Pastaza to the TCA. **c** Avulsions in the TCA, this area was active around 9,198 ± 200 years Cal BP ou 8,476+/112 years Cal BP, **d** Modern morphology of the drainage network resulting form the southward avulsion of the Rio Pastaza and the abandonment of the Rio Tigre/Corrientes area. This configuration is dated after 9,198 ± 200 years Cal BP or 8,476 ± 112 years Cal BP (see text for further explanations)

abandoned channels in the TCA indicates that the abandon was younger than in the MPA. This is confirmed by the fact that the eastward avulsions in the MCA from which originated the channels of the PCTB area and the TCA derived from the southward-flowing paleo-Pastaza which fed the MPA megafan. The curved streams of the MCA appear to be superimposed on the apex of the MPA megafan and can be thus considered to be younger. In terms of ages, the apex of the MPA megafan being situated at the debouchement of the Rio Pastaza from the Puyo plateau, the formation of this megafan and the avulsions therein are younger than the diversion of the Pastaza in the Puyo plateau. This diversion being a result of arching and backtilting of the plateau surface (Mera surface), the MPA megafan was younger than 17,920 ± 100 ^{14}C years BP (Bes de Berc et al. 2005), or ∼21,160 ± 260 Cal years BP according to Reimer et al.'s (2004) IntCal calibration.

The relative chronology between the MCA and the PCTB avulsions is less easy to establish. However, if we take into account the chronology of avulsions and the outward progression of the curved stream network pattern in the MCA on one hand and the chronology of avulsions in the western PCTB on another hand, it appears that the last diversion in the MCA corresponds to the first diversion in the PCTB (Fig. 8B). Therefore, one can consider that the avulsions in the MCA are older than those in the TCA. Ages of 9,200 ± 200 years and 8,480 ± 110 Cal years BP have been obtained by (Räsänen et al. 1992) in the floodplain of the Rio Corrientes in the northern TCA. The development of this floodplain being a result of the avulsions at the origin of the TCA, the abandon of the MPA was older than 9,200 ± 200 years Cal years BP.

If we group the avulsions older than the first occupation of the TCA floodplain, i.e., those in the MPA, the MCA and the PCTB, 84 avulsion sites have been defined, including 17 'supposed' sites. If the date of 8,480 ± 110 Cal years BP is considered as the age of the first occupation, then the frequency is ∼0.66 ± 0.2/100 years and the recurrence time is ∼150 years (142 ± 6 years accepting all sites and 179 ± 7 years excepting the 'supposed' sites). Assuming a first occupation age of 9,200 ± 200 Cal years BP, the frequency is ∼0.7/100 years and the recurrence time is ∼170 years (151 ± 4 years accepting all sites and 189 ± 6 years excepting the 'supposed sites').

Table 3 Avulsion recurrence and frequency data in the Rio Pastaza megafan and other fluvial systems known for their frequent avulsions: the Rhine-Meuse delta (Stouthamer and Berendsen 2000, 2001); the Saskatchewan river (Morozova and Smith 1999, 2000), the Kosi river megafan (Gole and Chitale 1966) and the Rio Taquari megafan (Assine 2005)

	Rio Pastaza Megafan			Rhine-Meuse delta		Saskatchewan	Kosi Megafan	Taquari Megafan	Brahmaputra river
	This study			Stouthamer and Berendsen (2000, 2001)		Morozova and Smith (1999, 2000)	Gole and Chitale (1966)	Assine (2005)	Bristow (1999)
Avulsions	108[(1)]	84[(2)]	24[(3)]	27[(4)]	87[(4)]	9	12	3	7
Interval (years)	~21,000	~12,300	~8,500	3,875	6,370	5,400	246 (1731–1977)	30 (1973–2003)	202 (1776–1978)
Recurrence (years)	~195	~145	~354	143	73	600	20.5	10	29
Average frequency (years)	0.51/100	0.68/100	0.28/100	0.7/100	1.4/100[(4)]	0.17/100	4.88/100	10/100	3.47/100

(1) entire Pastaza megafan; (2) MPA, MCA, and western PCTB; (3) TCA; (4) coeval avulsions taken into account for comparison purpose (see Stouthamer and Berendsen for the actual values)

Avulsion in the TCA, eastern PCTB and modern Pastaza

As shown earlier, avulsions in the TCA occurred around 9,200 ± 200 Cal years BP and 8,480 ± 110 Cal years BP. The last avulsion to occur in the PCTB was the diversion to the south of the Pastaza "Great Diversion" leading to the abandon of the eastern PCTB and the TCA (Fig. 8D). As a consequence, avulsions in the eastern PCTB are supposed to have occurred after the last avulsions in the TCA (8,480 ± 110 Cal years BP). The overall present-day course (and thus the "great diversion") of the Pastaza is figurate in a map published in 1691 (Samuel Fritz map reproduced by Gomez 1994), indicating that the "Great Diversion" was older than AD 1691.

In the TCA and the eastern PCTB, 26 avulsion sites have been numbered. If the date of 8,480 ± 110 Cal years BP was that of the first occupation of the eastern PCTB and TCA and the date of 1691 AD that of the last avulsion, the avulsion frequency was ~0.31/100 years and the recurrence time reduces to ~350 years (342 ± 5 years for all sites to 391 ± 6 years accepting the 'supposed' sites). If the age of first occupation of the eastern PCTB and TCA were 9,200 ± 200 Cal years BP, then the average frequency of avulsions was 0.29/100 years and the time of recurrence was ~400 years (372 ± 9 years for all sites and 426 ± 10 years excepting the 'supposed' sites).

The present-day activity of the underfit streams reoccupying the pre-existing channels of the TCA is due to the fact that these streams have been re-alimented by streams newly formed in the upper Villano surface in front of the Puyo landslides (including the Rios Tigre and Corrientes, Bes de Berc et al. 2005). The relatively recent age of the Pastaza "Great Diversion" is also attested by the beheading of the SW-flowing rivers formed after the abandon of the MPA megafan.

Significance of frequencies

The frequencies and average recurrence times of the avulsions in the TCA appear to be significant because of the homogeneity of the area and the similarity of the avulsion features. In contrast, the avulsions older than the occupation of the TCA floodplain formed in at least 3 differing contexts: construction of an alluvial megafan (MPA), piedmont of a propagating thrust-related fold (MCA) and construction of an avulsion belt (PCTB). Therefore, it is likely that the mean recurrence time varied from one area to another, and the average time of ~350 years can be considered as an order of magnitude.

Discussion

Avulsion frequency

Data relating to avulsions frequency exist for a few modern rivers in various contexts including avulsion belts, megafans and deltas. Stouthamer and Berendsen (2001, Table 3) present such data as interavulsion periods (=period of channel activity minus avulsion duration). Because our study cannot provide neither avulsion duration nor the number of coeval avulsions, interavulsion periods cannot be determined and the recurrence time referred to in the present paper assumes 'instantaneous' avulsions. Average frequencies (=total number of avulsions having occurred during a given period divided by the duration of this period) being independent of the duration of the avulsions have been preferred in the following discussion. Table 3 presents average frequencies in the areas considered by Stouthamer and Berendsen (2001) to which have been added the Brahmaputra River (Bristow 1999) and the Taquari megafan (Assine 2005).

The average avulsion frequency of 0.51/100 years for the whole Pastaza megafan complex is of the same order of magnitude as for the Rhine-Meuse delta (0.88/100 Cal years, Stouthamer and Berendsen 2001) but much less than for the Lower Brahmaputra River (3.47, Bristow 1999), the Kosi megafan (4.88, Gole and Chitale 1966), or the Taquari megafan (~10, Assine 2005) which have, however, been observed during much shorter periods of time (202, 246 and 30 years, respectively, see Table). In contrast, this avulsion frequency of 0.51/100 years is greater than those of the Saskatchewan River (0.17, Morozova and Smith 1999, 2000), the Po River (0.25, Nelson 1970 in Mackey and Bridge 1995) or the Yellow River (0.21, Li and Finlayson 1993).

When considering the different entities constituting the Pastaza megafan complex, the western domain formed by the MPA, the MCA and the western PCTB records a higher avulsion frequency (~0.6–0.7) than the eastern domain (~0.3). The former value is probably underestimated because many older channels in the MPA are likely to have been masked by the large aggradation having occurred in this area. A comparison between the MPA megafan and the other megafans (Kosi, Taquari) is difficult because we have no age for the MPA alone and the situation or geometry of these megafans differs markedly. The Kosi megafan appears as a piedmont megafan like the MPA but it is very flat compared with the MPA and is affected by a monsoonal climate. This may allow the mechanism proposed by Wells and Dorr (1987) to operate in this megafan and not in the more bulging MPA, thus explaining the much higher avulsion frequency in the former. In fact, the avulsion frequency in the MPA is the closest to that in the Rhine-Meuse delta which has formed in a much different context but is closely controlled by aggradation (Stouthamer and Berendsen 2000, 2001).

The value obtained in the PCTB-northern PCA floodplain avulsion belt is very close to those obtained in floodplain avulsion belts having similar areas (Saskatchewan and Po Rivers) or much larger areas (Yellow River) during similar spans of time but much lower than in the Brahmaputra floodplain, which has, however, been observed during a much shorter period. This suggests that the avulsions forming avulsion belts in low gradient floodplains might have similar long-term average frequencies, but highly varying short-term average frequencies. In this respect, floodplain avulsion belts should be similar to deltas such as the Rhine-Meuse where avulsion frequency varies in the time from 2.43 between 8,000 and 7,300 Cal years BP to 0.85 between 7,300 and 3,200 Cal years BP (Stouthamer and Berendsen 2001).

Style, local causes and triggers of avulsions in the Pastaza megafan complex

The origin of avulsions has been thoroughly discussed by Jones and Schumm (1999) and Singerland and Smith (2004) in their reviews of river avulsions.

Jones and Schumm (1999) consider 4 groups of causes and eventually triggers of avulsion. The first two groups involve an increase in the ratio of the slope of the potential avulsion course to the slope of the existing channels. The third group involves a reduction in the capacity of a channel to convey all of the water and sediment delivered to it. The fourth group involves other processes than those of groups 1–3, as various as animal trails and stream capture. In the context of the Amazonian basin, the group 4 processes are precluded or unlikely. Intrinsic processes related to sedimentation and extrinsic (external) processes are involved in any of the groups 1–3. External processes such as tectonic uplift/subsidence or lateral tilting are thought by Jones and Schumm (1999) to be capable of causing (and not only triggering) avulsion. Slingerland and Smith (2004) used a theoretical stability analysis of bifurcating channels and a thorough review of the papers dealing with the style and frequency of avulsions. They concluded that avulsion frequency increases with increasing aggradation whatever the exact cause of aggradation and the trigger (even though the authors acknowledged that avulsions may occur in the case of limited or no aggradation). According to them, avulsions are promoted by rapid alluviation of the main channel, a wide unobstructed floodplain able to drain down-valley, and frequently recurring floods of high magnitude. According to this viewpoint, it should be appealing in a megafan to distinguish between causes and triggers of avulsions. In this case, the cause should be the huge amount of sediment transported into the megafan (see e.g., Wells and Dorr 1987, or Leier et al. 2005), and the trigger should be "opportunistic" (Slingerland and Smith 2004), intrinsic (e.g., high floods) as well as extrinsic (e.g., tectonics). Accordingly, only the cause of the high sedimentary load should be researched as the cause of the avulsions in the entire modern Pastaza megafan complex, tectonic events being considered as opportunistic triggers. However, Jones and Schumm (1999, their Table 1) consider tectonics as a cause as well as a trigger of avulsion because tectonic uplift may decrease channel slope or increase the slope of the potential avulsion course as this is obvious in the case of piggy back basins formed upstream of growing anticlines (see e.g., Burbank et al. 1996; Burbank and Anderson 2001 p. 194; Humphrey and Konrad 2000; van der Beek et al. 2002). This is less obvious in the case of small relative increases in elevation such as those in front of the

Cangaime anticline (see, however, Bridge and Leeder 1979; Alexander and Leeder 1987; Dumont and Hanagarth 1993) and this point will be discussed hereafter in each of the studied areas.

Styles of avulsions as defined by Slingerland and Smith characterize 3 different ways by which avulsions are achieved in the floodplain: (a) avulsion by annexation by which an existing channel is appropriated or reoccupied; (b) avulsion by incision, where new channels are scoured into the floodplain surface; and (c) avulsions by progradation, characterized by extensive deposition and multi-channelled distributive networks.

The avulsions in the MPA

The MPA represents an ancient megafan disconnected from the Pastaza system by a regional avulsion related to the propagation of the Cangaime thrust-fold. The high volume of sediment forming this megafan has been sufficient for the fan crest to constitute the divide between the Morona and Pastaza drainage basins until today, long after the abandon. In spite of the surimposition of the MCA over its very apical part, the organization of the megafan is well apparent in satellital images. As in other megafans having a moderate average slope such as the Kosi megafan in the Himalayan piedmont (Gole and Chitale 1966; Wells and Dorr 1987), large aggradation occurred and avulsions associating progradation and annexation predominate as suggested by the high amount of sediment distributed in the megafan and the multi-channelled distributive network. The switch of a channel into an adjacent one (which must not be confused with diverging/rejoining channels, see Wells and Dorr 1987, fig. 2) can be interpreted as in the Kosi megafan (Wells and Dorr 1987) as evidence of the lateral shifting of a single channel sweeping across the fan. Wells and Dorr (1987) interpreted the avulsions at the origin of the shifting of the Kosi River as results of overflow of both highly aggraded active rivers (alluvial ridges) and less aggraded pre-existing non-active or less active rivers in the inter-ridges areas, promoting drainage into the topographic lows at the cessation of flooding. No unusually large floods have been recorded in the upper Amazonian basin in the historical period which is probably more humid than the early Holocene when the MPA formed (see Weng et al. 2002). This constitutes a difference with the Kosi fan where huge floods have been recorded in the modern and recent times. In fact, Wells and Dorr (1987) demonstrated in the Kosi fan that major avulsions were not correlated with unusually high floods of any origin but were a result of 'normal' floods. However, 'normal' floods in the Kosi cover very large areas because of the very flat topography of the fan. The MPA fan is more bulged than the Kosi fan, and the precipitation regime is not monsoonal. Therefore, wide annual floods are more difficult to invoke as triggers of avulsions in the MPA than in the Kosi system and the absence of wide annual floods like those occurring in the Kosi might explain the much lower frequency of avulsion in the MPA.

Other causes/triggers of avulsion in the MPA might be tectonics and volcanism. An influence of tectonics on avulsions is here rather unlikely because the MPA is relatively far from the active Subandean Frontal Trust and the Cutucu/Cangaime thrust-fold dome, and earthquakes recorded in the Amazonian domain are deep events with a relatively low magnitude.

The large-scale volcanic eruptions eventually capable of influencing the hydrologic regime of the Pastaza system when the MPA was active were a large rhyolitic eruption of the Cotopaxi, the first pyroclastic flows and associated lahars of the Chimborazo at 8000–5400 BC (Table), and the collapse of the Sangay II. Cotopaxi and Chimborazo volcanoes are far from the Amazonian domain, and no traces of these events are found downstream of Baños in the western Eastern Cordillera (Bes de Berc et al. 2005). We have no information on the presence of products of the Sangay II collapse in, and downstream of, the terraces of the Rio Palora. The uncertainty of the date of this event (>14,000 years BP, Monzier et al. 1999) does not assure that it was contemporary with the construction of the MPA. Even though it were so, the along-stream distance between the MPA and the crater ($\sim$180 km) is very long when we consider than the 8 km^3 avalanche resulting from the 3,000-year-old collapse of the Tungarahua II travelled 'only' 21 km along the valley and that no traces of lahars following this event have been found in the Pastaza terraces near Mera at 60 km from the volcano (Bes de Berc et al. 2005). Therefore, the Sangay II collapse could hardly have caused the abandon of the MPA megafan and it is unlikely that it might be a direct cause or trigger of the avulsions. However, the gradual erosion and transport in the fluvial system of the huge quantity of material provided by the volcanic eruptions coeval with, or older than, the MPA might have constituted a large part of the material accumulated in this area.

The avulsions in the MCA

In the MCA, the curved shape of the rivers shaping the propagation of Cangaime anticline and the avulsions only occurring in the downslope side of the rivers indicate that not only river migration but also avulsions have been controlled, at least in part, by tectonics. The local curved courses of rivers otherwise flowing south along the regional slope show that these rivers adapt locally to the new domal topography created by the propagation of the thrust-fold structure. The divergences at the origin of the successive

paths, the clear separation between them and the scarceness of meander mosaics (except locally in the west of path # 4 in Fig. 2) suggest that avulsion was there a more efficient process than progressive shifting to achieve this adaptation, even though progressive shifting may have locally occurred. At point A in Fig. 3, the avulsion from path #1 (Fig. 2) to path #2 (Fig. 2) is clearly a result of the lateral propagation of the Cangaime fold defeating path #1 and transforming the water gap passing through the nose of the fold into a wind gap. In this case, fold growth is the major if not the unique cause of the avulsion (if a pure "mechanical" diversion like this one can be actually considered as a diversion). This is not the same for the other avulsions of the MCA. LANDSAT images of the streams affected by these avulsions indicate deposition along the valleys but the topographic sections normal to the rivers show V-shaped incised valleys with no evidence of levees or exhausted beds which could have shown that aggradation was the direct cause of avulsion. It might be objected that these V-shaped valleys have been incised by the rivers having reoccupied the abandoned valleys, but it is unlikely that the abandoned alluvial ridges would have been entirely removed as a result of incision by underfit streams. Therefore, even though the sedimentary/water discharges were probably as large as in the other parts of the Pastaza megafan complex, tectonic uplift resulting from the lateral/frontal propagation of the Cangaime thrust-fold seems here to have been the direct cause of the avulsions. This interpretation is also supported by the localization of the avulsions near the northern nose of this fold. Earthquakes such as the 1980 El Asnam (Algeria) earthquake (Philip and Meghraoui 1983) capable of causing local rapid uplift of river beds could be possible triggers. Because of the absence of levees to be breached, seismic shaking alone as invoked by e.g., Stouthamer and Berendsen (2000) in the Rhine-Meuse delta could hardly be taken as a possible trigger in the MCA in spite of markedly greater earthquake magnitudes. In contrast, intrinsic factors such as large floods may be considered as possible triggers even in this tectonically active context because aggradation may have elevated the river bed sufficiently for the flow to take advantage of the tectonic slope.

The avulsions in the PCTB and the northern TCA

In the TCA and the PCTB, no field observations of avulsion features are available and satellite images only provide information on the size and arrangement of channels. However, the principal characteristic of these areas is the presence of diverted/rejoining channels forming anastomosing patterns still apparent in spite of vegetation growth. This suggests sustained avulsive flow transforming a floodplain into an avulsion belt showing abandoned anastomosed channels and small isolated flood basins as in the modern Saskatchewan River (Morozova and Smith 2000; Slingerland and Smith 2004) or other avulsion belts formed under various climatic regimes (e.g., Schumm et al. 1996; Smith et al. 1997; Bristow 1999; Ethridge et al. 1999; and other refs in Slingerland and Smith 2004). According to Slingerland and Smith's (2004) review, anastomosing reaches are results of progradational avulsions (Morozova and Smith 2000) characterized by deposition out of the parent channel into the invaded floodplain and favoured by slow runoff promoted by low floodplain slopes (Slingerland and Smith 2004, p. 264). The meandering streams occupying alluvial ridges such as the middle Rio Corrientes could be the new dominant meandering channel constituting the outcome of the evolution of the avulsion belt (fig. 2 in Slingerland and Smith 2004). In most of the modern avulsion belts such the Saskatchewan River (Morozova and Smith 2000), the Niobrara River (Ethridge et al. 1999), the Ovens and King rivers, Australia (Schumm et al. 1996) or the Brahmaputra River (Bristow 1999), the causes of avulsions are entirely autocyclic and related to the high sedimentary discharge and deposition of these rivers even though the trigger was occasionally extrinsic (e.g., damming as for the Niobrara River, Ethridge et al. 1999). However, for Smith et al. (1997), neotectonic movement is the underlying cause of avulsion and anastomosis in the panhandle (upper entry corridor) of the Okavango fan situated in a 'relative' valley gradient depression inferred to represent a small graben. In the case of the PCTB and TCA, the avulsion belt is situated much too far from the active tectonic region, and the earthquake foci are too deep and their magnitude too low for tectonics to be the cause or trigger of the avulsions. For the same reasons as in the MPA, and notably the great distance to the volcanoes, volcanic eruptions, although frequent at the time when the PCTB and the MCA formed (see Table 2), cannot have been a direct cause or trigger of avulsion in these areas.

The avulsions in the southern TCA and surrounding areas

In the southern part of the TCA, the fan shape is essentially apparent in the arrangement and shape of the numerous swamps of this region (Fig. 1). Well-characterized avulsions are rare. The style, cause and triggers of avulsions seem to be researched in the very shallow attitude of the topography like in the 'losimean' megafans (Stanistreet and McCarthy 1993) such as the Okavango (Stanistreet and McCarthy 1993; Stanistreet et al. 1993) or the Taquari (Assine 2005; Assine and Soares 2004). In fact, the arrangement and shape of the swamps is likely to reflect the configuration of the floodplain and may be fed by temporary breaching of channel banks with short new channels being formed (Stanistreet et al. 1993). The predominance

of low sinuosity channels is also a characteristic common to the southern TCA and the Okavango fan. We have no evidence in the southern TCA that channels are confined by vegetated and/or peat levees but no more evidence that they are not, and the similarity between the southern TCA and other very shallow humid fan such as the Okavango or the Taquari suggests that they might be.

Remote causes of the avulsions in the Pastaza megafan complex

As discussed earlier, aggradation played a major role in the generation of avulsions in the different areas studied in the present paper, even in the MCA where tectonics prevails. This conclusion agrees with that of many authors having studied avulsions in various contexts, scale and time lapses (see refs above). The origin of this large aggradation as a remote cause of avulsion is crucial in the Pastaza megafan complex where the catchment area (13,700 km^2) is much smaller than the depositional area (51,400 km^2). Table 4 shows characteristics of piedmont megafans in the Bolivian Andes (Rio Grande, Rio Pilcamayo, and Rio Parapeti, after Horton and DeCelles 2001) and of the Kosi megafan compared with the Pastaza megafan complex. These characteristics include catchment and fan surfaces, fan/catchment ratio, water discharge, stream power per length unit and incision rate. The entire Pastaza megafan complex has a much greater fan/catchment ratio (3.75 instead of 0.72 for the Rio Parapeti and 0.20–0.30 for the other systems). The contrast between the Pastaza megafan and the other megafans reduces if we consider only the MPA which is the first entity to have been formed and was abandoned when the eastern entities formed. If so, the fan/catchment ratio reduces to 1, which remains much higher than the other systems having similar stream powers per unit length. If we consider that the surface of the megafan is proportional to the volume of sediments preserved, then the volume of sediment transported per unit stream length was much greater for the Rio Pastaza than for the other systems presented in Table 4. Table 4 also shows that the Rio Parapeti which has a catchment surface close to that of the Rio Pastaza has a lower streampower and formed a much smaller fan, which would suggest that streampower is determinant in the construction of the fan. However, a comparison between the MPA and the Kosi indicate that the ratio of the catchment surfaces MPA/Kosi is 0.26 whereas the ratio of the fan surfaces MPA/Kosi is $\sim$1.14. This means that the volume of material extracted from a unit surface might have been 4 times greater in the Pastaza catchment than in the Kosi catchment whereas the streampower of the Kosi River is twice that of the Pastaza. Now, if we compare the average values of incision rates for the Sun Kosi and Arun rivers (the junction of which gives birth to the Kosi river) in the Main Boundary Thrust—which are of 1.5–2.5 mm $year^{-1}$ (Lavé and Avouac 2001)—with those for the Pastaza in the Eastern Cordillera—which are of $\sim$4–5 mm $year^{-1}$ (Bes de Berc et al. 2005)—, it appears that the incision rates in the Pastaza are twice those in the Kosi. Because the streampower is twice lower in the Rio Pastaza than in the Kosi River, it is likely that the faster incision rate in the Pastaza do reflect the rate of uplift of the Eastern Cordillera combined with a rapid adaptation of the river profile (Bes de Berc et al. 2005). Another cause must therefore be researched to the larger amount of material input into the Pastaza system.

In their study of tropical megafans, Leier et al. (2005) emphasized the contrast between the peak of discharge and the mean annual discharge, as a characteristic of all the megafans. The Rio Pastaza, like many other equatorial rivers (Latrubesse et al. 2007), does not display such a contrast in hydrologic cycles. Even during ENSO events, the ratio peak of discharge/mean annual discharge remains stable even though the mean annual discharge increases. Annual or episodic contrasts in hydrologic cycles are thus

Table 4 Comparison of morphological parameters between the Pastaza Megafan and its catchment and other megafans

	Catchment surface (km^2)	Fan surface (km^2)	Fan/catchment ratio	Discharge ($m\ s^{-3}$)(1)	Streampower ($W\ m^{-1}$)(2)	Incision values ($mm\ year^{-1}$)
Rio Pastaza	13,700	51,400	3.75	458	2.64×10^4	4.3(4)
MPA	13,700	13,750	1	458	2.64×10^4	4.3(4)
Rio Grande, Bolivia	$\sim$ 70,000(5)	$\sim$12,600(5)	0.18	2,195	5.10×10^4	n/a
Rio Pilcamayo	81,300(5)	$\sim$22,600(5)	0.28	2,534	2.76×10^4	n/a
Rio Parapeti	$\sim$ 8,000(5)	$\sim$5,800(5)	0.72	273	2.73×10^2	n/a
Kosi River	51,370(6)	$\sim$10,000(7)	0.19	1,631	5.12×10^4	1.5–2.5(8)

(1) Water discharge computed following the formula $Q = ka{\cdot}A^{\alpha}$ with Q: discharge in $m\ s^{-3}$, A: surface of the drainage basin in km^2, $ka = 0.049$ and $\alpha = 0.96$ (Talling and Sowter 1998). (2) Streampower by length unit $\Omega = \gamma Qs$, with γ, specific weight of water (9,810 $N\ m^{-3}$), Q: discharge in $m\ s^{-3}$, local slope in mm^{-1}. (3) and (4): (Bes de Berc et al. 2005). (5), after (Horton and DeCelles 2001). (6), after (Lavé and Avouac 2001). (7) after (Singh et al. 1993). (8) incision values of (Lavé and Avouac 2001) corresponding to the Main Boundary Thrust area for the Arun and Sun Kosi rivers, close to the Apex of the Kosi megafan

unable to explain the very large amount of sediment deposited by a fluvial system having a relatively small catchment. In any event, if this sediment were extracted by erosion from the bedrock of the catchment, this should imply a very rapid denudation and uplift of the entire Eastern Cordillera and eastern Western Cordillera of Ecuador during the late glacial period. The average denudation rate inferred by Vanacker et al. (2007a, b) from their radionuclide studies in small basins of the eastern Cordillera is 0.2 mm year^{-1}. This value is considered to be high by these authors. However, such a denudation rate acting during the 11,000 years of activity of the MPA would have provided only $\sim$30 km^3 of material if we assume that the denudation rate was the same over the entire Pastaza basin (and less if the denudation rate was lower in the Interandean Depression as observed by Vanacker et al. (2007a, b). Moreover, the uplift rate of 4–5 mm/year uplift since the LGM observed by Bès de Berc et al. (2005) cannot be considered as a rapid uplift when values of $\sim$2 cm/year have obtained in areas such as the Southern Alps of New Zealand). Volcanism may be another solution to this problem. As discussed earlier, it is unlikely that sedimentary pulses generated by volcanic eruption as previously proposed by Räsänen et al. (1990) were a direct cause or trigger of avulsions in any of the areas studied here. However, it is obvious that fluvial reworking of volcanic material associated to runoff and local landsliding in the easily erodable volcanic deposits has input volcanic material into the system. However, the estimate of the total volume of material provided by the volcanoes is of about 20 km^3 (see above). It should be pointed out that the addition of the material provided by the volcanic eruption and the denudation as inferred from the study of the cosmogenic radionuclides is only of $\sim$50 km^3, which is small compared with the $\sim$140 km^3 of the MPA. In any event, it is likely that the heavy volcano-sedimentary and sedimentary load transported down to the Amazonian lowland promoted aggradation and then avulsions as soon as the slope decreased. Even where the local cause or trigger of avulsion was not aggradation (e.g., the MCA), aggradation promoted by the heavy volcano-sedimentary load made the channel close to the avulsion threshold (Jones and Schumm 1999) such that any 'opportunistic' event (Slingerland and Smith 2004) can trigger avulsion. Conversely, aggradation may have triggered avulsion in areas such as the northern MCA where tectonic tilting has created a lateral slope more favourable to the avulsive channel but where the parent channel is confined by incised walls. In another ground, the prevalence of progradational avulsions in all the studied areas except the MCA could be taken as evidence that the high sedimentary load of the Pastaza system was the underlying cause of avulsion and and of the construction of very large megafans.

Conclusions

Remote sensing imagery mapping of the successive channels of the Rio Pastaza enabled us to evidence 108 sites of avulsion in the Rio Pastaza megafan. The location of these sites, the available radiocarbon ages as well as historic maps of the seventeenth century, allow us to propose an evolution of the migration and avulsions of the Rio Pastaza since the Last Glacial Maximum.

The first avulsions of the Rio Pastaza occurred after the LGM roughly parallel to the Subandean front and gave rise to a well-defined fan-shaped distributary pattern (Fig. 8A). In response to thrust-related anticline forelimb tilt, the Rio Pastaza and the apex of the megafan were progressively shifted eastward until the "Great Diversion" of the Rio Pastaza changed its course to the east-southeast towards the present-day Rios Tigre and Corrientes (TCA) (Fig. 8B). Around 9,200 $\pm$ 200 or 8,480 $\pm$ 110 Cal years BP, avulsions occurred in the TCA (Fig. 8C). The Rio Pastaza abandoned then its east-southeast course and the Tigre-Corrientes area to follow its present-day southerly course. This last avulsion was older than 1691 AD (Fig. 8D).

The average recurrence time of avulsions in the Marañon-Pastaza area, probably overestimated, ranges between 142 $\pm$ 6 years and 189 $\pm$ 6 years whereas in the Tigre-Corrientes areas, the average recurrence time of avulsions is underestimated and ranges from 342 $\pm$ 5 years to 426 $\pm$ 10 years.

Regional tectonics is active in the northwest of the Maranon-Pastaza area and responsible for thrust-related anticline eastward forelimb tilt, and lateral propagation is believed to have controlled most of the avulsions in this area. No such tectonic control seems to have acted in the south of the MPA and the TCA. The characteristics of the hydrologic cycles of the Rio Pastaza doe not allow "hydrologic" driven avulsions such as those known in areas characterized by contrasted hydrologic cycles invoked by Leier et al. (2005) in other megafans. Climatic fluctuations or pulses in sedimentary fluxes, not clearly related to volcanic activity as previously proposed by Räsänen et al. (1990), seem to be the most likely cause of avulsions in those areas.

Acknowledgments This study benefited of the logistic and financial support of the IRD (French Institute for Research in Development). This investigation was supported by a doctoral Alban fellowship (no E05D057404EC) and Université Toulouse III, Paul Sabatier grants.

References

Alexander J, Leeder MR (1987) Active tectonic control of alluvial architecture. In: Ethridge FG, Flores RM, Harvey MD (eds) Recent developments in fluvial sedimentology. Special Publication. SEPM (Society for Sedimentary Geology), pp 243–252

Assine ML (2005) River avulsions on the Taquari megafan, Pantanal wetland, Brazil. Geomorphology 70:357–371

Assine ML, Soares PC (2004) Quaternary of the Pantanal, west-central Brazil. Quat Int 114:23–34

Autin WJ, Burns SF, Miller BJ, Saucier RT and Snead JL (1991) Quaternary geology of the lower Mississipi Valley. In: Morrison RB (ed) Quaternary nonglacial geology: conterminous U.S. Geology of North America. Geological Society of America, pp 547–582

Baby P, Rivadeneira M, Christophoul F, Barragán R (1999) Style and timing of deformation in the Oriente of Ecuador. In: Orstom (ed) 4th international symposium of Andean geodynamics. ORSTOM, Göttingen, pp 68–72

Barba D, Robin C, Samaniego P, Eissen J-P (2008) Holocene recurrent explosive activity at chimborazo volcano (Ecuador). J Volcanol Geotherm Res 176:27–35

Barberi F, Coltelli M, Ferrara G, Innocenti F, Navarro J-M, Santacroce R (1988) Plio-quaternary volcanism in Ecuador. Geol Mag 125(1):1–14

Baret F, Guyot G (1991) Potentials and limits of vegetation indices for LAI and APAR assessment. Remote Sens Environ 35:161–173

Barragann R, Baudino R, Marocco R (1996) Geodynamic evolution of the Neogene intermontane Chota basin, Northern Andes of Ecuador. J South Am Earth Sci 9(5–6):309–319

Behling H, Hooghiemstra H (1998) Late quaternary palaeoecology and palaeoclimatology from pollen records of the savannas of the Llanos Orientales in Colombia. Palaeogeogr Palaeoclimatol Palaeoecol 139:251–265

Behling H, Hooghiemstra H (1999) Environmental history of the Colombian savannas of the Llanos Orientales since the last glacial maximum from lake records El Pinal and Carimagua. J Paleolimnol 21:461–476

Bès de Berc S (2003) Tectonique de chevauchement, surrection et incision fluviatile (exemple de la zone subandine équatorienne, haut bassin amazonien). PhD thesis, University of Toulouse, 181p

Bes de Berc S, Soula J-C, Baby P, Souris M, Christophoul F, Rosero M (2005) Geomorphic evidence of active deformation and uplift in a modern continental wedge-top—foredeep transition: example of the eastern Ecuadorian Andes. Tectonophysics 399(1–4):351–380

Blair TC, McPherson JG (1992) The Trolheim fan and facies model revisited. Geol Soc Am Bull 104(6):762–769

Bridge JS, Karssenberg D (2005) Simulation of flow and sedimentary processes, including channel bifurcation and avulsion, on alluvial fans. 8th international conference of fluvial sedimentology, TU Delft, pp 70

Bridge JS, Leeder MR (1979) A simulation model of alluvial stratigraphy. Sedimentology 26:617–634

Bristow CS (1999) Gradual avulsion, river metamorphosis and reworking by underfitd streams: a modern example from the Brahmaputra River in Bangladesh and a possible ancient example in the Spanish Pyrenees. In: Smith ND, Rogers J (eds) Fluvial sedimentology VI. Special Publication of the International Association of Sedimentologists #28, pp 221–230

Burbank DW, Meigs A, Brozovic N (1996) Interactions of growing folds and coeval depositional systems. Basin Res 8:199–223

Burbank DW, Anderson RS (2001) Tectonic geomorphology. Blackwell Science, Oxford 274 pp

Burgos JD (2006) Mise en place et progradation d'un cône alluvial au front d'une chaîne active: exemple des Andes équatoriennes au néogène. Phd Thesis, Université Paul Sabatier, Toulouse 3, Toulouse, 373 pp

Castro M, Mothes P, Hidalgo J, Samaniego P, Hall ML, Galarraga R, Yepes H, Andrade D, Ruiz AG (2006) Recent numerical modeling of Cotopaxi's lahars, Ecuador, Abstract Cities on Volcanoes 4, Quito, 23–27 January 2006

Christophoul F, Baby P, Soula J-C, Rosero M, Burgos JD (2002) Les ensembles fluviatiles néogènes du bassin subandin d'Equateur et implications dynamiques. Compte Rendus Géosciences 334: 1029–1037

Clapperton CM, Hall M, Mothes P, Hole MJ, Still JW, Helmens KF, Kuhry P, Gemmel AMD (1997) A younger dryas icecap in the Ecuadorian Andes. Quat Res 47:13–28

Cobb KM, Charles CD, Cheng H, Edwards RL (2003) El Niño Southern Oscillation and tropical Pacific climate during the last millenium. Nature 424:271–276

Demoraes F, d'Ercole R (2001) Cartografıa de riesgos y capacidades en el Ecuador. Diagnostico previo a planes de intervencion de las ONGs, International report. COOPI-IRD-OXFAM, Quito (Ecuador)

Dumont J-F (1996) Neotectonics of the Subandes-Brazilian craton boundary using geomorphological data: the Marañon and Beni Basin. Tectonophysics 257:137–151

Dumont JF, Hanagarth W (1993) River shifting and tectonics in the Beni Basin (Bolivia). In: Proceedings of the 3rd international conference of geomorphology, 23–29 August, Hamilton

Ethridge FG, Skelly RL, Bristow CS (1999) Avulsion and crevassing in the sandy, braided Niobrara River: complex response to base-level rise and aggradation. In: Smith ND, Rogers J (eds) Fluvial sedimentology VI. Special Publication of the International Association of Sedimentologists #28, pp 180–191

Frost I (1988) A holocene sedimentary record from Añangucocha in the Ecuadorian Amazon. Ecology 69:66–73

Gohain K, Parkash B (1990) Morphology of the Kosi Megafan. In: Rachoki AH, Church M (eds) Alluvial fans: a field approach. Wiley, London, pp 151–178

Gole CV, Chitale SV (1966) Inland delta building activity of Kosi River. Am Soc Civil Eng J Hydraul Div HY-2:111–126

Gomez N (1994) Atlas del Ecuador, Geografia y Economia. Imagenes de la Tierra, 3. Editorial Ediguias C. Ltda, Quito 114 pp

Guth PL (2006) Geomorphometry from SRTM: comparison to NED. Photogramm Eng Remote Sens 72(3):269–277

Hall ML (1977) El volcanismo en el Ecuador. Publicacion del Instituto Panamericano de Geografıa e Historıa, Seccion Nacional del Ecuador., Quito 120 pp

Hall ML (coord) (1991) The March 5, 1987 Ecuador earthquake, mass wasting and socioeconomic effects. The national academic Press, Washington DC, 144 pp

Hall M, Beate B (1991) El volcanismo Plio-Cuaternario en los Andes del Ecuador. Estudios Geograficos 4:5–38

Hall ML, Robin C, Beate B, Mothes P, Monzier M (1999) Tungurahua Volcano, Ecuador: structure, eruptive history and hazards. J Volcanol Geotherm Res 91(1):1–21

Hall ML, Samaniego P, LePennec J-L, Johnson JB (2008) Ecuadorian Andes volcanism: a review of late pliocene to present activity. J Volcanol Geotherm Res 171:1–6

Hansen BCS, Rodbell DT, Seltzer GO, Leon B, Young KR, Abbott M (2003) Late-glacial and Holocene vegetational history from two sites in the western Cordillera of southwestern Ecuador. Palaeogeogr Palaeoclimatol Palaeoecol 194:79–108

Hastenrath S (1981) The glaciation of the Ecuadorian Andes. Balkema, Rotterdam

Hastenrath S, Kutzbach J (1985) Late Pleistocene climate and water budget of the South American Altiplano. Quat Res 24:249–256

Heine K (1994) The Mera site revisited: ice-age Amazon in the light of new evidence. Quat Int 21:113–119

Heine K (2000) Tropical South America during the Last Glacial Maximum: evidence from glacial, peri-glacial and fluvial records. Quat Int 72:7–21

Heine K, Heine JT (1996) Late glacial climatic fluctuations in Ecuador. Glacier retreat during the Younger Dryas time. Arctic Alp Res 28:496–501

Horton BK, DeCelles PG (2001) Modern and ancient fluvial megafans in the foreland basin system of the Central Andes, Southern Bolivia: implications for drainage network evolution of fold-thrust belts. Basin Res 13:43–63

Humphrey NF, Konrad SK (2000) River incision or diversion in response to bedrock uplift. Geology 28:43–46

Hungerbühler D, Steinman M, Winkler W, Seward D, Egüez A, Peterson DE, Helg U, Hammer C (2002) Neogene stratigraphy and Andean geodynamics of southern Ecuador. Earth Sci Rev 57:75–124

IGEPN (2009) http://www.igepn.edu.ec. Instituto Geofisico de la Escuela Politecnica Nacional, Quito, Ecuador

Jones LS, Schumm SA (1999) Causes of avulsion: an overview. In: Smith ND, Rogers J (eds) Fluvial sedimentology VI. Special Publication of the International Association of Sedimentologists. Blackwell Science, Oxford, pp 171–178

Keefer DK, Moseley ME, deFrance S (2003) A 38000-year record of floods and debris flows in the Ilo region of southern Peru and its relation to El Niño events and great earthquakes. Palaeogeogr Palaeoclimatol Palaeoecol 194:41–77

Kennerley JB (1980) Outline of the geology of Ecuador. Overseas Geol Miner Resour 55:1–16

Lang HR, Welch R (1994) «Algorithm theoretical basis document for ASTER digital elevation models:», Jet Propulsion Laboratory, May 31, 1994, draft report to the EOS Project

Latrubesse EM, Stevaux JC, Sinha R (2007) Tropical Rivers. Geomorphology 70(3–4):187–206

Lavé J, Avouac J-P (2001) Fluvial incision and tectonic uplift across the Himalaya of Central Nepal. J Geophys Res 106(B11):26561–26591

Lavenu A, Noblet C, Bonhomme MG, Egüez A, Dugas F, Vivier G (1992) New K-Ar age dates of neogene and quaternary volcanic rocks from the Ecuadorian Andes: implications for the relationship between sedimentation, volcanism, and tectonics. J South Am Earth Sci 5(3–4):309–320

Ledru M-P, Bertaux J, Sifeddine A, Suguio K (1998) Absence of last glacial maximum records in lowland tropical forests. Quat Res 49:233–237

Leeder MR, Harris T, Kirby MJ (1998) Sediment supply and climate change: implications for basin stratigraphy. Basin Res 10:7–18

Leier AL, DeCelles PG, Pelletier JD (2005) Mountains, monsoons and megafan. Geology 33(4):289–292

LePennec J-L, Jaya D, Samaniego P, Ramon P, Moreno Yanez S, Egred J, Van der Plicht J (2008) The AD1300–1700 eruptive periods et Tungurahua vocano, Ecuador, revealed by historical narratives, stratigraphy and radiocarbon dating. J Volcanol Geotherm Res 176:70–81

Li S, Finlayson B (1993) Flood management on the lower Yellow River: hydrological and geomorphological perspectives. In: Fielding CR (ed) Current research in fluvial sedimentology. Sed Geol, vol 85, pp 285–296

Mackey SD, Bridge JS (1995) Three dimensional model of alluvial stratigraphy: theory and application. J Sed Res B65(1):7–31

McClay KR (1992) Glossary of thrust tectonics. In: McClay KR (ed) Thrust tectonics. Chapman and Hall, London, p 447

Molina I, Kumagai H, Garcia-Aristizabal A, Nakano M, Mothes P (2008) Source process of very-long-period events accompanying long-period signals at cotopaxi volcano (Ecuador). J Volcanol Geotherm Res 176:119–133

Montufar R, Pintaud J-C (2006) Variation in species composition, abundance and microhabitat preferences among western Amazonian Terra Firme palm communities. Bot J Linn Soc 151:127–140

Monzier M, Robin C, Samaniego P, Hall ML, Cotten J, Mothes P, Arnaud N (1999) Sangay volcano, Ecuador: structural development, present activity and petrology. J Volcanol Geotherm Res 90(1–2):49–79

Morozova GS, Smith ND (1999) Holocene avulsion history of the lower Saskatchewan fluvial system, Cumberland Marshes, Saskatchewan-Manitoba, Canada. In: Smith ND, Rogers J (eds) Fluvial sedimentology VI. Special Publication. International Association of Sedimentologists, pp 231–249

Morozova GS, Smith ND (2000) Holocene avulsion styles and sedimentation patterns of the Saskatchewan River, Cumberland Marshes, Canada. Sed Geol 130:81–105

Mothes P, Hall ML, Janda RJ (1998) The enormous Chillos Valley Lahar: an ash-flow-generated debris flow from Cotopaxi volcano, Ecuador. Bull Volcanol 59:233–244

Moy CM, Seltzer GO, Rodbell DT, Anderson DM (2002) Variability of El Niño/Southern Oscillation activity at millennial timescales during the Holocene epoch. Nature 420:162–165

Nelson BW (1970) Hydrography, sediment dispersal and recent historical development of the Po River Delta, Italy. In: Morgan JP, Shaver RH (eds) Deltaic sedimentation, modern and ancient. Special Publication. SEPM, pp 152–184

Philip H, Meghraoui M (1983) Structural analysis and interpretation of the surface deformation of the El Asnam earthquake of October 10, 1980. Tectonics 2(1):17–49

Potts LV, Akyilmaz O, Braun A, Shum CK (2008) Multi-resolution dune morphology using Shuttle Radar Topography Mission (SRTM) and dune mobility from fuzzy inference systems using SRTM and altimetric data. Int J Remote Sens 29:2879–2901

Pratt WR, Duque P, Ponce M (2005) An autochthonous geological model for the eastern Andes of Ecuador. Tectonophysics 399(1–4):251–278

Ramsay J (1967) Folding and fracturing of rocks. MacGraw-Hill, New York 568 pp

Ramsay JG, Huber MI (1987) The techniques of modern structural geology, vol 2: folds and fractures. Academic Press, London 307 pp

Räsänen ME, Salo JS, Jungnert H, Romero Pittman L (1990) Evolution of the western Amazon lowland relief: impact of Andean foreland dynamics. Terra Nova 2:320–332

Räsänen ME, Neller R, Salo J, Jungner H (1992) Recent and ancient fluvial deposition systems in the Amazonian foreland basin, Peru. Geol Mag 129:293–306

Reimer PJ, Baillie MGL, Bard E, Bayliss A, Beck JW, Bertrand CJH, Blackwell PG, Buck CE, Burr GS, Cutler KB, Damon PE, Edwards RL, Fairbanks RG, Friedrich M, Guilderson TP, Hogg G, Hughen KA, Kromer B, McCormac G, Manning S, Ramsey CB, Reimer RW, Remmele S, Southon JR, Stuiver M, Talamo S, Taylor FW, Van der Plicht J, Weyhenmeyer CE (2004) INTCAL04 Terrestrial Radiocarbon age calibration, 0–26 Cal kyears BP. Radiocarbon 46(3):1029–1058

Reynaud C, Jaillard E, Lapierre H, Mamberti M, Mascles G (1999) Oceanic plateau and island arcs of southwestern Ecuador: their place in the geodynamic evolution of northwestern South America. Tectonophysics 307:235–254

Rodbell DT, Seltzer GO, Anderson DM, Abbott MB, Enfield DB, Newman JH (1999) A high resolution 15,000 record of El-Nino driven alluviation in southwestern Ecuador. Science 283:516–519

Roddaz M, Baby P, Brusset S, Hermoza W, Darrozes J (2005) Forebulge dynamics and environmental control in Western Amazonia: the case study of the Arch of Iquitos (Peru). Tectonophysics 399(1–4):87–108

Rosseti D, Valeriano MM (2007) Evolution of the lowest amazon basin modeled from the integration of geological and SRTM topographic data. Catena 70:253–265

Saucier RT (1994) Geomorphology and quaternary geologic history of the Lower Mississipi Valley. US Army Corps Eng 1:1–364

Schumm SA, Mosley MP, Weaver WE (1987) Experimental fluvial geomorphology. Wiley Interscience, New York, 411 pp

Schumm SA, Erskine WD, Tilleard JW (1996) Morphology, hydrology, and evolution of the anastomosing Ovens and King Rivers, Victoria, australia. Geol Soc Am Bull 108(10):1212–1224

Seltzer GO, Rodbell PA, Baker SC, Fritz PM, Tapia HD, Rowe RB, Dunbar RB (2002) Early warming of Tropical South America at the last glacial transition. Science 296:1685–1686

Singh IB, Parkash B, Gohain K (1993) Facies anlysis of the Kosi Megafan deposits. Sed Geol 85:87–113

Slingerland R, Smith ND (2004) River avulsion and their deposits. Annu Rev Earth Planet Sci 32:257–285

Smith ND, McCarthy TS, Ellery WN, Merry CL, Ruther H (1997) Avulsion and anastomosis in the panhandle region of the Okavongo Fan, Botswana. Geomorphology 20:49–65

Spikings RA, Crowhurst PV (2004) (U/Th)He thermochronometric constraints on the late Miocene Pliocene development of the northern Cordillera Real and Interandean depression. J South Am Earth Sci 17:239–251

Spikings RA, Seward D, Winkler W, Ruiz G (2000) Low temperature thermochronology of the northern Cordillera Real, Ecuador: tectonic insights from zircon and apatite fission track analysis. Tectonics 19:648–649

Stanistreet IG, McCarthy TS (1993) The Okavango fan and the classification of subaerial fan systems. Sed Geol 85:115–133

Stanistreet IG, Cairncross B, McCarthy TS (1993) Low sinuosity and meandering bedload rivers of the Okavango fan: channel confinement by vegetated levees without fine sediment. Sed Geol 85(1–4):135–156

Stinton AJ, Sheridan MF (2008) Implications of long-term changes in valley geomorphology on the behavior of small-volume pyroclastic flows. J Volcanol Geotherm Res 176:134–140

Stouthamer E, Berendsen HJA (2000) Factors controlling the holocene avulsion history of the Rhine-Meuse Delta (The Netherlands). J Sed Res 70(5):1051–1064

Stouthamer E, Berendsen HJA (2001) Avulsion frequency, avulsion duration and interavulsion period of the holocene channel belts in the Rhine-Meuse Delta, The Netherlands. J Sed Res 71(4):589–598

Talling PJ, Sowter MJ (1998) Erosion, deposition and basin wide variations in stream power and bed shear stress. Basin Res 10:87–108

Törnqvist TE (1994) Middle and late Holocene avulsion history of the River Rhine (Rhine-Meuse Delta, Netherlands). Geology 22:711–714

Tschopp HJ (1953) Oil explorations in the Oriente of Ecuador. Am Assoc Petroleum Geol Bull 37:2303–2347

van der Beek P, Champel B, Mugnier J-L (2002) Control of detachment dip on drainage development in regions of active fault-propagation folding. Geology 30(5):471–474

Vanacker V, von Blanckenburg F, Govers G, Kubik PW (2007a) Transient landscape evolution following uplift in the Southern Ecuadorian Andes. Geochimica Cosmogenica Acta 71:A1052

Vanacker V, von Blanckenburg F, Govers G, Molina A, Poesen J, Deckers J, Kubik PW (2007b) Restoring natural vegetation reverts mountain erosion to natural levels. Geology 35:303–306

Welch R, Marko W (1981) Cartographic potential of spacecraft line-array camera system: stereosat. Photogramm Eng Remote Sens 47(8):1173–1185

Wells NA, Dorr JA (1987) Shifting of the Kosi River, Northern India. Geology 15:204–207

Weng C, Bush MB, Athens JS (2002) Holocene climate changeand hydrach succession in lowland Amazonian Ecuador. Rev Palaeobot Palynologt 120:73–90

Winkler W, Villagomez D, Spikings R, Abegglend P, Toblere S, Egüez A (2005) The Chota basin and its significance for the inception and tectonic setting of the inter-Andean depression in Ecuador. J South Am Earth Sci 19(1):5–19

Yepes H, Chatelain J-L, Guillier B, Alvarado A, Egred J, Ruiz M, Segovia M (1996) The Mw 6.8 Macas Earthquake in the Subandean Zone of Ecuador, October 3, 1995. Seismol Res Lett 67:27–32

Zandbergen P (2008) Applications of shuttle radar topography mission elevation data, geography compass, Earth observation. doi:10.1111/j.1749-8198.2008.00154.x

Annexe C

Christophoul, F., Regard, V., Martinod, J., Darrozes, J. ***(soumis)***
Geomorphology

Cet article est issu d'un projet interne au groupe de géomorphologie de l'UMR 5563 GET. Il dérive d'un enseignement de terrain "classique" du cursus en Sciences de la Terre de l'Univ. Toulouse "Cartographie des terrasses de la Garonne". Cette étude basée sur une cartographie des chenaux préservés dans le remplissage de la basse terrasse de la Garonne. La mise à disposition du public par l'IGN d'une part importante des campagnes de photographies aériennes nous a permis de mettre en place une base de donnée couvrant 120 km^2 de cette terrasse. La réponse spectrale sur ces photographies panchromatiques révèle, dans certains cas et en fonction de la saison de prise de vue, en lien avec l'humidité du sol, via la couleur des sols nus ou une croissance différentielle de la végétation, un "pattern" (constant au cours du temps mais avec des variations d'intensité) révélant la morphologie des chenaux sous-jacent, préservés dans le remplissage de la dernière terrasse de la Garonne.

Résumé :

Tout au long du Quaternaire, la Garonne a développé un important réseau dissymétrique de terrasses d'abrasion. La dernière d'entre elles est contemporaine de la dernière glaciation. La cartographie des paléochenaux qui constituent le remplissage de cette dernière terrasse a été effectué par traitement d'image sur les diverses campagnes de photographie aériennes disponibles. Cette cartographie nous permet de discuter les différents facteurs qui ont contrôlé la transition tresses-méandres en lien avec la fin de la dernière glaciation. Trois morphologies fluviales sont préservées dans les sédiments de la dernière terrasse de la Garonne. Ces morphologies sont, dans l'ordre chronologique :

1. une morphologie en tresses, mise en place avant 30 Ka,
2. des méandres à graviers à faible sinuosité formés entre 30 ka et 14 ka,
3. des méandres à graviers à forte sinuosité déposés entre 14 ka et la fin du Younger Dryas.

Les datations ainsi que lies données palynologiques disponibles permettent de relier ces changements de morphologie aux évènements climatiques s'étant produits durant la fin du pléniglaciaire et le tardiglaciaire. La transition tresse-méandres s'est produite il y a 30 ka et la sinuosité a brusquement augmenté à 14 ka. Cette transition, dans le contexte du retrait glaciaire dans la partie amont du bassin versant résulte des interférences entre la croissance de la végétation et les caractéristiques du régime hydrologique qui évolue progressivement d'un type "Glaciaire" avec de hautes eaux au printemps/été à un régime "Pluvio-nival" avec des hautes en hiver/printemps, laissant les barres de gravier à découvert pendant la période de germination des végétaux.

Morphodynamics of the Upper Pleistocene Garonne River (SW France): conditions of braiding/meandering transition

Frédéric Christophoul [(1)(2)], Vincent Regard [(1)], Joseph Martinod [(1)], José Darrozes [(1)]

[(1)] Géosciences Environnement Toulouse (GET), Observatoire de Midi-Pyrénées – Université de Toulouse – CNRS – IRD, 14 Av, Edouard Belin, F-31400 Toulouse, France. frederic.christophoul@get.obs-mip.fr

[(2)] Centre de Recherches Pétrographiques et Géochimiques (CRPG), 15 Avenue Notre Dame des Pauvres, 54501 Vandœuvre lès Nancy, cedex

Abstract :
The Garonne River developed through the Quaternary a huge network of asymmetric strath terraces. The last terrace is contemporary to the last glaciation. The mapping of the paleochannels preserved below the last Terrace of the Garonne River (southwest of France), by mean of remote sensing based on aerial photographs and field data, allows us to investigate the factors controlling factors of the transition braiding meandering related to the end of the last glaciation in the Pyrenees. Three channels patterns preserved in the infill of the lowest terrace of the Garonne River, could be evidenced. In chronological order, these patterns are: 1- braided channels before 30 ka, 2- low sinuosity gravel meandering channels until 15 ka and 3- high sinuosity gravel meandering channels before the end of the Younger Dryas. The available datings and palynologic data allow us to link this changes in fluvial morphology to the end of the last glaciation in the Pyrenees. The braided/meandering transition occurred 30 ka ago and the sinuosity sharply increased after 14 ka. This transition, in the context of the glaciar retreat in the upstream Garonne valley is the result of interplay between vegetation and hydrologic regime of the river, which evolved from a glacial regime with high water stage in spring/summer to a pluvio-nival regime with high water stage in winter/spring leaving uncovered gravel bars by the time of vegetation germination.

Keywords:
Fluvial dynamics, meandering, braiding, fluvial terrace, Garonne, France, würmian glaciation

1 – Introduction

The study of fluvial planforms is a classic tool used in fluvial geomorphology for tracing changes in rivers dynamics. In ancient fluvial systems, fluvial styles are inferred from facies associations by mean of facies models (Miall, 1996). Only a few examples of observed ancient fluvial planform are available in the literature (Cuevas Martinez et al., 2009) and none of them deal with braided or meandering streams. Nevertheless, examples of ancient fluvial systems in which fluvial style can be observed both in planforms and outcrops (Rhine valley, southeastern coast of New Zealand) are available in quaternary systems but have not been studied up to now. Studies of the evolution of ancient fluvial forms could be of great interest in order to constrain the morphological changes associated with stages of lateral and vertical incision involved the formation and abandonment of quaternary fluvial terraces.

Since Penck and Brückner (1909) and their study of the terrace network of the alpine rivers, the link between the timing of quaternary glacial cycles and alluvial terrace abandonment has been widely studied and precised (Vandenberghe and Maddy, 2000; 2001; Bridgland and Westaway 2008a; 2008b). In the case of the Pyrenean rivers, recent studies emphasized the link between climatic fluctuations and alluvial terraces formation (Delmas et al., 2011; Stange et al., 2013). Though the terrace network was widely studied (Hubschman, 1975a; 1975b; Revel and Bourgeat, 1981; Bourgeat et al., 1984) in terms of geometry and pedology, almost nothing is known about the morphological characteristics of the rivers that gave birth to these alluvial terraces.

The Garonne River is the longest tributary issued from the northern side of the Pyrenees. On its middle course, on the north pyrenean piedmont, this river has carved an impressively wide (up to 25 km) and deep (175m) network of asymmetric stepped alluvial terraces all along Quaternary times. We focused our study on the lowest terrace of the Garonne. Due to its extensive preserved surface and its young age this terrace provides an exceptional

This article is aimed at showing the first extensive survey of a river planform evolution contemporary to the formation of a strath terrace as a response to the end of the last glacial cycle over a 40 km long reach, representing the 120 km^2 swept

by the river between the beginning of aggradation on the last terrace and its abandonment. This study is based on outcrop description, well log interpretations and remote sensing based on aerial photography. The transition between the different styles identified and the timing of changes in fluvial processes in reponse to climate change at the end of the last glaciation will be the base of our discussion.

2 – Geological and geomorphological settings

The Garonne river (southwest of France) is 647 km long, It rises on the slopes of Aneto Peek (highest summit of the Pyrenees). Its catchment covers 55 000 km2, it is the major drain of the southwest of France. This terrace network developed through Quaternary times (Icole, 1974, Huschman, 1975 a, b).

Southward from Boussens, the substratum of the terrace network is made of alternating synclines and anticlines of the sub-pyrenean zone made of series from Upper cretaceous to Paleocene to Eocene limestone bearing series (Fig. 1).

To the north, this substratum is made of the syn-orogenic to post-orogenic molasses of the north Pyrenean foreland basin (Aquitaine basin). These molasses consist in fluvial deposits made of clays, marls, lacustrine/palustrine limestones and channelized sandstones and conglomerates. The age of these molasses ranges, in the studied area, from Oligocene to Miocene (Crouzel, 1957; Cahuzac et al., 1995; Dubreuilh et al., 1995; Antoine et al., 1997; Biteau et al., 2006). The molasses are sometimes overlain by alluvial deposits of the Lannemezan Formation, probably Pliocene to Lower Quaternary in age (Icole, 1974). The cumulated vertical incision of the Garonne river within the Lannemezan Fm. and molasses is up to 200 m.

Six main stepped terraces levels were identified (Hubschmann, 1975a; 1975b), labelled thereafter T1, the youngest to T6, the oldest (Fig. 1). The five oldest terraces are only known on the left bank of the Garonne. The youngest (T1 on Fig. 1) is mainly developed on the left bank, and poorly developed on the right bank due to the migration of the Garonne River toward the east (Fig. 1).

The chronology of these terraces is poorly constrained. The oldest and highest one (T6 on Fig.1) re-incised Pliocene to Lower Quaternary deposits of the Lannemezan Fm. (Icole, 1974). No precise datings are available, lower quaternary (Günz) age was attributed to this terrace (Icole, 1974) due to it position at the top of the terrace network and by analogy with Penck and Brückner (1909) stratigraphy of quaternary times. Terraces T5 to T2 are neither dated, ages were attributed to Mindel and Riss due to their elevation and infill weathering (Hubschman, 1975a,b ; Stange et al., (2013).

The youngest terrace is the only one whose age is satisfactorily constrained. Charcoal sampled a few meter above the base of the infill gave 10,651+/-457 yrs Cal BP and 11,242+/-593 yrs Cal BP (Bourgeat et al., 1984; calibration CalPal). ^{10}Be exposure dating in pits by Stange et al. (2013) indicates an abandonment age of T1 at 14.6 +9.6/-4.3 ^{10}Be ka in Plaine de Rivière (upstream from Boussens, Fig. 1) and 13.1 +6.7/-3.9 ^{10}Be ka in Cazères (Fig.1). Downstream from Toulouse (Fig. 1) several recent studies (Bruxelles et al. 2010, Bruxelles and Jarry, 2011, Carozza et al., 2013) based on radiocarbon dating constrained the age of silts covering the channel deposits of T1. After the abandonment of T1, the Garonne River started incising its molassic substratum carving several local terraces between T1 and the modern channel (Stange et al., 2013). Nowadays, in the studied area, upstream from Toulouse, the Garonne River flows on the molassic substratum. The post-T1 incision varies from south to north from 5 to 10m (Fig. 1). Though differences, datings indicate terrace T1 was abandoned during tardiglacial times.

We focused our study on a 40 km long segment of the up-to-5km-wide lower terrace between the topographic front of the Pyrenees (located to the north of the “Petites Pyrénées”, Fig. 1) to the south and the confluence with the Ariège River (10 km south of Toulouse) to the north.

3 – Data and methods

3.1– Remote sensing

Remote sensing based on the huge database of aerial photographs of the IGN (French Geographical Survey) allowed us to map the paleo-channels of the Garonne when it flew on the last terrace. We used panchromatic aerial photographs and orthorectified colour aerial photographs. The database includes all the aerial campaigns led between 1942 and 2008. Ground resolution, depending of the campaign flight altitude and camera type varies from 25 to 60 cm-wide pixels. Depending of the period of the year of the flight, the ground may exhibit a singular pattern (Figures 3 and 4). This pattern can correspond to: 1) differences in soil moisture on non-vegetated fields (fall and winter campaigns), 2) differences in vegetation growth (spring and summer campaigns) in response to soil moisture variations. Contrast intensity varies from a campaign to another but the pattern drawn on the same parcel remains the same through years.

Due to spectral response differences, each parcel was treated separately on the selected photographs. The treatment consists in a threshold filtering (leading to binarization on low contrast parcels) in order to enhance the original contrast (see examples later, Figs. 3 and 4).

3.2- Well log database

We interpolated an isopach map of the

quaternary sediments preserved below the terrace (Fig. 7) using the well log database of the BRGM (French geological survey) available through its online GIS Infoterre (http://infoterre.brgm.fr). This database takes into account all the pits, piezometers, pit quarries and wells cored in the sediments preserved below the terrace for quarry exploitation and water supply purposes. More than 950 logging reports were checked and re-interpreted. 300 wells crossed the base of the terrace deposits and went into the underlying substratum made of the oligocene "Molasses". Wells that did not cross the base of the gravel deposits were also used as minimum value of thickness. Thickness data were then interpolated. Considering the heterogeneity of the wells spatial distribution, we used a minimum curvature algorithm in order to avoid bull eyes effects.

4 – Paleochannel mapping

The channel patterns reconstructed by mean of remote sensing provide a vision of successive channels of the Garonne. Toward the North, the long-term urbanization and land use of the city of Muret and the southern suburbs of Toulouse (prior to the 40's), together with the poor quality of the 1940's and 1950's aerial photographs, do not allow for mapping the paleochannels clearly enough. The map of the Garonne paleochannels preserved below terrace T1 is shown on Figure 2.

4.1 – Fluvial styles

Two fluvial styles can be interpreted from the processed aerial photographs: braided pattern (Fig. 3) and meander belts (Fig. 4). Several braided areas could be recognised as well as three meander belts.

4.1.1- Braided streams

Braided streams were identified on 4 braided areas (BA: BA 1 to 4 from south to north on Fig. 2). Braided patterns are shown on Figure 3. Figure 3B exhibits the typical channel pattern encountered on the four braided areas. The pattern is made of low angle bifurcations (B, Fig. 3B) and downstream junctions (J, Fig. 3B, Ferguson, 1993) separating diamond shaped bars. Head channels disappearing upstream at the top of braid bars can also be identified (H, Fig. 3B). Channels width varies from 25 to 100m and shows the classical hierarchy of braided channels (Bridge, 1993) with wide central channels (1, Fig 3B) and narrow cross bar channels (2, Fig. 3B) isolating diamond shaped braid bars.

In BA 1, braided channels width varies from 25 to 45m. Mean channels direction indicates paleocurrents striking N38E.Northwards, BA 2 is the largest braided area identified on terrace T1 (Fig. 2). BA 2 is bounded to the left by terrace T2 scarp and to the right by meander belts (see § 4.1.2 below). BA 2 is 19 km long and its mean width is 1.6 km. On BA 2, braided channel width reaches 75 to 125 m. Mean channel direction varies from N60E-70E to the south, then it describes a gentle northward curve in the Laffite Vigordane area, reaching values N10E-20E to the north. To the north paleocurrents reveal another curve to the northwest with values of N30E and local bends till N70E.

BA 3 (Fig. 2, Fig. 3B) is located in the central part of the study area to the northwest of Carbonne. BA 3 is bounded on its left and right bank by meander belts. Braided channel geometry is similar than in BA 2 and paleocurrent trends are parallel to those of BA 2 in the same reach (N30E with bends reaching N70E). It suggests that BA 2 and 3 belong to the same ancient braided reach of the Garonne.

The northernmost braided area (BA 4 on Fig. 2) is located southward from Muret, it is bounded to the northwest and to the southwest by meander belts. In this area, braiding pattern is radically different than in the three other braiding areas. Channels are more sinuous and exhibit a better downstream continuity. Nevertheless it exhibits numerous bifurcations and junctions and the same hierarchy in channel width (Fig. 3C). Due to curvier channels, the diamond shape of braid bars is difficult to identify (Fig. 3C). Despite these similarities, this pattern also exhibits lateral accretion surfaces characteristic of meandering channels (M, Fig. 3C). We interpret this planform as a wandering channel pattern (Brierley and Hickin., 1991, Fig. 3C). Though different in shape than the other braiding areas this area cannot be considered as contemporaneous to the meanders. It would better represent a downstream evolution of the braided pattern as it is observed in several modern rivers (Brierley and Hickin, 1991).

Similarities and continuity in paleocurrents and a similar morphology seem to indicate that the four braided areas identified belong to a single stage of evolution of the river morphology. Younger channels separated then these braided areas.

4.1.2 – Meander belts

Three meander belts can be identified based on their channel pattern, sinuosity and their geometric relationships. Figure 4 exhibits the fluvial patterns corresponding to these meander belts. On Figure, we can see the pattern is made of a single band, with weak downstream variations. This band is sinuous and corresponds to the former channel. Inside the bends, arcuate lines, locally crosscutting the others can be identified (PB on Fig. 4B). These arcuate lines correspond to lateral accretion surfaces and depict a point bar. In the inner part of the first pointbar, another channel can be seen (CCh on Fig. 4B), due to its location, this channel can be interpreted as a chute channel.

The first Meander belt is MB1 (Fig. 2, Fig. 4), it is the major feature of terrace T1 (Fig. 2). In the southern part of T1, between Boussens and Cazères, MB1 occupies most of the terrace surface. In this southern part, channels exhibit poor downstream continuity due to numerous meander cut-off. Channels exhibit width

60-90m and sinuosity up to 1.4 (Fig. 4C). MB1 is bounded to the right by MB2 (Fig. 2). North of Cazères, MB1 divides into two branches isolating BA1. Northeastward, MB1 bounds BA2 and disappears as it is cut by MB2 over a 3km reach. MB1 re-appears northward to the south of Laffite Vigordane, bounding to the left BA2 and still bounded to the right by MB2. Northward, between Laffite Vigordane and Carbonne MB1 divides newly into two branches. The left one crosscuts the braided deposits, separating BA2 and BA3. This branch is the results of the limited wandering of an only meandering channel. This branch is 750m to 1 km wide what corresponds to the amplitude of the meanders observed in the area (Fig. 4B). Channel width increases to 125 m. The right branch bypasses BA3 to the right. MB1 is preserved here due to the disappearance of MB2. To the northeast of Carbonne, this branch disappears, crosscut by the reappearing MB2. To the north MB1 extends the left branch mentioned above. Between Carbonne and Muret MB1 completely replaces BA2 and reaches terrace T2 scarp, isolating BA4. To the north of BA4, MB1 is replaced by MB2. In terms of topography, the surface on top of MB1 remains at the same elevation than Braided Areas (BA 1 to 4, Fig. 2) such that no scarp allows discriminating them on the field.

The second meander belt, MB2 (Fig.2) only occurs on the right part of terrace T1, close to the scarp separating T1 from the modern channel of the river. MB2 is made of more sinuous channels than MB1. This higher sinuosity can be seen looking at the shape of the left MB2 boundary exhibiting numerous well-preserved meander loops. Meanders of MB2 mainly show lateral accretion and less downstream migration than meanders of MB1 (Fig.2). Channels are XXX m-wide. MB2 appears downstream from Boussens (south of Fig. 2). Here, MB2 channels crosscut MB1 meanders. MB2 develops then downstream, with fluctuating width. To the northeast of Cazères MB2 completely cuts MB1, making it disappear and also crosscuts BA2. MB2 abruptly disappears a few kilometrers south from Carbonne, close to the confluence with the Arize River. It reappears a few kilometres downstream from Carbonne, crosscutting BA3 and then, northward newly cutting MB1 channels. Northward, it bounds BA 4 to the right. Finally, to the southwest of Muret, to the north of BA4, MB2 crosscuts MB1 meanders, reaching the scarp of terrace T2. Toward Muret MB2 occupies the whole width of terrace T1.

In terms of topography, to the south (between Boussens and Cazères) a 5 m high scarp separates MB2 from MB1. Downstream, this scarp elevation diminishes, occurring punctually along the boundary (relics of the former cutbanks?). It finally disappears between Cazères and Carbone. Downstream, MB2, MB1, BA2 and BA3 remain at the same elevation.

A third meander belt was identified (MB3). MB3 is poorly preserved. It only locates in the inner part of modern meanders of the Garonne River (Fig. 2). They result from the modern meander scroll. On a topographic point of view these accretion surfaces testifying of the recent motion of the Channel are located below the terrace T1 level and above the modern channel. Hence, we can think these accretion surface are contemporary to the incision which provoked the final abandonment of T1.

4.2 - Relative chronology

In Terms of chronology, braided channels seem to be the oldest because they have been superimposed by meander belts. Meander of MB1 eroded and/or reworked sediments of Braided Channels. To the northwest of Cazères (Fig. 2) the terrace scarp between T2 and T1 exhibits a "re-entrant" showing channels of MB1 eroded the former braided deposits as well as T2 scarp. To the south (north of Cazères, Fig.1), MB1 meanders crosscut BA1. To the north (Carbonne), MB1 separates BA2 and BA3.

MB2, due to its location on the right part (southeast) of the terrace, close to the modern river and the meander loops cutting BA2, BA3 and MB1 meanders indicate these meanders are younger; this seems confirmed by its position at lower elevation. The radiocarbon ages by Bourgeat et al. (1984), significatively younger than the other ages presented in introduction were performed on samples issued from the base of the sediments of MB2 (Fig.1). They seem to confirm that MB2 postdates BA2, BA3 and MB1. MB3, located close to the modern course of the Garonne River is younger than MB2 and represents the last stage of the river course before or during the final abandonment of terrace T1.

5– Sedimentology

Thanks to the numerous quarries excavating the deposits of the lower terrace of the Garonne, the first meters below the terrace and above the water table can be easily studied in terms of facies analysis (Figure 1.5).

The deposits consist in non-cemented round pebbles to cobbles with sandy matrix interbedded with sandy lenses. Outcrops exhibit decametre to hectometre-wide and metre-deep channels made of stacked gravel bars partly interbedded with sand dunes organized in lateral accretion bedforms. Channels exhibit low depth compare to the thickness of sediments preserved on the terrace.

5.1. Braided Channels

In the area of Laffite Vigordane (Fig.1, Fig. 5), a quarry front illustrates the typical facies associations encountered. Before the exploitation of the quarry a well was cored (Fig. 5A). Figure 5C shows the lithologic log of the sediments encountered in the well, from base to top: 1) from 14 m to 13,30 m: sandy marls and limestones of the Oligocene molasses. 2) from 13,30 to 3,00 m: gravels with sandy matrix, 3) from 3,00 to 2,60 m: grey-blue medium sands, 4) from 2,60m to 1,40m: gravels with grey sandy matrix, 5) From 1,40 to 0,60m : gravels with sandy matrix

cemented by iron and manganese oxides resulting from the pedogenesis below the terrace surface after its abandonment, 6) brown clayish and silty sands and 7) humus and clays horizon. The working face of the quarry pit helped us to understand better the geometry of the gravel and sand bodies in the first meters below the terrace. This working face illustrates the five first meters below the surface. Figure 5 represents the face of the pit quarry as seen on June 2012. From top to base on Figure 5B, the face exhibits light brown clays and silts, unconsolidated sands interfingered within the underlying gravels. Below these deposits, most of the face is made of unconsolidated sandy matrix gravels interbedded with medium to coarse sands lenses. The gravels are organized into decametre-wide and metre-deep concave up and flat-topped swales. These swales exhibit a single-storey fill made of apparently lateral migrating bars exhibiting low angle centimetre thick heterolithic stratifications. No significant erosional surfaces were identified within the swale fill. Imbricated clasts reveal currents striking N32E, mostly obliquous toward the working face and in accordance with the channel strike observed on aerial photographs (Fig. 5A). The sandy lenses identified are metre-wide and centimetre-thick. Their shape is flat-based and convex up topped. These sands exhibit planar and trough cross bedding (Fig. 5D).

The overall geometry (symmetric, weak depth), size (decametre wide and decimetre deep) of the channels identified together with the grain size of the infill supports the interpretation of braided channels. The good preservation of sand bars within the channel fills as well as the lack of erosional surfaces within and between channels infill indicate high conditions of aggradation during deposition.

5.2. Gravel bed meandering channels

In the area of Cazères (Fig.1) another quarry pit allowed us to investigate the sedimentology of the meandering channels. Like in Laffite Vigordane, a well cored in the deposits of the terrace reached the molassic substratum. The sedimentary log on Figure 6A shows, compared to braided channel deposits (Fig. 5C) more variations in grain size. The column is made of metre-thick alternating sands, pebbly sands and pebble beds organized in seven fining upward sequences. The base of the terrace infill was reached at 13.5 m

Figure 6B exhibits the pit quarry face. At first sight, this outcrop presents great similarities with the outcrop of braided channels presented in §5.1. Sediments have the same grain size. Nevertheless we can observe on Figure. 6B there is more heterogeneity in grain size distribution as observed in well (Fig. 6A). In terms of architectural elements, the outcrop, from left to right, is made of alternating pebbles and sandy pebbles. Geometry of these beds is planar and inclined. To the left of the outcrop, apparent dip changes following the change in direction of the working face. Inclined planar beds occupy the left half of the outcrop. To the right, apparent dip slightly diminishes. Beds are then cut by more inclined beds. To the right, these beds exhibit a regular decrease of dip until they remain flat, describing a half swale. At the base of this swale, gravels are organized in planar inclined beds corresponding to the lee-side of a gravel bar. Paleocurrents measured on the planar beds reveals a N47E-striking mean current showing the flow was mostly perpendicular to the working face in the axis of the channel. Apparent flat stratification corresponds in fact to planar inclined surfaces dipping perpendicularly to the outcrop. The overall architecture of the outcrop consists in a lateral accretion macroform passing to a channel axis filled by downstream accreting gravel bars. The outcrop depicts a meander pointbar and its neigbouring channel. Considering plaeocurrents, the point bar is the left bank of the channel. The cutbank to the right of the channel could not be recognized.

The channel identified on the right part of the outcrop is 120 m-wide and 4 m-deep. The width of this channel has the same order of magnitude than those observed on the map (Fig. 2) in the same area. Compared to braided channel previously described, the gravel bed meandering channel of the Cazères pit quarry is wider and deeper. It also exhibits outcrop-scaled sigmoidal stratifications associated to heterogeneity in grain size, with alternating sandy pebbles and pebbly sands. Together with their inclined geometry can be interpreted as an equivalent of the IHS (Inclined Heterolithic Sandstones) for gravel meandering channels. IHS are widely described in sandy meandering rivers (Thomas et al., 1987) as corresponding to lateral accretion macroforms (Miall, 1996) and are characteristic of meandering channels.

6 – Sediment thickness

The thickness of sediments of the terrace infill observed in wells and pits ranges 3 to 19 m (Fig. 7A). Sediment thickness roughly diminishes from south to north. To the south, a few kilometres northeast of Boussens, local strong variations in thickness occur. In this area, terrace T1 substratum corresponds to the north-dipping Upper Cretaceous to Eocene sedimentary series of the subpyrenean folds. These sediments are made of alternating limestones and marls. The sharp changes in thickness observed correspond to local pools and riffles carved in the strath by differential erosion due to lithologic contrasts. These pools and riffles can be observed on the topographic maps of the strath, to the south (Fig. 7B).

A depoaxis with thicknesses around 12-16 m occurs between Boussens and Carbonne along the boundary with terrace T2 (northwestern boundary of the terrace). Southeastward from this depoaxis, the thickness diminishes rapidly to 6 m and less. This area of low thickness locates along the boundary between T1 and the Garonne River. Comparing thickness map with the paleochannel

map (Fig. 2), we can quote the abatment in thickness is associated with the transition between braiding patterns and meandering belts. It suggests that more agradation occurred during braidplain deposition than meanders.

A sharp decrease of thickness can be observed downstream, to the northwest of Carbone. There, thickness varies from 17 m to 5 m over 5 km. Northward Muret thickness remains low (1 to 6 m) with weak variations. As observed southward, areas of low thickness are also located along the boundary between T1 and the Garonne River.

The comparison of the isopach map with the paleochannels map on Figure 2 shows the depoaxis described above is associated with the deposits of the Braided Area 2 (BA2) though low thicknesses areas are associated with meanders. To the north, between Carbonne and Muret, sediment thickness remains low. In this area, the lowest thicknesses (6 to 4m and less) are associated to Braided Area 4 (BA4) while slightly higher thicknesses (5 to 7m) corresponds to Meander Belt 1 (MB1 on Fig. 2). It would indicate that, in this part of the terrace, less fluvial aggradation occurred by the time of deposition of braided streams than in the south of the terrace, though aggradation of meanders of MB1 was as equivalent or slightly higher than braided streams aggradation. As observed southward, deposits located close to the eastern boundary of terrace T1 exhibit the lowest thicknesses and are associated with MB 2 deposits.

7 – Discussion

7.1 – Chronology and end of the würmian glaciation

Our results allow us to refine the conditions of the abandonment of the T1 terrace at the end of the Würmian glaciation. Recently, Stange et al., (2013) showed evidence for the role of the quaternary climatic fluctuations on the abandonment of the terraces of the Garonne. In their study, Stange et al., (2013) provide datings of the sediment of the Barbazan Lake, (see figure 8). The curve represents the age vs. depth in the core. The gradient of the curve represents the sedimentation rate.

Andrieu-Ponel et al. (1988) also studied the sediments of the Barbazan Lake in terms of sedimentology, palynology and radiometric datings. In terms of sedimentology, Andrieu-Ponel et al. (1988) showed the base of the column is made of glacial deposits (rythmites and lacustrine turbidites). In contrast, above 10m (i.e. following ~30 ka), sediments lack glacial influence and are only resulting from decantation processes. It shows that the Barbazan Lake was no more under the influence of the retreating glacier and that sedimentary input was directly controlled by the precipitation in the source catchment (Fig. 8).

Evolution of palynomorphs through time shows a drastic change in the vegetation surrounding the lake around 30 000 yrs Cal BP. Before, vegetation was mainly made of *Abies*, *Picea* and *Fagus* whereas following 30 ka, vegetation was dominated by *Artemisia,* showing vegetation becomes bushy as a response to a dryer climate until 16 900 yrs Cal BP (Van Campo, 1985; Jalut and Turu I Michels, 2006). This dryer climate is corroborated by the occurrence of loess deposits in the Garonne valley and its tributaries in the Toulouse area since 26366 +/- 1773yrs Cal BP (Revel and Bourgeat, 1981). During the Bölling/Allerød (16 900 – 14 075 yrs Cal BP), rapid changes in the vegetation are observed with the appearance of *Juniperus, Betula, Abies* (Jalut and TuruiMichels, 2006). This dynamic of colonization by warmer climate species stops during the older Dryas (12 895 -11 700 yrs Cal BP, Jalut and TuruiMichels, 2006). After the end of the younger Dryas (8320-8070 yrs Cal BP, for Carozza et al., 2014), vegetation changes to deciduous trees such as *Quercus, Ulmus, Salix* and *Corylus*(Jalut and Turu I Michels, 2006; work *in progress* cited in Carozza et al., 2014).

Correlation between channel belt datings, climatic and vegetation data show a strong relation between climate evolution and river morphodynamics. Indeed, though they are not dated, braided stream of BA1-4 can be contemporary to the pleniglacial stage and the beginning of the glacial retreat in the Pyrenees. The change in sedimentation in the Barbazan Lake (around 30 000 yrs Cal BP) associated with a drier climate and different vegetation seems to indicate a change in the hydrologic regime of the Garonne which can originate a change in fluvial patterns from braided to meandering (Fig. 8).

Dates on terrace T1 exhibited on Figure 9 reveals the abandonment of MB1 occurred around 14 000 yrs Cal BP. It corresponds to the period of the Bölling/Allerød. Hence we propose the abandonment of MB1 is related to hydraulic events related to the warm period of the Bölling, mainly an increase in precipitation as shown by the increase in sedimentation rate in the Barbazan Lake (Fig. 8). Available dates from the literature are younger for MB2 channels than for other channels (Fig. 9; Bourgeat et al., 1984). Moreover, these ages are maximum values as they do not come from silts above the channel deposits. These observations made us correlate the increase in sinuosity of the Garonne with the Younger Dryas event and more precisely with the warming and increase in precipitations in the Garonne catchment at the end of this period, as shown by the increase in sedimentation rates in the Barbazan Lake (Fig. 8, Stange et al., 2013). Consequently, surface exposure ages by Stange et al. (2013) would not show the final abandonment of T1 but only the abandonment of MB1, the final abandonment of T1 occuring later, following the abandonment of MB2 at the end of the Younger Dryas (Fig. 9). This chronology is

summarized on figure 10.

This analysis of the morphodynamic evolution of the Garonne river by the times of formation of T1 confirms the climatic control of the terraces abandonment previously proposed by Stange et al. (2013 Considering datings, it seems the Older to Younger Dryas terrace identified by Stange et al. (2013) upstream from our study area disappears downstream and makes an only terrace level together with the Würmian (MIS 2) terrace (T1 terrace in this study).

7.2 – Braiding /meandering transition

As shown in the previous paragraph the change in fluvial style between BA 1-4, MB1 and MB2 (mainly an increase in sinuosity) can be correlated with climatic events contemporary to the last pleniglacial and late glacial Würm as indicated by datings and correlations with sedimentary dynamics in glacial lakes (Stange et al., 2013; Andrieu-Ponel et al., 1988) and vegetation evolution shown by palynology (Andrieu-Ponel et al., 1993; Andrieu,-Ponel, 1991; Jalut et al., 2006). Nevertheless, we can wonder how these events controlled the morphology of the Garonne River. Such kind of data gives us indication of the climatic context but they cannot be interpreted in terms of river hydrologic dynamics.

The braiding/meandering transition generated, a huge literature since the 50's (see review by Métivier and Barrier 2012). Through years influence of several parameter was discarded. Bridge (1993) pointed out the lack of influence of discharge: "Discharge variability does not exert a major influence on the existence of the different channel patterns because they can all be formed in laboratory channels at constant discharge". More recent studies confirmed this statement (see review in Métivier and Barrier, 2012).

Channel slope was also invoked as a key parameter in the transition braided/meandering. Lane (1957) ; van den Berg, (1995) stated that threshold slope values controls this transition with meandering channel below the threshold value and braided channels above. Schumm and Kahn (1972) showed with analog modelling of channels that stable meanders could occur for higher slope values than braided streams, depending on sediments grain size and discharge. Other studies showed that channel slope is the result of the combination of other parameters and cannot be considered as an independent parameter (Carson, 1984 ; Lewin and Brewer, 2001; Métivier and Barrier, 2012).

Grain size can also play a role in the braided meandering transition (Schumm and Kahn, 1972 ; Métivier and Barrier, 2012). In the case of the Upper Pleistocene Garonne River, grain size is not likely to play a role in the braided/meandering transition because grain size of material observed in braided streams (Fig. 5) and in meanders (Fig. 6) is the same. It seems the gravel meanders only reworked material previously deposited by braided streams. This observation seems to be quite common in gravel meandering rivers and was yet proposed by Brierley and Hickin (1991).

In the last years, two parameters referred to play a role in this transition were object of attention: 1) cohesive material on channel banks increasing resistance to erosion (Smith, 1998; Rowntree and Dollar, 1999) and 2) role of vegetation and its role in fixing bedforms and pointbars (Tal and Paola, 2007; 2010; Brauderick et al., 2009; Ghibling and Davies, 2012).

The occurrence of cohesive materials in the terrace T1 infill is scarce. As shown on figure 5 and 6, channel deposits are made of pebbles and sands. The only silty or clayish sediments are observed at the top of the channel deposits. The silts observed above the channel deposits (Fig. 5 and 9) are widespread all over the terrace covering both the braided and meandering channels. outcrops exposed in quarry pits do not exhibit silt or clay within channels but only at the top of both channels and pointbars (Fig. 6). Moreover when present, silts and clay represent only rather thin beds (< 50cm). Anyway, at least part of these silts deposited after the abandonment of the terrace by low order tributaries superposed to the terrace. Another part is contemporary to the progressive abandonment and wandering of channels, silts and clays filling former channels during floods. Cohesive sediment such as silts or clays are classically not observed in braided channels, which suggests that silts and clays covering the braided channels are not contemporary to the channel activity but deposited after the braided channels abandonment. In the case of meanders, gravel meandering rivers were poorly considered (Bluck, 1971; Ori, 1979; Arche, 1983; Brierley and Hickin, 1991) but facies models for gravel meandering rivers (Miall, 1996) show silts and clays are scarce in such rivers and play no major role in increasing bank stability (Rowntree and Dollar, 1999).

The role of vegetation in the stabilization of meander at the onset of MB1 (Fig. 2) is more difficult to evidence. The change in vegetation at 30 000 yrs Cal BP (Andrieu-Ponel et al, 1988) is registered in the Barbazan Lake. It indicates a change in vegetation at regional scale correlated with a dry event known in whole Europe (Van Campo, 1985). Nevertheless this regional change in vegetation does not depict the characteristics of the riparian vegetation, which, even if the climate becomes dryer, remains in moist condition due to the water discharge in the stream. In their studies dedicated to the conditions stabilization of meanders, Tal and Paola (2007; 2010) and Brauderick et al. (2009) showed the role of vegetation in stabilizing meanders. Indirectly, they also show it is important to have fluctuations in

water discharge in streams. Indeed, with fluctuating discharge, the top of bedforms remains uncovered between discharge peaks allowing germination and the growth of vegetation. This vegetation helps then the bedform to resist erosion during the following flood. In studies presented by Tal and Paola (2007; 2010) and Braudrick et al. (2009), meanders could not be stabilized because, the discharge being constant, sand bars remained under water which did not allow germination and sufficient growth of plants. Considering the time needed for germination and growth of vegetation on bedforms, it would indicate the fluctuations of discharge varies from an annual to pluri-annual cycles, which is the typical time scale of an hydrological regime of a river. In the modern Garonne River, sand or gravel bars need at least to years for germination of seedling of a pioneer specie such as *Populus nigra* and even more time in order to stabilize the bedform (Corenblit et al., 2013).

Another key point in the role of the vegetation for stabilizing meanders is the relationship between time of germination and the high water stage in the river. Indeed, germination and growth start generally in spring. In rivers exhibiting a glacial hydrologic regime in Western Europe, high water stage occurs in July and August with discharge starting to increase in April (case of swiss alpine rivers). This would indicate that bars in channels are covered by water by the time of germination. On the contrary, in pluvio-nival hydrologic regime (such as the modern Garonne River), high water stage occurs in February and March and low water stage occurs in summer. This indicates that bars remain uncovered within the time of germination of the vegetation. Hence, we can think that, at the end of the last glaciation, the hydrologic regime of the Garonne River progressively changed from a glacial to a pluvio-nival hydrologic regime and, as a consequence, the shift of the high water stage from summer to winter allowed the vegetation to settle the gravel bars and stabilized meanders.

Thus, in the case of the transition from BA 1-4 to MB1, the stabilization of meanders may result from a change in the hydrological regime allowing sand bars to remain uncovered by flow during dry periods and to be colonized by pioneer vegetation. In the case of the transition between MB1 and MB2, the change in hydrologic and vegetation characteristics allowing new species growing faster to develop in the riparian vegetation, increasing meanders stability and sinuosity.

As whole, morphological adjustments of the Garonne River could be better a response of the river channels to changes in hydrological regimes passing from a glacial hydrological regime to a pluvio-nival regime shifting the high water stage to the end of winter and spring and putting it in phase with the cycle of germination and growth of the vegetation.

8 – Conclusions

The mapping of the paleochannels preserved in the infill of the lowest terrace of the Garonne by mean of remote sensing based on aerial photographs and field data allows us to reconstruct the evolution of fluvial styles in time and space at the end of the Würmian glaciation. Fluvial aggradation on top of the strath started after 35,000 BP associated with a braided morphology (BA 1 to 4 on Fig. 2 and 10), contemporary to the retreat of Pyrenean glaciers (Andrieu et al., 1991, Delmas et al. 2011; Stange et al. 2013) and the increase of water discharge at some periods of the hydrologic cycle allowing more bedload transport. The Garonne changed its morphology to a low sinuosity gravel bed meandering stream (MB1 on Fig. 2 and 10) contemporary to the intensification of glacial melting identified in the Barbazan Lake around 25 600 +/- 800 yrs^{14}C (30 456 +/- 831 yrs Cal BP, Andrieu-Ponel et al., 1988). This change in morphology would be the consequence of the change in hydrologic regime of the Garonne River passing from a glacial to pluvio-nival hydrologic regime associated to the development of bushy vegetation on pointbars at low water stage provoking meander stabilization of meanders. MB1 was abandoned after 15,000 BP. The Garonne evolved then toward a high sinuosity gravel meandering river contemporaneous of MB2 which was active till the end of the Younger Dryas. This drastic change in morphology could be the consequence of changes in hydrologic regime at the end of the Younger Dryas associated to the end of the "dry climate" allowing the development of denser riparian vegetation.

The abandonment of MB2 and final abandonment of Terrace T1 is so younger than the Younger Dryas.

Our study shows this terrace is composite, recording below an only flat surface a complex history made of partial abandonments and reworking contemporaneous of hydrologic regime changes and interplay with vegetation changes related with the end of the last glaciation.

Acknowledgments

This study benefited of the free access to the data of the Bureau des Recherches Géologiques et Minières (BRGM, French Geological Survey) and the Institut Géographique National (IGN, French Geographical Survey) through the "Infrastructure for Spatial Information in Europe"(INSPIRE) directive of the European Union. The IGN is also thanked for providing additional topographic and photographic data through a "non profit teaching and research" agreement between French universities and state administrations. The authors thank S. Bonnet, S. Carretier and G. Hérail for fruitful discussion about this study. This article is a

contribution to the project “PYRAMID” funded by the ANR (French agency for research funding).

References

Andrieu-Ponel, V., Hubschman, J., Jalut, G., Hérail., G., (1988). Chronologie de la déglaciation des Pyrénées françaises. Dynamique de sédimentation et du contenu pollinique des paléolacs : application à l'interprétation du retrait glaciaire. *Bulletin de l'Association Française pour l'Etude du Quaternaire*, 25 : 55-67. doi :10.3406/quate.1988.1866

Andrieu-Ponel, V. (1991).Dynamique du paléoenvironnement de la vallée montagnarde de la Garonne (Pyrénées centrales, France) de la fin des temps glaciaires à l'actuel. *PhD thesis*, Université Toulouse 2, 330pp.

Andrieu, V., Eicher, U., Reille, M., (1993).Le fin du dernier pléniglaciaire dans les Pyrénées (France) : données polliniques, isotopiques et radiométriques. *Comptes-Rendus de l'Académie des Sciences Paris série II*, 316 :245-50.

Antoine, P-O., Duranthon, F., Tassy, P., (1997). L'apportdes grands mammifères (Rhinocérotidés, Suoïdés, Proboscidiens) à la connaissance des gisements du Miocène d'Aquitaine (France). In Aguilar, J-P., Legendre, S., Michaux, J. (eds) BiochroM'97, *Mémoires de Travaux de l'Ecole Pratique des Hautes Etudes, Institut de Monptellier,* 21 : 581-590.

Arche, A. (1983) Coarse-grained meander lobe deposits in th Jarama River, Madrid, Spain. In : Collinson J.D. & Lewin, J. (eds) Modern and ancient fluvial systems. International Association of Sedimentologists Special Publication 6 :313-321.

Biteau, J-J., Le Marrec, A., Le Vot, M., Masset, J-M. (2006). The Aquitaine Basin. *Petroleum Geosciences*, 12 : 247-273, doi: 10.1144/1354-079305-674.

Bridge, J.S., (1993) The interaction between channel geometry, water flow, sediment transport and deposition in braided rivers. *Geological Society, London, Special Publications*, 75: 13-71, doi: 10.114/GSL.SP.1993.075.01.02

Bluck, B.J. (1971) Sedimentation in the meandering River Endrick. *Scottish Journal of Geology*, 7 :93-138.

Bourgeat, F., Andrieu-Ponel, M., Revel, J-C., (1984). Les Terrasses Alluviales Dans Les Petites-Pyrénées et L'avant-pays Molassique. *Bulletin de l'Association Française pour l'Etude du Quaternaire*, 21 : 60-66.

Bridgland, D.R., Westaway, R., (2008a). Climatically Controlled River Terrace Staircases : a worldwide Quaternary phenomenon. *Geomorphology*, 98 : 285-315. doi : 10.1016/j.geomorph.2006.12.032

Bridgland, D.R., Westaway, R., (2008b). Preservation Patterns of LateCenozoic Fluvial Deposits and Their Implications. *Quaternary International*, 189 :5-38.Doi : 10.1016/j.quaint.2007.08.036.

Brauderick, C.A., Dietrich, W.E., Leverich, G.T., Sklar, L.S. (2009). Experimentalevidence for the conditions necessary to sustainmeandering in coarse-beddedrivers. *Proceedings of the National Academy of Sciences*. 106 : 16936-16941. Doi :10.1073/pnas.090941710

Brierley, G.J., Hickin E.J., (1991). Channel Planform as a Non-controlling Factor in Fluvial Sedimentology: The Case of the Squamish RiverFloodplain , British Columbia. *SedimentaryGeology*, 75 : 67-83.

Bruxelles, L., Pons, F., Magnin, F., Bertrand, A. (2010). Ages et modalistées de la mise en place de la couverture limoneuse de la basse plaine de la Garonne d'après l'exemple du site de Fontréal (Castenau-d'estrétefonds, Haute Garonne. *Quaternaire*, 21 : 475-484.

Bruxelles, L., Jarry, M. (2011) Climatic conditions ; settlement patterns and cultures in the paleolithic : The example of the Garonne Valley (Southwest France). *Journal of Human Evolution,* 61 : 538-548. doi:10.1016/j.jhevol.2011.05.009

Cahuzac, B., Jannin, M-C., Steurbaut, E., (1995). Biostratigraphie de l'Oligo-Miocène du Bassin d'Aquitaine fondée sur le nannofossiles calcaires. Implications Paléogéographiques. Géologie de la France, 1995 : 57-82.

Carozza, J-M., Valette, P., Carozza, L., Llubes, M. Ferdinand, L., Edou Obame, S., Sévègnes, L. (2013). L'architecture morpho-sédimentaire de la basse plaine de la Garonne moyenne en aval de Toulouse : premiers résultats. *Quaternaire*, 24 : 397-406.

Carozza, J-M., Carozza, L., Valette, P., Llubes, M., Py, V., Galop, P., Danu, M., Ferdinand, L., David, M., Sévègnes, L., Bruxelles, L., Jarry, M., Duranthon, F. (2014). The subfossil tree depositsfrom the Garonne Valley and their implications on Holocene alluvial plain dynamics. *Comptes Rendus Géosciences*, doi : 10.1016/j.crte.2014.01.001

Carson, M.A., (1984). The meandering-braiding river threshold : a reappraisal. *Journal of Hydrology*, 73 :315-334.

Corenblit, D., Steiger, J., Gonzalez, E., Gurnell, A.M., Charrier, G., Darrozes, J., Dousseau, J., Julien, F., Lambs, L., Larrue, S., Roussel, E., Vautier, F., Voldoire, O., (2014). The biogeomorphological life cycle of poplarsduring the fluvial biogeomorphological succession : a special focus on *Populusnigra* L. *Earth Surface Processes and Landforms*, doi : 10.1002/esp.3515

Courbouleix, S., Barnolas, A. (2008). Carte géologique du Quaternaire des Pyrénées à 1/ 400 000. BRGM, IGME, eds.

Crouzel, F., (1957). Le Miocène continental du Bassin d'Aquitaine. *Bulletin des Services de la Carte Géologique de la France*, 54 : 1-265.

Cuevas Martínez, J.L., Cabrera Pérez, L., Marcuello, A., Arbués, P., Marzo, M., Bellmunt, F., (2009). Exhumed channel sandstone networks within fluvial fan deposits from the Oligo-Miocene Caspe Formation, South-east Ebro Basin (North-east Spain). *Sedimentology*, 57:1365-3091, doi: 10.1111/j.1365-3091.2009.01096.x

Danzeglocke, U., Jöris, O., Weninger, B., 2013. CalPal-2007^{online}. http://www.calpal-online.de/, accessed 2013-09-14.

Delmas, M., Calvet, M., Gunnell, Y. Braucher, R., Bourlès, D., (2011). Palaeogeography and ^{10}Be exposure–age chronology of Middle and Late Pleistocence glacier

systems in the northern Pyrenees : Implication for reconstructing regionalpalaeoclimates. *Palaeogeography, Palaeoclimatology, Palaeoecology* 305:109–122. doi:10.1016/j.palaeo.2011.02.025

Dubreuilh, J., Capdeville, J-P., Farjanel, G., Karnay, G., Platel, J-P., Simon-Coinçon, R., (1995). Dynamique d'un comblement néogène et quaternaire : l'exemple du bassin d'Aquitaine. *Géologie de la France*, 4:3-26.

Ferguson, R.I., (1993). Understanding braiding processes in gravel-bed rivers : progress and un solved problems. *Geological Society, London, Special Publications*, 75: 73-87, doi: 10.114/GSL.SP.1993.075.01.03

Ghibling, M.R., Davies, N.S. (2012) Palaeozoic landscapes shaped by plant evolution. *Nature Geosciences*, 5:99-105. doi: 10.1038/NGEO1376

Hubschman, J. (1975a). Les terrasses récentes de la Garonne et leur évolution. *Bulletin de l'Association Française pour l'Etude du Quaternaire*. 12 : 137-147, doi : 10.3406/quate.1975.1261

Hubschman, J. (1975b). L'évolution des nappes alluviales antérissiennes de la Garonne, dans l'avant-pays molassique. *Bulletin de l'Association Française pour l'Etude du Quaternaire*. 12 :149-169,doi : 10.3406/quate.1975.1262

Icole, M., 1974. Géochimie des altérations dans les nappes d'alluvions du piedmont occidental nord-pyrénéen. Eléments de paléopédologie quaternaire. *Sciences Géologiques*, mémoire #40. Université Louis Pasteur, Strasbourg, France, 200 pp.

Jalut, G., Turu i Michels, V. (2006). La végétation des Pyrénées françaises lors du dernier épisode glaciaire et durant la transition Glaciaire interglaciaire (Last Termination). In Fullola, J.M., Valdeyron, M., and Langlais, M. (eds). Els Pireneus i los areescircumdants durant el tardiglacial. Mutacions i filiacionstecnoculturals, evoluciopaleoambiental. Homenatge Georges Laplace. XIV Col.loqui internacional d'arquelogia de Puigcerda, 10-11 November 2006. Institut d'Estudis Ceretans.

Lane, E.W. (1957). A study of the Shape of Channels Formed by Natural Streams flowing in Erodible Material. United States Army Corps of Engineers, Missouri River Division, Omaha, NB. Missouri River Division Sediment Series 9.

Lewin, K., Brewer, P.A., (2001). Predicting channel patterns. *Geomorphology*. 40 :329-339.

Lisiecki, L.E., Raymo, M.E., 2005. A Pliocene-Pleistocene stack of 57 globally distributed benthic d18O records. *Paleoceanography* 20, PA1003. doi:10.1029/ 2004PA001071.

Martinson, D.G., Pisias, N.G., Hays, J.D., Imbrie, J., Moore, T.C., Shackleton, N.J., 1987. Age dating and orbital theory of the Ice Ages: Development of a high-resolution 0 to 300,000-year chronostratigraphy. *Quaternary Research,* 27: 1–29.

Métivier, F., Barrier, L., (2012). Alluvial landscape evolution: what do we know about metamorphosis of Gravel-bed meandering and braided streams. In: Church, M., Biron, P.M., Roy, A.G., Gravel-bed rivers : Processes, Tools, Environments. Chapter 34: 474-501

Miall, A. (1996). The geology of fluvial deposits : sedimentary facies, basin analysis and petroleumgeology. Springer Verlag, Berlin & Heidelberg, 598pp.

Ori, G.G., (1979). Barre di meandre nelle alluvioni ghiaiose del fiume Reno (Bologna). Bolletino della Societa Geologica Italiana. 98 :35-54.

Penck, A.F.K, Brückner, E., (1909). *Die Alpen im Eiszeitalter*, Chr. Herm. Tauchnitz., Leipzig, 1199pp.

Reille, M., Andrieu, V., (1995). The latePleistocene and Holocene in the Lourdes Basin, Western Pyrénées, France : a new pollen analytical and chronological data. *VegetationHistory and Archebotany*, 4 :1-21

Revel, J-C., Bourgeat, F., (1981). Sols fossiles du terrefort toulousain, leur signification paléoclimatique. *Bulletin de l'Association Française pour l'Etude du Quaternaire*. 7-8 :149-159

Rius, D., Vannière, B., Galop , D., (2012). Holocene history of fire, vegetation and land use from the central Pyrenees (France). Quaternary Research, 77 : 54-64, doi : 10.1016/j.yqres.2011.09.009

Rowntree, K.M., Dollar, E.S.J., (1996). Controls on channel from and channel change in the Bell River, Eastern Cape, South Africa. *South African Geographical Journal*, 78 :20-28.

Schumm, S.A., Kahn, H.R., (1972). Experimental study of channel patterns. *Geological Society of America Bulletin*. 83: 1755-1970.

Stange, K.M., van Balen, R.T., Kasse, C., Vandenberghe J., Carcaillet, J. (2013) Linking morphology across glacio fluvial interface : A ^{10}Be supported chronology of glacier advances and terrace formation in the Garonne River, northern Pyrenees, France. *Geomorphology*, doi : 10.1016/j.geomorph.2013.10.028.

Tal, M., Paola, C., (2007). Dynamic single-thread channels maintained by the interaction of flow and vegetation. *Geology*, 35 :347-350, doi : 10.1130/G23260A.1

Tal, M., Paola, C. (2010). Effects of vegetation on channel morphodynamics : results and insights from laboratory experiments. *Earth Surface Processes and Landforms*. 35 :104-1028, doi : 10.1002/esp.1908

Thomas, R.G., Smith, D.G., Wood, J.M., Visser, J., Calverley-Range, A., Koster, E.H., (1987). Inclined Heterolithic Stratification—Terminology, Description, Interpretation and Significance. *Sedimentary Geology*, 53 : 123-179, doi :10.1016/S0037-0738(87)80006-4.

Van Campo, M., (1985). Relation entre la végétation de l'Europe et les températures de surface océaniques après le dernier maximum glaciaire. *Pollen et Spores*, 26 :497-518

van den Berg, J.H., (1995). Prediction of alluvial channel pattern of perennial rivers. *Geomorphology*, 12 :259-279

Vandenberghe, J., Maddy, D., (2000). The Significance of Fluvial Archives in Geomorphology. *Geomorphology*, 33 : 127-130, doi : 10.1016/S0169-555X(99)00119-1

Vandenberghe, J., Maddy, D., (2001). The Response of River Systems to Climate Change. *Quaternary International*, 79 : 1-3, doi :10.1016/S1040-6182(00)00118-X

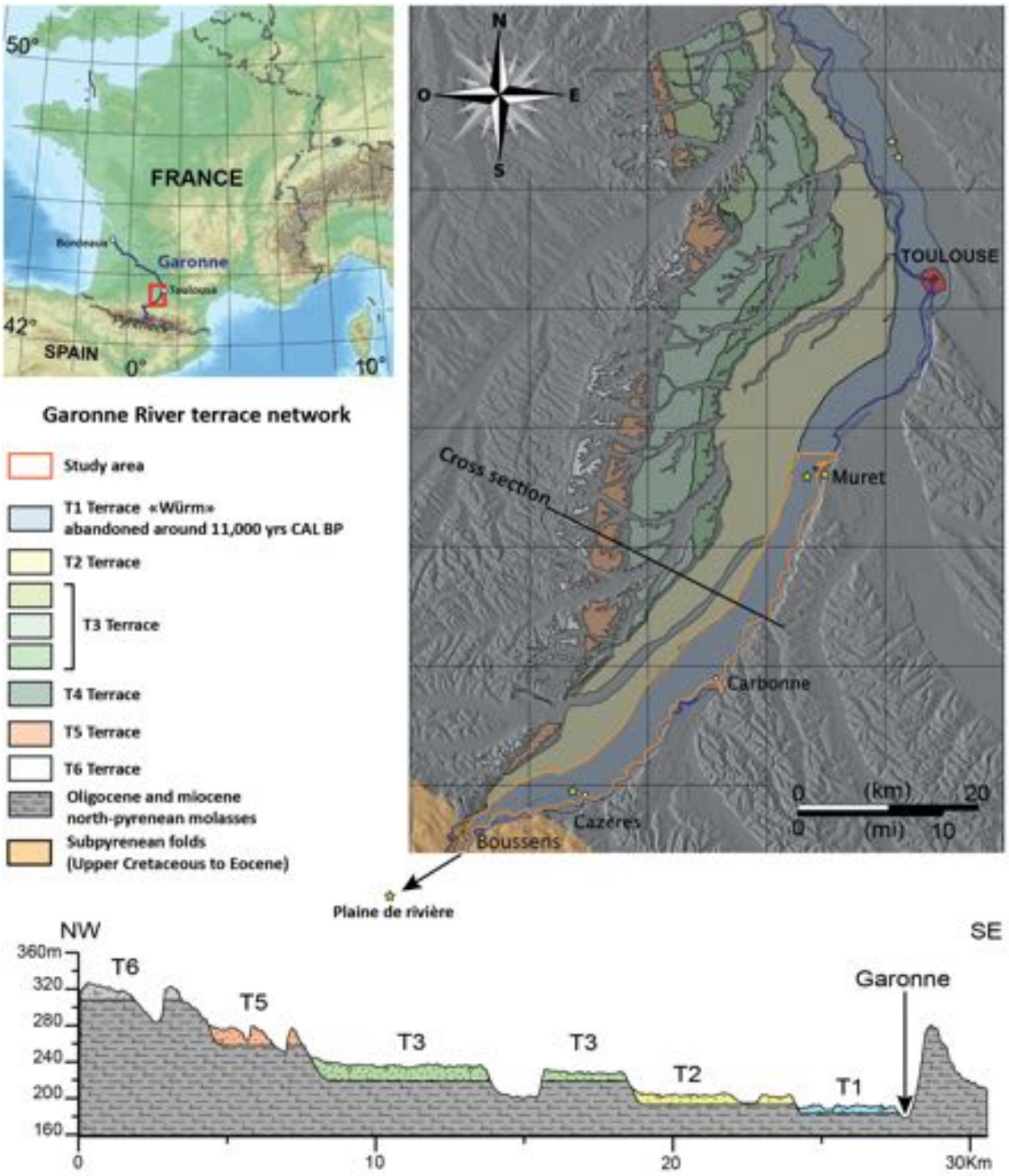

Figure 1: Geological map of the north-pyrenean foothill along the Garonne,location of the study area and geological cross section (modified from Hubschmann, 1975a, b; Courbouleix and Barnolas, 2008). Yellow stars: datings (north: Bruxelles et Jarry 2011, south of Muret: Bourgeat et al., 1984, Cazères and out of the map: Stange et al., 2013). Yellow stars: datings sites exhibited on figure 8.

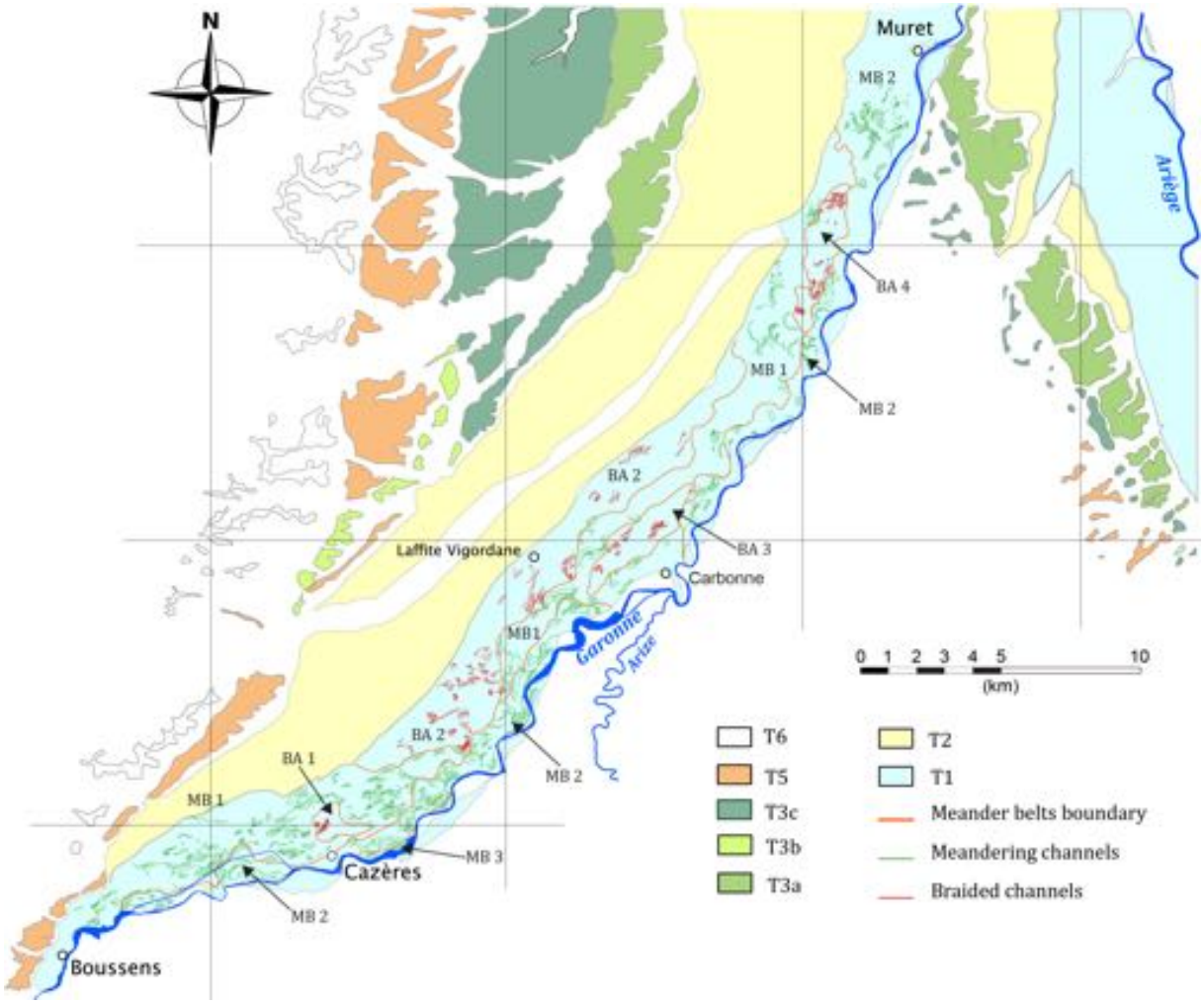

Figure 2: Map of the fluvial planforms of the Garonne river preserved below the lowest terrace (T1). In yellow: boundary of the lowest Terrace (T1), in red: braid channels, in green: meandering channels, in orange: boundaries of the main fluvial belts, in blue: channel preserved below the second terrace (T2), in light blue: modern Garonne river boundary. BA 1 to 4: Braided areas. MB 1 to 3: Meander Belts.

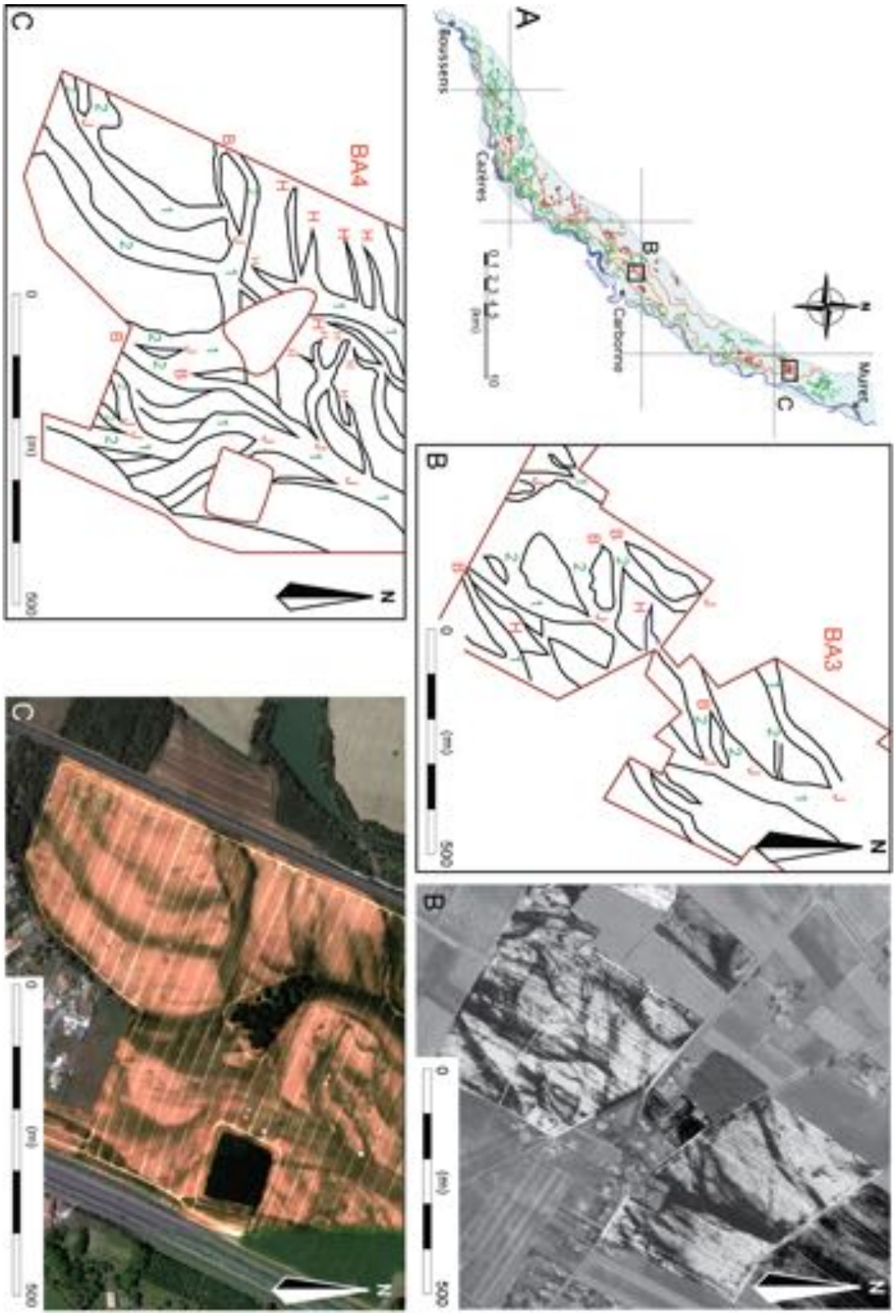

Figure 3: Braided pattern of the Garonne lowest terrace highlighted by remote sensing based on aerial photographs. A: Location of B and C. B: Braiding pattern of BA3. C: Braided channel in BA4; note that the difference in shape of the channels: they are more sinuous than B. Topological classifications of channel nodes (Ferguson, 1993): J: junction; B: bifurcation, H: channel head. Channels orders: 1 and 2 (Bridge, 1993).

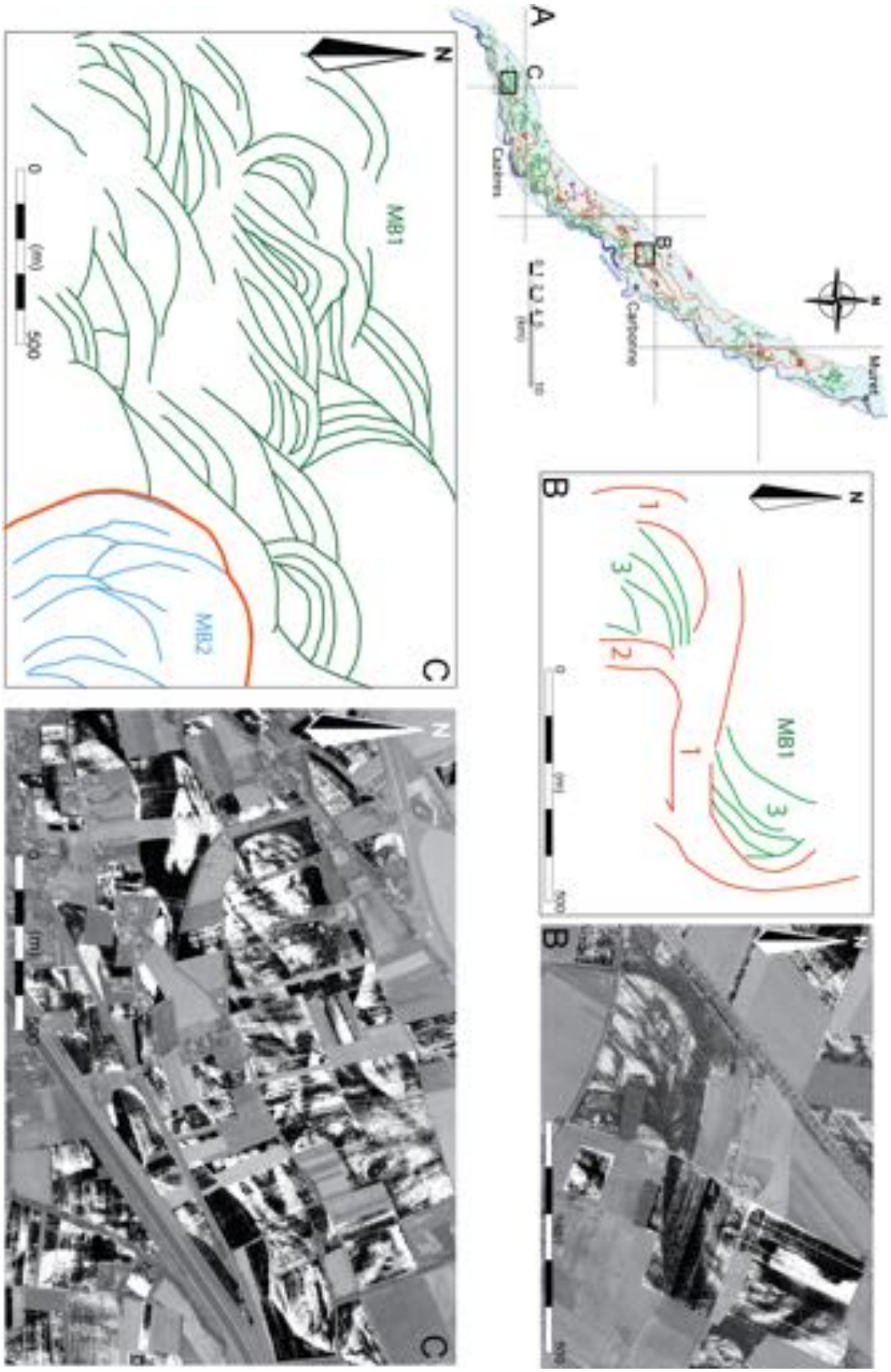

Figure 4: Meandering planforms of the Garonne lowest terrace evidenced by remote sensing based on aerial photographs. A: Location of B and C. B: Meander of MB1. C: Meander loops of MB1 between Cazères and Boussens.

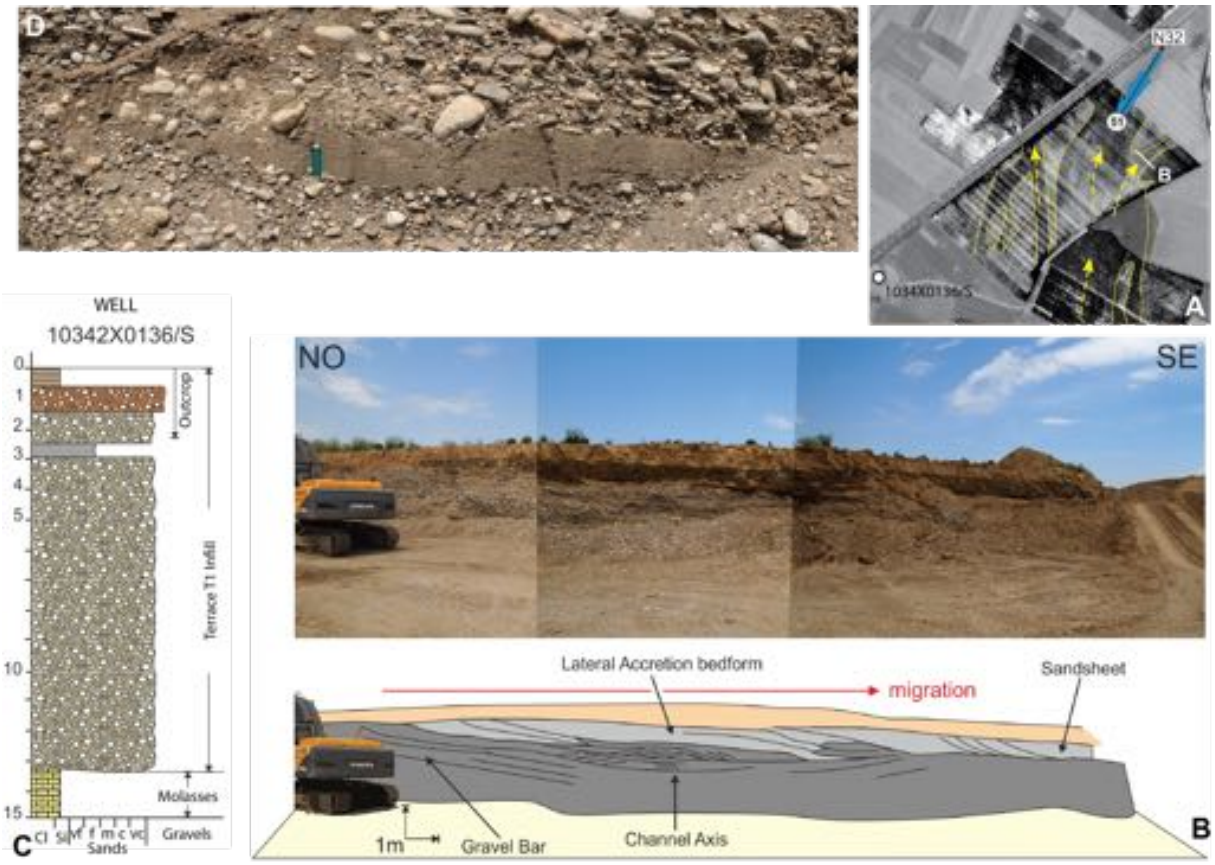

Figure 5: Outcrops of the braided channels of the Garonne lowest terrace. A: location of the outcrops in the pit-quarry and paleocurrents. B: Well log cored previous to the exploitation of the quarry (location on A). C: Outcrop showing the transition between the two main channels identified on aerial photographs. Channels. D: Structure of the southeastern channel. E: Gravel bar preserved in the northwestern channel. Paleocurrent rose diagram on A was measured on this outcrop. F: Detail of a sandy lens.

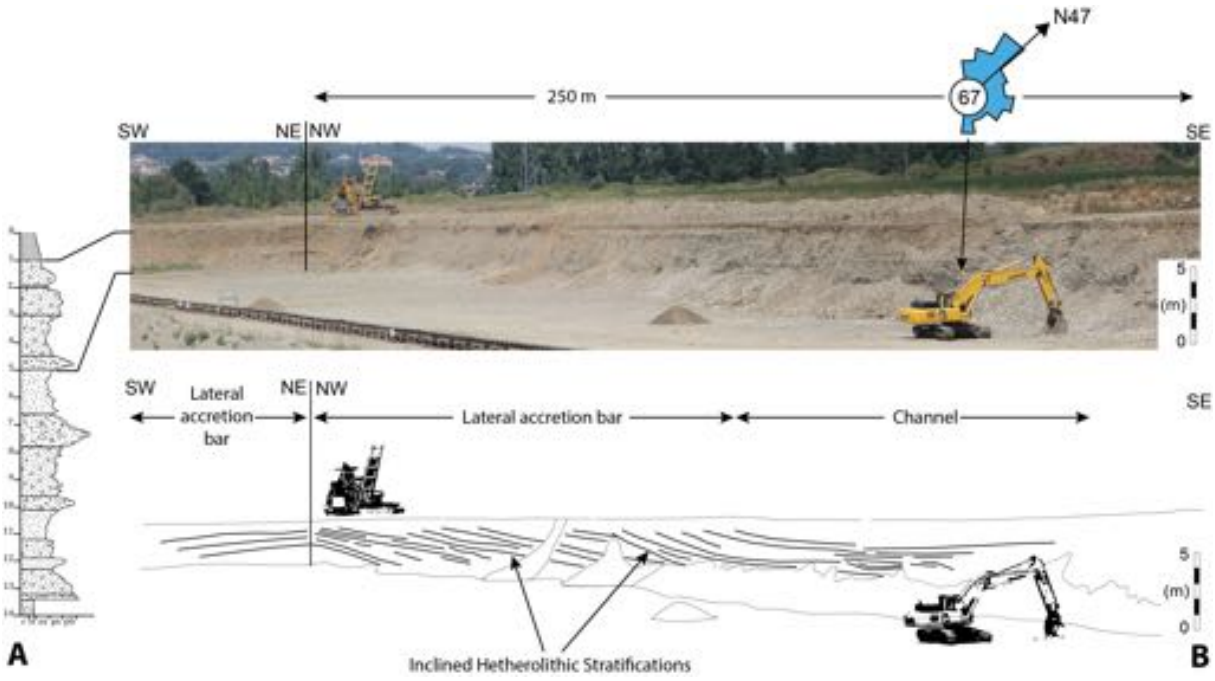

Figure 6: Outcrop of the gravel meandering channels of the Garonne lowest terrace in Cazères. Channels belong to MB1 (Fig. 2). Remark the increasing depth of channel and the steep slope of IHS compared to braided channel exhibited on Figure 5.

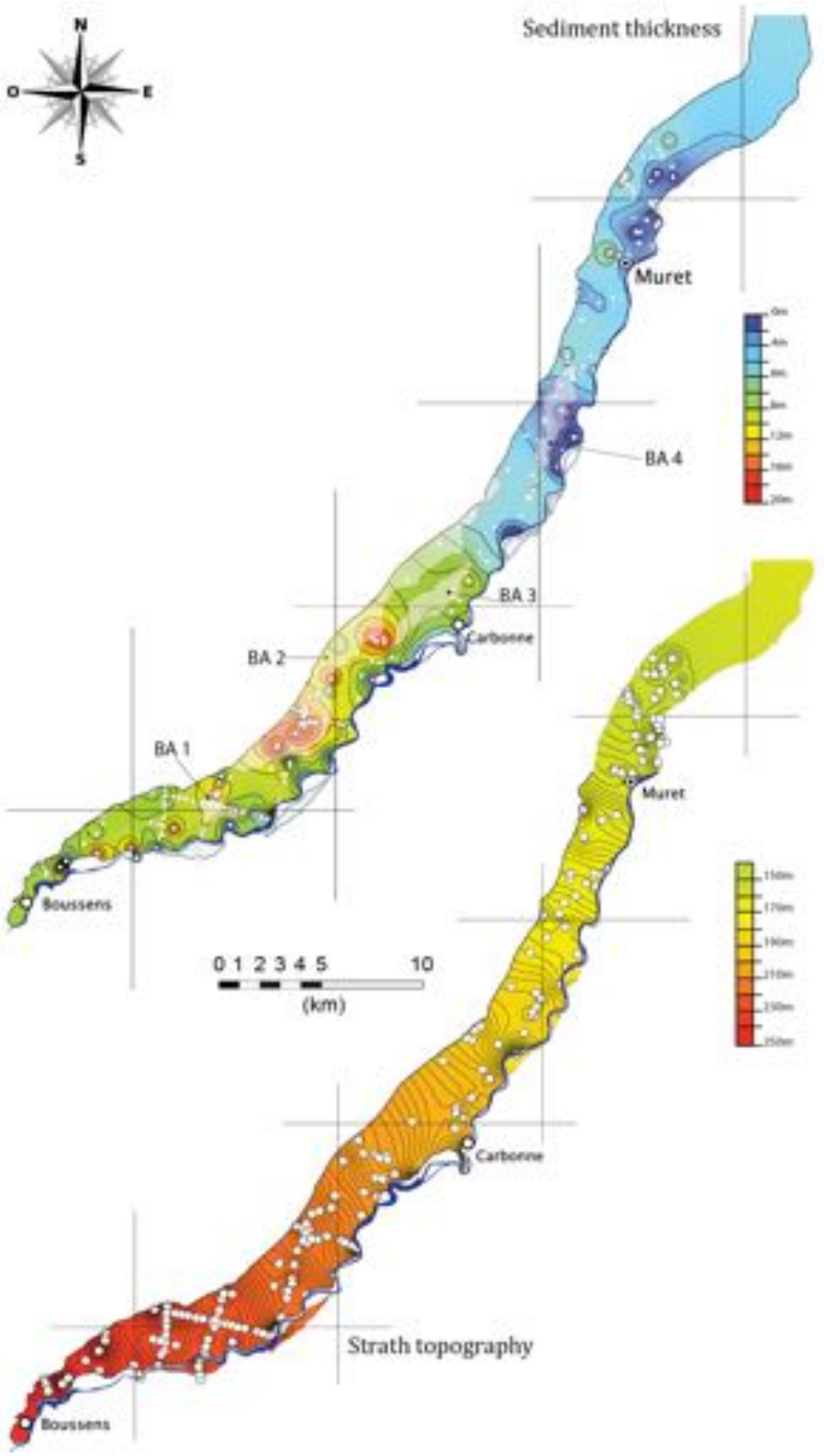

Figure 7: Strath topography and Isopach map of the sediments preserved below the lowest terrace of the Garonne River. White dots: boreholes, curves spacing: 2 m.

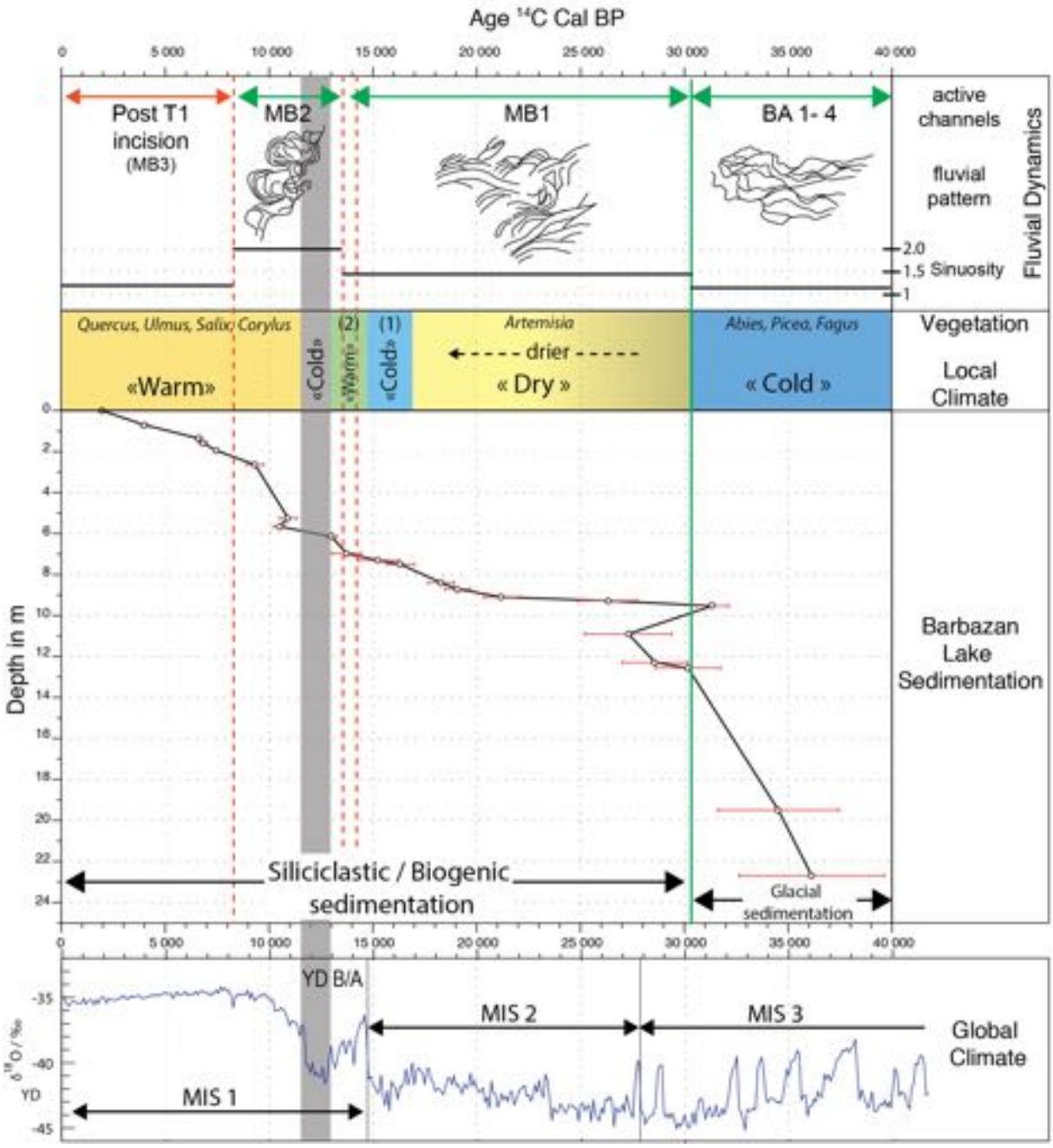

Figure 8 : Correlation between sedimentation rates in the Barbazan glacial lake (modified from Stange et al., 2013). $\delta^{18}O$ curve from Lisiecki and Raymo (2005), Martinson et al., (1987). Sedimentation data after Andrieu-Ponel (1991).^{14}C ages calibrated with CalPal2007^{online} (Danzeglocke et la., 2013). Vegetation and climate from Andrieu-Ponel et al. (1988), Reille and Andrieu, (1995) Jalut and Turu i Michels (2006), Rius et al., (2012), Carozza et al., (2014). (1) Vegetation between 16 900-14 700 yrs Cal BP: *Artemisia, Juniperus*. (Jalut et Turu i Michels, 2006), (2) Vegetation between 14 700 – 12 895 yrs Cal BP: *Abies, Betula, Quercus* (Jalut et Turu i Michels, 2006).

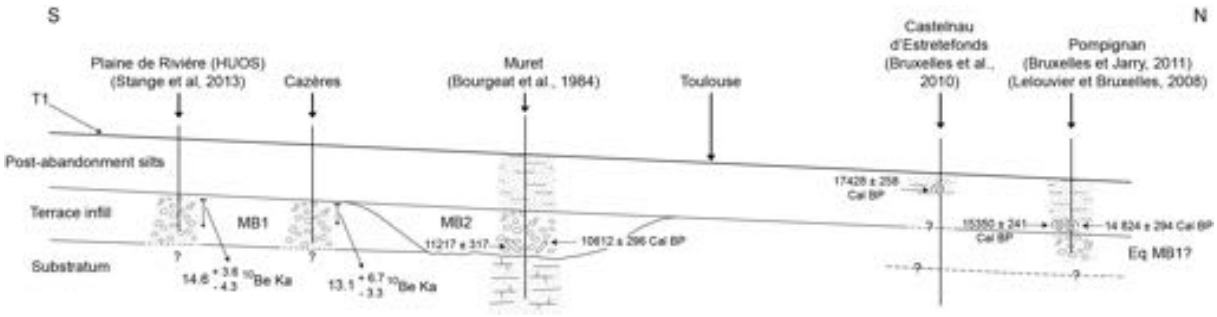

Figure 9 : Downstream correlations of datings of the terrace T1 of the Garonne River.^{10}Be exposure ages after Stange et al., (2013). Radiocarbon datings from Bourgeat et al., (1984), Bruxelles et al., (2010), Bruxelles and Jarry, (2011), Lelouvier and Bruxelles(2008). ^{14}C ages calibrated with CalPal2007^{online} (Danzeglocke et al., 20013). Location of dated sites : yellow stars on Figure 1. No scale.

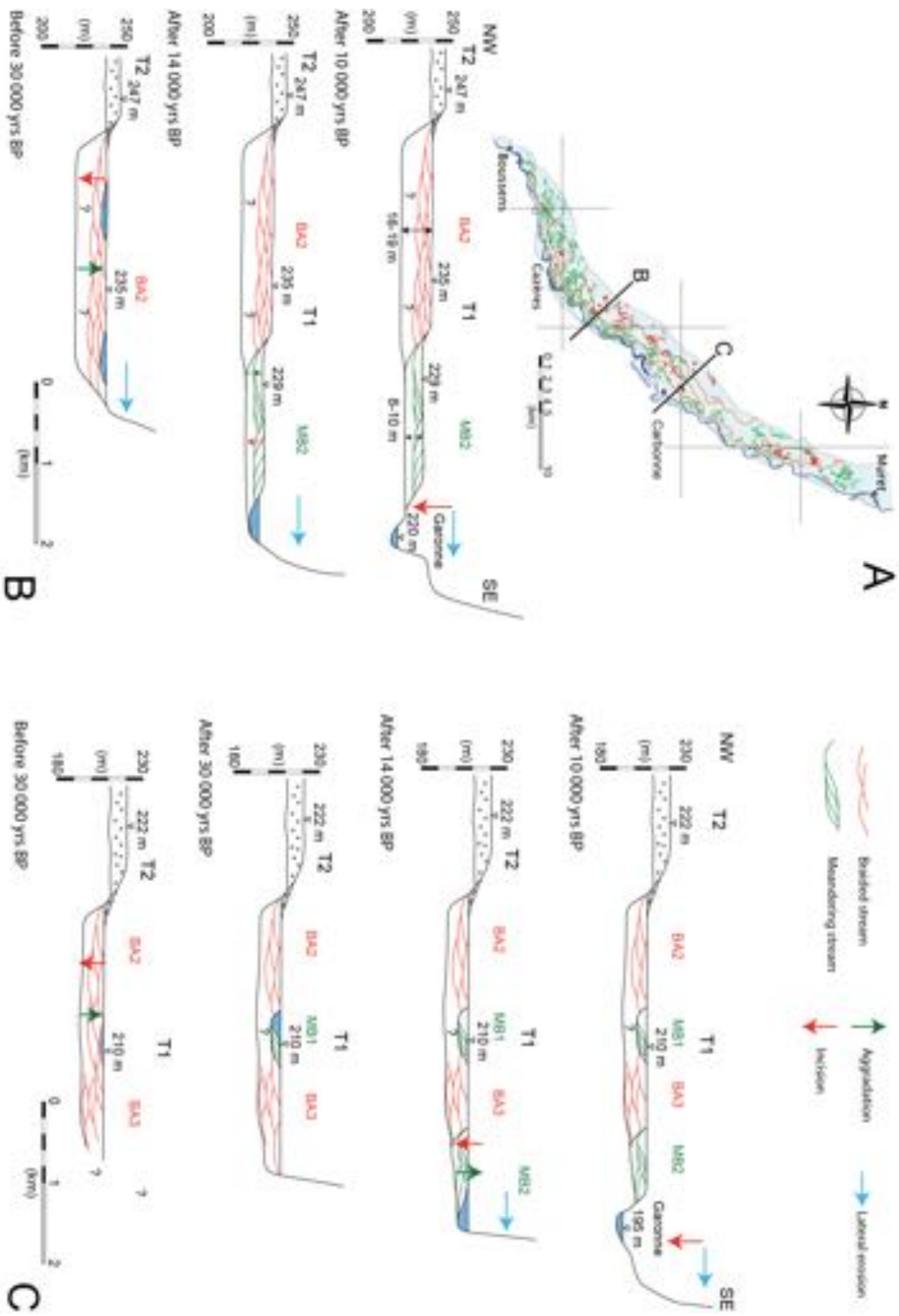

Figure 10 : Upper Pleistocene and Holocene evolution of the last terrace of the Garonne River along two transverse cross sections. Channel belts refer to figure 2. Sediment thicknesses represented correspond to Figure 7. Observe the weak incision between the base of the terrace infill and the modern Garonne River (bottom not constrained)

Annexe D

Bernal, C., Christophoul, F., Darrozes, J., Soula, J-C., Baby, P., Burgos, J. (2011)
International Journal of Earth Sciences (Geologische Rundschau)

Cet article, issu des travaux de thèse de Carolina Bernal montre comment les avulsions successives d'un tributaire amazonien ont généré un des plus grands mégafan du bassin de l'Amazone. Cette étude établit la chronologie la fréquence des avulsions à l'origine du mégafan et met en évidence les forçages contrôlant ces avulsions.

Résumé :

La cartographie géomorphologique, au moyen d'images satellites du Mégafan du Rio Pastaza (Equateur-Nord Pérou) met en évidence la présence de 108 sites d'avulsions. La localisation de ces sites, les datations disponibles dans la littérature ainsi que des cartes historiques nous permettent de proposer une histoire de la migration et des avulsions du Rio Pastaza depuis le Dernier Maximum Glaciaire (LGM).

Les premières avulsions se sont produites, après le LGM, au voisinage du front subandin alors que le Rio Pastaza s'écoulait globalement nord-sud entre les actuels Rio Morona et Pastaza. Ces avulsions ont mené à un réseau hydrographique éventail. Ce réseau s'est mis en place en réponse au basculement du forelimb d'un pli sur chevauchement lié à la mise en place du front subandin. Ce basculement a provoqué la migration vers l'est de l'apex du cône. Cette migration a pris fin par le Grand Déversement du Rio Pastaza (GDP) vers le sud-est. Suite au GDP, le Rio Pastaza occupe la région des actuels rio Tigre et Corrientes. Ces avulsions se sont produites entre 9 200 et 8 500 ans Cal BP. Par la suite, le Rio Pastaza adopte son cours actuel. Cette dernière avulsion est antérieure à 1 691 ap. J.C..

Avant 9 200 ans Cal BP, la fréquence des avulsions (sûrement surestimée) est de 100 à 200 ans. Suite au GDP, la fréquence (sous-estimée) des avulsions est de 300 à 400 ans. La tectonique active sur le Front Subandin a contrôlé le déclenchement des avulsions avant le GDP. Le facteur contrôlant les avulsions après le GDP est moins clair. Cependant, les caractéristiques de la distribution des débits (présence de pics de débits tranchant fortement avec le débit moyen), mentionné pour expliquer les avulsions dans les mégafans ne semble pas applicable au cas du Rio Pastaza.

Int J Earth Sci (Geol Rundsch)
DOI 10.1007/s00531-012-0752-9

ORIGINAL PAPER

Gradual diversions of the Rio Pastaza in the Ecuadorian piedmont of the Andes from 1906 to 2008: role of tectonics, alluvial fan aggradation, and ENSO events

Carolina Bernal · Frédéric Christophoul · Jean-Claude Soula · José Darrozes · Luc Bourrel · Alain Laraque · José Burgos · Séverine Bès de Berc · Patrice Baby

Received: 8 April 2011 / Accepted: 12 January 2012

Abstract The successive courses of the Rio Pastaza in the upper Amazonian Puyo plateau (Ecuador) during the past century have been followed using historical maps, aerial photographs, satellite imagery, topographic and river long profiles, and field studies. The abrupt change in direction of the Rio Pastaza from transverse to longitudinal was a result of two avulsions occurred between 1906 and 1976 at the braided-meandering transition of the former alluvial plain. These avulsions are related to aggradation at the toe of a braided piedmont fan prograding on to a hinterland-dipping topographic slope formed by ongoing tectonic backtilting. The main avulsion proceeded by annexation of a south-dipping depression created in front of the cordillera by backtilting of the plateau. A partial and gradual avulsion having occurred upstream of the former site between 1976 and 2008 is marked by the progressive predominance of a newly formed inner branch. Tectonic backtilting enhanced aggradation upstream of the initial site while it offered the newly avulsed channel a still more favorable way along the cordillera by creating a westward lateral slope. The correlation between ENSO events and the occurrence of the 1976–2008 avulsions strongly suggests that the triggers of the avulsions were the floods caused by the high water and sediment discharges associated with ENSO (La Niña) events contrasting with the regular monthly discharge and the lack of actual 'normal' floods during the inter-ENSO periods.

Keywords Avulsion · Tectonics · Sedimentation · Fluvial morphology · Andes · Ecuador

C. Bernal · F. Christophoul (✉) · J.-C. Soula · J. Darrozes · L. Bourrel · A. Laraque · P. Baby
UMR 5563 GET, Université de Toulouse-CNRS-IRD-OMP-CNES, 14 Avenue Edouard Belin, 31400 Toulouse, France
e-mail: frederic.christophoul@get.obs-mip.fr

C. Bernal
e-mail: chavelacarola@yahoo.com.mx

J.-C. Soula
e-mail: soula@get.obs-mip.fr

J. Darrozes
e-mail: darrozes@get.obs-mip.fr

L. Bourrel
e-mail: bourrel@get.obs-mip.fr

A. Laraque
e-mail: alain.laraque@ird.fr

P. Baby
e-mail: patrice.baby@ird.fr

J. Burgos
Petroamazonas, Av. Naciones Unidas E7-95 y Shyris, Quito, Ecuador, 4to piso, Quito, Ecuador
e-mail: jose_burgos@petroamazonas.ec

S. Bès de Berc
BRGM, Direction Régionale Réunion et Interrégionale Océan Indien, 5, Rue Sainte-Anne, BP 906, 97478 Saint-Denis Cedex, France
e-mail: s.besdeberc@brgm.fr

Introduction

The present paper presents an example of migrations of a river of the Ecuadorian Andes, the Rio Pastaza in the regional context of a low amplitude active tectonic backtilting over the past century (1906–2008). As often on an orogenic foothill, these migrations are results of avulsion, the process whereby a river abruptly changes its course. These avulsions occurred on a 400 km^2 area where the Rio Pastaza exits a 13,700 km^2 drainage basin by mean of a deep gorge incised in the Eastern Cordillera after a 155 km long course. The occurrence of these avulsions in such a

Published online: 31 January 2012

context provides a good opportunity of investigating the conditions of the morphological response of a river in a context of tectonic-driven surface tilting in an orogenic active foothill and alluvial sedimentation.

The parameters favoring and/or triggering these avulsions such as sediment supply, tectonic tilting, and ENSO-controlled local climatic characteristics will be discussed. This study is based on historical maps, aerial photography, satellite images, field data, and interviews with inhabitants.

Background

Structure of the Ecuadorian Andes

The Amazonian versant of the Ecuadorian Andes (Fig. 1) can be divided into four morphotectonic units.

The Western Cordillera and Interandean depression consist of Upper Cretaceous-Paleogene formations (Kennerley 1980; Lavenu et al. 1992; Reynaud et al. 1999) unconformably overlain by Neogene/Quaternary deposits (Barberi et al. 1988; Lavenu et al. 1992; Barragán et al. 1996; Hungerbühler et al. 2002; Winkler et al. 2005).

The Eastern cordillera is comprised of Paleozoic through Upper Cretaceous metamorphic rocks blanketed by late Miocene to Pliocene volcanic/volcaniclastic formations involved in a large-scale fault-bend fold, and intruded by Quaternary volcanoes (Baldock 1982; Barberi et al. 1988; Lavenu et al. 1992).

The Subandean Zone is separated from the Eastern cordillera by the west dipping Subandean Thrust fault and includes the Abitagua cordillera (essentially granitic) and two antiformal thrust stack culminations, the Cutucu and Napo domes made up of Jurassic to Neogene strata

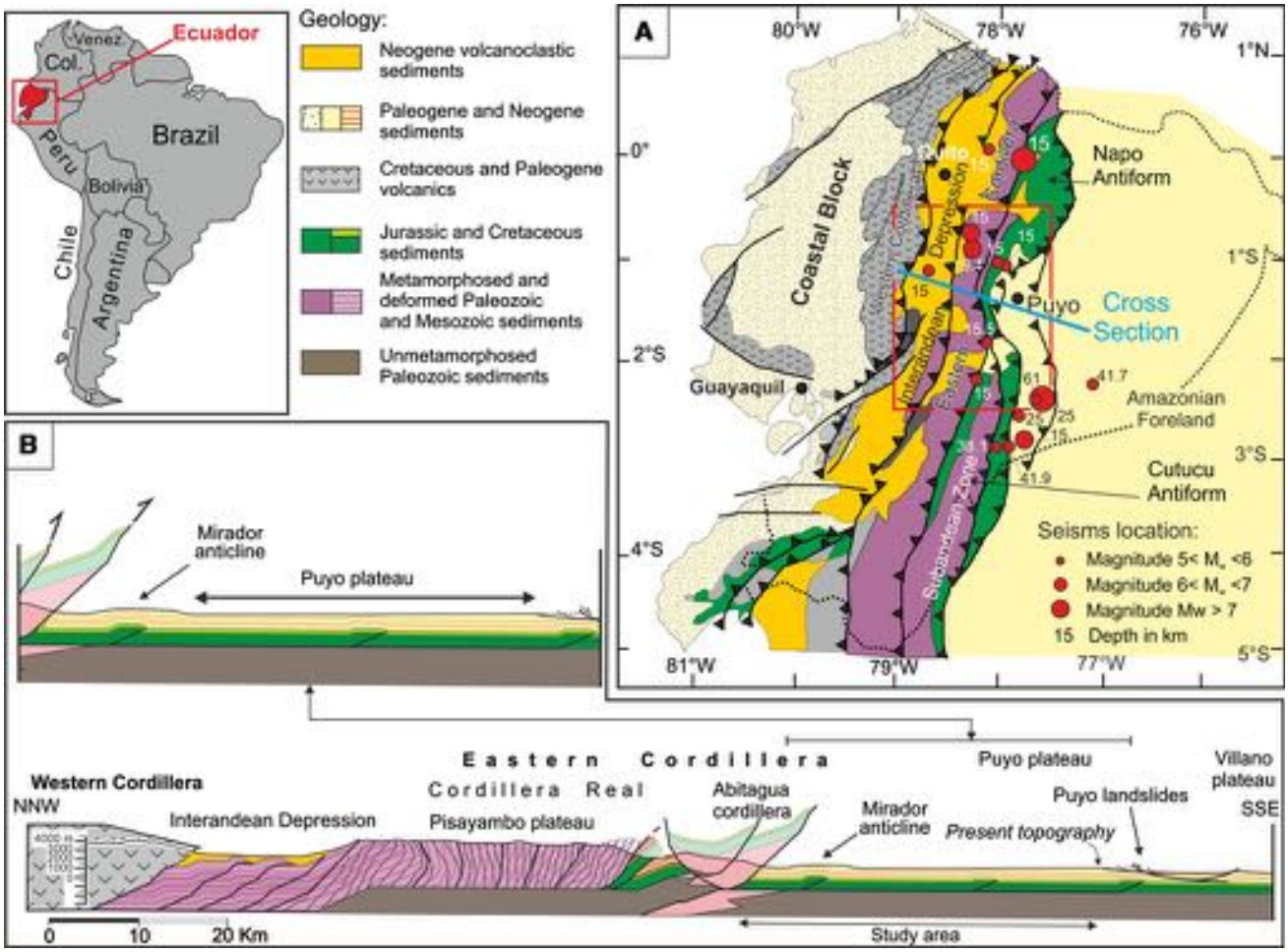

Fig. 1 Simplified geological map of Ecuador, structural cross-section, location of the seismic. **a** Simplified geological map of the Ecuadorian Andes and location of the seismic activity. *Solid black lines*: mains thrusts faults of Ecuadorian Andes. *Solid red line*: location of **b**. Location and depth of earthquakes with magnitude greater than M_w 5 in the study area, between 77°W and 79°W and between 1°N and 3°S between 1976 and 1999 (Harvard Catalog 1999). **b** Depth of earthquakes with magnitude greater than M_w 5 in the study area, between 77°W and 79°W and between 1°N and 3°S, between AD 1976 and 1999 (Harvard Catalog 1999). **b** Structural cross-section across the western cordillera, the interandean depression, the eastern cordillera, the subandean zone, and the amazonian foreland. Cross-section is striking NW–SE, location on the geological map exhibited in **a**

(Baby et al. 1999; Bès de Berc et al. 2005). These culminations are separated by an axial depression in which occurred the studied avulsions. The Subandean Zone is bounded to the east by the Subandean Frontal Thrust fault which emerges at the base of the Cutucu and Napo thrust stacks related antiforms (Fig. 1a). Between 2.77 Ma and 190 ka, the depression was affected by a basaltic volcanism, leaving lavas and scoria cones (Hoffer et al. 2008). A piedmont megafan (Mera fan) had formed there during the Pleistocene (Tschopp 1953; Baby et al. 1999; Bès de Berc et al. 2005). The apex of this fan was cut by an oxidized and hardened surface (Mera surface, Heine 1994, 2000; Bès de Berc et al. 2005) which formed during the LGM, 21,000 cal. years ago (Bès de Berc et al. 2005; Bernal et al. 2011). Since then, the Mera surface—geographically known as the Puyo plateau—has been affected by tectonic backtilting and arching (Bès de Berc et al. 2005; Bernal et al. 2011) (Figs. 2, 3a).

The Puyo and Villano plateaus

The Puyo plateau (=the Mera surface) was originally the western part of a piedmont pediment, gently dipping eastward, now separated from its eastern prolongation, the Villano surface, by an erosional depression (Bès de Berc et al. 2005; Bernal et al. 2011) formed along a low-angle normal fault (Fig. 1b). The Puyo plateau (Fig. 2) has now a westward dip of 0.6° in average and 0.9° in its central part including the study area. Its elevation varies from 1,100 m asl in its central-eastern edge to 900 m asl at the northern and southern tips and along its inner boundary, in front of the cordillera. In a south-north profile, the Puyo plateau appears as a 70-km-wide gentle arch with an amplitude of 190 m (Bès de Berc et al. 2005) (Fig. 3a). This arch forms an east–west culmination east of the town of Puyo (Puyo high, Bès de Berc et al. 2005) (Figs. 2, 3a). This culmination

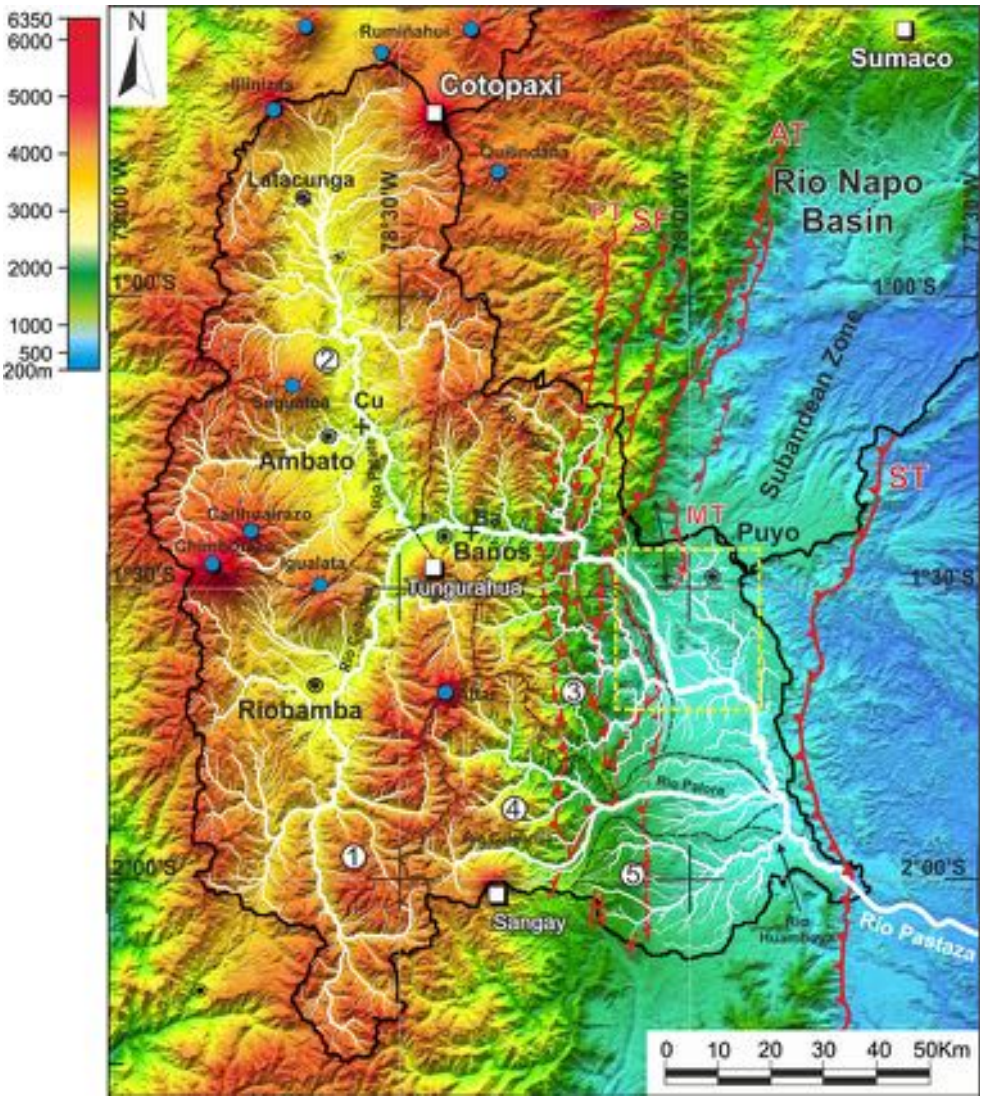

Fig. 2 SRTMV3 DEM (90 m accuracy) of the Ecuadorian Andes. *White squares*: active volcanoes. *Blue spots*: inactive volcanoes. *Solid black line*: watershed divide of the Rio Pastaza and Napo basins. *Dashed black lines*: sub-basins divide, *1* Rio Cebadas, *2* Rio Patate, *3* Rio Llushin, *4* Rio Culebrilla, *5* Rio Huamboya. *Solid white lines*: hydrographic network, thickness of *lines* grows with Stralher order (tributaries represented have order >3). *Solid red lines*: main thrusts faults of the eastern cordillera and subandean zone. *PT* Pallatanga Thrust, *SF* Subandean Fault, *AT* Abitagua Fault, *MT* Mirador Thrust, *ST* Subandean Thrust. *Yellow dashed lines*: area of avulsions of the Rio Pastaza. The Puyo Plateau is the *light blue* to *light green* (750–1,100 m asl) area comprised between the ST to the east and the thrust-faults at the front of the Eastern Cordillera (involving the MT) to the west. *Black crosses*: location of hydrometeorological stations which provided data exposed on Fig. 4. *Cu* Cusubamba Station, *Ba* Baños Station

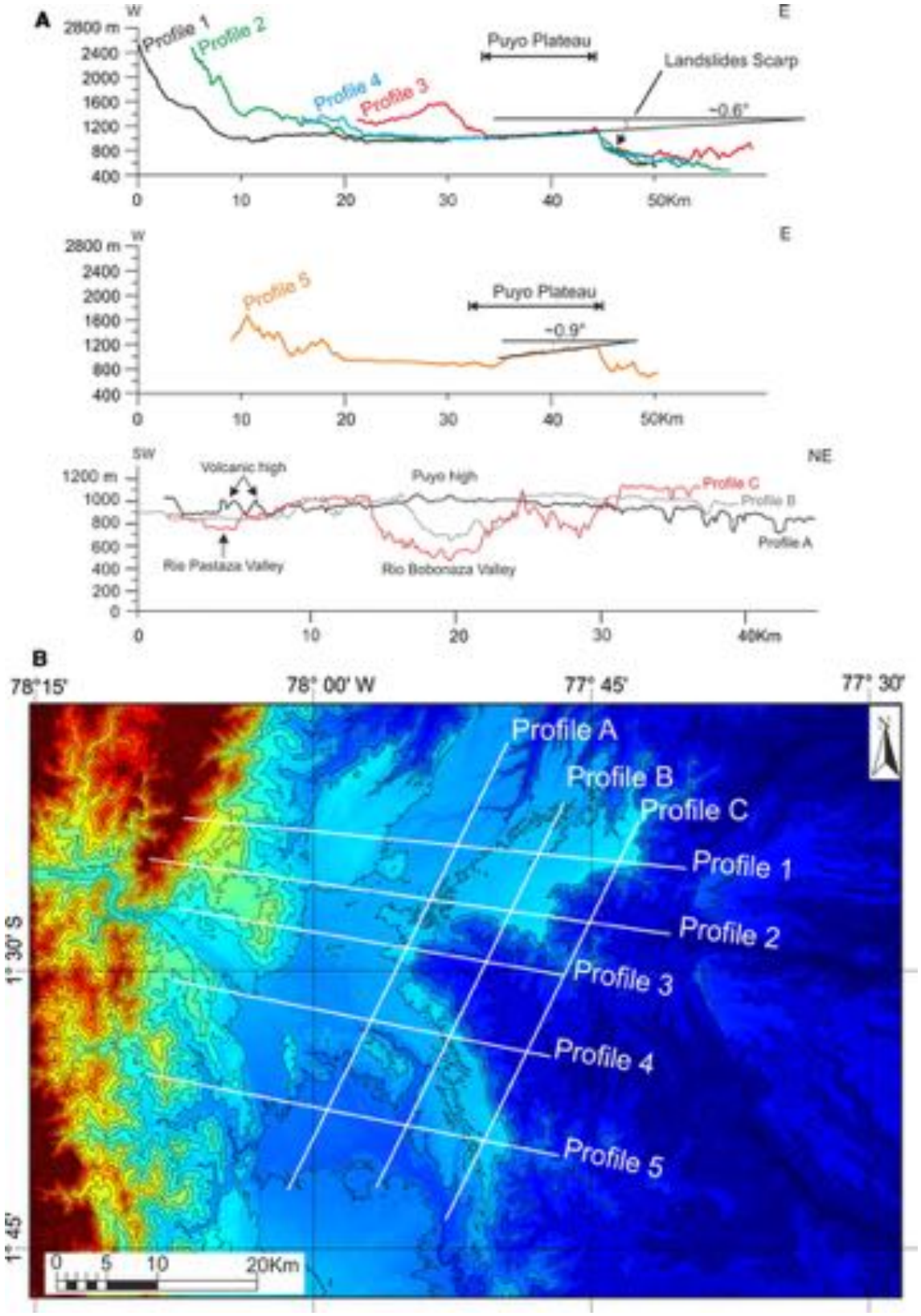

Fig. 3 Transverse and longitudinal topographic profiles across the Puyo plateau extracted from the ASTER DEM processed with B3 (VNIR_Band3N) and B4 (VNIR_Band3B) stereoscopic bands and SRTM V3 DEM. **b** Topographic profiles location map

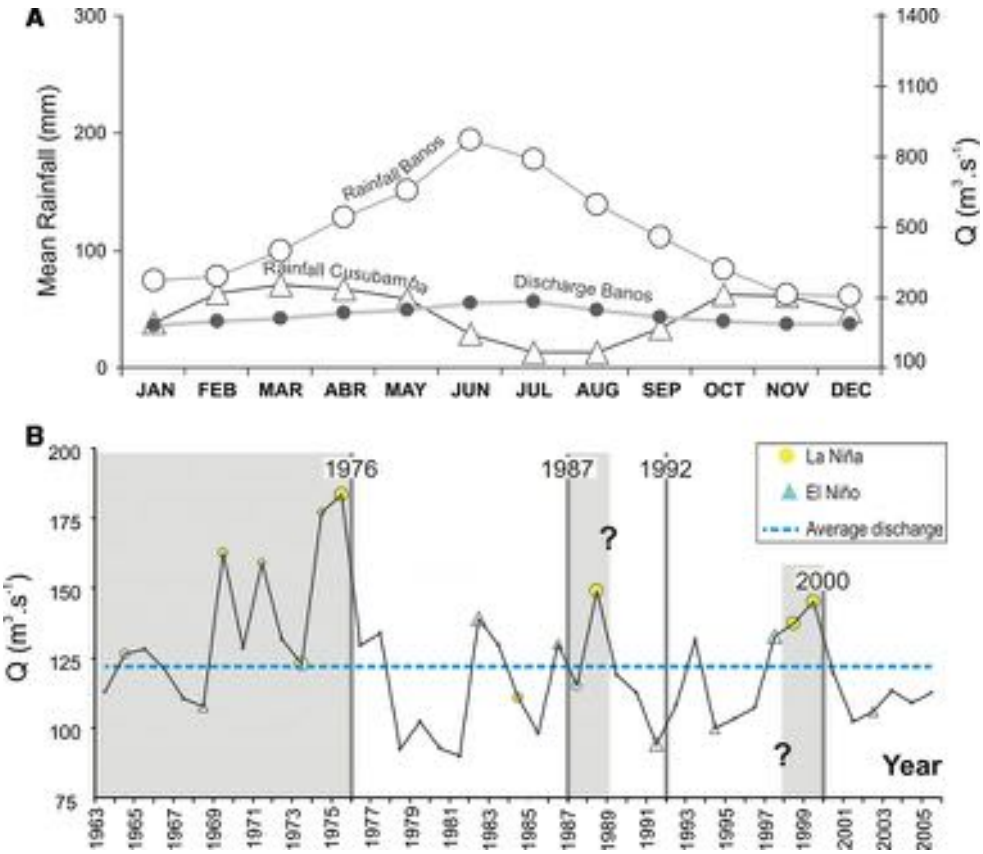

Fig. 4 **a** Average monthly precipitations at Baños (Eastern Cordillera) and at Cusubamba (Interandean Depression) and average monthly discharge of the Rio Pastaza at Baños. **b** Influence of ENSO events on the annual discharge of the Rio Pastaza at the Hydroagoyan dam near Baños (after Laraque et al. 2009). The *thick gray vertical lines* mark the date at which were taken the aerial photographs and satellital images showing the changes in course of the Rio Pastaza. The *gray rectangles* indicate the periods of time in which these changes in course may have occurred

constitutes the main divide between the drainage basin of the Rio Pastaza and that of the Rio Napo, which is the other major river of the region. The Villano surface has kept a shallow dip (<0.3°) to the east. Its elevation in its western edge is 800–500 m asl. The restoration of the original surfaces from a series of cross-sections shows a normal offset of 300–400 m (Fig. 1b). The normal fault is related to the propagation of the Subandean frontal thrust and fold. The average tilting rate of the Puyo plateau since the LGM is $\sim 3\text{–}4.5 \times 10^{-5\circ}$ year^{-1} (0.5–0.8 μrad year^{-1} or 0.008 cm km^{-1} year^{-1}). The average uplift of the plateau edge with respect to its inner boundary is of 0.6–0.85 cm yr^{-1}, higher than in the cordilleras for the same period (4–6 mm year^{-1}, Bès de Berc et al. 2005).

Two local topographic highs appear in the Puyo plateau (Fig. 3b). In the north, the fault-related Mirador anticline culminates at ~1,400 m asl (Bès de Berc et al. 2005) (Fig. 1b). In the south, the volcanic edifice formed by the preserved Pliocene lavas and scoriae (Hoffer et al. 2008) culminates at ~1,100 m asl, ~80–100 m above the plateau (Fig. 3b).

The Rio Pastaza in the Ecuadorian Andes

The Rio Pastaza is sourced in the Western Cordillera (Fig. 2) and is the only Ecuadorian river that traverses the Eastern Cordillera. Upstream of the Subandean front, its catchment covers an area of 13,700 km^2.

The Rio Pastaza sensu stricto is transverse and formed by the junction of two longitudinal branches flowing in the Interandean Depression (Fig. 2). Downstream of the confluence, the Rio Pastaza traverses the Eastern Cordillera and the Abitagua cordillera through a narrow and deep valley ~12 km wide and 2,900–1,300 m deep. Where debouching into the Puyo plateau, the valley widens abruptly and the river slope decreases to form an alluvial fan with a ~6 km radius. The Rio Pastaza diverges into two branches which form an abrupt bend to the south and flow southward along the front of the Eastern Cordillera where it has formed a wide braidplain in continuity with the Puyo fan. These two branches rejoin immediately south of the Volcanic Complex (Fig. 2). The Rio Pastaza receives two major transverse tributaries from the west, the Rios Llushin (basin area = 1,015 km^2) and Palora (basin area = 2,350 km^2) (Fig. 2). At its confluence with the Rio Llushin, the course of the western branch of the Rio Pastaza forms a sharp eastward bend in prolongation of the western course of the Rio Llushin (Figs. 2, 5a) while the eastern branch forms a more rounded bend before rejoining the western branch. Downstream, the Rio Pastaza exits the Puyo plateau after having flowed ~12 km along the plateau edge (Fig. 2). The deposits on the younger terraces of

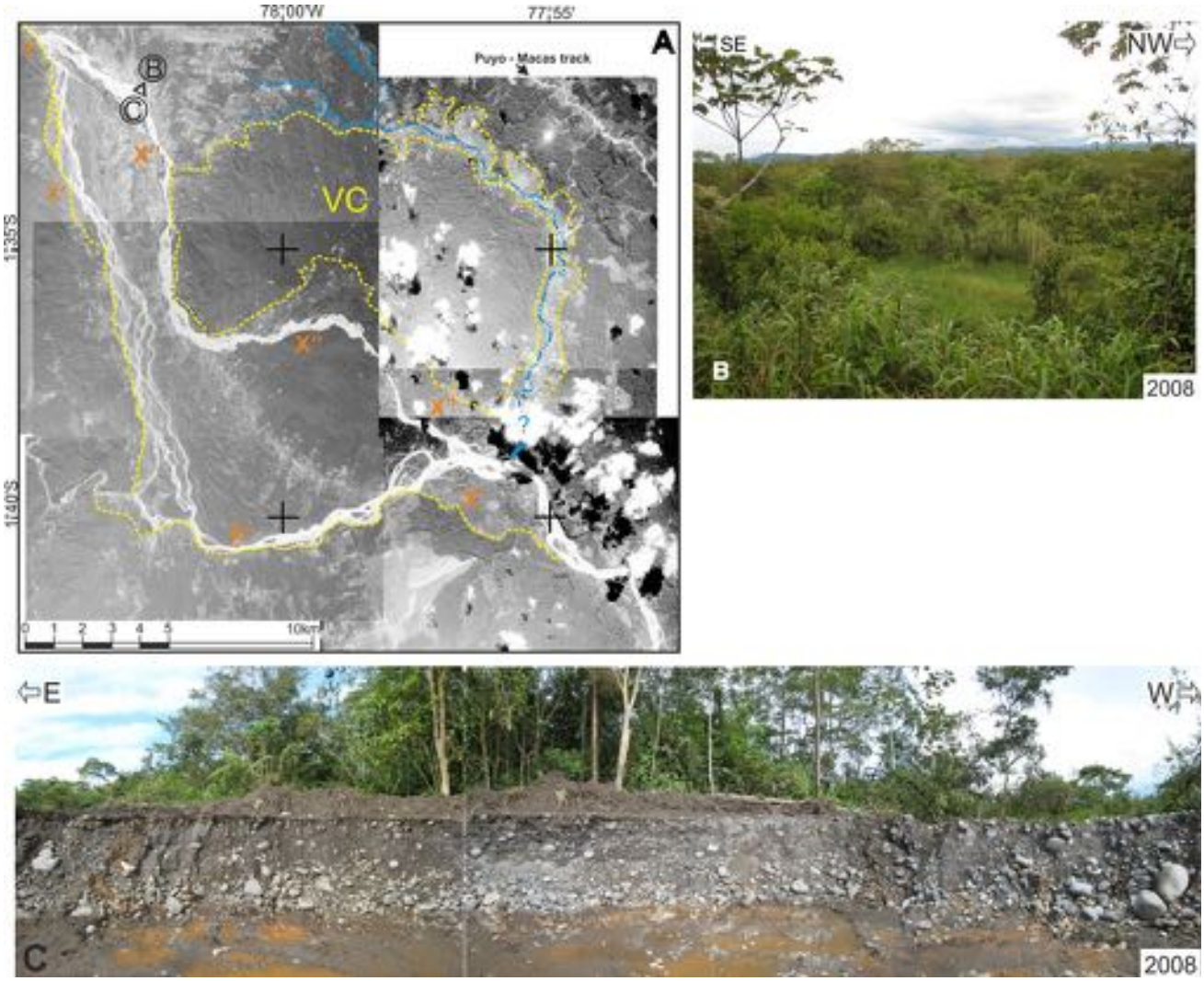

Fig. 5 **a** Mosaic of 1976 aerial photographs of the southern Puyo plateau (Instituto Geographico Militar de Ecuador). *Yellow dashed line* corresponds to the boundary of the thalwegs of the Rio Pastaza from 1906 to 2008. *Blue dashed pointed lines* correspond to the Rio Puyo and its tributary resulting from the beheading of 1906 path. The snapshot shown in **b** is viewed from point *B*. *C* Indicates location of snapshot shown in **c**. *1* is the avulsion point of 1976, X′ is the western branch, and X″ the eastern branch resulting of the partial avulsion. *1* X and X″ are the same than those presented on Fig. 8. **b** Present-day aspect of the eastern channel of the Rio Pastaza abandoned between 1976 and 2002. Vegetation is represented by arborescent shrubs and rare trees. **c** Snapshot of the 1976 channel as it appears in July 2008. An outcrop of the gravel bar preserved in the channel abandoned after 1976. Observe the height of the vegetation developed on the gravel layers

the Pastaza grade downstream into aggrading modern deposits forming the Puyo fan and the southern Pastaza braidplain (Fig. 7). These modern deposits are rather coarse (boulders up to 50 cm in diameter) and their thickness is greater than 7–8 m.

The average annual discharge of the Rio Pastaza from 1917 to 2004 is 121 $m^3\ s^{-1}$ at the Hydroagoyan dam, near Baños, and varies between $\sim$185 $m^3\ s^{-1}$ in 1975 (La Niña event) to 85–90 $m^3\ s^{-1}$ in 1981 and 1991 (El Niño event) (Laraque et al. 2009) (Fig. 4b). The average monthly discharge varies from 181 $m^3\ s^{-1}$ in July and 82.5 $m^3\ s^{-1}$ in January (Laraque et al. 2009) (Fig. 4a).

Climatic setting

The present climate in the Ecuadorian Amazonia is hot and wet, especially in the piedmont with average annual precipitation of over 3,000 mm all along the cordillera front, and $\geq$4,500 mm near Puyo at 1,000 m asl (Hastenrath 1981; Gomez 1994). At Puyo, the monthly average rainfall is greater than 300–350 mm all year, with a maximum in March and April (Gomez 1994). At Baños (Fig. 4a, location on Fig. 2), 35 km upstream of our study area, the monthly average rainfall varies from $\sim$80 mm in January to $\sim$200 mm in June. At the Cusubamba station in the

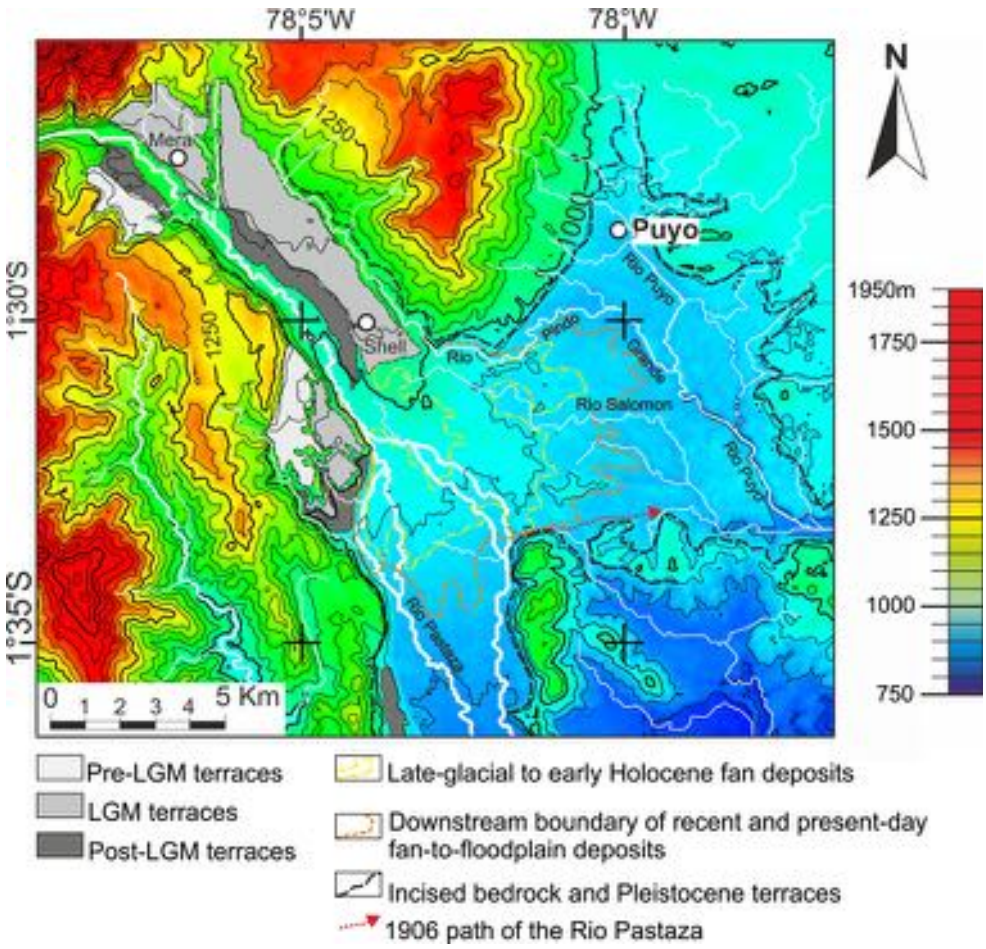

Fig. 6 Map of Pleistocene and Holocene alluvial terraces and alluvial fan deposits of the Puyo area (modified from Bès de Berc et al. 2005 and Burgos 2006)

northern Interandean Depression (Fig. 3a), the average annual precipitation is considerably lower and the monthly average rainfall varies from ~15 mm in July and August to ~75 mm in March and November (Laraque et al. 2009) (Fig. 4a).

The recent migrations of the Rio Pastaza in the Puyo plateau

The migrations of the Rio Pastaza in the past century (from 1906 to 2008) have been traced using a topographic map published in 1906, aerial photographs taken in 1976, satellital images and field observations between 1992 and 2008. 1976 paths were constructed using 6 photographs taken during the aerial photography campaign of the Instituto Geografico Militar of Ecuador. Photographs were georeferenced, orthorectified, and then mosaicked. The resulting mosaic is shown in Fig. 6. The paths of 1987 and following years (1992, 2000, and 2002) are based on Landsat and Aster satellite images. These images were georeferenced, orthorectified, and then binarized in order to enlight the active channels (Fig. 8). Field observations were carried out during the years 2003–2008 (Fig. 5). No press documents have been found, even for the more recent avulsions. Eye witnesses have a clear memory of the avulsions having occurred since 1976 (but not of the exact time when they occurred). No one remember the time when the Rio Pastaza flowed to the east along the Volcanic Complex but peoples over 70 still living in the area are rare. The exact time when the avulsions occurred thus remains unknown, in particular in the 1906–1976 period. However, the snapshots in the evolution of the river system provided by the images enable us to distinguish 6 'stages' (Fig. 8). Complexity of the braid channels network will be described by the Braiding Index (BI). BI is defined as the sum of the active channels length divided by the reach length.

Stage 1 (observed in 1906)

The 1906 map shows that the Rio Pastaza flowed along the northern and then eastern boundaries of the Pliocene Volcanic Complex (Figs. 5a, 8). Today, the eastern portion of this path is occupied by the Rio Puyo a left-bank tributary of the former Rio Pastaza (Fig. 8), which forms a sudden 90° bend toward the east at the junction with the former

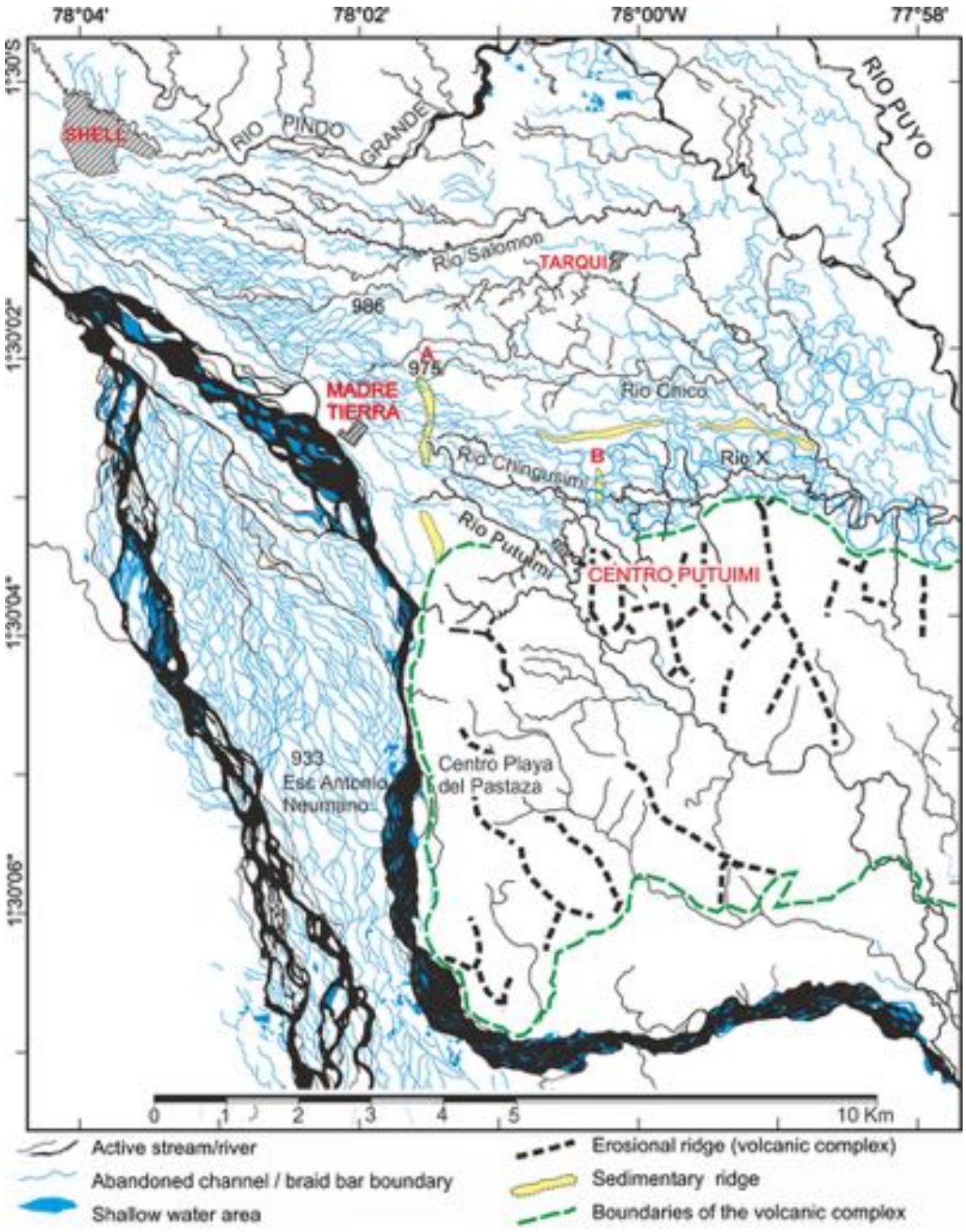

Fig. 7 Photograph-interpretated map of the fluvial features of the Puyo area. Map based on aerial photographs exhibited on Fig. 5a. Active channels in 1976 are represented in *black*, braid *bars* in *blue*. *Yellow areas* correspond to topographic highs interpreted as sedimentary ridges deposited on the former banks of the channels. Inactive and abandoned channels are represented with *blue lines*. To the west, in the north–south reach of the Rio Pastaza, the pattern of inactive and abandoned channels is typical of a braided river. In the north (east of Madre Tierra and Tarqui), the abandoned channel patterns evolves from west to east from a braided to meandering channel pattern. The active reach (north–south) and the abandoned one (west–east) are separated by the volcanic complex (bounded by a *dashed green line*)

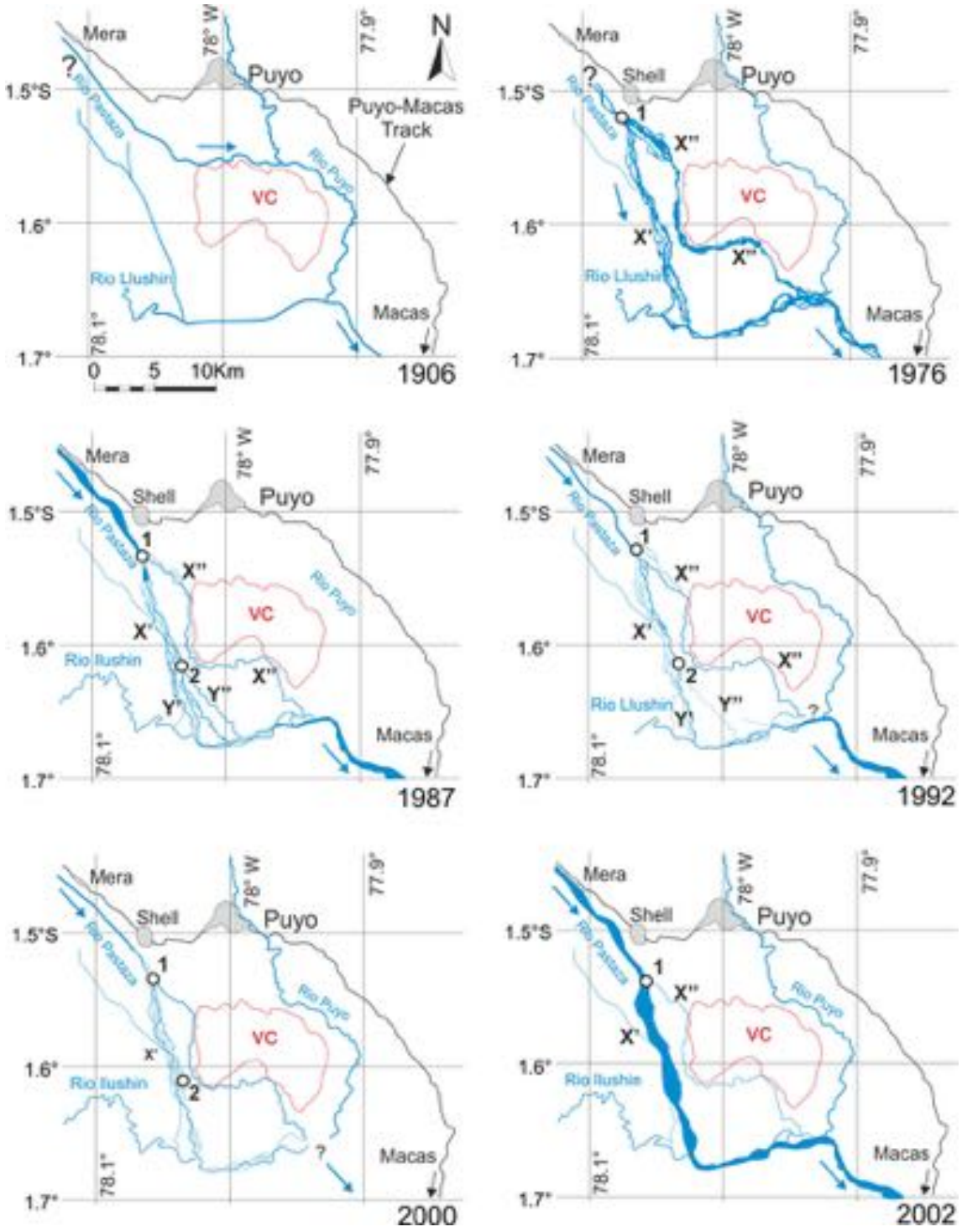

Fig. 8 Evolution of the Rio Pastaza in the southern Puyo plateau since 1906. Each map illustrates the following stages: 1906, 1976, 1987, 1992, 2000, 2002. 1906 is deduced from a map. 1976 is based on aerial photography mosaic exhibited on Fig. 5. 1987, 1992, 2000, and 2002 stages are based on Landsat satellite images. *1* and *2* refer to bifurcation points. X′, X″ and Y′, Y″ correspond to the channel, respectively, origined downstream of the bifurcations *1* and *2*

Pastaza valley. A distance of 7 km separates this junction from the eastern branch of the Pastaza. The eastern part of the abandoned valley is now occupied by the unnamed river we termed 'Rio X' (Fig. 8). The western portion of this abandoned valley is presently occupied by the upper Rio Chigunsimi. This document also reveals the presence of a minor left-bank tributary of the Rio Llushin flowing along the front of the cordillera.

The poor quality of the 1906 document did not enable us to characterize the channel pattern of the Rio Pastaza and the characteristics of the Pastaza valley at this time. However, information on this valley is provided by the 1976 photographs (Figs. 5a, 7). Although the area was already highly vegetated (in the east) or occupied by tea plantations (in the west), the 1976 photographs show evidence of an abandoned floodplain oriented west–east along the northern boundary of the volcanic complex between the Pastaza braidplain in the west, and the eastward bend of the Rio Puyo in the east (Fig. 7). This floodplain is wider (1–2 km) than the present-day valleys of the Rio X and Rio Puyo and incised by these rivers. Tracing the abandoned drainage network reveals a braided/distributary pattern changing eastward into a relatively wide meander belt (Fig. 7). Some of the rivers (Rio Pindo Grande, Rio Salomon, Rio Chico in the north; Rio Chigunsimi and Rio X in the center; Rio Putuimi in the south) are still active but have acquired since then a contributory pattern. In the west, around and southeast of the village of Shell, bifurcating-rejoining channels are frequently seen separating 250-m-wide amygdaloidal swells, which are likely to represent former longitudinal baidbars. This abandoned braidplain is similar in size and morphology to the better preserved or active Pastaza braidplain in the south. In the east, the abandoned meander loops have wavelength and amplitude in general greater than those of the present-day rivers and extend to the north in the area now drained by the lower Rios Pindo Grande and Salomon (Fig. 7) which now flow southward. The area where the 1906–1976 avulsion occurred corresponds to the braiding-meandering transition of the ancient valley and only a sedimentary ridge constitutes the divide between the present-day Rio Pastaza and Rio Puyo drainage basins.

Stage 2 (observed in 1976)

In 1976, the Rio Pastaza was divided into two branches (X′ and X″ in Fig. 8), issued from a bifurcation located south of the village of Shell (1 in Figs. 5a, 8).

The western branch X′ flows southward along the Eastern Cordillera for 14 km and forms a sharp 90° bend at the confluence with the Rio Llushin, changing its direction from N 165°E to N 75°E (Fig. 8). North of the confluence with the Rio Llushin, the western branch consists in a braidplain varying from 250 to 1,500 m in width comprising 1–8 braided channels. The width of individual braid channels never exceeds 250 m. East of the confluence, the downstream reach becomes less braided and evolves into a low-sinuosity channel with numerous mid-channel bars which may characterize a wandering morphology (Brierley 1989). Individual channel width increases and exceeds 500 m when approaching the confluence with the eastern branch. All along the western branch, the most active channels are on the right of the braidplain, against the cordilleran front. A series of abandoned diverging channels separated from the main channels are still visible (Figs. 5a, 7, 8).

The eastern branch X″ flows south-eastward along the Puyo fan axis for 5 km, then southward (6 km) and eastward (6 km) along the western and southern boundaries of the Volcanic Complex, and finally south-eastward until the present Pastaza-Puyo confluence (Figs. 7, 8). Downstream of the bifurcation 1, a 1,000-m-wide upstream reach striking SW–NE (130) is composed of wide braided channels. At the contact with the Volcanic Complex, the river becomes a single channel for $\sim$1.7 km, and then widens and recovers its braided morphology. The active channels are located in the left side of the baidplain in contact with the Volcanic Complex.

The 1976 photographs also reveal that two avulsions are at the origin of the abandon of the pre-1976 floodplain and both occurred between 1906 and 1976. The sedimentary ridge constituting the wing gap between the eastern branch of the Pastaza 1976 and the Pastaza 1906 (the present Rio Chigunsimi) is somewhat higher than the Pastaza braidplain ($\sim$15 m), thus indicating a large accumulation of sediment. The present windgap between the Rio Chingusimi and the Rio X is only 4–6 m higher than the site of the avulsion of the Rio Chingusimi into the Rio Putuimi (Fig. 7). As for the Pastaza—Chigunsimi divide, the ridge is sediment-made. A well-marked knick point appears in the long profile of the Rio Chigunsimi strongly suggesting either a capture of the Chigunsimi by the Rio Putuimi or an annexation of the Rio Putuimi by the Rio Chigunsimi. As the Putuimi valley is relatively deep but narrow, this avulsion must have occurred after the Pastaza avulsed to the south. It is noteworthy that both avulsion sites are situated at the braiding-meandering transition of the pre-1976 floodplain (Fig. 7).

Stage 3 (observed in 1987)

In 1987 (Fig. 8), the Río Pastaza has the same overall configuration as in 1976. The western branch X′ exhibits braided channels characterized by a low braiding parameter (BI = 1.8, cf. Schumm 1977). Compared to 1976, this branch exhibits the same width but less active channels. The morphology of the eastern branch X″ varies from single channel to braided with a very low braiding parameter (BI = 0.5). This branch is less wide and exhibits less active channel than in 1976. To the south, a series of diverging channels separate from the main channel and rejoin the river downstream of the Llushin confluence. The remaining southward-flowing main channel (Y′) presents the same braiding characteristics (BI = 1.6) as upstream of

the divergence point 2. The separate channels (Y″) appear as single meandering streams.

Stage 4 (observed in 1992)

In 1992 (Fig. 8), the point of bifurcation between the branches X′ and X″ is displaced ~1.8 km to the south. The branch X″ is reduced to a straight single channel. The branch X′ has a braiding parameter BI = 1.8. The channels, active in 1987 having separated from X′ at bifurcation point 2 (channels Y″), are now abandoned except the eastern one. Downstream of point 2, the braiding parameter of the main channel decreases (BI = 0.9).

Stage 5 (observed in 2000)

In 2000 (Fig. 8), the overall configuration is similar as in 1992 and 1987, but the eastern branch X″ is now very narrow. No active channels separate from the western branch X′, but traces of abandoned parallel channels have been observed east of the main stream. The braiding parameter of this western reach increased (BI = 3.1) to the south of the point 1 and BI = 2.0 to the south of point Y′.

Stage 6 (observed in 2002)

The 2002 image (12/09/2002, Fig. 8) does not differ much from 2000. The branch X″ keeps reducing its width. The channel X″ is inactive and the main channel X′–Y′ preserves its high braiding parameter (BI = 3.0) north of point 2 and BI = 2.0 south of point 2. The braid channels are wider and the braid islands narrower, which strongly suggests that practically all the flow was directed into the western branch.

No satellite image and air photograph are available since 2002 but a series of field observations in 2008 highlight the changes happened in the eastern braidplain between 1976 and 2008 (Fig. 5b, c). Figure 5b, c represent a south-eastward looking photograph taken in July 2008, which shows that the active braidplain of 1976 (Fig. 5a) is completely abandoned and highly vegetated with trees exceeding 20 m in height. Even though vegetation growth is rapid in the region, this confirms that no channel activity has occurred for several tens years.

Geomorphological analysis

River long profiles of either active or abandoned streams were extracted from the DEM based on stereoscopic 3N and 3B bands of an ASTER scene and the SRTM DEM.

River long profiles

The Rio Pindo Grande that constitutes the northern and eastern boundary of the Puyo fan preserves a low gradient upstream of its confluence with the Rio Puyo. The Rio X shows the steeper and most regular gradient (Fig. 9a), and the profile preserves the same regularity until the confluence with the present Rio Pastaza, with no marked change at the confluence with the Rio Puyo. The gradient of the upper Rio Puyo remains relatively low in the plateau but increases when approaching the confluence with the Rio X (Fig. 9a). As the gradient of the Rio X remains rather regular in this area, this clearly shows that the greatest part of the over-incision imposed by the backtilt of the plateau was achieved by the 'Pastaza 1906' and predated the avulsions.

The profile of the Rio Pastaza 1906 has been reconstructed by joining the upper portion of the eastern branch of the Pastaza, the western portion of the Rio Chigunsimi, the Rio X, and the lower Rio Puyo. This profile shows two narrow highs only 15 and ~5 m above the profile (Fig. 8b), which are the sedimentary ridges related to the two avulsions that occurred between 1906 and 1976. The profile is, however, rather regular with an average slope (585 cm km^{-1} for the 16 km preceding the confluence with the Rio Puyo) steeper than those of the upper Rio Puyo and Rio Pindo Grande (375 and 384 cm km^{-1}, respectively) (Fig. 9a). The valley/stream profile of the Pastaza 1906 becomes convex upward in the area where the avulsions occurred (Fig. 9b). The profiles of the western and eastern branches of the Pastaza show the steepest slopes (743 and 707 cm km^{-1}, respectively) (Fig. 9b). In detail, the profiles of both branches of the present Rio Pastaza downstream of Mera show a marked increase in slope in the area where the main avulsion occurred with an increase, followed by a decrease, in river gradient not related to any bedrock change (Fig. 9b, c).

River long profile of the 1906 path and plateau profiles

The reconstructed long profile of the Pastaza 1906, between the avulsion sites and the southward bend, has been compared with two transverse profiles of the plateau in the same area. The first profile is along a straight line at ~1 km from the 'river' (XX′ profile on Fig. 10). The second profile is along the northern divide of the former drainage basin and projected onto the plane of the first profile (yellow dashed line on Fig. 10a). The two profiles are remarkably similar except the presence along the divide of a local residual relief. The eastern (upper) portion of this diagram shows the Pastaza (present eastern branch) incising the upper fan. The convex-upward central portion between the two windgaps (Pastaza—Chigunsimi and

Chigunsimi—Rio X) corresponds to a low in the plateau profile with the same slope as the reconstituted river. The eastern portion represents the backtilted surface of the plateau incised by the Pastaza 1906 and presently occupied by the lower Rio Puyo (Fig. 10). The incision increases up to ~150 m near the southward bend at ~4.5 km to the plateau edge (Fig. 10). If considering that incision commenced at the LGM, this yields a minimum average incision rate of 7.5 mm year^{-1}. This rate is consistent with the average uplift rate of the plateau edge (6–8.5 mm year^{-1}, see above).

Discussion

No other documents than the 1906 map, the 1976 aerial photographs, and the satellite images are presently available on the avulsions and the relations between these avulsions and the volcanic, climatic, and seismic events having occurred in the twentieth century cannot be directly observed. However, the eventual role of these events and of longer-term events such as aseismic tectonic tilting in the genesis of the avulsions may be discussed in light of the above data.

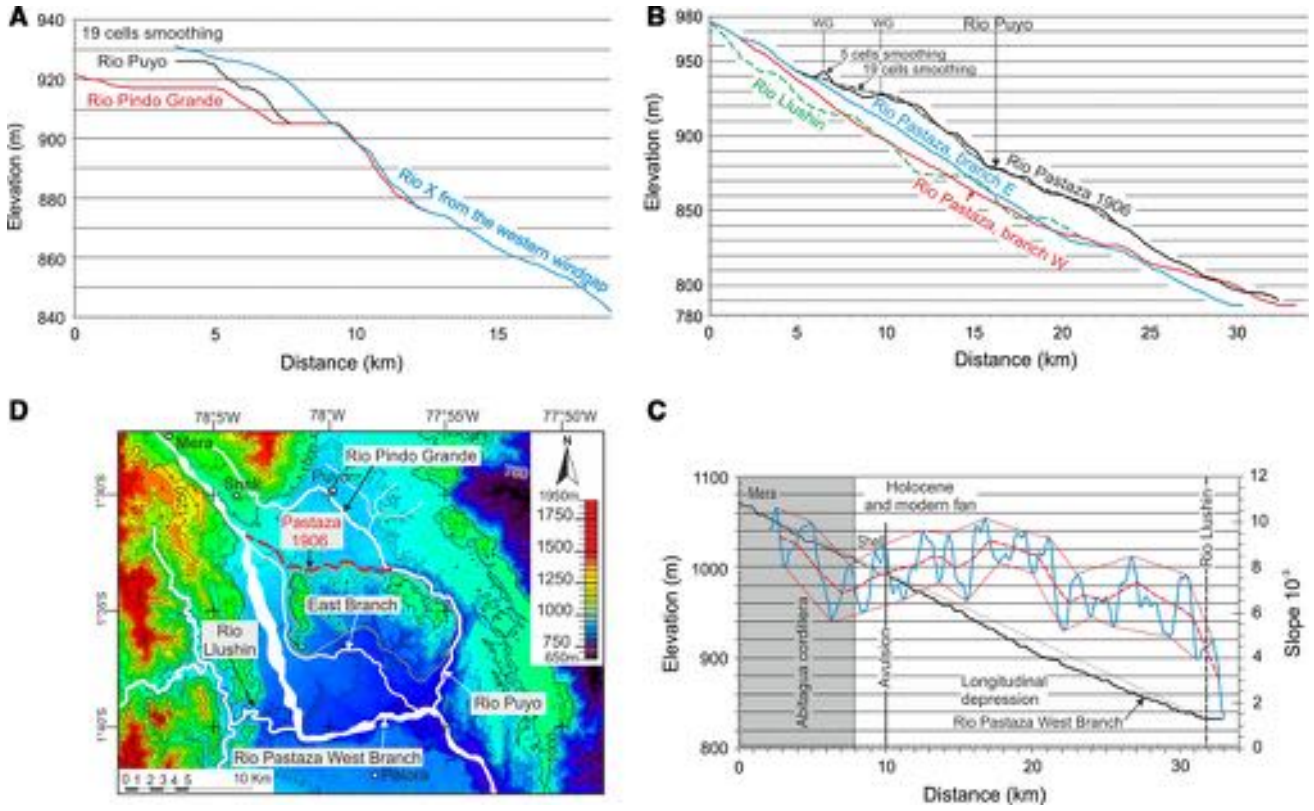

Fig. 9 Long profiles of the main rivers flowing in the central Puyo plateau. Elevations in m; distances in km. **a** Profiles of the Rio X, Rio Puyo, and Rio Pindo Grande down to the 90° bend of the Rio Puyo from the SRTM DEM. The profiles have been smoothed using average value in a 19 cells (~1,700 m) moving windows filter. The Rio X continued by the lower Rio Puyo downstream of the confluence of these rivers shows the most regular profile. No change in the profile of the Rio X is observed at the confluence whereas the gradient of the Rio Puyo abruptly deceases ~3 km upstream of this confluence. **b** Profiles of the eastern and western branches of the Pastaza starting from the divergence area compared with the reconstituted profile of the Rio Pastaza (1906). The present-day wind gaps well appear using a 5 cells moving window filter and are smoothed by using a 19 cells moving window filter. In any case, the profile takes a convex-upward shape in the area where the avulsions occurred. Note that both branches of the Pastaza have a steeper gradient than the original course. The profile of the transverse Rio Llushin in the front of the cordillera has been added. Although being more irregular because of alternating longitudinal and transverse reaches, this profile shows an average gradient similar to those of both branches of the Pastaza. **c** Long profile and slope of the Pastaza (eastern branch) from Mera to the confluence with the Rio Llushin. The gradient appears to be steeper in the longitudinal depression immediately downstream of the avulsion site than between Mera and Shell where the river traverses the Abitagua cordillera. The slope (*blue line*) decreases between Mera and Shell, then increases in the upper part of the longitudinal depression, and finally, decreases toward the confluence with the Rio Llushin. Slopes values are computed with 5 pixels segments (*blue line*). The *red lines* above and below the *blue curve* corresponds to the minimum and maximum envelope curves of slope values. **d** Location map of the profiles presented in **a**–**c**. The topographic map is based on the DEM used for profiles extraction

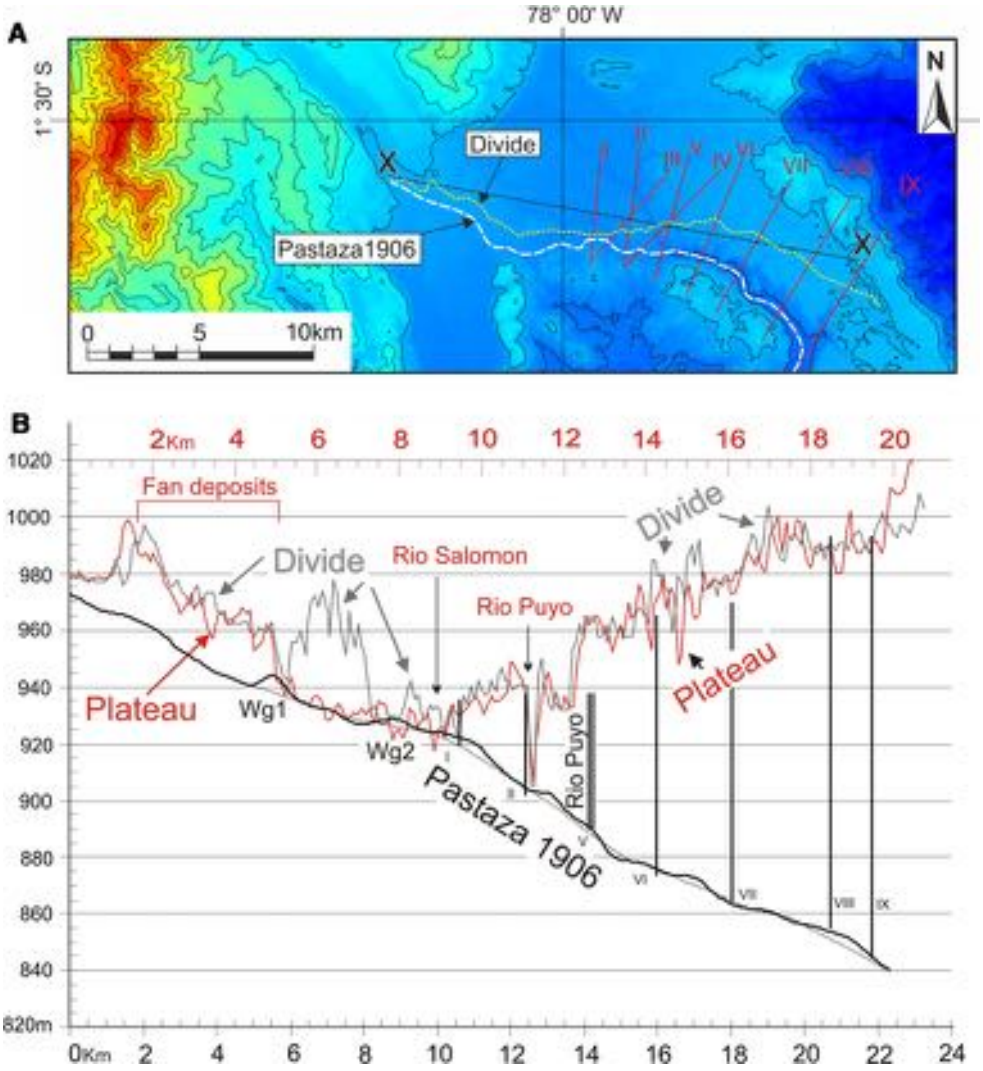

Fig. 10 Reconstituted long profiles of the 'Pastaza 1906' (*black*), transverse profile parallel to the overall direction of the 'Pastaza 1906' (*red*), and profile along the northern drainage divide (*gray*). **a** Location map of topographic profiles represented below. **b** The along-divide and river profiles have been projected onto the plane of the transverse profile. *Wg* wind gap. The *double vertical line* marks the confluence between the Rio X and the Rio Puyo. The *single lines* are the traces of the transverse profiles shown in Fig. 9a. The *top* of each *line* is the elevation of the *hinge line* between the valley flank and the plateau surface. The *scale* in the *bottom* of the diagram refers to river and divide profiles. The *scale* on the *top* refers to the transverse profile. The convex-upward portion of the river profile corresponds to the area where the 1906–1976 avulsions occurred. This area is situated in a flat-lying area between the fan and the backtilted plateau surface. The high in the divide profile is a residual relief situated 1 km to the north of the river. Elevations in m, distances in km. **d** Location map of the profiles exhibited in **a**–**c**

Earthquakes and volcanic eruptions

Major earthquakes occurred in 1949, 1987 (M_w 7.1), and 1995 (M_w 7.0) (Yepes et al. 1996; Legrand et al. 2005, Fig. 1a), that is, between the making up of the 1906 map and 1976, just before or after the 1987 photographs, and between the 1992 and 2000 images. Relatively high magnitudes earthquakes are frequent (Fig. 1a). However, the stepped terraces that bound both branches of the Pastaza (Bès de Berc et al. 2005; Fig. 6) show that aggradation has proceeded there without constructing levees to be breached by earthquakes as, for example, in the Rhine-Meuse delta (Stouthamer and Berendsen 2000; Cohen et al. 2002). There are no more evidences of transverse faults having diverted the Pastaza.

Major eruptions of Tungurahua volcano producing pyroclastic flows and ash falls occurred in 1916–1918 and 2006–2008 (Le Pennec et al. 2008; IGEPN 2009). However, the amount of material delivered to the Pastaza was relatively limited and none of these major eruptions was capable of transporting ash surges or lahars necessary for triggering avulsions down to the study area (Le Pennec et al. 2008; IGEPN 2009).

Tectonic tilting

The westward migration of the Pastaza and the development of the western branch at the expense of the eastern branch apparently agree with the interpretation that the Pastaza simply migrated westward as a result of tectonic backtilting opposing the normal eastward flow and/or creating more favorable slopes toward the south. However, even though the uplift rate generated by backtilting is relatively high, such a 'mechanical' increase in slope diverting the river course may appear by itself insufficient for having caused the 1906–1976 avulsion if we consider that the presently modest Rio Puyo has been able to maintain its eastward course.

Figures 6 and 10 show that the area where the avulsions occurred is in fact situated in the topographic depression between the east-sloping Puyo fan and the west-sloping plateau surface and is marked by a reduction in slope of the 'Pastaza 1906'. The abrupt increase in width and decrease in river gradient when debouching on to a piedmont (see Fig. 5) reduces bed shear stress, thus enhancing braiding and aggradation, and promoting avulsion (Schumm et al. 2000). In another hand, it has been established that subtle warping is sufficient to induce changes in planform geometries (Ouchi 1985; Holbrook and Schumm 1999). Again, according to Jones and Schumm (1999): 'gradient reduction in meandering streams may result in bedload deposition where the slope decreases, clogging of the channel, and finally avulsion'. The 1906–1976 avulsion in fact occurred at the braiding-meandering transition in an area where the reconstituted profile of the 'Pastaza 1906' effectively shows a decrease in slope (Figs. 9b, 10). An association of gradient reduction and abrupt river widening may also be invoked for the 1976–2008 gradual avulsion which occurs in the same piedmont area where the Pastaza both decreases in slope as a result of tectonic backtilting and enlarges after having been confined in the cordilleran valley. The progressive dominance of the western branch over the eastern branch might have been a result of progressive starving of the eastern branch by tectonically enhanced aggradation upstream of the initial avulsion site. Aggradation enhanced by tectonic tilting seems, therefore, to have played a major role in the genesis of the avulsions by leading the system close to the avulsion threshold as stated by Jones and Schumm (1999). Previous steepening and narrowing of the valley downstream of the avulsion site might explain why a former left-bank tributary of the Pastaza—the Rio Puyo—could have continued to flow in this valley after the Pastaza was beheaded.

Capture/annexation of a pre-existing river

The longitudinal depression in which flow the present western and eastern branches of the Pastaza was created by tectonic backtilting tilting and arching (Fig. 3). This depression has had a slope steeper than the original slope of the river, which may have provided a more favorable way to the Pastaza (Jones and Schumm 1999; Slingerland and Smith 2004; Humphrey and Konrad 2000). This depression was occupied by a former tributary to the Rio Llushin potentially able to capture the Pastaza by headward erosion (e.g., Summerfield 1991). Another possibility should be that the Pastaza, made unstable because of increasing aggradation and decreasing slope, annexed this tributary [avulsion by annexation according to Slingerland and Smith (2004); 'capture par déversement' (=capture by overflow) as opposed to capture by headward erosion in the French literature, see e.g., Tricart (1952) or Coque (2002, p. 120–121)]. This latter interpretation will be preferred as it accounts for both the shape of the long profile of both branches of the Pastaza and the wind gaps being constituted by an accumulation of sediment at the braiding/meandering transition.

ENSO events

Severe ENSO events occurred in 1916, 1942, 1949, 1955, 1969–1970, 1971–1972, 1974–1975, 1975–1976, 1982–1983, and 1997–1998 (Aalto et al. 2003). The major avulsions observed in our study area occurred between 1906 and 1976, between 1987 and 1992, and between 1992 and 2000. The hydrograms available for our study area (Baños hydrometeorological station, Fig. 2) only cover the period 1963–2006. Figure 4 shows that the peaks in annual discharge associated with La Niña events occurred in periods preceding the avulsions. The partial avulsion having formed the western branch may have been triggered by the 1975–1976 and 1974–1975 La Niña events (highest discharges yet measured) and/or the preceding 1971–1972 and 1969–1970 events. The 1988–1989 La Niña events occurred in the period 1987–1992. The 1998–1999 and 1999–2000 La Niña events immediately preceded the changes observed in 2000. The peaks in annual discharge during La Niña events are not much higher than the average: $\sim$185 m^3 s^{-1} for the 1975–1976 and 1974–1975 events, $\sim$165–170 m^3 s^{-1} for the 1971–1972 and 1969–1970 events, and $\sim$150 m^3 s^{-1} for the 1998–1999 and 1999–2000 events versus 121 m^3 s^{-1} for the average annual discharge but significantly higher than the 'normal' variations (see Fig. 4b). As observed by Wells and Dorr (1987) in the Kosi megafan and discussed by Jones and Schumm (1999), exceptional floods are not necessary for triggering avulsions if other conditions make the river close to the avulsion threshold. However, the Kosi fan is 'very flat' and aggradation rapid (Wells and Dorr 1987) and 'normal' flood are important because of this flat attitude of the fan and of the monsoonal regime of the region. In the Puyo area and the Amazonian domain in general, floods were not registered in the hazard records, except during La Niña events (Demoraes and D'Ercole 2001). In fact, the flat shape of the average monthly discharge curve (Fig. 4a), due to different precipitation regimes in various parts of the upper catchment, does not allow large 'normal' floods and leaves them no great chance of triggering avulsions. As actual floods only occur during La Niña events, the correlation between stronger ENSO events and the avulsions cannot be a simple coincidence. According to Aalto et al. (2003) not only water but also sediment discharge considerably and rapidly increased during La Niña events (Aalto et al. 2003) and most of the aggradation in the Andean floodplains has occurred during La

Nina events. Therefore, La Niña events should have enhanced aggradation in the same time as they caused flooding.

The main avulsion from the Pastaza 1906 to the eastern branch and the avulsion of the Rio X into the Rio Putuimi are obviously much older than 1976 as it is clear that in 1976 the vegetation in the abandoned meander belt was too high for the abandon to have occurred recently. These avulsions may have been triggered by ENSO events older than those recorded in the hydrograms of the Baños station, probably the 1942 or 1916 La Niña events as suggested by the height of the trees greater than 20–30 m and the state of evolution of the forest.

Conclusions

The study of the migrations of the Rio Pastaza in the eastern Subandean Zone of Ecuador (Puyo plateau) over the last century reveals 3 westward avulsions. The main avulsion was achieved in the period 1906–1976 by the annexation of a smaller river flowing in a south-sloping wide tectonic depression formed along the front of the cordillera. A second, smaller-sized, avulsion affecting the beheaded portion of the river occurred in the same period. The third avulsion occurring in the period 1976–2008 is characterized by a gradual shift of flow from the previous avulsive channel to a newly formed westward channel. This partial avulsion involves two branches which have co-existed for more than 30 years. The eastern branch formed first with its channel pattern evolving from highly braided to single channel. All these three avulsions have been controlled by the interplay of the progradation of a braided alluvial fan formed by the Rio Pastaza and tectonic tilting continuously increasing the hinterland-dipping topographic slope. Tectonic backtilting may have acted by enhancing aggradation upstream of the initial site to generate a second avulsion site, in the same time as it offered the avulsed channel a more favorable longitudinal way along the cordillera.

In this framework, the cause and trigger of avulsions could be (1) tectonic backtilting on top of the propagating Subandean Front creating a favorable topographic and sedimentary setup for avulsions, and (2) ENSO (La Niña) events which are responsible for much higher water and sediment discharges and in the climatic context of the study area are the only events able to cause floods and enhance aggradation.

Acknowledgments This study benefited of the logistic and financial support of the IRD (French Institute for Research in Development). This investigation was supported by a doctoral Al*β*an fellowship (no E05D057404EC). The authors thank RSI-France (Envi®) for its technical support. The authors thank J.M. Holbrook, J.-D. Champagnac, and a third anonymous reviewer for their help in improving this article.

References

Aalto R, Maurice-Bourgoin L, Dunne T, Montgomery DR, Nittrouer C, Guyot J-L (2003) Episodic sediment accumulation on Amazonian floodplains influenced by El Niño/Southern Oscillation. Nature 425:493–497

Baby P, Rivadeneira M, Christophoul F, Barragán R (1999) Style and timing of deformation in the Oriente of Ecuador. In: ORSTOM (ed) 4th international symposium of Andean geodynamics, vol 1. ORSTOM, Göttingen, pp 68–72

Baldock JW (1982) Boletín de Explicación del Mapa Geológico del Ecuador. DGGM, Quito

Barberi F, Coltelli M, Ferrara G, Innocenti F, Navarro JM, Santacroce R (1988) Plio-quaternary volcanism in Ecuador. Geol Mag 125:1–14

Barragán R, Baudino R, Marocco R (1996) Geodynamic evolution of the Neogene intermontane Chota basin, northern Andes of Ecuador. J South Am Earth Sci 9:309–319

Bernal C, Christophoul F, Darrozes J, Soula J-C, Baby P, Burgos JB (2011) Late Glacial and Holocene avulsions of the Rio Pastaza Megafan (Ecuador-Peru): frequency and controlling factors. Int J Earth Sci (Geol Rundsch) 100:1759–1782. doi:10.1007/s00531-010-0555-9

Bès de Berc S, Soula J-C, Baby P, Souris M, Christophoul F, Rosero J (2005) Geomorphic evidence of active deformation and uplift in a modern continental wedge-top—foredeep transition: example of the eastern Ecuadorian Andes. Tectonophysics 399:351–380

Brierley GJ (1989) River planform facies models: the sedimentology of braided, wandering and meandering reaches of the Squamish River, British Columbia. Sed Geol 61:17–35. doi:10.1016/0037-0738(89)90039-0

Cohen KM, Stouthamer E, Berendsen HJA (2002) Fluvial deposits as a record for Late Quaternary neotectonic activity of the Rhine-Meuse delta, The Netherlands. Neth J Geosci/Geologie en Mijnbouw 81:389–405

Coque R (2002) Géomorphologie, 6th edn. Armand Colin, Paris

Demoraes F, D'Ercole R (2001) Cartografía de riesgos y capacidades en el Ecuador. Diagnóstico previo a planes de intervenciones de las ONG's. Internal report. COOPI-IRD-OXFAM, Quito (Ecuador)-Université de Savoie (France) Internet site, 65

Gomez N (1994) Atlas del Ecuador, Geografia y Economia. Imagenes de la Tierra, 3, Editoria Ediguias C. ltda, Quito, 114 pp

Harvard Catalog (1999) Hervard seismology, CMT catalog search (updated 1999). http://www.seismology.harvard.edu/CMTsearch.html

Hastenrath S (1981) The glaciation of the Ecuadorian Andes. Balkemma, Rotterdam

Heine K (1994) The Mera site revisited: Ice-age Amazon in the light of new evidence. Quat Int 21:113–119

Heine K (2000) Tropical South America during the Last Glacial Maximum: evidence from glacial, peri-glacial and fluvial records. Quat Int 72:7–21

Hoffer G, Eissen J-P, Beate B, Bourdon E, Fornari M, Cotten J (2008) Geochemical and petrological constraints on rear-arc magma genesis processes in Ecuador: the Puyo cones and Mera lavas volcanic formations. J Volcanol Geotherm Res 176:107–118

Holbrook J, Schumm SA (1999) Geomorphic and sedimentary response of rivers to active deformation: a brief review and critique of a tool for recognizing subtle epiorogenic deformation in modern and ancient settings. Tectonophysics 305:287–306

Humphrey NF, Konrad SK (2000) River incision or diversion in response to bedrock uplift. Geology 28:43–46

Hungerbühler D, Steinmann M, Winkler W, Seward D, Egüez A, Person DE, Helg U, Hammer C (2002) Neogene stratigraphy and Andean geodynamics of southern Ecuador. Earth Sci Rev 57:75–124

IGEPN (2009) Instituto Geofisico de la Escuela Politecnica Nacional, Quito, Ecuador. http://www.igepn.edu.ec

Jones LS, Schumm SA (1999) Causes of avulsion: an overview. In: Smith ND, Rogers J (eds) Fluvial sedimentology VI, special publication of the International Association of Sedimentologists, Blackwell Science, 28:171–178

Kennerley JB (1980) Outline of the geology of Ecuador. Overseas Geol Miner Resour 55:1–16

Laraque A, Bernal C, Bourrel L, Darrozes J, Christophoul F, Fraizy P, Pombosa R, Guyot J-L (2009) Sediment budget of the Napo River, Amazon Basin, Ecuador and Peru. Hydrol Process 23:3509–3524. doi:10.1002/hyp.7463

Lavenu A, Noblet C, Bonhomme MG, Egüez A, Dugas F, Vivier G (1992) New K–Ar age dates of Neogene and Quaternary volcanic rocks from the Ecuadorian Andes: implications for the relationship between sedimentation, volcanism, and tectonics. J South Am Earth Sci 5:309–320

Le Pennec JL, Jaya D, Samaniego P, Ramon P, Moreno Yanez S, Egred J, van der Plicht J (2008) The AD 1300–1700 eruptive periods at Tungurahua volcano, Ecuador, revealed by historical narratives, stratigraphy and radiocarbon dating. J Volcanol Geotherm Res 176:70–81

Legrand D, Baby P, Dorbath C, Bès de Berc S, Rivadeneira M (2005) The 1999–2000 seismic experiment of Macas swarm (Ecuador) in relation with rift inversion in Subandean foothills. Tectonophysics 395:67–80

Ouchi S (1985) Response of alluvial rivers to slow active movement. Geol Soc Am Bull 96:504–515

Reynaud C, Jaillard E, Lapierre H, Mamberti M, Mascle G (1999) Oceanic plateau and island arcs of south-western Ecuador: their place in the geodynamic evolution of north-western South America. Tectonophysics 307:235–254

Schumm SA (1977) The fluvial system. The Blackburn Press

Schumm SA, Dumont J-F, Holbrook JM (2000) Active tectonics and alluvial rivers. Cambridge University Press, Cambridge

Slingerland R, Smith ND (2004) River avulsion and their deposits. Annu Rev Earth Planet Sci 32:257–285

Stouthamer E, Berendsen HJA (2000) Factors controlling the Holocene avulsion history of the Rhine-Meuse delta (The Netherlands). J Sed Res 70:1051–1064

Summerfield MA (1991) Global geomorphology. An introduction to the study of landforms. Longman, Harlow

Tricart J (1952) La partie orientale du bassin de Paris, étude morphologique. Sédes, Paris

Tschopp HJ (1953) Oil explorations in the Oriente of Ecuador. Am Assoc Pet Geol Bull 37:2303–2347

Wells NA, Dorr JA (1987) Shifting of the Kosi River, Northern India. Geology 15:204–207

Winkler W, Villagomez D, Spikings R, Abegglen P, Tobler S, Egüez A (2005) The Chota basin and its significance for the inception and tectonic setting of the inter-Andean depression in Ecuador. J South Am Earth Sci 19:5–19

Yepes H, Chatelain J-L, Guillier B, Alvarado A, Egred J, Ruiz M, Segovia M (1996) The Mw 6.8 Macas earthquake in the subandean zone of Ecuador, October 3, 1995. Seismol Res Lett 67:27–32

Annexe E

Christophoul et al., *en révision*,
Geological Society of London Special Publication

Cet article découle des travaux de thèse de José Burgos. Le piémont amazonien des Andes d'Equateur, de part son contexte particulier dans la structure des Andes : chaîne étroite et prisme chevauchant caractérisé par une tectonique de type thick-skin, induisant un raccourcissement faible (Baby et al., 2013) a favorisé la préservation, en seul dépocentre, de l'histoire Miocène à actuelle d'un piémont orogénique actif. Ce contexte tectonique fait de ce piémont le lieu privilégié pour la compréhension de l'évolution des séries sédimentaire impliquées dans l'évolution morphologique et sédimentologique d'un piémont orogénique actif.

Résumé :

L'étude du remplissage du bassin subandin amazonien des Andes d'Equateur est l'occasion de discuter l'évolution, au cours du temps, des systèmes sédimentaires menant à la mise en place des systèmes fluviaux distributifs (DFS) observables à l'heure actuelle sur le piémont amazonien des Andes.

Le remplissage néogène est constitué de formation fluviales et marines. L'analyse des faciès et des mesures de paléocourants montrent une structuration du réseau de drainage (axial puis transverse) influencée par la structure du bassin et son évolution dans le temps. L'architecture stratigraphique du système montre un schéma progradant comportant une accélération brusque au miocène supérieur. Cette progradation généralisée du système fluvial est aussi perceptible dans l'architecture du DFS quaternaire du Rio Pastaza.

Au premier ordre, la progradation du système est contrôlée par la tectonique andine et plus précisément par la propagation du prisme orogénique vers l'avant-pays. La propagation de ce prisme provoque le soulèvement et l'érosion de l'apex du système alluvial et son déplacement vers l'est. Cette érosion successive des zones d'apex du DFS ainsi que l'évolution du bassin d'avant-pays d'un stade "filled" à "overfilled" montre un faible potentiel de préservation de ce genre de système sédimentaire dans l'enregistrement stratigraphique dans un tel contexte.

Onset and development of a Distributive Fluvial System in the amazon basin (Neogene of the Oriente basin of Ecuador)

Frédéric Christophoul

UMR 5563 GET, Université de Toulouse – CNRS – IRD - CNES, 14 Av, Edouard Belin, F-31400 Toulouse, France

Tel: 00 33 (0)5 61 55 26 70

Fax : 00 33 (0)5 61 33 25 60

frederic.christophoul@get.obs-mip.fr

José David Burgos Zambrano

Petroamazonas, Av. Naciones Unidas E7-95 y Shyris, 4to piso, Quito, Ecuador

Tel: 00 593 (2)467 500 ext 8495

jose_burgos@petroamazonas.ec

Martin Roddaz

UMR 5563 GET, Université de Toulouse – CNRS – IRD - CNES, 14 Av, Edouard Belin, F-31400 Toulouse, France

Tel : 00 33 (0)5 61 55 26 50

Fax : 00 33 (0)5 61 33 25 60

martin.roddaz@get.obs-mip.fr

Carolina Bernal

Facultad de Geologia y Petroleos, Escuela Politecnica Nacional del Ecuador, Ladron de Guevarra E11 – 253 Quito, Ecuador.

Tel : 00 593 2507127 ext. 2533

isabel.bernal@epn.edu.ec

Pierre-Olivier Antoine

UMR - CNRS 5554 ISEM, Université MONTPELLIER 2, Place Eugène Bataillon, F-34095 MONTPELLIER Cedex 05 FRANCE

Tel: 00 33 (0)4 67 14 32 51

Fax : 00 33 (0)4 67 14 36 10

pierre-olivier.antoine@univ-montp2.fr

Jean-Claude Soula

UMR 5563 GET, Université de Toulouse – CNRS – IRD - CNES, 14 Av, Edouard Belin, F-31400 Toulouse, France

Tel : 00 33 (0)5 61 55 26 50

Fax : 00 33 (0)5 61 33 25 60

jean-claude.soula@get.obs-mip.fr

Patrice Baby

UMR 5563 GET Université de Toulouse – CNRS – IRD - CNES; 14 Av, Edouard Belin, F-31400 Toulouse, France

Tel : 00 33 (0)5 61 55 26 72

Fax : 00 33 (0)5 61 33 25 60

patrice.baby@ird.fr

Abstract

The study of the neogene sedimentary infill of the the amazonian subandean foreland basin of Ecuador allows us to investigate the evolution through time, of the sedimentary systems leading to the Distributive Fluvial Systems observed nowadays on the Amazonian foothill of the Andes.

The neogene infill is made of several fluvial and marine formations. Facies analysis and paleocurrents measurements of these formations reveals a distributive pattern and drainage axis influenced by the foreland basin structure and evolution. The stratigraphic architecture of the neogene facies shows a prograding pattern accelerating at the end of Miocene times. This prograding pattern can also be identified in the recent evolution of the Rio Pastaza DFS. At first order, the progradation of the system through neogene times is controlled by andean tectonics and more precisely by the outerland propagation of the subandean orogenic wedge. This propagation of the orogenic wedge progressively uplifts the apex of the DFS, submitting it to erosion. This erosion of the proximal part of the DFS, together with the overfilled stage of the foreland basin seem to indicate a poor potential of preservation of this DFS in the future.

Key words: Foreland basin, Neogene, lithofacies, Andes, DFS, Ecuador.

Introduction

Distributive Fluvial Systems are common geomorphic features and sedimentary systems observed all around the world (Hartley et al., 2010). DFS are characterized by distributive drainage pattern resulting from bifurcations or avulsions and they include alluvial fans, fluvial megafans and alluvial plains. In the last years a great attention was given to the knowledge of DFS in terms of morphology and stratigraphic record of these objects (Hartley et al. 2010; Weissman et al., 2013) evidencing the role of bifurcation and avulsions in their prograding stratigraphic architecture. Weissmann et al., (2013) also pointed out the need of new studies in order to understand the factors originating the prograding trend oberserved in the last studies.

On the Amazon foothill of the Andes, several DFS have been identified from Ecuador to the north (Christophoul et al., 2002; Bernal et al., 2011), Northern Peru (Dumont, 1996; Wilkinson et al., 2010), Southern Peru (Wilkinson et al., 2010) and Bolivia (Horton and DeCelles, 2001; Strub, 2006; Hartley et al., 2010) to the south. The modern Andean foothill of the Amazon basin is made of coalescent distributive fluvial systems described as "Megafans" (Wilkinson et al., 2010). These DFS are separated by inherited structures such as the Miocene forebulge of the north Amazonian foreland basin (Roddaz et al., 2005; 2010) or the topographic high of the Fitzcarrald Arch related to the flat subduction of the Nazca Ridge (Espurt et al., 2007).

During upper Miocene times the nature of the sedimentary system is debated. It was a "marine like megalake" Pebas system (Hoorn et al., 2010; Roddaz et al, 2010) or a fluvial system (Latrubesse et al. 2012). Nevertheless, the origin of the genesis of the widespread distributive fluvial systems of the Amazon basin remains poorly described. The DFSs of the Amazonian Andean Foothill are part of the retro-arc foreland basin and their onset and evolution though times is closely related to the history of the foreland basin (Horton and DeCelles, 2001; Roddaz et al., 2010).

This study focuses on the northernmost DFS of the Andean Amazonian Foothill known as the Pastaza Megafan (Räsänen et al., 1992, Christophoul et al., 2002; Bernal et al., 2011). Due to the incision in its proximal part (Bes de berc et al., al, 2005)

(1) to define the architecture and depositional environment of the Neogene formations of the Ecuadorian foreland basin in relation with andean tectonics, (2) to propose a model of evolution of the neogene sedimentary systems ending up in the modern distributive fluvial systems known nowadays in

96 the Amazon Basin (Horton and DeCelles, 2001 ; Wilkinson et al. 2010; Bernal et al., 2011), (3) to
97 investigate the potential of preservation of this DFS in the sedimentary record taking in account the
98 history of the Amazonian retro-foreland basin.
99 The present study is based on facies analyses of the sedimentary formations of the Ecuadorian
100 amazonian foreland basin together with an updating of the chronostratigraphy and geomorphic mapping.
101
102 **2. Geological background**
103 The Ecuadorian Andes are divided into five fold-thrust belts, which are, from west to east, the
104 coastal plain, the Western Cordillera, the Interandean depression, the Eastern Cordillera and the
105 Subandean zone (Fig. 1 and 2) which overthrusts the Amazonian foreland. The Oriente Basin of Ecuador
106 (Dashwood & Abbots, 1990; Alemán & Marksteiner, 1993), filled with deposits ranging from the upper
107 Cretaceous to the Holocene, constitutes the western part of the wider of the bend-controlled foreland
108 basins of the northern Andes (Fig. 1A).
109 A balanced cross-section trough the front of the Western Cordillera, the Interandean Depression,
110 the Eastern Cordillera and the Subandean Zone shows that the structure of the range in this area results
111 from a complex arrangement of fold-and-thrust structures. The large-scale structure includes, from east
112 to west, basement-involved frontal fold-thrusts (Abitagua Cordillera, Napo dome, Cutucu Cordillera), a
113 large-scale basement-cored fold forming most of the Eastern Cordillera, and a series of imbricate fault-
114 related folds developed in the Interandean Depression (Fig. 2).
115 Growth strata formed in the upper part of the Miocene Chambira-Arajuno formation described
116 below indicate that frontal the Abitagua cordillera and the Napo dome were active in the late Miocene
117 (Christophoul et al., 2002a, b). The Paleozoic to upper Cretaceous rocks constituting the basement of the
118 Eastern Cordillera were deformed and metamorphosed during latest Cretaceous-Paleocene shortening
119 (Pratt et al., 2005). The structures were then eroded and blanketed by a widespread volcanic and
120 volcaniclastic series, the Pisayambo formation aged of 9-10 to 6 Ma (Lavenu et al., 1992; Barberi et al.,
121 1988) that also covers the Interandean Depression and the eastern Western Cordillera (Baldock, 1982),
122 and by lavas issued from the volcano Altar aged of <3.5 Ma (Lavenu et al., 1992). Deformation and/or
123 transport by the Eastern Cordilleran fault-bend fold of these volcanic and volcaniclastic series and of a
124 rather well preserved pediment indicate that the Eastern Cordillera was younger than the late Pliocene
125 (Burgos, 2006). In the Interandean Depression, syntectonic deposits have been dated at 8.5 – 7.9 Ma from

Zircon fission tracks combined with paleomagnetic measurement in the south (Nabon basin, Hungerbühler et al., 1995), at ~6.3 Ma and 3.6 Ma from K-Ar measurements in the north (Chota basin, Barberi et al., 1988; Barragan et al., 1996), and 2 to 1.5 Ma from K-Ar measurements in the central part (Lavenu et al., 1992).

The Oriente Basin is shared between the Subandean Zone to the west and the Amazonian foredeep to the east (Fig. 1), being traversed by the Subandean Frontal Thrust fault, which has transported the Subandean Zone over the Amazonian foreland. The Subandean Zone involved in the Oriente basin is constituted by two frontal 'pop-up'-like antiformal culminations, the Napo dome to the north and the Cutucu cordillera to the south (Balkwill et al., 1995; Baby et al., 1999; Kley et al., 1999, Bès de Berc et al., 2005), separated by an axial depression, known as the 'Pastaza depression' (Fig. 1). The Napo and Cutucú antiforms deform Jurassic formations (the volcanic Misahuallí Formation in the Napo antiform and the sedimentary Santiago and Chapiza Formations, in the Cutucú antiform), and Cretaceous/Tertiary formations, (the Hollín, Napo, Tena, Tiyuyacu, and Orteguaza Formations., Baldock, 1982) (Fig. 1B). In the 'Pastaza depression', the pre-Miocene sedimentary strata are unconformably overlain by the Neogene strata studied in the present paper.

To the east, the Amazonian lowlands contain sedimentary formations ranging from Cretaceous to Quaternary (Christophoul et al., 2002b). The pre-Miocene strata are weakly deformed by the positive tectonic inversion of NNE-SSW Triassic-Jurassic grabens (Balkwill et al., 1995; Baby et al., 1999; Barragán et al., 2004, 2005) and topped by the Miocene, Pliocene and Pleistocene deposits of the Pastaza Megafan (Räsänen et al., 1990, 1992; Christophoul et al., 2002b, Bès de Berc et al., 2005; Roddaz et al., 2005).

3. Stratigraphy

Four formations have been recognized in the Neogene of the Oriente Basin (Tschopp, 1953, Bristow & Hoffstetter, 1977; Baldock, 1982) and approximately dated (Fig. 3): the Chalcana Formation of Upper Oligocene through Miocene age, the Arajuno Formation of Upper Miocene age, the Chambira Formation of Upper Miocene through Pliocene age. The Curaray Formation is considered as the easterly equivalent of the Arajuno Formation. We can add to these formations the quaternary and modern Rio Pastaza DFS (Bernal et al., 2011).

In order to define their age, all the available biostratigraphic ages of the Neogene formations (Labogeo: 1991, 1992a, b, and c) were synthesized and integrated in the most recent Neogene

biostratigraphic charts established in northern South America (Lorente, 1986; Muller et al., 1987; Rull, 2002; Hoorn, 1993, 1994; Whatley et al., 1996; Wesselingh et al., 2002). These biostratigraphic ages were compared with AFT ages.

3.1. Chalcana Formation

The Chalcana Formation (Tschopp 1953) reaches a total thickness of approximately 800 m in its type locality (geological map of Tena, scale 1:100 000, INEMIN, 1986) and crops out along the eastern flank and southern nose of the Napo antiform (Fig. 1A). The Chalcana Formation comprises variegated clays, intercalated with fine grained sandstones and siltstones. The Villano-2 well (western part of the basin, Fig. 1) yields impoverished miospore assemblages in the upper part of the Chalcana Formation (*Laevigatosporites* sp.), associated with freshwater alga *Pedastrium delicatites* (Edwards, 1993). In the Vinita well (northern part of the Oriente Basin) sporomorphs (*Cicatricosisporites criatus*, *Magnastriatites howardi* and *Verrucatosporites usmensis)* were also encountered. The *Magnastriatites – Cicatricosporites dorogensis* Zone documents the Oligocene in Venezuela (Lorente, 1986) and Northern South America (Muller et al., 1987), whereas the *Verrutricolporite*s - *Cicatricosisporites* Zone is reported in the Early Miocene (Lorente, 1986). The Chalcana Formation yields also charophytes oogones (*Tectochara* cf. *ucayaliensis*), which is known in the Peruvian Chambira Formation (quite different from the Ecuadorian Chambira Formation described below) of the Marañon Basin (Gutierrez, 1975). The 19-23 Ma AFT age of the lower part of the overlying Arajuno Formation (Ruiz, 2002) excludes the top of the Chalcana Formation to be younger than the earliest Miocene. Thus, in agreement with Zambrano et al. (1999), we assign a Late Oligocene to earliest Miocene stratigraphic range for the Chalcana Formation.

3.2. Arajuno Formation

The Arajuno Formation (Tschopp 1953) crops out along the Arajuno River (right bank tributary of the Napo River), (Fig. 1A). The bounding surface between the Arajuno and Chalcana Formations is conformable and gradual (Campbell, 1970). The following fossils were reported: foraminifera *Bathysiphon* sp., *Psammosphaera* sp., *Trochammina* sp., and *Valvulina*? (Bristow & Hoffstetter, 1977). The Villano-2 well yielded frequent *Echiperiporites* and only one specimen of *Echitricolporites maristellae*. Freshwater fern spores *Azolla* are also common in this interval. *Echitricolporites maristellae* is a fossil guide from late Early Miocene Zone 27 (Late Aquitanian - Burdigalian), covering a range of ~22 - 16.2 Ma (Muller et al., 1987;

186 Rull, 2002). AFT and Zircon Fission Tracks (ZFT) ages of 22 Ma (earliest Miocene) have been found by
187 Ruiz (2002) in samples of volcanic origin from the base of the formation. The age of the upper part of the
188 Arajuno formation is less constrained.
189
190 **3.3. Chambira Formation**
191 The Chambira Formation is absent in the Napo and Cutucú antiforms, but crops out in the Pastaza
192 Depression near the southern nose of the Napo Antiform (Talag syncline, west of Tena).
193 The Chambira formation is considered to be barren of fossils. Nevertheless, in the uppermost part
194 of the section of the Villano-2 well, in the western part of basin, the highest occurrence of *Verrucatotriletes*
195 *etayoi* is described in cutting samples (Edwards, 1993). The first downhole appearance of
196 *Crassoretitriletes vanraadshoovenii* in the lowermost interval of the section indicates the Middle Miocene
197 (Muller et al, 1987). Hoorn, (1993) confirms the occurrence of this species in the Late Miocene. Thanks to
198 biostratigraphic markers and stratigraphic relations with the underlying Arajuno Formation, we can
199 consider the Chambira Formation to be Middle to Late Miocene in age. More precise dating is impossible
200 with the presently available data. Previous interpretations attributing a Pliocene age to this formation
201 (Tschopp, 1953) cannot be entirely ruled out but might only apply to the uppermost part of it.
202
203 **3.4. Curaray Formation**
204 The Curaray Formation crops out along the Curaray River (Tschopp, 1953). This formation is
205 quite problematic for its vertical and spatial extension is not very well known (Tschopp, 1953; Bristow &
206 Hoffstetter, 1977; Sauer, 1965; Baldock, 1982). The fauna comprises fish and crustacean remains, turtles,
207 teeth and bones of crocodiles, molluscs, ostracods and arenaceous foraminifera. An assemblage of
208 arenaceous foraminifera found in the eastern part of the basin (Tiputini well, Fig. 1A) is described as
209 "*Ammobaculites* B" fauna by Tschopp (1953). It comprises: *Ammobaculites* (2 sp.), *Sigmoilina* sp.,
210 *Polytstomella* sp.. *Rotalia* sp. pelagic foraminifera were also encountered. Other fossils reported here such
211 as *Cytheridea* cf. *kollmani* indicative of Late Miocene, and *Cyprideis* aff. *howei* (today *Vetustocytheridea*
212 *bristowi*) have also be found in the Loyola and Mangán Formations of the Miocene Cuenca Basin, southern
213 Ecuador (Bristow & Hoffstetter, 1977; Hungerbühler et al.,2002). The Loyala formation was dated with
214 zircon fission tracks (ZFT) at 13.9±1.4 and 11.1±1.0 Ma (Serravallian-Early Tortonian, Hungerbühler et al.,
215 2002) and the Mangán Formation at 9.9±1.2 to 9.5±1.0 Ma (Tortonian, Hungerbühler et al., 2002). In the

Vinita well, *Retitricolporites guianensis*, *Zonocostites ramonae, Laevigatosporites* sp. and the foraminifera *Ammonia beccarii* were encountered (Labogeo, 1991). On the basis of these biostratigraphic markers and correlated radiometric ages, we can consider the Curaray Formation to be Middle to Late Miocene in age. This age confirms that the Curaray Formation is a lateral equivalent of both the Arajuno and Chambira formations.

3.5 Mera Formation

The Mera Formation crops out in the subandean zone, the best exposure locates along the Rio Pastaza in the Puyo area (Fig. 1). It is made of conglomerates made of quartz and volcanic clasts. Due to the coarse grained deposits, no biostratigraphic data are available. The top of the formation consist in a pediment (Bes de Berc et al., 2005) which datings show agave 40 000 to 20 000 yrs Cal BP (Bes de Berc et al., 2005). Due to its stratigraphic position (above the Chambira Fm.), a Pliocene and Pleistocene age was attributed to this formation by Tschopp, (1953) and Baldock, (1982).

4. Sedimentology

4.1. Paleocurrents

New outcrops provided by road enlargements were studied in terms of facies analysis of fluvial deposits following the architectural elements method, Miall (1978, 1985) and Best (2003). Paleocurrent measurements were performed on planar bedding, trough cross bedding, and imbricated clasts and processed by mean of classical methods (Potter & Petitjohn, 1963; DeCelles et al., 1983)

In the Chalcana Fm., paleocurrents (mainly measured on lee side of ripples and megaripples) indicate two main directions of paleoflow: NNW-SSE which would correspond to the protoandean tributaries and N-S which would indicate a longitudinal drainage, parallel to the strike of the Andean orogen (Fig.4A).

In the Arajuno Fm, paleocurrents measurements (performed on the lee side of ripples and megaripples) reveal easterly and north-south main paleoflow directions as in the Chalcana Formation but the easterly paleocurrents are dominant, in particular in the west, and the longitudinal drainage axis is shifted eastward (Fig. 4B). Paleocurrents measured in the Chambira formation show that this system was flowing from southwest to northeast in the west and from east to west in the east of the basin (Fig. 4C).

The paleocurrents measured show a progressive change in drainage pattern from a transverse drainage issued from the Andean cordillera leading to a transverse drainage parallel to the Andean range.

The axial drainage axis is located in the modern subandean zone. Later, during the deposition of the Arajuno and Curaray Fm. , this drainage pattern remains the same but an eastward shift of the axial drainage axis can be observed. Finally, the drainage pattern changes to a transverse drainage pattern with the deposition of the Chambira Fm. Since these times, the drainage pattern remained transverse as it can be seen nowadays.

4.2- Facies and paleoenvironments

In the next paragraphs, facies associations will be described. Facies associations mainly dominated by fine deposits are designated by F, dominated by sands by S and dominated by gravels by G. On the various sections and outcrops presented in this study, 15 Lithofacies were identified. They are presented on Table 1.

4.2.1. Chalcana Formation

a - Facies associations

The best exposed sections of the Chalcana Formation are along the Aguarico River (northern part of the basin). Deposits are very fine to fine and mainly consist in reddish laminated shales (Fl lithofacies, Miall, 1996, see Table 1).

F1:These reddish shales are sometimes rooted (Fr lithofacies) and exhibit variegated rooted beds (P lithofacies). These lithofacies are classically interpreted as more (P: Bk Horizon) or less (Fr) mature entisols (Retallack, 2000). The sandstones can be grouped into 3 types:

S1: Very fine to fine sandstones forming some 10 cm thick and >10 m long tabular beds with lithofacies Sh, Fr, Fl.

S2: Concave up-based and flat-topped lentiforms made up of fine to medium-grained sandstones exhibiting Sh, St and Sr lithofacies.

S3: Coarser-grained and fining-upward deposits only found in the Apuya River section, showing from base to top the succession of lithofacies Gt, Gt-St, St, Sp and Fl (Fig. 5).

b - Interpretation

The association of fine deposits (Fl, P, Fr) constitute FF architectural elements (Miall, 1985, 1996) and is likely to characterize floodplain environments (Fig. 5). The occurrence of P lithofacies is believed to indicate a quite stable floodplain allowing a long-term weathering. Very fine to fine sandstones (group (1) can be interpreted as LS architectural elements (laminated sandsheets, Miall, 1996). Concave up based

and flat topped sandstones (group (2) can be interpreted as a multi-storey channel infill (CH element, Miall, 1996). The last type of sandy bodies (group (3) exhibits a succession of lithofacies showing a progressive abatment of current velocity. This is classically interpreted as a result of the migration of a sandy macroform (Miall, 1996, Best, 2003). The paleocurrent data (Christophoul et al. 2002b), indicate that this migration (mostly E-W) is transverse with respect to the main current direction (NW-SE, see Fig. 4A). So, this macroform can be interpreted as a Lateral Accretion macroform (LA architectural element, Miall, 1996).

The previously described lithofacies and architectural elements enable us to interpret the Chalcana Formation in terms of fluvial environments. The abundance of fine-grained deposits and the predominance of shales indicate low energy environments, where fine sediments are dominant. The LS architectural elements interbedded with floodplain deposits (FF, Table 2) are interpret as crevasse splays recording the periodic influx in the floodplain of sediments issued from nearby channels. The occurrence of LA architectural elements indicate a fluvial style (Miall, 1985) dominated by lateral accretion as observed in meandering rivers (Miall, 1978, 1996, Best, 2003). In contrast, the CH elements cannot be interpreted as main channels in a meandering system because they have symmetrical geometries and limited extents (several meters at most). It is likely that these fine-grained CH elements were crevasse channels. The occurrence of these CH elements, regularly interbedded with FF elements confirms this interpretation. The fluvial environment of the Chalcana Formation may be interpreted as a sandy load meandering system with a coeval floodplain periodically invaded by crevasse splays/channels and fine sediments during floods (Miall, 1996).

4.2.2. Arajuno Formation

a – Facies Associations

The Arajuno Formation is made up of reddish sandstones, shales and siltstones. The sandstones contain lithic fragments, predominantly black, rounded milky quartz pebbles, 2 to 3 cm wide, small andesitic clasts, and fine-laminated medium grey phyllites. The shales are predominantly reddish brown, blue grey, light green grey, and white. The siltstones are variegated, orange, white, cream, occasionally light green. The siltstones are occasionally observed grading to shales or as a silty matrix with floating fine sand grains grading to fine sandstone. On the whole, the Arajuno deposits are coarser than those of the underlying Chalcana Formation with conglomerates (almost absent in Chalcana Formation sediments),

306 and less frequent shales. The fine deposits represent here <25% of the thickness of the formation instead
307 of >50% in the Chalcana Formation.
308 Three sections of the Arajuno Formation are presented in Figure 6. The stratigraphic relationship between
309 these sections is displayed in Fig. 6A. The Arajuno River section (Fig. 6D) represents the base of the
310 Arajuno Formation while the Puyo-Arajuno and the Puyo-Canelos road sections (Fig. 6B and 6C) represent
311 its upper part.
312 The fine deposits are quite monotonous all along the three sections. We identified two facies associations:
313 **F1:** This facies association represents the major part of the fine sediments encountered along the three
314 cross sections (Fig 6A, 6B, 6C, 7A, 8 and 9). It is made of reddish shales, siltstones and occasionally fine-
315 grained sandstone exhibiting Fl and Fsm lithofacies. Locally, the material is rooted, display variegated
316 colors and exhibit Fr lithofacies. Occasionally are observed pedogenic features showing an incipient
317 differentiation of soils horizons with non-amalgamated calcareous rhyzoconcretions, (Bk horizon,
318 Retallack, 2000), P lithofacies (Table 1). F1 is similar to F1 of the Chalcana Fm (see previous praragraph).
319 **F2:** This facies association has been recognized in the lower part of the Puyo Canelos road cross section
320 (Fig. 6C). It is essentially made of meter thick variegated reddish shales and silts exhibiting Fr lithofacies.
321 These shales and silts are interbedded with reddish silts grading to fine sandstones organized in tabular
322 beds less than one meter-thick with St and Sh lithofacies. Interbedded within the shales, we identified
323 centimeter-thick wavy beds of carbonates (Cr lithofacies, Table 1) succeeded by laminated reddish shales
324 and siltstones with pedogenetic features (Fr and P) and exhibiting mudcracks (Fig. 8).
325 Sandstones and conglomerates are organized in simple or complex facies associations which correspond
326 to single and multi-storey channels. 6 different facies associations have been identified.
327 **S1:** it corresponds to fine-grained sandstones with occasional conglomeratic laminations containing clasts
328 up to 1 cm large. The sandstones show St lithofacies and are organized into concave up-based lenses ~10
329 cm thick. The conglomerates laminas exhibit well-rounded quartzitic clasts with a diameter up to 1 cm.
330 They form concave-up to sigmoidal based meter thick bodies with Sp, St and Sr lithofacies. These
331 sandstones bodies are interbedded with fine deposits. Their basal contact is sharp but shows no evidence
332 of scouring even though the top of the bodies exhibit a gradual fining upward transition with the overlying
333 fines (Fig. 7). This facies association is most frequent near the base of the section (Fig. 8).
334 **S2:** consists in a successions of fine- to medium-grained sandstones, exhibiting St, Sp and Sh lithofacies
335 organized into 1 to several meters thick tabular to wedge-shaped bodies. Sr lithofacies was identified in

meter-wide and centimeter-thick scours (cut-and-fill structures). The typical geometry of S2 is illustrated on Figure 9 B.

S3: was only encountered on the higher part of the Rio Arajuno section. It comprises red fine- to medium-grained sandstones exhibiting St, Sp and Sh lithofacies, organized into tabular bodies, or cut by conglomerates. These conglomerates contain milky quartz pebbles up to 5cm wide, mostly exhibiting Gp and Gt lithofacies. They are organized into thick concave-up lentiforms or tabular beds. The stacking pattern of conglomerates beds is complex with numerous reactivation surfaces. These conglomerates are topped either by red sandstones or, directly, by fine deposits showing F1 facies association. In both cases the contact is sharp and flat.

S4: is observed in the highest part of sections 6B and 6C. It is composed of meter thick pebbly sandstones with pebbles up to 1 cm, exhibiting most frequently Sh lithofacies (Table 1) but also Sp. The shape of these bodies is in general difficult to recognize because of the limited size of the outcrops. However, the larger outcrops (more than 10m along road) suggest that they are tabular bodies. No evidence of erosion is observed at the base of the pebbly sandstone beds and the contact with the underlying S3 sandstones is progressive. Each of these sequences of S4 facies association is several meters thick.

G1: The coarsest facies associations of the Arajuno Fm were identified in the upper part of the sections exhibited on Figure 6 D. It consists in metre thick tabular beds exhibiting Gt and Gh lithofacies. Beds exhibit no erosional base. Metre wide and centimeter thick sandy lenses interbeded between conglomeratic bed were identified, they exhibit Sr lithofacies. The paleocurrents showing a strike to the south on figure 4B were measured on imbricated clasts in this facies association.

b - Interpretations

In terms of architectural elements, the facies association F1 already found in the Chalcana Formation can similarly be interpreted as FF elements. In the Arajuno Formation, the immaturity of the paleosoils gives another support to this interpretation. The occurrence, at the base of the Puyo-Canelos road section (Fig. 6C) of limestones related to mudcracks and dolo/calcretes (F2) appears as a peculiarity of the Arajuno Formation. This would indicate that the floodplain deposits were submitted at this time to an intense drying. The association of limestone crusts with mudcracks has been described as characteristic of playa environments (Reading, 1978, p.89-91; Leeder & Gawthorpe, 1987). We have therefore differentiated this "dry" floodplain environment (architectural element PL, Table 2) from the "classic" floodplain environment (element FF).

366 The S1 facies association could be interpreted as Lateral Accretion macroforms (Miall, 1985, 1996) as
367 suggested by the lithofacies associations and the overall sigmoidal shape of the sand bodies and they have
368 yet been identified as such (meander bars in Ruiz, 2002). However, compared to typical LA elements (Fig.
369 7), these elements lack Gt lithofacies at their base, which might give less support to the interpretation. In
370 fact, in the classical models of pointbars (Bernard et al., 1962; Allen, 1963) or in LA elements as defined by
371 Miall (1985, 1996), the basal Gt lithofacies correspond to lag deposits resulting from reworking of the
372 channel floor. Such a reworking does not necessarily act all along the channel and the absence of Gt
373 lithofacies can not be considered as a major obstacle to the interpretation of F1 as lateral accretion bars.
374 The strike of the accretion surfaces (N-S) being perpendicular to the regional paleocurrent direction
375 determined by Christophoul et al. (2002b) (Fig. 4B) provides an independent support to this
376 interpretation.
377 The sandstones with S2 facies association can be interpreted as Downstream Accretion macroforms (DA,
378 Miall, 1996) because of their wedge-like shape and the presence of St, Sp and Sh lithofacies.
379 The pebbly sandstones of facies association S4 exhibit Gh, Gt lithofacies and show frequent imbrications of
380 clasts (laminas of pebbles). Although sand is predominant, these pebbly sandstones can be interpreted as
381 gravel bars according to Miall (1996) who showed that the maximum grain size traduces the main
382 characteristic of the transporting flow (GB element, Miall, 1985, 1996). The near-tabular shape of the beds
383 well agrees with this interpretation.
384 The complex arrangement of the lithofacies involved in the S3 facies association and the
385 numerous reactivation/erosion surfaces differs fundamentally from the simple internal geometry of the 3
386 other sandy facies associations (S1, S2 and S4). We can thus consider that S3 depicts multi-storey
387 channels whereas S1, S2 and S3 refer to single-storey channels. Accordingly, we interpreted the sequences
388 showing S3 facies association as CH elements (Table 2). As pointed out by Miall (1985), CH elements are
389 nothing less than a superposition of other architectural elements. Within the S3 facies association, we
390 could recognize the architectural elements by their facies rather than by the geometry of the bodies which
391 are truncated by erosional surfaces. Most of the conglomerates identified in S3 facies associations show Gt
392 and Gh lithofacies with clasts imbrications. We can interpret these facies as the expression of gravel bars.
393 The two facies Gt and Gh could represent gravel dunes. A gravel dune being rather long, this implies a low
394 angle for the stoss-side and considered at outcrop scale this part of the dune will appear to be more or less
395 horizontal (Gh). If so, the Gt facies could represent the lee-side of the dunes. The sandstones forming S3

396 associations (St and Sr lithofacies) are located on top of the conglomerates beds with no scouring of the
397 underlying conglomerates. This apparent continuity in the deposition of the conglomerates and
398 sandstones strongly suggests a continuous depositional process. This would indicate that the gravel/sand
399 succession marks an abatment in shear stress such as those observed during a hydrologic cycle (high
400 water stage / low water stage). The whole succession is therefore interpreted as a Gravel Bars (GB
401 architectural element, Miall, 1985).

402 As a whole, the Arajuno Formation exhibits the assemblage of LA, DA and GB elements. LA is
403 dominant in the lower part of the formation (Fig. 5A) whereas DA and GB are present only in the upper
404 part (Fig. 6B, 6C). In terms of fluvial environments, there is a unique model, the gravel-wandering rivers
405 (Church, 1983; Miall, 1996), where LA and DA elements co-exist. Nevertheless, we observed most of the
406 LA elements at the base of the Arajuno Formation (Fig. 6A) and most of the DA elements higher in the
407 section (Fig. 6A), together with GB elements. We interpret this succession as the consequence of a change
408 in fluvial style, from meandering rivers (characterized by LA elements) at the base and braided channels
409 (coarser and dominated by DA and then GB elements) at the top. This interpretation is confirmed by the
410 increase in grain size compared to the Chalcana Formation, and the reduction of the floodplain / channel
411 infill ratio.

412 **4.2.3. Chambira Fm.**

413 a. **Facies associations**

414 In the Talag syncline (Fig 10A and B), at the contact with the Eastern Cordillera frontal thrust
415 fault, the Chambira strata are overturned with an eastward dip. To the east of the contact, strata dip is to
416 the east and decreases progressively, showing a progressive unconformity (Fig. 11C). The Chambira Fm. is
417 made of quartz pebbles-bearing conglomerates (locally more than 90%) included in a quartz-rich clayish
418 matrix, with less the red beds which characterized the other formations. Granite clasts are absent. This
419 may be due to the intense weathering of granitoid rocks or more probably to the presence of a Mesozoic
420 cover then removed by erosion (Fig. 2C-2G). The average grain size in the Chambira Fm. is coarser than in
421 the Arajuno Fm.

422 Two sections were logged in the Talag syncline Vicinity. The first (Fig. 12A) was logged in the
423 progressive unconformity (western limb of the Talag syncline, fig 11A and B). The second (Fig 12B)
424 locates eastward on the forelimb of the Costa Azul anticline and shows the relations between the Arajuno
425 and Chambira Fms (Fig. 11B). On these two sections, three facies associations where encountered:

F1: This facies association was only identified in the distal part of the Chamibra Fm in the Talag Syncline (Fig. 12 B). Its is made of reddish shales exhibiting horizontal laminations (Fl lithofacies) and massive rooted shales (Fr).

G1: This facies association was mainly identified on the Costa Azul Anticline section. It corresponds to the interbedded with decimeter-thick and meter-wide concave-based and flat-topped sandy lenses. The conglomerates mainly exhibit lithofacies Gt (Miall, 1996, Table 1) but also Gh and Gp. The sandy lenses mainly exhibit St lithofacies. Higher in the section, the conglomerates are replaced by meter-thick beds of alternating conglomerates showing Gh, Gt lithofacies and pebbly sandstones with horizontal bedding (Gh/Sh) and low angle trough cross bedding (Gt). Fr lithofacies were encountered at the top of some concave-up based and flat-topped beds of pebbly sandstones (Fig. 11B).

S1: This facies association was encountered on both sections. It consists in pebbly sandstone exhibiting Sh/Gh (depending on the pebbles proportion) and St/Gt lithofacies. They are organized in tabular meter thick beds.

b - Interpretations

In terms of architectural elements, the facies Association G1 (Gt, Gh and Gp lithofacies associated with St sandy lenses) can be interpreted as migrating gravel bars (GB, table 2). These GB elements exhibit characteristics described by Smith (1990) as those of the different types of gravel sheets growth encountered in deep braided channel. The beds of pebbly sandstones (facies association S1) exhibiting Gh/Sh and low angle Gt lithofacies may correspond to Sandy Bedforms (SB, Table 2). However, considering that pebbles are located in laminas interbedded with Sh lithofacies, those deposits can be interpreted as high regime deposits (Fr>1). This interpretation fits well with the occurrence of low angle cross bedding, which is characteristic of high velocity currents (Miall, 1996). Facies association F1 can be interpreted as floodplain deposits. They are identical to those identified in the Arajuno Fm.

The association of the architectural elements GB and SB may characterize a high energy fluvial system. The bedforms GB and SB are known to be associated in gravel braided channels (Leopold et al., 1964; Schumm, 1977, Miall, 1985). This type of channels known for their rapid displacement is consistent with the low preservation of floodplain deposits (Fr lithofacies). Compared to a classic facies model, it would correspond to a Gravel Braided fluvial system (Miall, 1996).

4.2.4. Curaray Fm.

According to Tschopp (1953) *"This formation consist of well bedded light grey to blue-green or reddish, in some places gypsiferous clays which alternate with fine to medium grained sandstones. Tuffaceous admixtures, lignitic seams, and coally black clays are common in the upper part".* The lowermost part shows micaceous sandstones, with a green clay matrix, grading up to medium-grained sandstones, and culminating in pebbly sandstones with well rounded milky quartz and black metamorphic schists. This sandy interval has a thickness of 3 m. The facies are from bottom to top: sandstone massive (Sm), sandstone horizontal (Sh), and gravel horizontal (Gh), with an overall coarsening-upward trend. The section continues with an interval of 1.8 m of fine-grained deposits showing a sharply basal contact. At the base, structures such as "herring bones" were identified, which can represent bidirectional flux in a tide-influenced environment. Along the Puyo-Tena road, the Curaray Formation is made up of sandstones showing ripple cross lamination. Ripples show mostly "climbing ripples" and exhibit a heterolithic lamination that we interpret as mud couplets such as those preserved in subtidal environments (Hovikoski et al., 2005).

4.2.5 – Mera Fm and quaternary deposits

The Mera Fm overlays the Chambira and Curaray Fms (Fig. 1). The Mera Formation crops out in the subandean zone in the vicinity of Puyo (Fig. 1) where it corresponds to 50m high cliffs on the left Bank of the Rio Pastaza. The Mera Fm. is made of conglomerates with sandy matrix and sands. These sands and conglomerates exhibit two facies association.

G1 : Conglomerates are made of volcanic bearing and quartzitic clasts. Clasts grain size varies from 1 cm to several tenth centimetres, while matrix grain size ranges from medium to very coarse. They are organized in concave based and flat-topped and convex-up decimetre thick beds. They exhibit Gh, Gp and Gt lithofacies (Table 1). These deposits can be interpreted as gravel bars (Miall, 1985).

S1 : Sands are scarce, they exhibit mainly St lithofacies and Sp in a few cases. They are organized in centimetre thick and metre wide lenses. These lenses take place in swales between two conglomeratic gravel bars. They are in some cases affected by the erosional base of an overlying gravel bar. These sandy lenses can be interpreted as SB architectural elements corresponding to sand dunes covering gravel bars in secondary channels.

The association of GB and SB architectural elements let us to interpret the Mera Fm as corresponding to gravel bed braided streams, very similar to the modern Rio Pastaza (Bes de Berc et al., 2005; Bernal et al., 2012).

Bernal et al. (2011) investigated the late Pleistocene and Holocene evolution of the Rio Pastaza DFS. Since the Last Glacial Maximum, the Rio Pastaza DFS was the siege of 108 avulsions (Bernal et al., 2011). The location of the avulsion sites, the available radiocarbon ages as well as historic maps of the seventeenth century, shows an evolution of the migration and avulsions of the Rio Pastaza since the LGM. The first avulsions of the Rio Pastaza occurred after the LGM roughly parallel to the Subandean front and gave rise to a well-defined fan-shaped distributive pattern associated with meander belts (Fig. 13). In response to thrust-related anticline forelimb tilt, the Rio Pastaza and the apex of the megafan were progressively shifted eastward until the ''Great Diversion'' of the Rio Pastaza changed its course to the east-southeast towards the present-day Rios Tigre and Corrientes (TCA) (Fig. 13) where alluvial ridges exhibit straight channels in the proximal part and anastomosing pattern in the distal one. Around 9,200 ± 200 or 8,480 ± 110 Cal years BP, avulsions occurred in the TCA (Fig. 13). The Rio Pastaza abandoned then its east-southeast course and the Tigre-Corrientes area to follow its present-day southerly course. This last avulsion was older than 1691 AD (Fig. 13). The average recurrence time of avulsions in the Marañon-Pastaza area, probably overestimated, ranges between 142 ± 6 years and 189 ±6 years whereas in the TCA, the average recurrence time of avulsions is underestimated and ranges from 342 ± 5 years to 426 ± 10 years.

The map of the abandoned and active channel belts and the number of avulsions sites mapped (Fig. 13) show avulsion where more frequent in the proximal part of the Pastaza DFS (MCA on fig. 13) with juxtaposed wide channel belts, while the distal part of the DFS (TCA an PCTB), channel belts are narrower and exhibit a greater development of floodplain. The high concentration of channel belts and avulsion sites in the proximal and older part of the DFS (MCA) as well as the higher frequency of avulsions seem to indicate accommodation was lower while the distal part exhibits higher accommodation. We can interpret this scheme, with lower accommodation in the proximal part and higher in the distal one, in space and time, as the expression of the progradation of the DFS since the LGM from the subandean front to the Amazonian lowland.

In terms of controlling factors, regional tectonics is active in the northwest of the Marañon-Pastaza area (Bes de berc et al., 2005) and responsible for thrust-related anticline eastward forelimb tilt, and lateral propagation is believed to have controlled most of the avulsions in this area (Bernal et al., 2012). No such tectonic control seems to have acted in the distal part (MPA and TCA). The characteristics of the hydrologic cycles of the Rio Pastaza doe not allow ''hydrologic'' driven avulsions such as those

known in areas characterized by contrasted hydrologic cycles invoked by Leier et al. (2005) in other megafans. Climatic fluctuations or pulses in sedimentary fluxes, not clearly related to volcanic activity as previously proposed by Räsänen et al. (1990), seem to be the most likely cause of avulsions in those areas.

5. Discussion

5.1 - Evolution of the sedimentary system

The facies analyses and new age data presented above allow us to propose a new model of spatial and temporal evolution of the deposits in the Oriente Basin of Ecuador (Fig. 14).

The Chalcana Formation is known all over the Oriente Basin exhibiting the same facies association with no apparent proximal/distal changes (Christophoul et al., 2002a, 2002b). This formation is also isopachous (Christophoul et al., 2002a) and represents a shallow-dipping floodplain environment with unstable channels mainly oriented ~southeast.

The Arajuno Formation is observed in the Subandean Zone and pass westward (Talag syncline) to the base of the Chambira Formation (Fig. 14). Floodplain deposits are there more abundant in the lower than in the upper Chambira Formation and the series shows a coarsening upward trend, even though the same type of conglomerates is observed. The thickness decreases rapidly east of the Subandean Thrust where the Chambira Formation overlies the Arajuno Formation (Fig. 14). The Curaray Formation is only known in the east of the Oriente Basin.

This, and the fossil and AFT ages show that the time range of the Chambira Formation and Arajuno Formation are quite similar and these two formations must be considered as lateral equivalents (Fig. 14). The paleocurrents in the Arajuno and Chambira formations indicate map-scale transverse and diverging paleoflows, indicating a distribuary pattern. The large dispersion of paleoflows in the Curaray Formation is consistent with its distal position in the system.

Therefore, the different formations in this area can be considered to represent differing parts of an alluvial fan system. The Chambira Formation belonged to the proximal part of the alluvial fan system characterized by braided streams while the Arajuno Formation corresponded to the distal part characterized by wandering to meandering streams in an alluvial plain. The “Chambira” facies

associations overlapping the older “Arajuno” facies associations indicate eastward progradation of the fluvial fan.

The “marine” deposits of the Curaray Formation constituting eastward lateral equivalents of the Arajuno/ Chambira fluvial deposits show that this alluvial system debouched into the Maine-like Pebas Mega-lake. Replaced in the frame of the Neogene north western Amazonian basin, it is likely that the deposition of the Curaray Formation was contemporary with the Pebas “marine-like megalake” recognized in the Marañon Basin of Peru and dated of the middle and late Miocene (Wesselignh et al., 2002). The lack of sedimentological data between the areas where the Arajuno/Chambira Formations and the Curaray Formation crop out made us unable to characterize the transition (delta or estuary). Nevertheless, the progradation of the fan-like alluvial system and the high dispersion of paleoflow orientations strongly favors the delta hypothesis.

The observations reported in the present paper also show that the very apical part of the Miocene alluvial fan system of Ecuador is missing and was actually situated in place of the present-day Eastern Cordillera: (1) Outcrops of the Chambira Formation being seen at Talag, in the southern nose of the Napo Dome, and on the northern nose of the Cutucu dome, ~100 km to the south, indicate that the width of the fan was there rather large; (2) The paleocurrents in the Chambira-Arajuno Formation (see also Christophoul et al., 2002 a and b) converge toward a point situated in the westernmost Eastern Cordillera or the Interandean Depression, in prolongation of the upper Napo or Pastaza valley. Such a convergence of paleocurrents has been classically used for evidencing the apex of distributary fluvial systems (Howard, 1966, Petitjiohn et al., 1987, Horton and DeCelles, 2001, Uba et al, 2005). (3) The clasts in the westernmost Chambira Formation are relatively small-sized (<1 cm), well rounded, and almost exclusively constituted of quartz whereas bedrock at the vicinity or farther from the outcrops are metamorphic and volcanic rocks as well as granitic rocks. This indicates a mechanical selection of the more resisting material during a relatively long fluvial transport.

The western origin of the Neogene deposits of the Oriente basin was first demonstrated by means of petrographic studies (Baldock, 1982). Hoorn (1993, 1994, 1996), using heavy minerals studies invoked the role of Andean tectonics in the control of the sources of foreland sediment since the early to middle Miocene. Heavy minerals analyses of Ruiz (2002) show that the deposits in fact originated from the west of the present-day Eastern Cordillera since the Eocene. Again, Roddaz et al. (2005) demonstrate from a geochemical study that the sediment of the Curaray Formation was issued from an andesitic source.

574 Possible sources of andesitic material of Miocene or older age are situated in the Interandean
575 Depression and the eastern flank of the Western Cordillera, including the Saraguro group dated at 35.3-
576 26.8 Ma from K-Ar measurements (Lavenu et al., 1992; Kennerley, 1980), the Chinchillo Formation and
577 the Biblian-Azogues-Mangan Formations dated at 22 to 5.2 Ma from K-Ar measurements (Kennerley, 1980;
578 Barberi et al., 1988; Lavenu et al., 1992) in southern Ecuador and the Pisayambo Formation aged of 10-9
579 Ma (base) to 6 Ma (top) (Barberi et al., 1988; Lavenu et al., 1992) which is widespread over the western
580 Eastern Cordillera, the Interandean Depression and the eastern flank of the Western Cordillera (Baldock,
581 1982; Lavenu et al., 1992) in central Ecuador. Another possible andesitic source might have been the
582 Upper Cretaceous-Paleogene Macuchi formation which constitutes most of the basement of the Western
583 Cordillera under the volcanic formations (Reynaud et al., 1999).
584 The Oligocene and early/middle Miocene andesitic sources being situated to the south, the
585 southwest and the west-northwest, and the Upper Cretaceous/Paleocene sources to the southwest, west
586 and northwest, of the reconstructed apex indicate that the distribuary system which fed the fan was
587 situated in the western flank of the Western Cordillera in agreement with the above sedimentological
588 study
589 The sedimentary system also shows an evolution of the Neogene streams through time. Since the slope
590 of the channel belt can as a first approximation be considered as equal to the regional slope during pre-
591 steady state, such an increase in river slope is directly related to an increase in regional topographic slope.
592 This should be ascribed to a relative local base level fall. Because the elevation of the Amazonian plain
593 cannot have considerably fallen at this time – the Curaray/Pebas marine deposits being essentially
594 tidalites or other shallow water deposits all over the Pebas "marine-like meagalake" (Wesselingh et al.,
595 2002; Roddaz et al., 2005; Hovikoski et al., 2005) – the increase in regional slope was necessarily due to an
596 increase in elevation of the source area of the alluvial system. This means that the elevation and the
597 frontal slope of Western Cordillera increased during the Miocene.
598 The deformation of the late Miocene Pisayambo volcanic formation in the outer Western Cordillera and
599 the inner Eastern Cordillera gives another support to this interpretation. According to Lavenu et al. (1992)
600 the base of the Pisayambo formation is situated at 3600 asl on the eastern flank of the Western Cordillera.
601 The top of this formation crops out in the Subandean Depression with an elevation of 2800 m asl and on
602 top of the Eastern Cordillera (Pisayambo plateau) with an elevation of 4200 m. If we admit that the
603 thickness of this formation is between ≤ 1000 m (Lavenu et al., 1992 in the Interandean Depression), its

dip is 3-4° east in the outer Western Cordillera. This formation is subhorizontal in the Interandean Depression, and dips 15° west in the western flank of the Eastern Cordillera (Burgos, 2006) and 0.5° east on top of the Eastern Cordillera (Burgos, 2006). Because this widespread volcanic formation including lava flows and volcaniclastic deposits is likely to have been deposited on a shallow-dipping slope, it appears that the Eastern Cordillera did not exist and the slope of the outer Western Cordillera was much less than today in the late Miocene. The persistence of a shallow dipping and low elevation planation surface during the Miocene in place of the Eastern Cordillera is consistent with the very slow exhumation of only 200 m between 10 and 2 Ma revealed by (U Th)/He measurements in granitoids from the central-western Eastern Cordillera (Spikings & Crowhurst, 2004). The growth of the Eastern Cordillera is recorded by a relatively rapid and deep incision of ~2000 m in < 2 My of this cordillera by the Pastaza River (Burgos, 2006), beheading of the transverse rivers except the Pastaza (Burgos, 2006) and the deformation of the sedimentary deposits and volcanic strata beginning with the early Pleistocene in the Latatunga basin (2 to 1.5 Ma, Lavenu et al., 1992).

It should be thus considered that the Miocene-Pliocene alluvial fan system of Ecuador was a shallow-dipping fan passing eastward to a large-scale fan delta which evolved through time to a DFS prograding eastward, as a result of the growth of the Western Cordillera. The proximal fan was abandoned in the late Pliocene (?) – early Pleistocene with the growth of the Eastern Cordillera.

5.2 - Tectonic control of the progradation of the DFS

The results of the present study show that the tectonic controls of depocenter migration and megafan progradation in Ecuador differ from those in Peru and Colombia. The essential difference with the Peruvian belt is that no actual individual thrust-related sub-basins formed during the development of the Miocene megafan. Thrust-related folds formed within the proximal fan as shown by the growth strata in front of the Abitagua thrust sheet and the southern nose of the Napo dome. The growth of the Cutucu dome predating the deposition of the Pleistocene Mera Formation (Bès de Berc et al., 2005) suggests that this dome was also Miocene in age. However, paleocurrent patterns, sedimentary evolution, and provenances studies show that the organization of the Miocene megafan was poorly disturbed by these folds, which appear as isolated although complex antiforms. However, the ages of 2 to 1.5 Ma of the deformation of the Pisayambo Formation and of the deposits of the Latacunga basin (Lavenu et al., 1992) where we situate the apex of the fan confirm that this fan apex was not deformed before the late Pliocene-

early Pleistocene. In contrast, compressional deformation occurred on either side of the fan apex since 6 Ma (Barragan et al., 1996; Winkler et al., 2005) in the Chota basin to the north and at 8.5-7.9 Ma in the Nabon basin to the south (Hungerbühler et al., 1995). Therefore, the fan apex and practically the whole proximal part of the fan ('Pastaza depression') lay in a re-entrant of the deformational front, representing a zone of 'deficit of displacement' according to Burbank et al. (1999), during the middle to late Miocene deformation. It should be thus inferred that the development of the large-scale fan and its progradation toward the "Pebas marine-megalake" and the Amazonian lowland was allowed by the presence of a re-entrant in the Western Cordillera front and the well-marked axial depression between the antiformal culminations of the Napo and Cutucu. This differs from Colombia where the ongoing growth of the Eastern Cordillera in the late Miocene closed the issue to the east to transverse streams flowing across valleys between discontinuous hills during late Oligocene-Early Miocene time (Gomez et al., 2003). In another ground, the much smaller width (and mass) of the Napo and Cutucu domes if compared with the Eastern Cordillera of Colombia may be interpreted as a more limited transfer of deformation toward the east in Ecuador than in Colombia. The deformation remaining localized in the west is also recorded in Ecuador by the major control exerted on the Miocene-Pliocene sedimentation by the ongoing growth of the Western Cordillera while in Colombia, this control was predominantly exerted by the growth of the Eastern Cordillera. The restoration of the Miocene-Pliocene fan system in Ecuador also show the Eastern Cordillera of Ecuador is younger than the Central Cordillera of Colombia (Late Pliocene to early Pleistocene instead of pre-Middle Eocene, Gomez et al., 2003, 2005). Localization of deformation and ongoing tectonic loading in the Western Cordillera of Ecuador during the Miocene might be one of the reasons – if not the principal – why the Amazonian foreland basin has had there its maximum width.

5. 3 – Development and preservation of the DFS

The study of the Neogene sedimentary series of the subandean basin of Ecuador shows a coarsening upward trend together with a reduction of the preservation of floodplain deposits from base to top. Moreover, architectural elements analysis shows an evolution through time toward more powerful streams and paleocurrents show evidence of radial drainage pattern. These data seem to depict a long term DFS which began with the Chalcana Fm. during Miocene times. Compared to DFS models (Nichols and Fisher, 2007; Weissmann et al, 2013) our data provide no evidence of downstream decrease in size of channels. Nevertheless, the modern Pastaza DFS do not exhibit this pattern. The Rio Pastaza is the only

active stream crossing the whole DFS from the catchment to its confluence with the Rio Maranon. Moreover all along its course on the DFS, the Rio Pastaza drains its surrounding floodplain, making it increasing in size downstream. It appears in this case, as stated by Weissman et al., (2013) the DFS builts in time, due to avulsions and not necessarily a pattern observed at given time.

Progradation of DFS is a common trend, as shown by Nichols and Fisher (2007) and Weissmann et al., (2013). This way, the evolution of the sedimentary systems of the Neogene of the Ecuadorian subandean basin is typical of this kind of object. In the specific case of the Pastaza DFS, the main control on the sedimentary system is the tectonic evolution of the Ecuadorian Andes and its consequences on the subsidence in the foreland basin. Roddaz et al., (2010) synthesized the evolution of the Amazonian foreland basins of Colombia, Ecuador, Peru and Bolivia through tertiary times. The Rio Pastaza DFS, began during Miocene times. Roddaz et al., show by these times the subandean basins from Colombia to Bolivia are in a phase of "filled" foreland basin, as testified by the marine ingressions from the caribbean sea to the north and the initiation of the "Pebas marine-like megalake" (Hoorn et al., 2010). In the Pastaza DFS, these "marine-like" deposits correspond, in the Ecuadorian subandean basin to the Curaray Fm. This stage is characterized by and axial drainage system. Since the end of Upper Miocene, the Subandean foreland basins are in an "overfilled stage" (Roddaz et al., 2010)

We can consider that the evolution of the foreland basin influenced the architecture of the DFS. The transition from filled to overfilled corresponds to an increase of sediment input, overpassing flexural subsidence (Roddaz et al., 2010). In this context, the Pastaza DFS, together with the eastward propagation of deformation (see above), firstly filled accommodation at its apex and then toward its distal part, initiating a prograding trend.

As seen here, the development of the DFS take place in the last stage of evolution of the retroforeland basin. Comparing this case with classical foreland basin (Molasse Basin of the Alps, Homewood et al., 1986; Indo-gangetic plain, Burbank, 1992;
DFS are also characteristic of the overfilled stages of the foreland basin and in some cases evolve later to contributive system due to incision. This would show that DFS developing in tertiary foreland basins overfilled stages exhibit poor potential of preservation as reservoir.

6. Conclusions

693 The Neogene infill of the Ecuadorian Amazonian foreland basin comprises a thick (1350 to 2800 m
694 from the basin margin to the depocenter) of non-marine deposits (Chalcana et Arajuno/Chambira
695 formations) passing eastward to shallow marine deposits (Curaray formation). The Chalcana and
696 Arajuno/Chambira Formations form a series of coarsening upward deposits displaying instable
697 meandering channels in a flood plain environment passing upward and westward to wandering braided
698 channels, with a general reduction of the flood plain/channel infill ratio. The convergence of the
699 paleocurrent directions in the upper series along with the channel instability shows that these deposits
700 formed a distribuary system with a fan-like arrangement. The sedimentary evolution thus records the
701 evolution through time of a shallow-dipping alluvial fan passing eastward to a large-scale fan delta to a
702 piedmont fan prograding eastward. The point of convergence of paleocurrent directions being situated
703 upstream of the present-day Eastern Cordillera reveals that the actual apex of the fan was situated at the
704 foot of the Western Cordillera, which is also supported by the size and the nature of the clasts and the
705 width of the westermost exposed part of the fan. The erosion of the very proximal part of this fluvial fan
706 system occurred as a result of the post-depositional (Plio-Pleistocene) growth of the Eastern Cordillera.
707 The non-marine deposits pass eastward and downward to the shallow marine deposits of the Pebas
708 “Marine like Megalake” of Wesselingh et al. (2002). Despite the absence of a visible transition, it should be
709 postulated that a delta marked here the transition from the fan-like piedmont deposits to the marine
710 deposits.
711 The coarsening upward of the series, the westward/upward passage from meandering to braided
712 streams and the reduction of the flood plain/channel infill ratio indicate a progradation of the
713 sedimentary system and maybe an increase in slope and in erosion rate of the Western Cordillera during
714 Middle Miocene through Pliocene time. The architecture of the upper quaternary DFS shows the same
715 prograding trend.
716 Although the Middle Miocene to Late Miocene-Pliocene sedimentary series of the Amazonian foreland
717 basin of Ecuador is grossly similar to those in Peru (Hermoza et al., 2005) and Colombia (Gomez et al.,
718 2003, 2005), the tectono-sedimentary organization differs. In Ecuador, the piedmont fan prograded, and
719 the Amazonian foreland basin was fed, as a result of the growth of the Western Cordillera until the late
720 Pliocene.
721

ACKNOWLEDGEMENTS: This study was carried out thanks to the Petroproducción-IRD agreement and received the financial support of the IRD, the INSU grant "Erosion des Andes" and the University Paul Sabatier grant BQR2003. The authors thank Alain Lavenu, Roberto Barragán, Miguel Ponce for stimulating discussions during field work and the redaction of this paper.

REFERENCES

Alemán, A. M., and Marksteiner, R. M., 1993. Meseozoic and Cenozoic evolution of the Marañon basin in south eastern Colombia, eastern Ecuador and northeastern Peru. *American Association of Petroleum Geologists Bulletin*, 77: 301.

Allen, J. R. L., 1963. The classification of cross stratified units, with notes on their origin. *Sedimentology*, 2: 93-114.

Baby, P., Rivadeneira, M., Christophoul, F., and Barragán, R., 1999, Style and timing of deformation in the Oriente of Ecuador, *in* 4th International Symposium of Andean Geodynamics (ISAG), Göttingen, 68-72.

Baldock, J. W., 1982, Boletín de Explicación del Mapa Geologico del Ecuador: DGGM, scale 1/1000000.

Balkwill, H. R., Rodrigue, G., Paredes, F. I., and J.P., A., 1995, Northern part of Oriente Basin, Ecuador: reflection seismic expression of structures, *in* Tankard, A. J., Suarez Soruco, R., and Welsink, H. J., eds., Petroleum basins of south America, AAPG Memoir #62, 559-571.

Barberi, F., Coltelli, M., Ferrara, G., Innocenti, F., Navarro, J. M., and Santacroce, R., 1988, Plio-Quaternary volcanism in Ecuador. *Geological Magazine*, 125: 1-14.

Barragán, R., Christophoul, F., White, H., Baby, P., Rivadeneira, M., Ramirez, F., and Rodas, J., 2004, Estratigrafía secuencial del Cretacico de la Cuenca Oriente del Ecuador., *in* Baby, P., Rivadeneira, M., and Barragán, R., eds., la cuenca Oriente: Geología y petroleo: Travaux de l'Institut des Etudes Andines, 144: 45-68.

Barragán, R., Baby, P., and Duncan, R., 2005, Cretaceous alkaline intra-plate magmatism in the Ecuadorian Oriente Basin: Geochemical, geochronological and tectonic evidence: *Earth and Planetary Science Letters*, 236: 670-690.

Bernard, H. A., Leblanc, H. J., and Major, C. J., 1962, Recent and pleistocene geology of southeast texas., *in* Rainwater, E. H., and R.P., Z., eds., Geology of the Gulf Coast and central Texas: guidebook for anual meeting, p. 175-224.

751 Bernal C., Christophoul, F., Darrozes, J., Soula, J-C., Baby, P., Burgos, J., 2011. Late glacial and holocene
752 avulsions of the Rio Pastaza Megafan (Ecuador-Peru): Frequency and controlling factors.
753 I*nternational Journal of Earth Sciences (Geologische Rundschau)*, 100: 1759-1782, doi
754 10.1007/s00531-010-0555-9.

755 Bernal, C., Christophoul, F., Soula, J-C., Darrozes, J., Bourrel, L., Laraque, A., Burgos, J., Bès de Berc, S., Baby,
756 P., 2012, Gradual diversions of the Rio Pastaza in the Ecuadorian piedmont of the Andes from
757 1906 to 2008: role of tectonics, alluvial fan aggradation and ENSO events, *International Journal of*
758 *Earth Sciences (Geologische Rundschau)*. DOI 10.1007/s00531-012-0752-9

759 Bes de Berc, S., Soula, J.-C., Baby, P., Souris, M., Christophoul, F., and Rosero, J., 2005, Geomorphic evidence
760 of active deformation and uplift in a modern continental wedge-top - foredeep transition:
761 example of the eastern Ecuadorian Andes: *Tectonophysics*, 399: 351-380.

762 Bridge, J. S., 2003, Rivers and Floodplains, forms, processes and sedimentary record. London, Blackwell
763 Science Ltd., 491 p.

764 Bristow, C. R., and Hoffstetter, R., 1977, Ecuador, Lexique Stratigraphique International: Paris, France,
765 CNRS éditions, 410 p.

766 Burbank, D.W., 1992, Causes of recent Himalayan uplift deduced from deposited patterns inthe Ganges
767 Basin. *Nature* 357 : 680 – 683, doi:10.1038/357680a0

768 Burgos, J. D., 2006, Mise en place et progradation d'un cône alluvial au front d'une chaîne active: exemple
769 des Andes équatoriennes au néogène [Phd thesis]: Université Paul Toulouse 3, France, 373 p.

770 Campbell, C. J., 1970, Guide to the Puerto Napo area, Eastern Ecuador with notes on the regional geology of
771 the Ecuadorian Oriente Basin: Quito, 40 p.

772 Christophoul, F., 1999, Discrimination des influences eustatiques et tectoniques dans les bassins liés a des
773 zones de convergences: exemples du bassin Subandin d'Equateur. [Phd thesis]: Université
774 Toulouse 3, France, 184 p.

775 Christophoul, F., Baby, P., and Dávila, C., 2002a, Stratigraphic responses to a major tectonic event in a
776 foreland basin: the Ecuadorian Oriente from Eocene to Oligocene times. *Tectonophysics*, v. 345:
777 281-298.

778 Christophoul, F., Baby, P., Soula, J.-C., Rosero, M., and Burgos, J. D., 2002b, Les ensembles fluviatiles
779 néogènes du bassin subandin d'Equateur et implications dynamiques: *Comptes Rendus*
780 *Géosciences*, 334 : 1029-1037.

781 Church, M., 1983, Pattern and instability in a wandering gravel bed channel, *in* Collinson, J. D., and Lewin, J.,
782 eds., Modern end ancient fluvial systems: IAS Special Publication, International Assocation of
783 Sedimentologists, p. 169-180.

784 Collinson, J.D., 1996. Alluvial sediments. *In* Reading, H.G. *(ed.)*, Sedimentary environments,: processes,
785 facies and stratigraphy. Blackwell. 37-82.

786 Cooper, and others, e., 1995, Basin development and tectonic history of the Llanos basin, Eastern
787 Cordillera, and the Middle Magdalena Valley, Colombia.: *American Association of Petroleum*
788 *Geologists Bulletin*, 79: 1421-1443.

789 Dashwood, M. F., and Abbots, I. L., 1990, Aspects of the petroleum geology of the Oriente basin, Ecuador, *in*
790 Brooks, J., ed., Classic petroleum provinces, Geological Society of London Special Publication, 50:
791 89-117.

792 Edwards, G. L., 1993, Villano-2 well, completion report, ARCO-Oriente, Quito, Ecuador, p. 4-13.

793 Gutierrez, M., 1975, Contribucion al conocimento microplaeontologico del Oriente Peruano. *Boletin de la*
794 *Sociedad Geologica del Peru.* 19: 25-52.

795 Hermoza, W., Brusset, S., Baby, P., Gil, W., Roddaz, M., Guerrero N., and Bolaños, R., 2005, The Huallaga
796 foreland basin evolution: Thrust propagation in a deltaic environment, northern Peruvian Andes.
797 *Journal of South American Earth Sciences*, 19: 21-34.

798 Homewood, P., Allen, P.A., Williams, G.D., 1986. Dynamics of the Molasse Basin of western Switzerland. In:
799 P.A. Allen and P. Homewood (eds), Foreland Basins, *Special Publication of the International*
800 *Association of Sedimentologists*, 8: 199-217.

801 Hoorn, C., 1993, Marine incursions and the influence of Andean tectonics on the Miocene depositional
802 history of northwestern Amazonia: Results of a palynostratigraphic study. *Palaeogeography;*
803 *Palaeoclimatology, Palaeoecology,* 105: 267-309.

804 Hoorn, C., 1994, Fluvial paleoenvironments in the intracratonic Amazonas Basin (Early Miocene-Early
805 Middle Miocene, Colombia). *Palaeogeography, Palaeoclimatology, Palaeoecology*, 109: 1-54.

806 Hoorn, C., 1996, Miocene deposits in the Amazonian Foreland Basin (Technical comments). *Science.* 273:
807 122,123.

808 Horton, B. K., and DeCelles, P. G., 2001, Modern and ancient fluvial megafans in the foreland basin system
809 of the Central Andes, Southern Bolivia: implications for drainage network evolution of fold-thrust
810 belts. *Basin Research.* 13: 43-63.

811 Hovikoski, J., Räsänen, M. E., Gingras, M. K., Roddaz, M., Brusset, S., and Hermoza, W., 2005, Miocene semi-
812 diurnal tidal rythmites in Madre de Dios, Peru. *Geology. 33:* 177-180.

813 Howard, J.D., 1966. Pattern of sediment dispersal in Fountain Formation, of Colorado. *Mountain Geologists*.
814 3: 147-153.

815 Hungerbühler, D., Steinmann, M., Winkler, W., Eguez, A., Seward, D., Heller, F., and Ford, M., 1995, An
816 integrated study of fill and deformation in the Andean intermontane basin of Nabón (Late
817 Miocene), southerrn Ecuador. *Sedimentary Geology.* 96: 257-279.

818 Hungerbühler, D., Steinmann, M., Winkler, W., Seward, D., Egüez, A., Peterson, D. E., Helg, U., and Hammer,
819 C., 2002, Neogene stratigraphy and Andean geodynamics of southern Ecuador: *Earth-Science*
820 *Reviews;* 57: 75-124.

821 Kley, J., Monaldi, C. R., and Salfity, J. A., 1999, Along-strike segmentation of the Andean foreland: causes
822 and consequences. *Tectonophysics*. 301: 75-94.

Labogeo, 1991. Informe bioestratigráfico del Pozo Vinita-1. PPG-91.

Labogeo, 1992a. Informe geológico del pozo Ishpingo-1. PPR GL 114A.

Labogeo, 1992b. Informe geológico del pozo Tiputini-1. PPR GL 161.

Labogeo, 1992c. Sedimentología-Bioestratigrafía-Geoquímica-Litoestratigrafía del Pozo: Secoya-24. Informe Técnico No 24, PPG-92.

Lavenu, A., Noblet, C., Bonhomme, M. G., Egüez, A., Dugas, F., and Vivier, G., 1992, New K-Ar age dates of Neogene and Quaternary volcanic rocks from the Ecuadorian Andes: Implications for the relationship between sedimentation, volcanism, and tectonics. *Journal of South American Earth Sciences.* 5: 309-320.

Leeder, M. R., and Gawthorpe, R. L., 1987, Sedimentary models for extensional tiltblock/half graben basins, *in* Coward, M. P., Dewey, J. F., and Hancock, P. L., eds., Continental extensional basins: Special Publication, Geological Society of London, p. 139-152.

Leopold, L. B., Wolman, M. G., and Miller, J. P., 1964, Fluvial Processes in Geomorphology: San Francisco, W. H. Freeman and Company, 522 p.

Lorente, M. A., 1986, Palynology and palynofacies of the Upper Tertiay in Venezuela. *Dissertationes Botanicae.* 99: 1-222.

Miall, A. D., 1978, A review of the braided river depositional environment. *Earth Science Review.* 13: 1-62.

Miall, A. D., 1985, Architectural element analysis: a new method of facies analysis applied to fluvial deposits. *Earth Science Review.* 22: 261-308.

Miall, A. D., 1996, The Geology of fluvial deposits, sedimentary facies, basin analysis and petroleum geology. London, Blackwell Science, 582 p.

Muller, J., de Di Giacomo, E., and Van Erve, A. W., 1987, A palynological zonation for the Cretaceous, Tertiary, and Quaternary of northern South America: American Association of Stratigraphic Palynologists Contributions Series, 19: 7-76.

847 Nichols, G.J., and Fisher, J.A, 2007. Processes, facies and architecture of fluvial distribitary syste deposits.
848 *Sedimentary Geology*, 195: 75-90

849 Potter, P. E., and Pettijohn, F. J., 1963, Paleocurrents and basin analysis.: Berlin, London, New York,
850 Springer Verlag, 326 p.

851 Pratt, W. R., Duque, P., and Ponce, M., 2005, An autochthonous geological model for the eastern Andes of
852 Ecuador. *Tectonophysics.* 399: 251-278.

853 Räsänen, M.E., Salo J.S., Jungnert, H., Romero Pittman, L. (1990) Evolution of the western Amazon lowland
854 relief: impact of Andean foreland dynamics. Terra Nova 2:320–332

855 Räsänen, M., Neller, R., Salo, J.S., Jungner, H. (1992) Recent and ancient fluvial deposition systems in the
856 Andean foreland basin, Peru. *Geological Magazine* 129, 293–306.

857 Roddaz, M., Baby, P., Brusset, S., Hermoza, W., and Darrozes, J. M., 2005, Forebulge dynamics and
858 environmental control in Western Amazonia: The case study of the Arch of Iquitos (Peru):
859 *Tectonophysics.* 399: 87-108.

860 Roddaz, M., Hermoza, W., Mora, A., Baby, P., Parra, M., Christophoul, F., Brusset, S. and Espurt, N, 2010.
861 Cenozoic sedimentary evolution of the Amazonian foreland basin system. *In* Hoorn, C., and
862 Wesselingh, F. (*eds*), Amazonia: a look into the past. Wiley, 61-88.

863 Roddaz, M., Christophoul, F., Burgos Zambrano, J.D., Soula, J-C., Baby, P., 2012. Provenance of Late
864 Oligocene to quaternary sediments of the ecuadorian foreland basin as inferred from major and
865 trace elements geochemistry and Nd-Sr isotopic composition. *Journal of South American Earth*
866 *Sciences.*37, 136-153. doi:10.1016/j.jsames.2012.02.008

867 Ruiz, G., 2002, Exhumation of the northern Sub-Andean Zone of Ecuador and its source regions: a
868 combined thermochronological and heavy minerals approach. [Phd thesis]: Swiss Federal
869 Institute of Technology Zurich, 260 p.

870 Ruiz, G., Seward, D., and Winkler, W., 2004, Detrital thermochronology - a new perspective on hinterland
871 tectonics, an example form the Andean Amazon Basin, Ecuador. *Basin Research.* 16: 413-430.

872 Rull, V., 2002, High-impact palynology in petroleum geology: Applications from Venezuela (northern
873 South America). *American Association of Petroleum Geologists Bulletin.* 86: 279-300.

874 Sauer, W., 1965, Geologia del Ecuador: Quito, 383 p.

875 Schumm, S. A., 1977, The Fluvial System. New York, Wiley & sons.

876 Smith, S. A., 1990, The sedimentology and accretionary style of ancient gravel-bed stream: the Budley
877 Salterton Pebbles Beds (Lower Triassic, Southwest England). *Sedimentary Geology.* 67: 199-
878 219.zaaswffgggy

879 Spikings, R.A., and Crowhurst, P.V., 2004. (U/Th)He thermochronometric constraints on the late Miocene
880 Pliocene development of the northern Cordillera Real and Interandean Depression.: *Journal of*
881 *South American Earth Sciences.* 17, 239 – 251.

882 Tschopp, H. J., 1953, Oil explorations in the Oriente of Ecuador. *American Association of Petroleum*
883 *Geologists Bulletin*. 7: 2303-2347.

884 Uba, C.J., Heubeck, C. and Hulka, C., 2005. Facies analysis and basin architecture of the Neogene Subandean
885 synorogenic wedge, southern Bolivia. Sedimentary Geology, 180 : 91-123.

886 Weissman, G.S., Hartley, A.J., Scuderi, L.A., Nichols, G.J., Davidson, S.K., Owen, A., Atchley, S.C., Bhattacharya,
887 P., Chakraborty, T., Ghosh, P., Nordt, L.C., Michel, L., Tabor, N.J. (2013) Prograding distributive fluvial
888 sysms – geomorphic models and ancient examples. SEPM Special Publication No104, New Frontiers in
889 Paleopedology and Terrestrial Paleoclimatology, 131-147.

890 Wesselingh, F. P., Räsänen, M. E., Irion, G., Vonhof, H. B., Kaandorp, R., Renema, W., Romero Pittman, L., and
891 Gingras, M., 2002, Lake Pebas: a palaeoecological reconstruction of a Miocene, long-lived lake
892 complex in western Amazonia. *Cainozoic Research*, 1: 35-81.

893 Wilkinson, M.J., Marshall, L.G., Lundberg, J.G. & Kreslavsky, M.H. 2010. Megafan environments in
894 northern South America and their impact on Amazon Neogene aquatic ecosystems. In: Hoorn,
895 C. & Wesselingh, F., eds. Amazonia: landscape and species evolution, a look into the past.
896 Oxford: Wiley Blackwell, pp. 162–184.

Winkler, W., Villagómez, D., Spikings, R., Abegglen, P., Tobler, S., and Egüez, A., 2005, The Chota basin and its significance for the inception and tectonic setting of the inter-Andean depression in Ecuador. *Journal of South American Earth Sciences.* 19: 5-19.

Whatley, R., Muñoz-Torres, F., and van Harten, D., 1996, Des ostracodes d'un lac salé Néogène à l'ouest du bassin Amazonien., *in* Third European Symposium on Ostracoda, Bierville, p. 25.

Zambrano, I., Ordóñez, M., and Jiménéz, N., 1999, Micropaleontología de 63 muestras de afloramientos de la Cuenca Oriental Ecuatoriana: Labogeo, Petroproducción, 016-PPG-99.

CAPTIONS

Tables

Table 1 - Nomenclature of the lithofacies identified in the fluvial deposits of the neogene infill of the Ecuadorian subandean Basin (modified from Miall, 1996)

Table 2 – Nomenclature of the architectural elements identified in the fluvial deposits of the neogene infill of the Ecuadorian subandean Basin (modified from Miall, 1985, 1996)

Figures

Figure 1 – Location and geologic map of the studied Area, A: Simplified map of the structural domain of Ecuador (modified from Baby et al., 1999). B : Geologic map of the subandean basin of Ecuador (modified from Baldock, 1982),

Figure 2 – Balanced cross section through the outer Western Cordillera, the Interandean Depression, the Eastern Cordillera and the frontal plateau of Ecuador. A) Pre-Miocene configuration (deposition of the Chalcana formation). Erosional surfacing (pediment?) affects the Paleozoic and Mesozoic rocks metamorphosed during late Cretaceous/early Paleocene time (Pratt et al., 2005). The Abitagua Jurassic granitoid (sill-like body) intruded into Paleozoic rocks. Structures in the metamorphic rocks on the basis of the structural data of Pratt et al. (2005), with internal structures constructed assuming antiformal thrust stack in the Cordillera Real. In order to account for the small angle between foliation and thrust ramps, we used an initial bedding-parallel shear $\gamma = 1$ giving rise to a foliation at 31.7° to bedding and at 17.6° to ramps initially at 25° to bedding, and flexural slip varying as a function of dip angle. B) Middle to late Miocene. Growth and erosion of the Western Cordillera with the deposition of the Chambira, Arajuno and Curaray formations and the propagation of the Miocene Pastaza megafan. Deposition of the Pisayambo volcanic formation in the immediate piedmont of the Western Cordillera in the late Miocene. Synchronous propagation of the Abitagua thrust forming growth stratal patterns in the Chambira deposits downstream of the apex (Talag syncline). Erosion did not attain the granitoid. The Napo and Cutucu domes formed at this time north and south of the cross section. C) Pliocene. Ongoing propagation of the Abitagua thrust. D) Late Pliocene – early Pleistocene. Onset of propagation of the Eastern Cordillera and

ongoing propagation of the Western Cordillera resulting in the formation of the Interandean Depression and the deformation of the Pisayambo volcanic formation. The Western Cordillera is assumed to have reached topographic steady state. The major rivers except the Rio Pastaza are defeated by the propagating Eastern Cordillera. The Subandean thrust faults formed at this time in front of the Eastern Cordilleran fault-bend fault. E – F - G) Pleistocene. Ongoing propagation of the Eastern Cordillera with accentuation of the Subandean thrust faults and backthrusting of the Abitagua cordillera. Thrust fault-related folds formed in the Interandean Depression and the back of the Eastern Cordillera.

Figure 3 – Stratigraphic Chart of the neogene formations of the subandean Basin of Ecuador (modified from Tchopp, 1953; Baldock, 1982; Baby et al., 1999; Burgos, 2006).

Figure 4 – Paleocurrent maps of the neogene formations of the subandean Basin of Ecuador. A: Chalcana formation, B: Arajuno/Curaray formations, C: Chambira/Curaray formations (modified from Christophoul et al., 2002b).

Figure 5 – Sedimentary column of the Chalcana formation (00°04'18''N-77°15'01''W); lithofacies and architectural elements codes are detailed in Tables 1 and 2. Horizontal axis represents granulometry with: Cl: Clays, S: Sands, f: fine, m: medium, c: coarse, G: gravels.

Figures 6 – Sedimentary columns of the Arajuno formation. Lithofacies and architectural elements codes are detailed in Tables 1 and 2, horizontal axis see Fig. 4. A: Structural cross section showing the stratigraphic relationships between sections B, C and D, location on Fig.1A; B: Puyo-Arajuno road section (from 01°29'42"S-77°59'59"W to 01°14'06"S-77°41'23"W); C: Puyo-Canelos road section (From 01°29'42"S-77°59'51"W to 01°26'03"S-77°45'30"W); D: Rio Arajuno section (From 01°03'03"S-77°31'30" to 01°09'31"S-77°40'49"W).

Figure 7 – Outcrop and sedimentary column characteristic of the base of the Arajuno Formation, along the Rio Arajuno (Lithofacies and architectural elements codes are detailed in Tables 1 and 2, horizontal axis see Fig. 4.

Figure 8 – Sedimentary column of the Arajuno Formation, from 77° 28' 24" W, 1° 54' 38" S to 77° 48' 12" W, 1° 54' 09" S. Lithofacies and architectural elements codes are detailed in Tables 1 and 2, horizontal axis see Fig. 4.

Figure 9 – A: Characteristics of the upper part of the Arajuno Formation. B: Floodplain facies of the Upper Arajuno Formation. Lithofacies and architectural elements codes are detailed in Tables 1 and 2, horizontal axis see Fig. 4.

Figure 10 – Outcrop showing Floodplain, crevasse Splay and Crevasse channel facies associations in the Arajuno Formation.

Figure 11 – Geological map and cross section of the Talag syncline. A: Geological map of the Talag syncline (Modified from Baby et al., 2001) location of Fig. 1. B: Cross sectin across the Talag syncline (location on the map above). Quote the eastward prograding pattern of the "coarse" Chambira Fm over the "finer" Arajuno Fm. C: detail of the contact between the Abitagua granitoid and the western overturned flank of the Talag Syncline. The rapid change of dip is interpreted as the result of a progressive unconformity.

Figure 12 – Sedimentary columns of the Chambira and Arajuno formation in the Talag Syncline (locations on fig. 10 B). Lithofacies and architectural elements codes are detailed in Tables 1 and 2, horizontal axis see Fig. 4. B: sedimentary column of the Chambira formation. C: Sedimentary columns of Chambira and Arajuno formations.

Figure 13 – A : Composite map of the Napo-Pastaza DFS (DEM SRTM 3'' resolution and Landsat 7). Solid

986 black lines: limits of the Napo and Pastaza catchments, solid white lines: modern Rio Napo and
987 Pastaza, red dashed lines: limits of the Plio-Pleistocene Napo Pastaza Megafan, yellow dashed
988 lines: post-LGM Pastaza Megafan. Blue points: volcanoes, white squares: actives volcanoes. NA:
989 Napo Antiform, PD: Pastaza Depression, CA: Cutucu Antiform, MCA: Morona Cangaime Area, MPA:
990 Morona Pastaza Area, TCA, Tigre Corrientes Area, PCTB: Pastaza Corrientes Transition Band. B :
991 Map of the catchment and the Rio Pastza DFS . To the northwest, with red lines: catchment of the
992 Rio Pastaza Megafan (extracted from the SRTM DEM). With green lines: drainage network.
993 Thickness of lines depends on the Stralher order of the streams. Thinnest lines correspond to
994 Order 3 streams. 1) Modern apex of the Pastaza Megafan, 2) avulsion sites, 3) supposed avulsion
995 sites, 4) abandoned stream, 5) abandoned stream re-annexed by the modern drainage network, 6)
996 supposed abandoned stream, 7) main modern streams, 8) eastern boundary of the subandean
997 tectonic structures, 9) Cangaime anticline axis (Modified from Bernal et al., 2011).

998 Figure 14 – Wheeler diagram of the neogene infill of the Ecuadorian subandean basin (Oriente Basin). See
999 text for details.

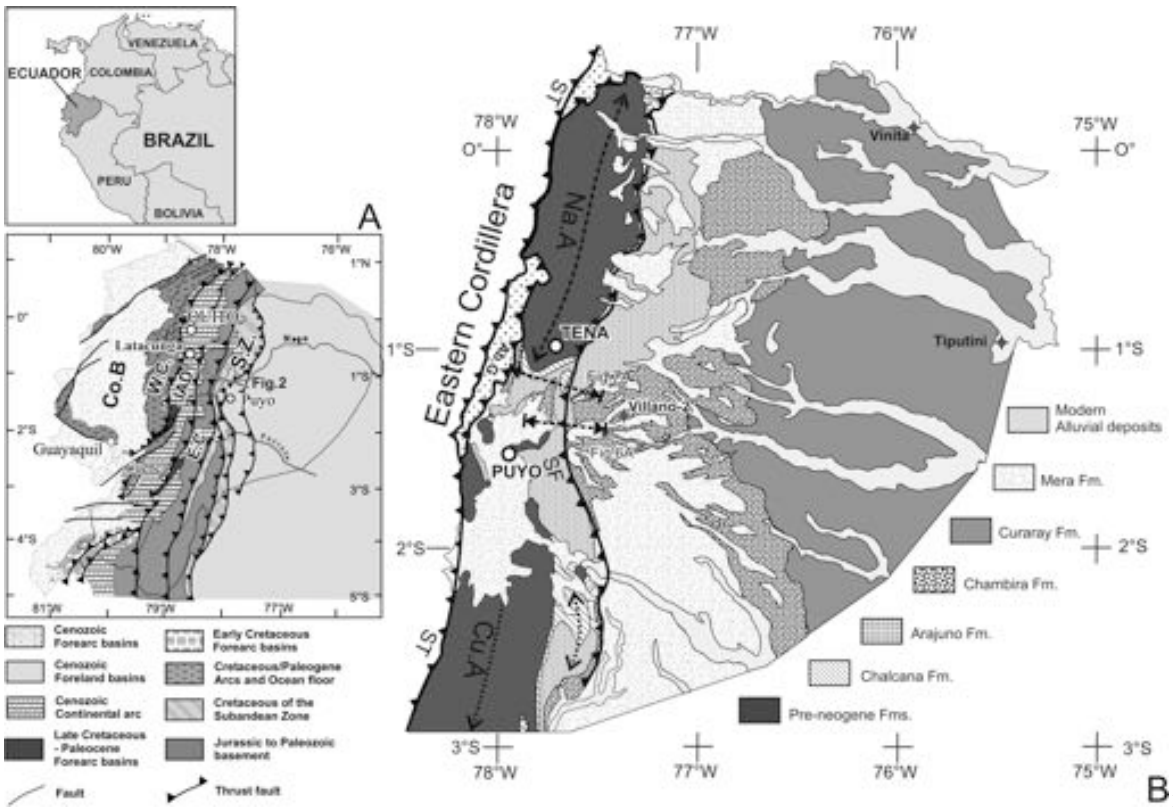
VENEZUELA
ECUADOR
COLOMBIA
BRAZIL
PERU
BOLIVIA
A
Guayaquil
Fig.2
Co.B
WC
IAD
CS
EB
Cenozoic Forearc basins
Cenozoic Foreland basins
Cenozoic Continental arc
Late Cretaceous - Paleocene Forearc basins
Early Cretaceous Forearc basins
Cretaceous/Paleogene Arcs and Ocean floor
Cretaceous of the Subandean Zone
Jurassic to Paleozoic basement
Fault
Thrust fault
77°W
76°W
78°W
75°W
0°
1°S
2°S
3°S
Eastern Cordillera
NAPO
ST
NAPO
CUTUCU
TENA
PUYO
Vinita
Tiputini
Villano
Modern Alluvial deposits
Mera Fm.
Curaray Fm.
Chambira Fm.
Arajuno Fm.
Chalcana Fm.
Pre-neogene Fms.
B

Figure 1

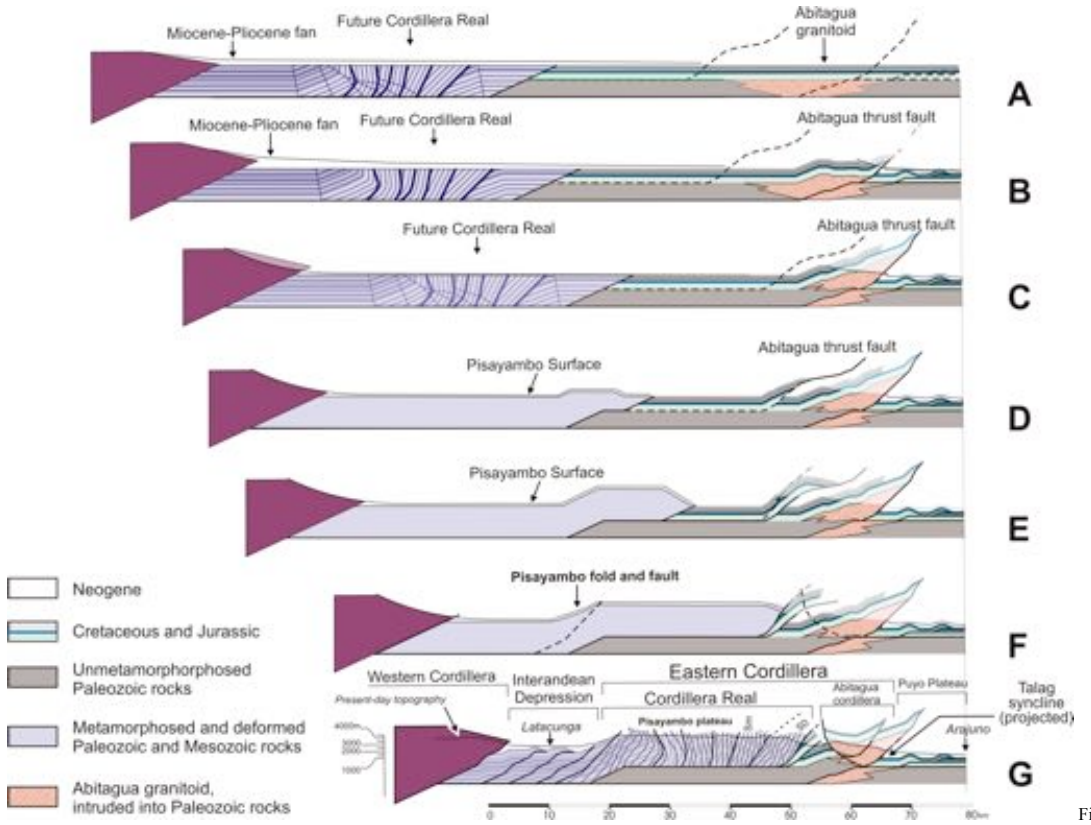
Miocene-Pliocene fan
Future Cordillera Real
Abitagua granitoid
A
Miocene-Pliocene fan
Future Cordillera Real
Abitagua thrust fault
B
Future Cordillera Real
Abitagua thrust fault
C
Pisayambo Surface
Abitagua thrust fault
D
Pisayambo Surface
E
Pisayambo fold and fault
F
Western Cordillera
Present-day topography
Interandean Depression
Eastern Cordillera
Cordillera Real
Abitagua cordillera
Puyo Plateau
Talag syncline (projected)
Latacunga
Pisayambo plateau
Arajuno
G
0
10
20
30
40
50
60
70
80km
Neogene
Cretaceous and Jurassic
Unmetamorphorphosed Paleozoic rocks
Metamorphosed and deformed Paleozoic and Mesozoic rocks
Abitagua granitoid, intruded into Paleozoic rocks

Figure 2

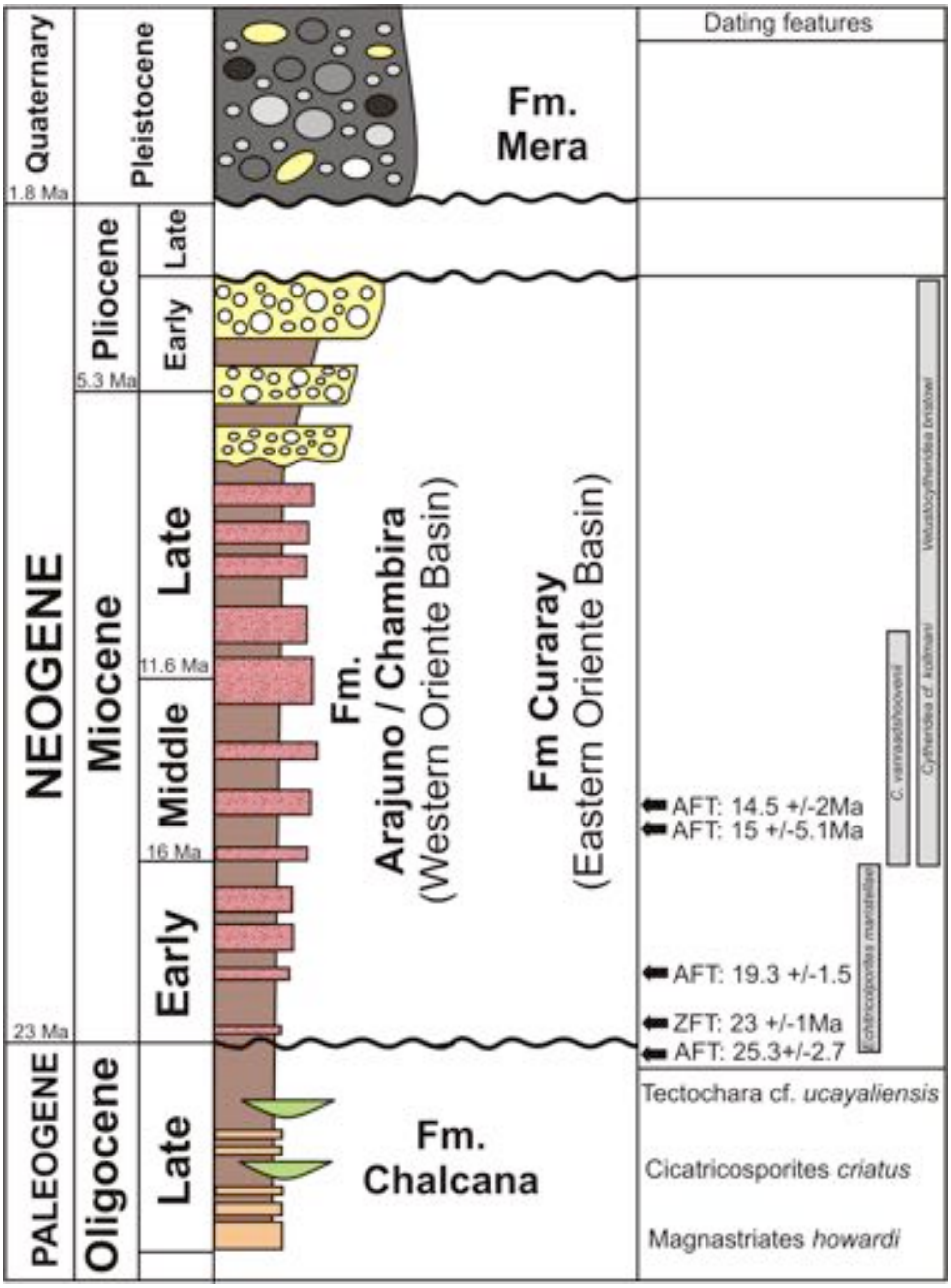
Quaternary
Pleistocene
1.8 Ma
NEOGENE
Pliocene
Late
Early
5.3 Ma
Miocene
Late
11.6 Ma
Middle
16 Ma
Early
23 Ma
PALEOGENE
Oligocene
Late
Fm. Mera
Fm. Arajuno / Chambira (Western Oriente Basin)
Fm Curaray (Eastern Oriente Basin)
Fm. Chalcana
Dating features
AFT: 14.5 +/-2Ma
AFT: 15 +/-5.1Ma
AFT: 19.3 +/-1.5
ZFT: 23 +/-1Ma
AFT: 25.3+/-2.7
Tectochara cf. ucayaliensis
Cicatricosporites criatus
Magnastriates howardi

Figure 3

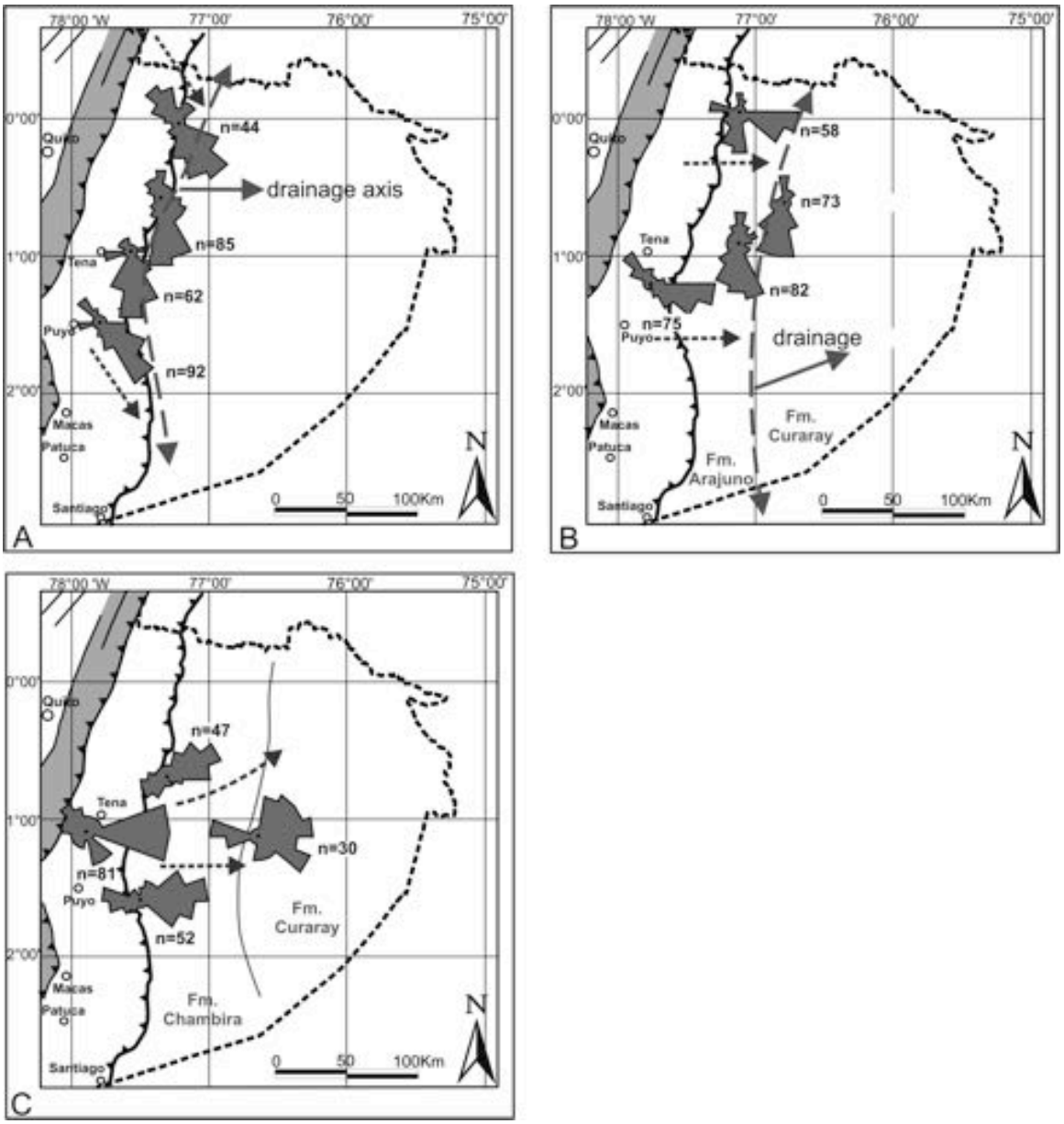
78°00 'W
77°00'
76°00'
75°00'
0°00'
1°00'
2°00'
Quito
Tena
Puyo
Macas
Patuca
Santiago
n=44
drainage axis
n=85
n=62
n=92
0
50
100Km
N
A
n=58
n=73
n=82
n=75
drainage
Fm.
Curaray
Fm.
Arajuno
B
n=47
n=30
n=81
n=52
Fm.
Curaray
Fm.
Chambira
C

Figure 4

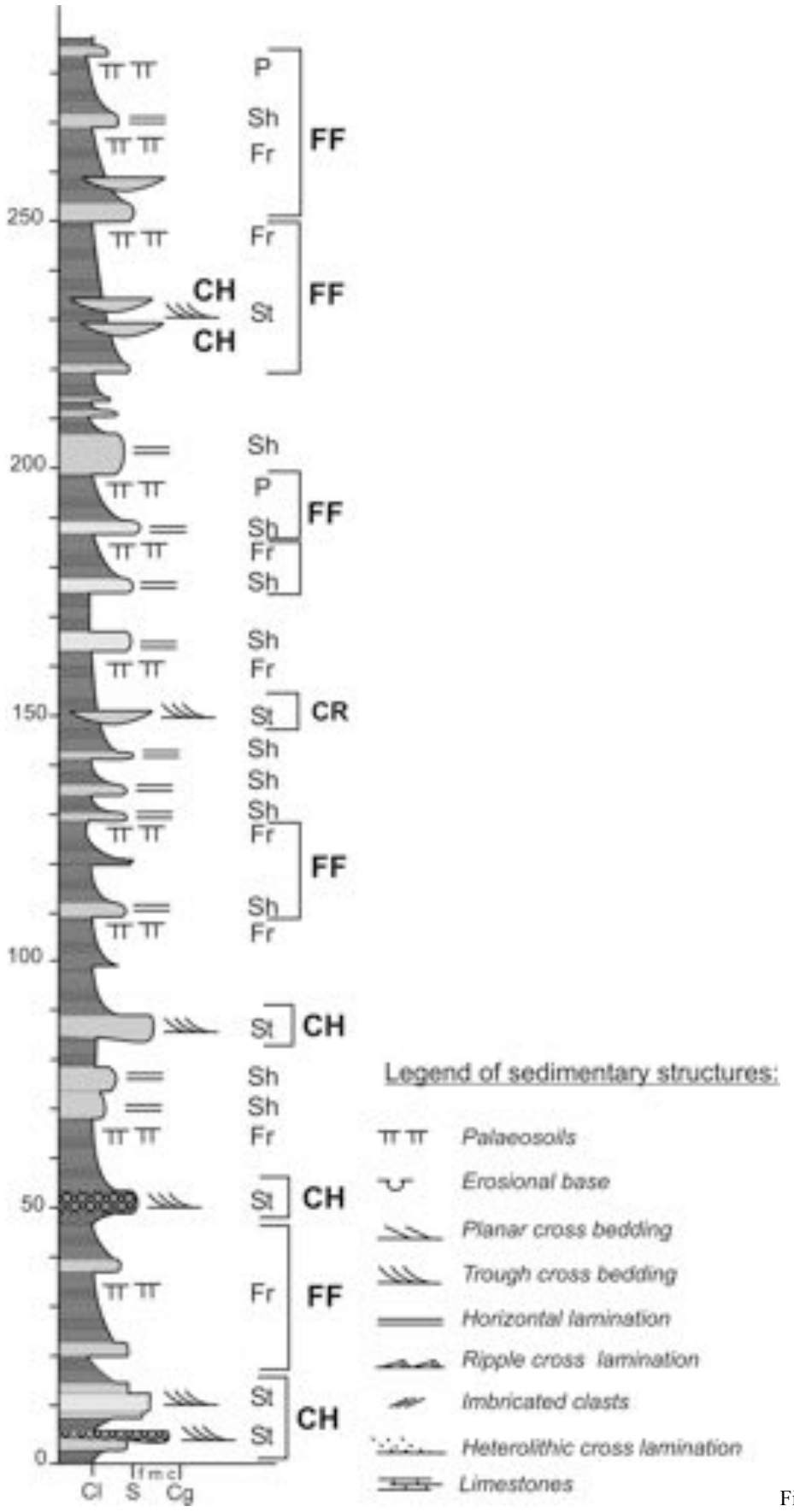
250
200
150
100
50
0
P
Sh
Fr
FF
CH
St
CR
Cl
S
Cg
f m c
Legend of sedimentary structures:
Palaeosoils
Erosional base
Planar cross bedding
Trough cross bedding
Horizontal lamination
Ripple cross lamination
Imbricated clasts
Heterolithic cross lamination
Limestones

Figure 5

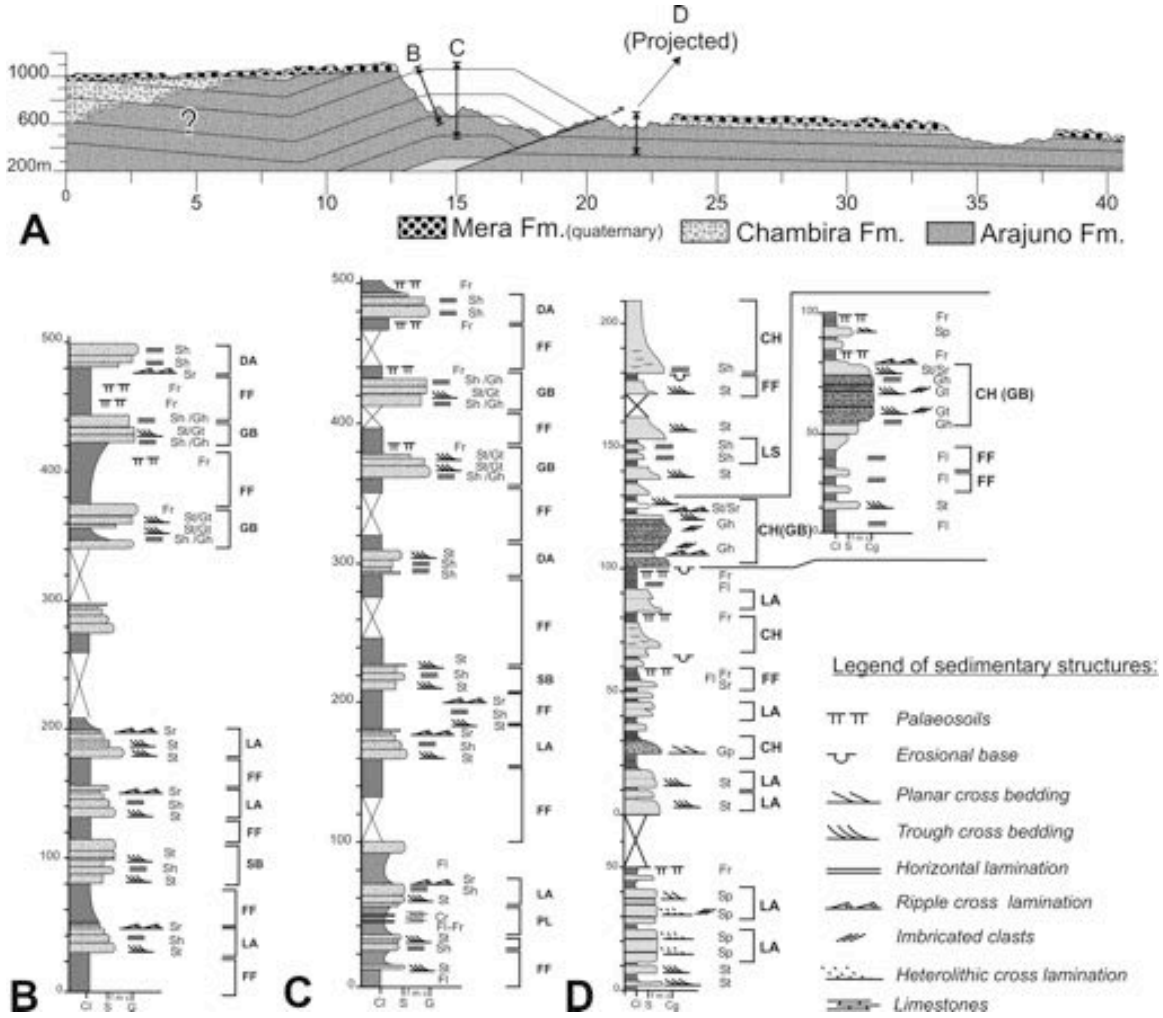
D
(Projected)
B
C
1000
600
200m
?
0
5
10
15
20
25
30
35
40
A
Mera Fm.(quaternary)
Chambira Fm.
Arajuno Fm.
B
C
D
Legend of sedimentary structures:
Palaeosoils
Erosional base
Planar cross bedding
Trough cross bedding
Horizontal lamination
Ripple cross lamination
Imbricated clasts
Heterolithic cross lamination
Limestones

Figure 6

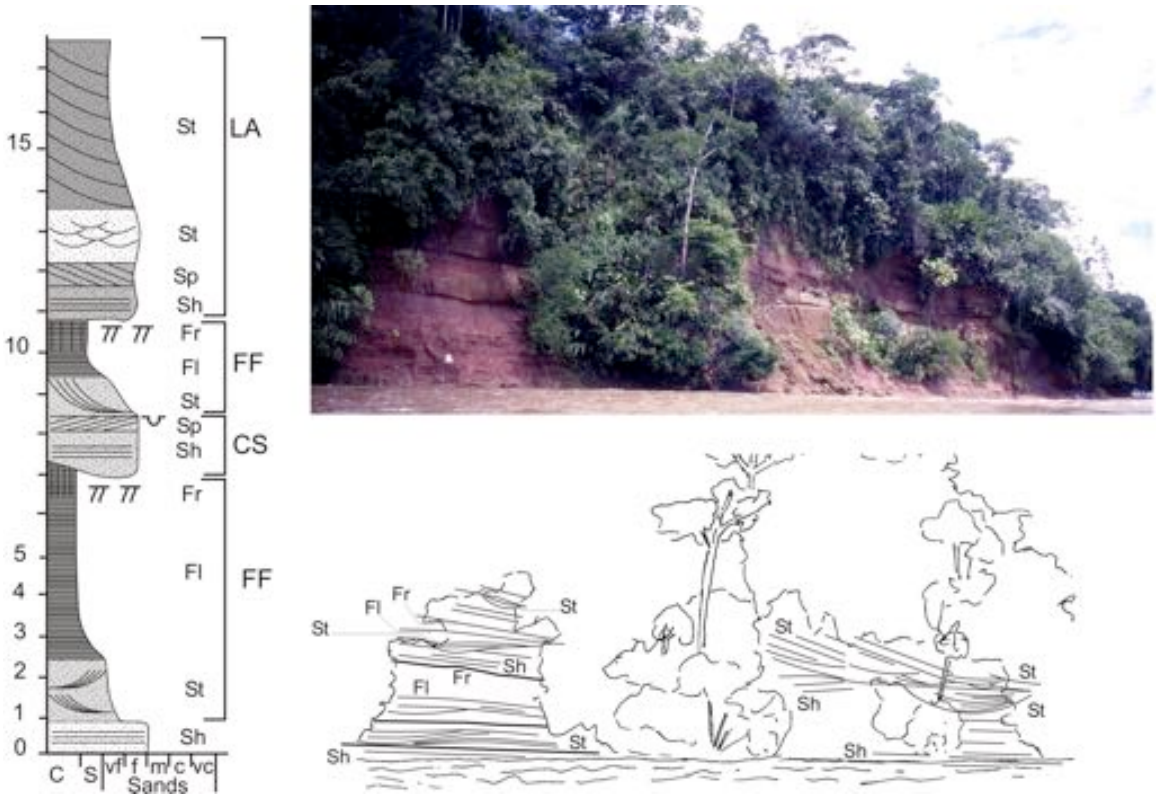
15
10
5
4
3
2
1
0
St
St
Sp
Sh
Fr
Fl
St
Sp
Sh
Fr
Fl
St
Sh
LA
FF
CS
FF
C
S
vf
f
m
c
vc
Sands
St
Fl
Fr
St
Sh
Fr
Fl
St
Sh
St
St
Sh
St
St
Sh

Figure 7

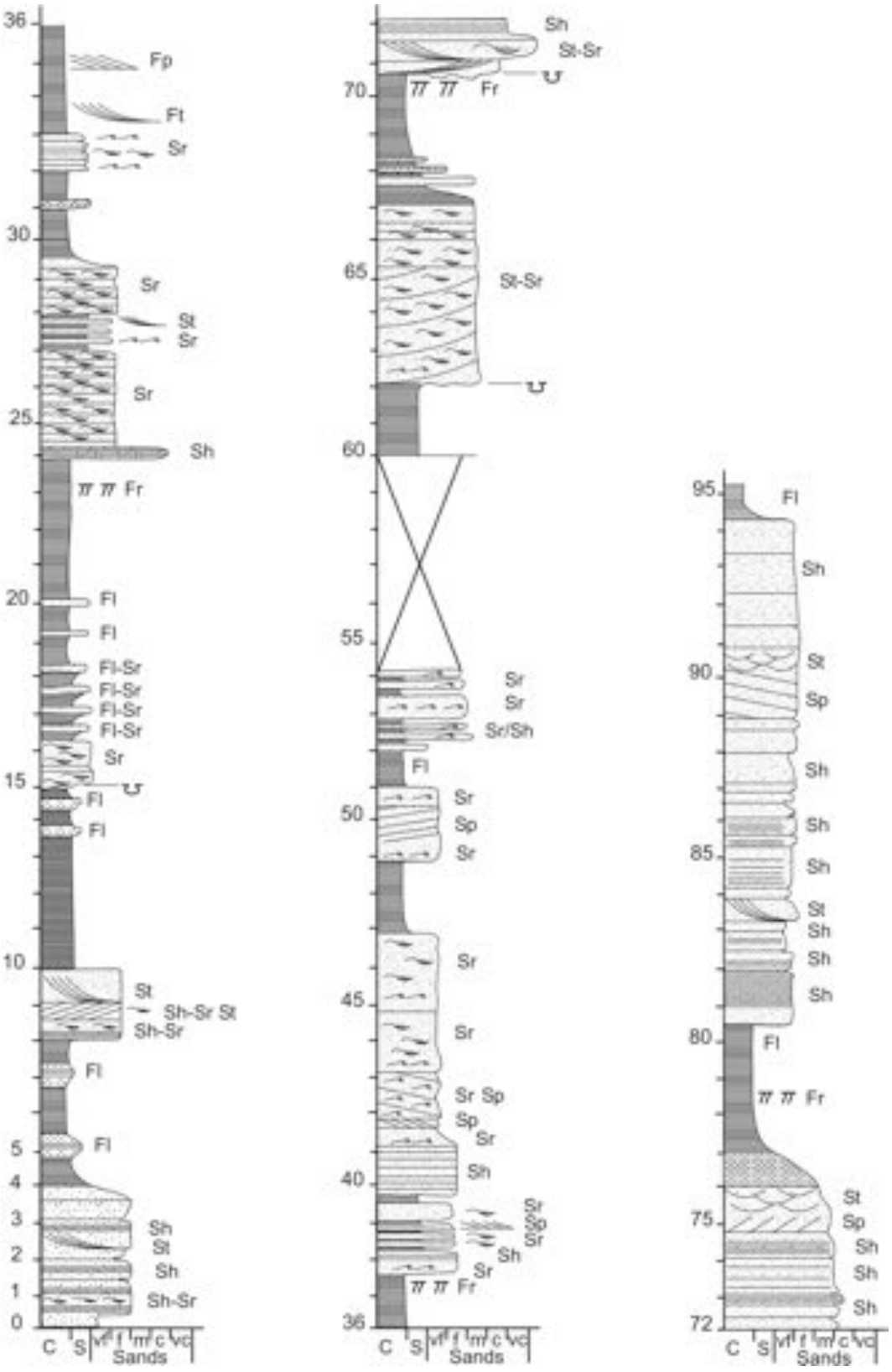
36
Fp
Ft
Sr
30
Sr
St
Sr
Sr
25
Sh
Fr
20
Fl
Fl
Fl-Sr
Fl-Sr
Fl-Sr
Fl-Sr
Sr
15
Fl
Fl
10
St
Sh-Sr St
Sh-Sr
Fl
5
Fl
4
3
Sh
2
St
Sh
1
Sh-Sr
0
C S vf f m c vc
Sands
70
Sh
St-Sr
Fr
65
St-Sr
60
55
Sr
Sr
Sr/Sh
Fl
50
Sr
Sp
Sr
Sr
45
Sr
Sr Sp
Sp
Sr
40
Sh
Sr
Sp
Sr
Sh
Sr
Fr
36
C S vf f m c vc
Sands
95
Fl
Sh
90
St
Sp
Sh
Sh
85
Sh
St
Sh
Sh
Sh
80
Fl
Fr
St
75
Sp
Sh
Sh
Sh
72
C S vf f m c vc
Sands

Figure 8

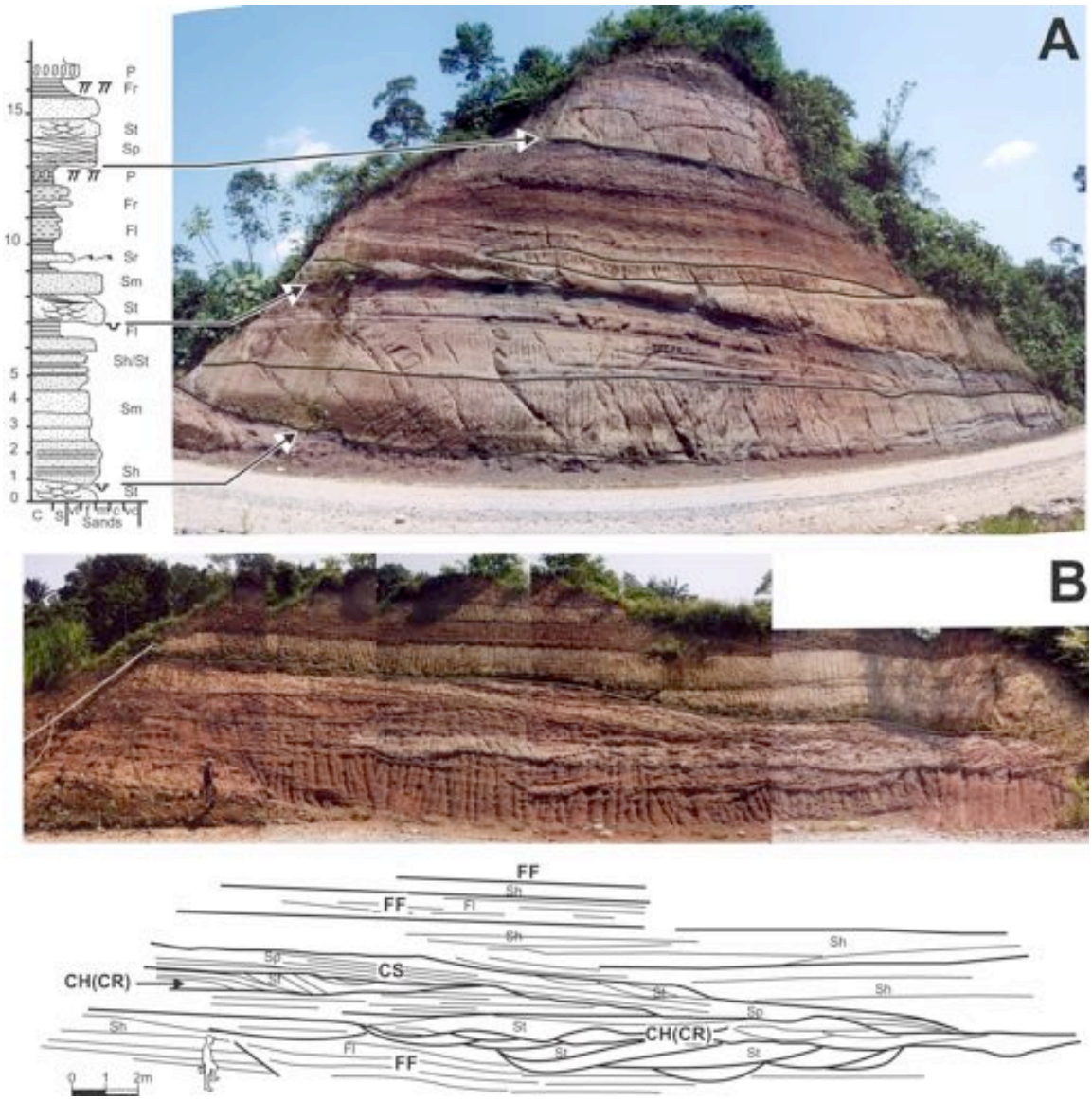
A
B
P
Fr
St
Sp
P
Fr
Fl
Sr
Sm
St
Fl
Sh/St
Sm
Sh
St
Sands
15
10
5
4
3
2
1
0
FF
Sh
FF
Fl
Sh
Sh
Sp
CS
CH(CR)
Fl
St
Sh
Sh
St
Sp
CH(CR)
Fl
FF
St
St
0
1
2m

Figure 9

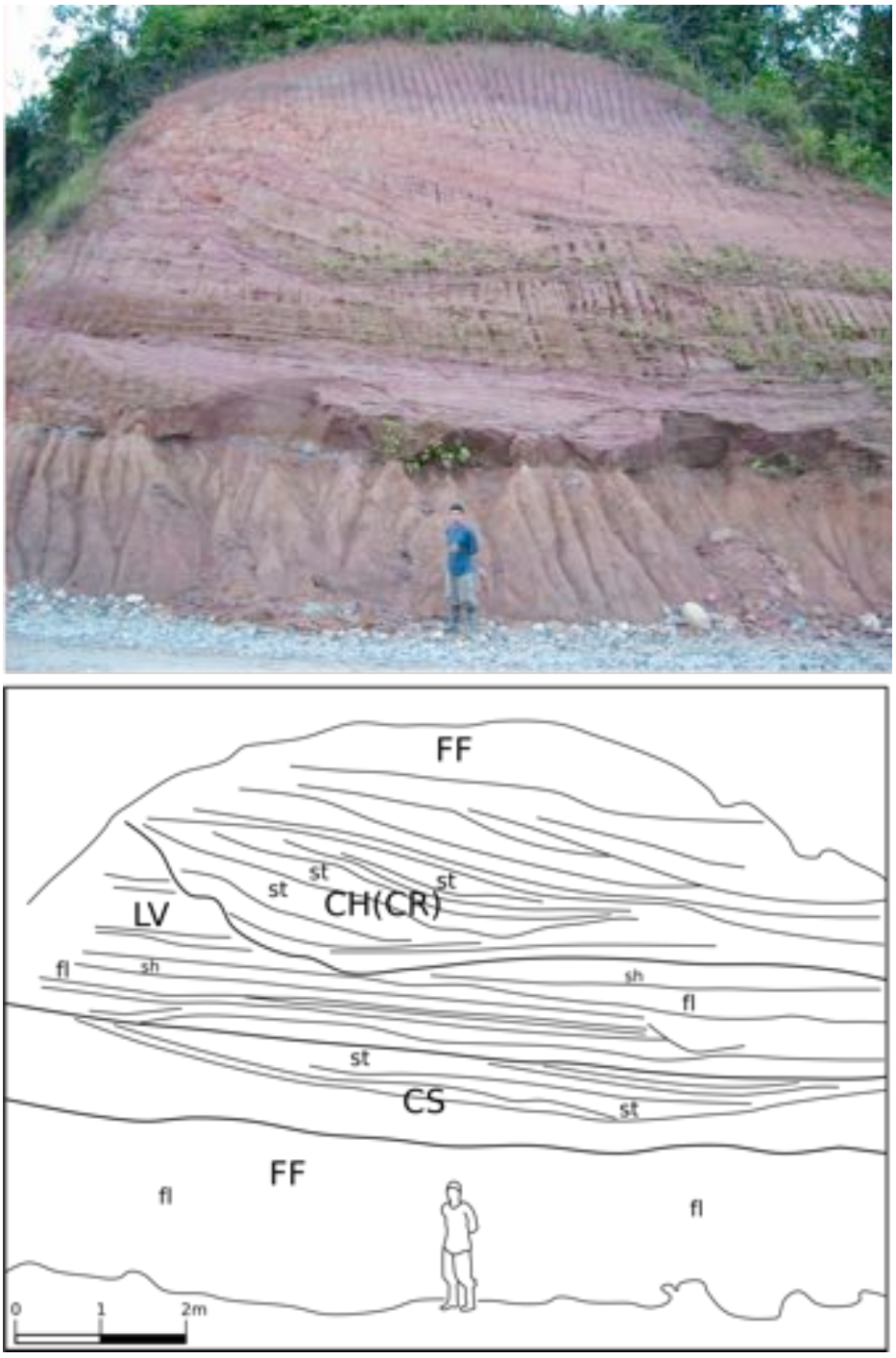

Figure 10

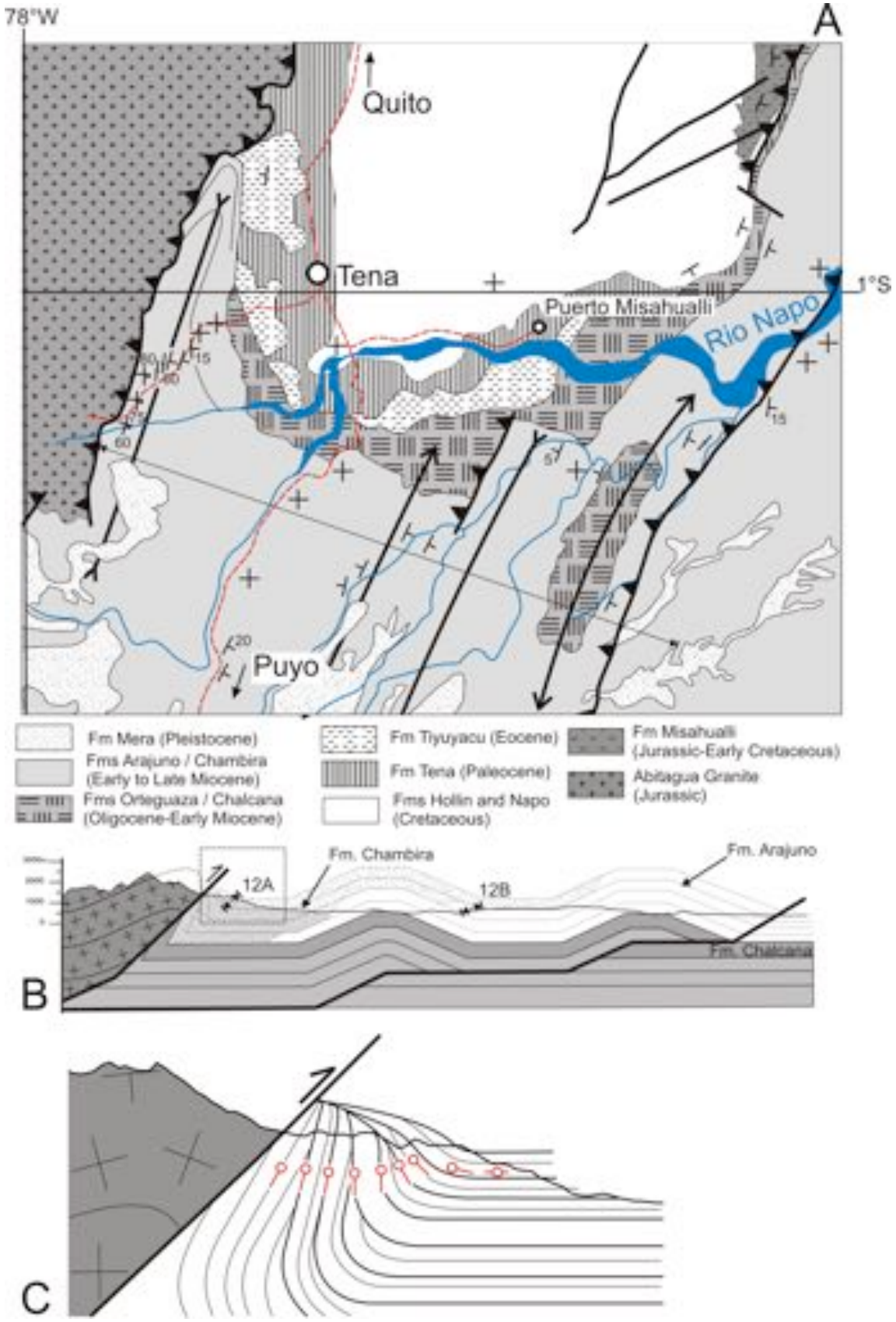
78°W
A
Quito
Tena
1°S
Puerto Misahualli
Rio Napo
Puyo
Fm Mera (Pleistocene)
Fms Arajuno / Chambira (Early to Late Miocene)
Fms Orteguaza / Chalcana (Oligocene-Early Miocene)
Fm Tiyuyacu (Eocene)
Fm Tena (Paleocene)
Fms Hollin and Napo (Cretaceous)
Fm Misahuallí (Jurassic-Early Cretaceous)
Abitagua Granite (Jurassic)
Fm. Chambira
Fm. Arajuno
12A
12B
Fm. Chalcana
B
C

Figure 11

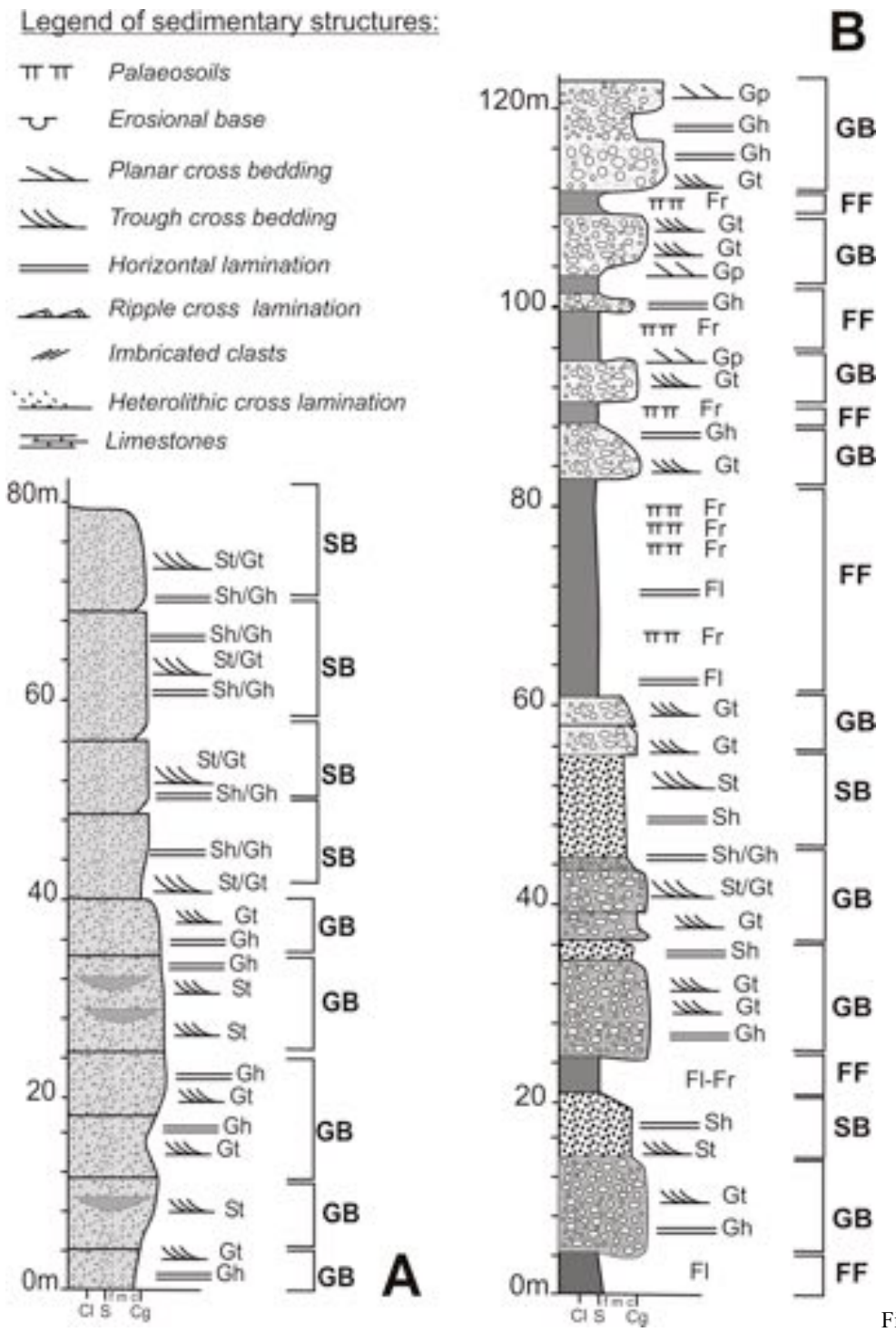
Legend of sedimentary structures:
Palaeosoils
Erosional base
Planar cross bedding
Trough cross bedding
Horizontal lamination
Ripple cross lamination
Imbricated clasts
Heterolithic cross lamination
Limestones
80m
60
40
20
0m
St/Gt
Sh/Gh
Gt
Gh
St
SB
GB
A
Cl S f m c Cg
B
120m
100
80
60
40
20
0m
Gp
Fr
Fl
Fl-Fr
FF
Cl S f m c Cg

Figure 12

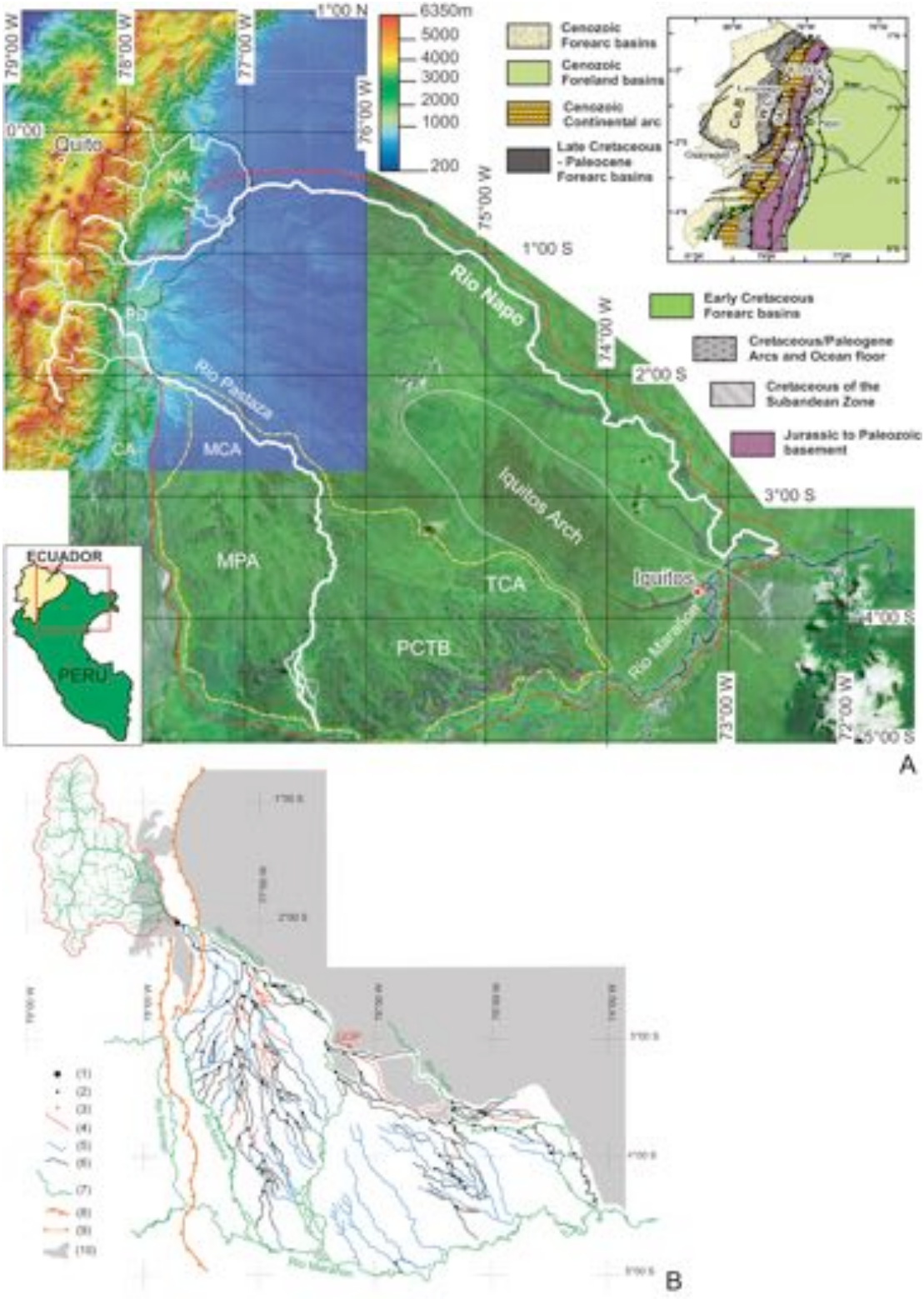
79°00 W
78°00 W
77°00 W
1°00 N
0°00
Quito
NA
PD
CA
MCA
6350m
5000
4000
3000
2000
1000
200
76°00 W
75°00 W
1°00 S
Cenozoic Forearc basins
Cenozoic Foreland basins
Cenozoic Continental arc
Late Cretaceous - Paleocene Forearc basins
Río Napo
Río Pastaza
74°00 W
2°00 S
Early Cretaceous Forearc basins
Cretaceous/Paleogene Arcs and Ocean floor
Cretaceous of the Subandean Zone
Jurassic to Paleozoic basement
3°00 S
Iquitos Arch
ECUADOR
PERU
MPA
TCA
Iquitos
PCTB
Río Marañón
73°00 W
72°00 W
4°00 S
5°00 S
A
B

Figure 13

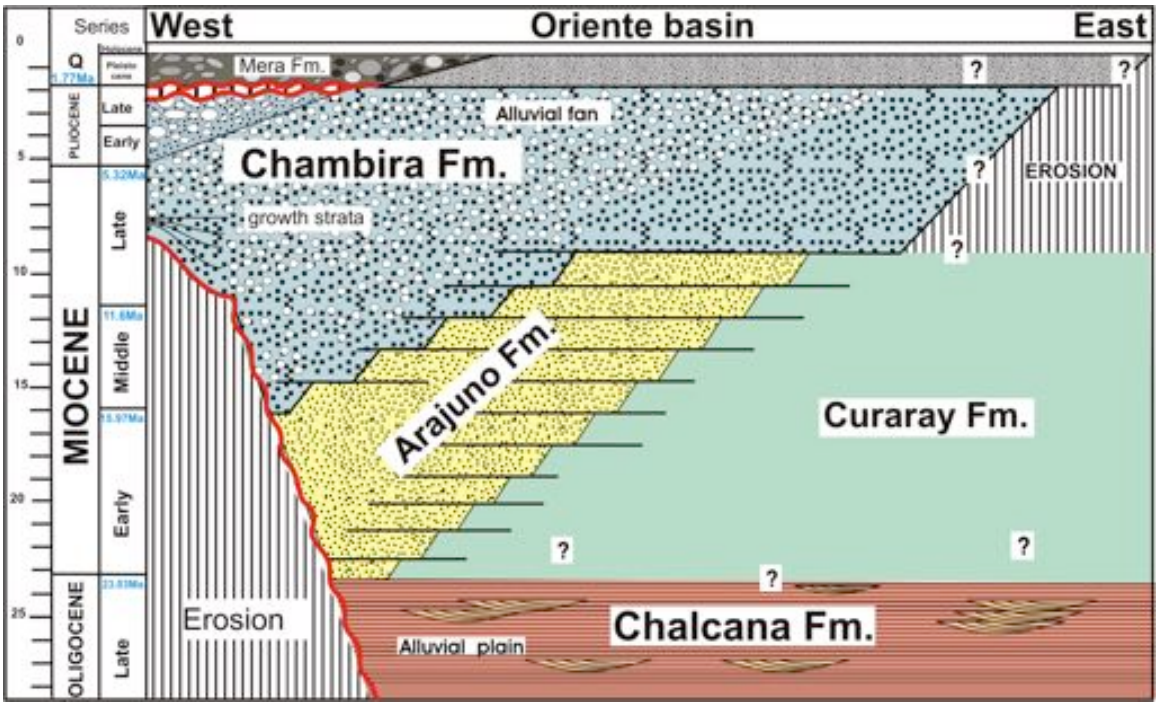
Series
West
Oriente basin
East
Q
Mera Fm.
PLIOCENE
Late
Early
MIOCENE
Late
Middle
Early
OLIGOCENE
Late
Alluvial fan
Chambira Fm.
growth strata
EROSION
Arajuno Fm.
Curaray Fm.
Erosion
Alluvial plain
Chalcana Fm.
?

Figure 14

Code		Description
Fines	**Fl**	Laminated shales and silts
	Fr	Rooted massive or laminated shales and silts
	Fg	Gypsum laminas interbedded in laminated shales and silts
	Fmc	Laminated shales or silts exhibiting mudcracks
	Fsm	Massive shales and silts
	Flc	Thinly laminated limestones and dolostones
	Ft	Trough cross thinly laminated shales and silts
Sands	**Sh**	Flat horizontal thinly laminated to thinly bedded sandstones
	Sr	Ripple crossed laminated sandstones (2D or 3D ripples)
	St	Trough cross laminated or bedded sandstones
	Sp	Planar cross laminated or bedded sandstones
Gravels	**Gh**	Flat horizontal thinly to very thickly bedded conglomerates
	Gp	Planar cross thinly to very thickly bedded conglomerates
	Gt	Trough cross thinly to very thickly bedded conglomerates
Others	**P**	Calcretes, varicouloured shales,

Code	Lithofacies	Geometry, stacking	Architectural element	Formation
FF	Fl, Fr, Fsm	Flat base, flat top, hectometric extension ? Thinly bedded regularly alternating Fl and Fsm, rooted horizons (Fr).	Floodplain	Chalcana Arajuno Chambira
PL	Fl, Flc, Fg, Fmc, P	Flat base, flat top, hectometric extension, meter to decameter thick. Mainly made of Fl alternating with very thinly bedded facies Flc, Fg, fmc and decimeter thick P (calcretes).	Playa type floodplain	Arajuno
LV	Fl, Sr	Flat non erosional base, Flat top. Meter thick	Natural levee	Arajuno
CS	Sr, Sh, Sp	Flat or lightly erosional base and flat to convex-up topped, meter thick, wide extension. Mainly made of Sr, Sp with Sh at the base in case of erosional base. (see Fig. 8A and 9B). Associated with FF, PL and LV.	Crevasse-splay	Arajuno
SB	Sp, Sh, St	Flat or lightly erosional base, flat topped, meter thick.	Sand bar	Arajuno Chambira
LA	St, Sh, Sp, Sr	Erosional base, no reactivation surface within the stack, meter thick, decameter to hectometer wide. Lithofacies succession within a fining upward trend : St, Sh, Sp, St, Sr.	Lateral Accretion macroform	Arajuno
CH(CR)	Sr, Fl, St	Concave down erosional base, flat topped, meter deep, decameter wide made of centrimetric alternating Sr and Fl (see Fig. 8A and 9B). Associated with LV and FF.	Crevasse channel	Arajuno
GB	Gt, Gh, Gp	Concave down erosional base, flat to convex-up top. Meter thick, decametric wide. Alternating Gt and Gh. Thickly to very thickly bedded Gp.	Gravel bar	Chambira
CH(GB)	Gt, Gh, St, Sr	Association of SB and GB organized in concave down erosional base and flat top bodies.	Gravel filled braided channel	Chambira
CH(S)	St, Sr, Sh,	Association of LA and SB organized in Flat to lightly erosional based and flat topped mater thick and hectometric extension.	Sand filled straight to low sinuosity channel	Chalcana Arajuno

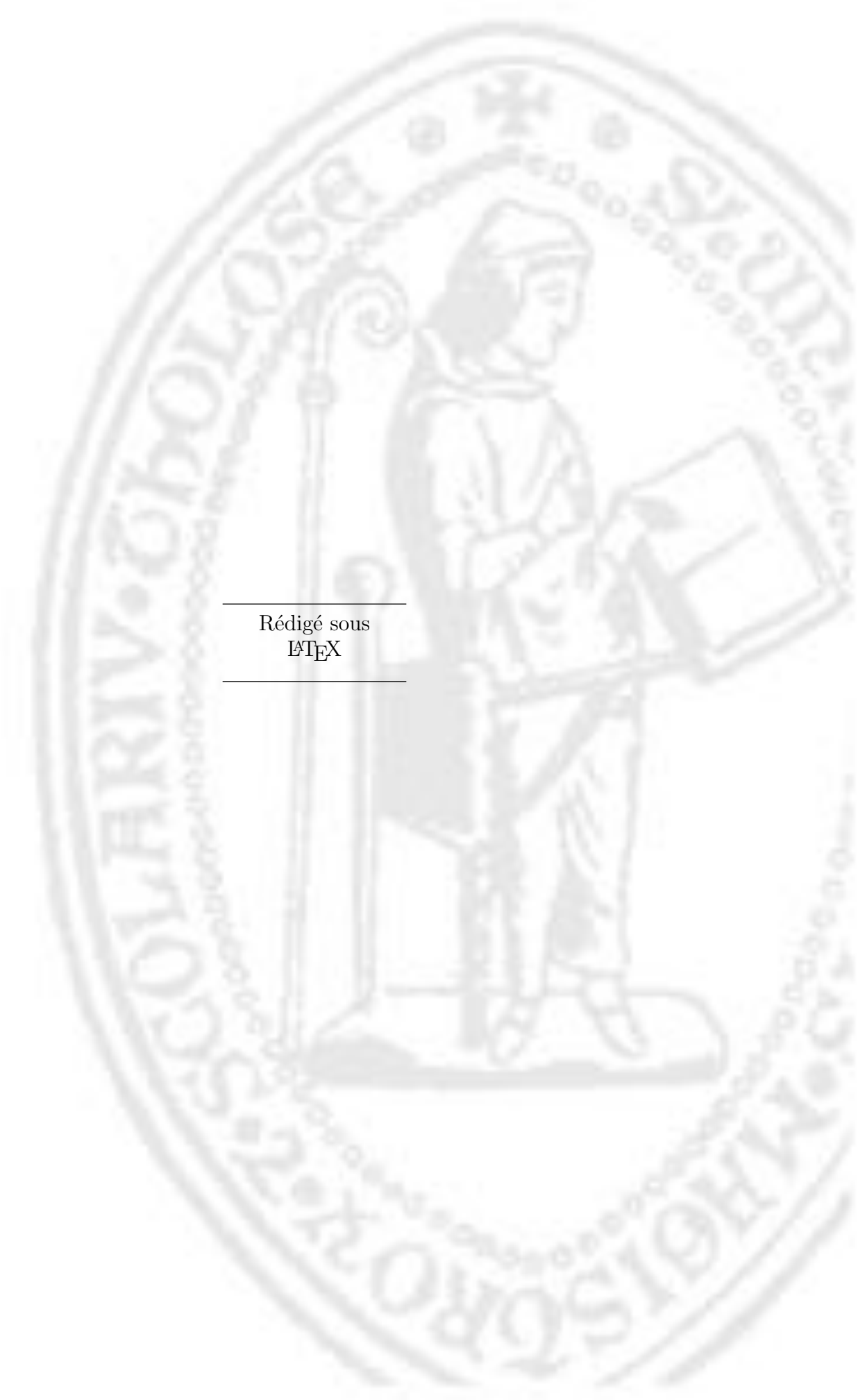

Rédigé sous
LaTeX